PHASE I: GENERAL CUMULATIVE EFFECTS

KEM-48: CUMULATIVE EFFECTS DUE TO MINING, GENERAL AND IN THE GRIJPSKERK AREA

Ministry of Climate and Green Growth

Project	23288 KEM-48
Title report	Phase I: general cumulative effects
Reference	KEM-48 | 202305009
Client	Ministry of Climate and Green Growth
Status	Definitief
Version	4.0
Date	10/07/2025
Authors	W.J.F. Hanckmann MSc, ir. M. Kodde, dr. ir. H. Velsink, dr. S. Baisch, dr. R. Vörös, dr. ir. S. Slob
Reviewed by	dr. ir. F.C. Vossepoel, dr. A.M.H. Pluymakers, dr. G. Giardana, dr. E.W. Meijles, dr. G. Siddiqi, prof.dr.ir. T. Olsthoorn, dr. ir. B. Alberts
Checked by	dr. ir. S. Slob, dr. T. Sweijen
Released by	dr. ir. ing. A.E.C. van der Stoel
File	KEM-48 Phase I literature study.docx

TABLE OF CONTENTS

EXECUTIVE SUMMARY

Background and objective

There are various underground activities in the northern part of the Netherlands, including natural gas extraction, salt mining, gas storage, and (waste) water injection. Although extensive research has been conducted on the individual aspects and effects of mining activities, there are still challenges in understanding their combined effects. Concerns have arisen regarding underground gas storage in Grijpskerk and its interactions with nearby gas fields, leading to the initiation of this KEM-48 research project. This project aims to investigate the interactions between underground activities in response to these concerns, with a focus on ground movement: subsidence and induced earthquakes. Phase I involves a literature review and initial data analysis to test the feasibility of the proposed method, while Phase II entails in-depth modelling studies of the Grijpskerk area. The project team consists of experts from various fields, with advisory and peer-review panels ensuring scientific integrity. This report covers the results of Phase I of the project.

Part 1: literature study

Subsidence

Subsidence of the ground surface results from various processes in the subsurface, occurring at different depths and rates. It is driven both by natural and anthropogenic factors. Natural subsidence in the Netherlands is mainly caused by long-term processes such as consolidation, post-glacial isostasy, and tectonics, with a maximum annual subsidence rate of less than 1 mm/year in the northern part of the Netherlands. Anthropogenic subsidence, resulting from human activities, includes shallow, intermediate, and deep mechanisms such as peat oxidation, groundwater extraction, and mining activities. Subsidence modelling varies by the mechanism. Gas extraction uses poroelasticity and reservoir-based models, while salt solution mining relies on models to account for cavern closure and creep. Gas storage considers elastic deformation. Shallow subsidence applies geotechnical principles and is strongly influenced by spatial variations. Groundwater extraction uses traditional models and more recent data assimilation for large-scale predictions.

In the northern part of The Netherlands the maximum shallow subsidence rate is 12 mm/year. The maximum deep subsidence rate for gas extraction is 6 mm/year, for gas storage 20 mm/year (including heave) and for salt mining 14 mm/year. Intermediate subsidence due to groundwater extraction is considered here negligible compared to the other mechanisms. Traditionally, subsidence monitoring is conducted through geodetic measurements, but the use of other technologies such as InSAR, GNSS, and LiDAR offer opportunities for large-scale and continuous monitoring, provided they are carefully interpreted and supplemented with traditional geodetic measurements.

Induced seismicity

The primary cause of induced earthquakes is stress changes in the subsurface induced by anthropogenic (human) activities. Various activities can be associated with induced earthquakes. In the Netherlands, induced earthquakes are caused by gas extraction, gas storage, geothermal energy, and water injection. The sensitivity with which earthquakes can be detected and the accuracy with which they can be located depend on the number of active and operational monitoring stations and their geometric configuration. When anthropogenic activities in the subsurface are closely spaced, as in the Netherlands, it is not always possible to unambiguously associate an observed earthquake with a specific activity in the subsurface.

Leakage

Methane leakage via damaged oil and gas wells after decommissioning is a known risk in the industry. Although leakage is often identified in the late (decommissioning) phase of a well's lifecycle, the root causes typically originate much earlier, during drilling, completion, and production phases, when high reservoir pressures are present. Poor well- and cement design, shrinkage, and chemical degradation can cause well integrity failure and subsequent leakage. International experiences indicate various relationships with factors such as well type, age, depth, plug status, geographical and geological conditions. For storage reservoirs, pressure fluctuates over time and by season, in contrast to producing reservoirs which generally experience continuous pressure depletion. Although methane leakage via natural faults occurs, well leakage is generally considered more significant. Understanding pressure redistribution after decommissioning and long-term fluid migration can provide information on leakage potential, especially on the scale of centuries for the Groningen gas field, where the cumulative effects with neighbouring gas fields are still unknown.

Effects

The impact of earthquakes on buildings has mainly been studied after the earthquake in Huizinge on August 16, 2012. Regarding damage, an empirical model has been developed for the Groningen field to predict peak ground velocities based on magnitude and distance to the hypocentre. The KNMI has developed specific models for earthquakes in small gas fields outside the Groningen field. By testing these model calculations against threshold values, the likelihood of damage can be determined. Deep subsidence, caused by mining activities, results in horizontal strain and angular distortion (relative rotation) in buildings, which can cause damage. There are both direct effects, such as horizontal strain, and indirect effects, such as changes in groundwater level that can cause differential settlements. Various aspects of subsidence are addressed, with attention to their varying effects on buildings. Therefore, various methods to determine horizontal deformation and angular distortion resulting from subsidence, and the resulting potential damage, are discussed.

Processes and interactions

Shallow subsidence is influenced by factors such as overburden, vibrations from cyclic loading, and hydrogeological changes, with varying impact depending on geological, hydrogeological, and anthropogenic conditions. Top loading affects the subsurface at a 45-degree angle, typically impacting depths and lateral distances up to 20 meters. Vibration-induced compaction from infrastructure work generally has a 10-meter radius. The impact area of deep subsidence due to gas extraction extends to a maximum of about twice the depth of the gas-water contact from the edge of the reservoir, typically 6 km, based on a depth of 3 km. The impact area of salt mining is due to the smaller widths of the caverns usually smaller, but the subsidence bowl is generally more pronounced.

Seismic activity can be caused by stress changes in the subsurface due to various activities, with the definition of threshold values being complex and dependent on subsurface fault conditions. The influence zone of an induced seismic event is strongly influenced by its magnitude. For magnitudes above 2.0, the affected area can extend for several kilometres from the epicentre, and this distance grows exponentially with larger magnitudes.

Fluid migration is influenced by pressure communication between subsurface layers and factors influencing vertical migration, such as lithology and underground activities. Subsidence and the hydrogeological system form a feedback mechanism influenced by natural and anthropogenic factors. The compaction caused by gas extraction in the reservoir affects the sealing salt layer and lateral fluid migration. International examples can be found on interactions between earthquakes, subsidence, and mining activities. In Northern Netherlands, specific examples include unexpected subsidence due to interaction between salt and gas extraction in Fryslân and complex interactions in the Veendam area.

Part 2: Project plan phase II

Case study area

The case study area of Grijpskerk is characterized by diverse set of landscapes and is divided into several regions, including De Marne, Lauwers, Middag-Humsterland, Reitdiep, Westerkwartier, and Oostergo. The area is partly situated in Groningen Province and partly in Fryslân Province. The deeper geology around the UGS Grijpskerk and surrounding gas fields is dominated by the formation of the Lower Rotliegend-Sandstone reservoir rock and the Permian sealing salt layer within the sub-basin of the Lauwerszee Trog. The Pleistocene ice ages have had a significant impact on sediment deposition and landscape formation. Human activities have strongly influenced the landscape in the last few thousand years. The hydrogeological system is influenced by polder water management, precipitation, evaporation, and seepage. Water management in the project area is supervised by two water boards (Wetterskip Fryslân and Noorderzijlvest). The concept of drainage is elaborated, which is essential in regulating water levels and its influence on groundwater levels and shallow subsidence.

Feasibility study using raw NAP data

A feasibility study has been conducted with the aim of exploring the potential of advanced modelling techniques and innovative deformation analysis to understand the cumulative effects and interactions of mining activities in the Lauwerszee Trog. The Annerveen gas field has been chosen as a showcase due to the presumed absence of complex cumulative effects on the south side of the field and because of the long-term gas production that has taken place there. Pressure measurements from production wells have been used to understand reservoir pressure variations, resulting in the identification of gas compartments. A historical matching of NAP (Amsterdam Ordnance Datum) level data before 1995 has been conducted, leading to an estimation of combined subsidence effects of Annerveen and nearby salt mining in Veendam. NAP data have been chosen for their long history, although they were not originally intended for deformation analysis. A new method, the DELTA method, has been developed to utilize raw NAP observations for subsidence analysis, resulting in improved precision and accuracy. This approach allows for the identification of points that actually represent deep subsidence. This innovative, new approach provides greater precision and accuracy in subsidence modelling than was previously possible and can be applied on a larger scale in the project area in Phase II of the research.

Recommendations for further study in Phase II

In this Phase I of the project, the feasibility of a new approach for calibrating multiple compaction sources based on differential elevation measurements has been demonstrated. This approach will be the primary focus of the Phase II study, along with investigating various other topics identified during literature review, the field visit, and consultation with local stakeholders. Phase II will focus on the impact of inelastic reservoir compaction, research into differences in published data, the possibility of felt vibrations not directly associated with recorded earthquakes, and the presence of potentially leaking wells.

The work process involves modelling of deep and shallow subsidence mechanisms, assessing the effect on surface objects, and evaluating their cumulative effects. Risks of mining-induced damage to buildings will be identified and placed in the context of non-mining-related processes. Ultimately, the goal of the study is to provide a comprehensive understanding of the impact of underground activities on ground movement, enabling a forecast of future effects.

MANAGEMENT SAMENVATTING

Aanleiding en doel

Er zijn verschillende ondergrondse activiteiten in het noorden van Nederland, waaronder aardgaswinning, zoutwinning, opslag van gas en (afval) waterinjectie. Hoewel er veel onderzoek is verricht naar de individuele aspecten en effecten van mijnbouwactiviteiten, zijn er nog uitdagingen bij het begrijpen van hun gecombineerde effecten. Er zijn zorgen over de ondergrondse gasopslag in Grijpskerk en de interacties ervan met nabijgelegen gasvelden, wat heeft geleid tot dit KEM-48 onderzoeksproject. Dit project beoogt naar aanleiding van deze zorgen de interacties tussen ondergrondse activiteiten te onderzoeken, met de nadruk op bodembeweging: bodemdaling en geïnduceerde bevingen. Fase I omvat een literatuurstudie en eerste data-analyse om de haalbaarheid van de voorgestelde methode te testen, terwijl in Fase II diepgaande modelstudies van het gebied Grijpskerk worden uitgevoerd. Het projectteam bestaat uit experts uit verschillende vakgebieden, waarbij advies- en peer-reviewpanels zorgen voor wetenschappelijke borging. Dit rapport behandelt de resultaten van Fase I van het project.

Deel 1: literatuurstudie

Bodemdaling

Bodemdaling aan het oppervlak is het gevolg van diverse processen in de ondergrond, met verschillende dieptes en snelheden. Bodemdaling wordt gedreven door natuurlijke en antropogene factoren. Natuurlijke bodemdaling in Nederland wordt voornamelijk veroorzaakt door lange termijn processen zoals inklinking, postglaciale isostasie en tektoniek, met een maximale jaarlijkse daling van minder dan 1 mm/jaar in het noorden van Nederland. Antropogene bodemdaling, voortkomend uit menselijke activiteiten, omvat ondiepe, tussenliggende en diepe mechanismen, zoals oxidatie van veen, grondwaterwinning en mijnbouwactiviteiten. Modellering van bodemdaling varieert per mechanisme. Gaswinning maakt gebruik van poroelasticiteit en reservoir-gebaseerde modellen, terwijl voor zoutwinning modellen worden gebruikt die gebaseerd zijn op krimp van de caverne en het kruipgedrag van zout. Modelleren van bodembeweging door gasopslag is gebaseerd op elastische vervorming. Voor ondiepe bodemdaling worden geotechnische principes toegepast, waar de ruimtelijke variatie een belangrijk aspect is. Grondwaterwinning gebruikt traditionele modellen en meer recent wordt data-assimilatie gebruikt voor grootschalige voorspellingen.

In het noordelijke deel van Nederland is de maximale ondiepe bodemdaling 12 mm per jaar. De maximale diepe bodemdaling voor gaswinning is 6 mm per jaar, voor gasopslag 20 mm per jaar (inclusief heffing), en voor zoutwinning 14 mm per jaar. De tussenliggende bodemdaling door grondwaterwinning kan als verwaarloosbaar beschouwd in vergelijking met de andere (diepe en ondiepe) mechanismen. Monitoring van bodemdaling gebeurt traditioneel met geodetische metingen, maar inzet van andere technologieën zoals InSAR, GNSS en LiDAR bieden kansen voor grootschalige en continue monitoring, mits zorgvuldig geïnterpreteerd en aangevuld met de traditionele geodetische metingen.

Geïnduceerde aardbevingen

De hoofdoorzaak van geïnduceerde aardbevingen zijn spanningsveranderingen in de ondergrond veroorzaakt door antropogene (menselijke) activiteiten. Verschillende activiteiten kunnen in verband worden gebracht met geïnduceerde aardbevingen. In Nederland worden geïnduceerde aardbevingen veroorzaakt door gaswinning, gasopslag, geothermie en waterinjectie. De gevoeligheid waarmee aardbevingen kunnen worden gedetecteerd en de nauwkeurigheid waarmee ze kunnen worden gelokaliseerd, hangt af van het aantal actieve en operationele meetstations en hun onderlinge

geometrische configuratie. Als antropogene activiteiten in de ondergrond dicht bij elkaar liggen, zoals in Nederland, is het niet altijd mogelijk om een waargenomen aardbeving eenduidig in verband te brengen met een specifieke activiteit in de ondergrond.

Lekkage

Methaanlekkage via beschadigde olie- en gasputten na buitenbedrijfstelling is een bekend risico in de industrie. Hoewel lekkage vaak pas in de late (buitenbedrijfstelling) fase van de levenscyclus van een put wordt vastgesteld, liggen de oorzaken meestal veel eerder, tijdens de boor-, voltooiings- en productie-fasen, wanneer er sprake is van hoge reservoirdrukken. Slecht put- en cementontwerp, krimp en chemische degradatie zijn de oorzaken van put falen en daarmee lekkage. Internationale ervaringen geven verschillende relaties met bijvoorbeeld put type, leeftijd, diepte, plugstatus, geografische- en geologische omstandigheden. Bij opslagreservoirs varieert de reservoirdruk cyclisch in de tijd en per seizoen als gevolg van injectie- en onttrekkingsactiviteiten, terwijl producerende reservoirs doorgaans een gestage drukdepletie vertonen door voortdurende productie. Hoewel methaanlekkage via natuurlijke breuklijnen voorkomt, wordt putlekkage over het algemeen als belangrijker beschouwd. Inzicht in drukherverdeling na buitenbedrijfstelling en lange termijn vloeistofmigratie kan informatie verschaffen over lekkagepotentieel, vooral op de schaal van eeuwen voor het Groningen gasveld, waarbij de cumulatieve effecten met naburige gasvelden nu nog onbekend zijn.

Effecten

De impact van bevingen op gebouwen is voornamelijk onderzocht na de aardbeving bij Huizinge op 16 augustus 2012. Met betrekking tot schade is voor het Groningenveld een empirisch model ontwikkeld om piekgrondsnelheden te voorspellen op basis van magnitude en afstand tot het hypocentrum. Het KNMI heeft specifieke modellen ontwikkeld voor aardbevingen in kleine gasvelden buiten het Groningenveld. Door deze modelberekeningen te toetsen aan grenswaarden, kan de kans op schade worden bepaald. Diepe bodemdaling, veroorzaakt door mijnbouwactiviteiten, resulteert in horizontale rek en hoekverdraaiing (relatieve rotatie) in gebouwen, wat schade kan veroorzaken. Er zijn zowel directe effecten, zoals horizontale rek, als indirecte effecten, zoals veranderingen in de grondwaterstand die differentiële zettingen kunnen veroorzaken. Verschillende aspecten van bodemdaling worden behandeld, met aandacht voor hun variërende effecten op gebouwen. Er worden derhalve verschillende methoden om horizontale vervorming en hoekverdraaiing als gevolg van bodemdaling, en de daaruit eventueel resulterende schade te bepalen, behandeld.

Processen en interacties

Ondiepe bodemdaling wordt beïnvloed door onder andere bovenbelasting, trillingen door cyclische belasting en geohydrologische veranderingen, met wisselende impact, afhankelijk van de geologische, geohydrologische en door mensenhanden veroorzaakte omstandigheden. Bovenbelasting beïnvloedt de ondergrond onder een hoek van 45 graden, wat meestal invloed heeft op dieptes en laterale afstanden tot 20 meter. Trillingsverdichting door bouwwerkzaamheden heeft over het algemeen een straal van 10 meter. Het invloedsgebied van diepe bodemdaling door gaswinning strekt zich uit tot een maximum van ongeveer twee keer de diepte van het gas-watercontact vanaf de rand van het reservoir, doorgaans ongeveer 6 km, gebaseerd op een diepte van 3 km. Het impactgebied van zoutwinning is door de kleinere breedtes van de cavernes meestal kleiner, maar de bodemdalingskom is over het algemeen steiler en dieper.

Seismische activiteit kan worden veroorzaakt door spanningsveranderingen in de ondergrond door verschillende activiteiten, waarbij de definitie van grenswaarden complex en afhankelijk van ondergrondse breukcondities is. Het invloedsgebied van een geïnduceerde beving wordt sterk beïnvloed door de magnitude ervan. Voor magnitudes boven de 2.0 kan het invloedsgebied zich over enkele kilometers vanaf het epicentrum uitstrekken, en deze afstand groeit exponentieel bij grotere magnitudes.

Vloeistofmigratie wordt beïnvloed door drukcommunicatie tussen ondergrondse lagen en factoren die verticale migratie beïnvloeden, zoals lithologie en de ondergrondse activiteiten. Bodemdaling en het geohydrologische systeem vormen een terugkoppelingsmechanisme beïnvloed door natuurlijke en menselijke factoren. De door de gaswinning veroorzaakte compactie in het reservoir, beïnvloedt de afsluitende zoutlaag en de laterale vloeistofmigratie. Internationale voorbeelden zijn te vinden over interacties tussen aardbevingen, bodemdaling en mijnbouwactiviteiten. In Noord-Nederland zijn concrete voorbeelden uit te lichten zoals de onverwachte bodemdaling door interactie tussen zout- en gaswinning in Fryslân en complexe interacties in het Veendam-gebied.

Deel 2: Projectplan fase II

Projectgebied

Het projectgebied rondom Grijpskerk wordt gekenmerkt door een divers landschap en wordt onderverdeeld in verschillende regio's, waaronder De Marne, Lauwers, Middag-Humsterland, Reitdiep, Westerkwartier en Oostergo. Het gebied ligt gedeeltelijk in Groningen en gedeeltelijk in Fryslân. De diepere geologie rondom de UGS Grijpskerk en omliggende gasvelden, wordt gedomineerd door de vorming van het Lower Rotliegend-zandsteen reservoirgesteente en de afsluitende zoutlaag tijdens het Perm binnen het sub-bekken van de Lauwerszee Trog. Veel later hebben de Pleistocene ijstijden grote invloed gehad op sedimentafzettingen en landschapsvorming, Menselijke activiteiten hebben het landschap de laatste paar duizend jaar sterk beïnvloed. Het geohydrologisch systeem wordt beïnvloed door polderwaterbeheer, neerslag, verdamping en kwel. Het waterbeheer in het projectgebied staat onder toezicht van twee waterschappen (Wetterskip Fryslân en Noorderzijlvest). Het concept drooglegging wordt uitgewerkt, belangrijk in het reguleren van het waterpeil en de invloed hiervan op de grondwaterstand en ondiepe bodemdaling.

Haalbaarheidsonderzoek gebruik ruwe NAP data

Een haalbaarheidsstudie is uitgevoerd met als doel het potentieel van geavanceerde modelleringstechnieken en innovatieve deformatieanalyse te onderzoeken, om zo de cumulatieve effecten en interacties van mijnbouwactiviteiten in de Lauwerszee Trog te begrijpen. Het Annerveen gasveld is gekozen als showcase vanwege de veronderstelde afwezigheid van complexe cumulatieve effecten aan de zuidzijde van het veld en vanwege de langjarige gaswinning die daar heeft plaatsgevonden. Drukmetingen van productieputten zijn gebruikt om reservoirdrukvariaties te begrijpen, resulterend in de identificatie van gascompartimenten. Een historische matching van NAP-peilgegevens tot vóór 1995 is uitgevoerd, wat heeft geleid tot een schatting van gecombineerde bodemdalingseffecten van Annerveen en nabijgelegen zoutwinning in Veendam. NAP-gegevens zijn gekozen vanwege hun lange historie, hoewel ze oorspronkelijk niet bedoeld waren voor deformatieanalyse. Een nieuwe methode, de DELTA-methode is ontwikkeld om ruwe NAP-waarnemingen te gebruiken voor bodemdalingsanalyse, resulterend in een verbeterde precisie en nauwkeurigheid. Deze aanpak maakt het mogelijk om punten te identificeren die daadwerkelijk diepe bodemdaling weergeven. Deze innovatieve, nieuwe benadering biedt een grotere precisie en nauwkeurigheid in bodemdaling modellering dan tot op heden mogelijk was en kan op grotere schaal worden toegepast in het projectgebied in fase II van het onderzoek.

Aanbevelingen voor het fase II onderzoek

In deze fase I van het project is de haalbaarheid van een nieuwe aanpak voor het kalibreren van meerdere compactie-bronnen op basis van differentiële hoogtemetingen gedemonstreerd. Deze aanpak zal de primaire focus zijn van fase II, samen met het onderzoeken van verschillende andere onderwerpen die zijn geïdentificeerd tijdens literatuuronderzoek, veldbezoeken en in overleg met de omwonenden. Fase II zal zich onder meer richten op de impact van inelastische reservoircompactie,

onderzoek naar de verschillen in gepubliceerde gegevens, de mogelijkheid van gevoelde trillingen die niet direct geassocieerd zijn met vastgestelde aardbevingen en de aanwezigheid van potentieel lekkende putten.

Het werkproces omvat het modelleren van diepe en ondiepe bodemdaling mechanismen, het beoordelen van het effect op aan het oppervlak gelegen objecten en het beoordelen van de cumulatieve effecten. Risico's van door mijnbouw veroorzaakte schade aan gebouwen zullen worden geïdentificeerd en in de context van niet-mijnbouw gerelateerde processen worden geplaatst. Uiteindelijk is het doel van de studie om een uitgebreid begrip te bieden van de impact van ondergrondse activiteiten op bodembeweging, wat een prognose van toekomstige effecten mogelijk maakt.

1

INTRODUCTION

1.1 Background

The subsurface in the northern region of the Netherlands is characterized by intensive mining activities that have been ongoing for decades. Gas extraction, primarily from the vast Groningen field, has been the most prominent activity, complemented by numerous smaller natural gas fields dispersed across Fryslân, Groningen, and Drenthe. Additionally, active salt solution mining takes place in Groningen and Fryslân, while salt caverns and gas fields serve as storage facilities for natural gas and nitrogen. There are considerations for repurposing these abandoned salt caverns for the storage of green energy, such as compressed air or hydrogen. While not a mining activity in the strict sense, the extraction of geothermal energy is also gaining interest in this region.

There are several areas where these subsurface activities interact. The Veendam area serves as an illustrative example, where subsidence from salt solution mining intersects with subsidence from the Groningen and Annerveen gas fields. Moreover, induced earthquakes from the Groningen field affect parts of this area. Disentangling these effects to identify the most influential mining activity and analysing cumulative effects poses significant challenges. Ongoing research is addressing some of these complexities. The Underground Gas Storage (UGS) in Norg exemplifies seasonal subsidence and heave, in addition to general deep subsidence and seismicity from the Groningen field, with potential cumulative effects. The primary focus of this KEM project revolves around the Underground Gas Storage (UGS) facility in Grijpskerk. Initially developed as a gas field in 1997, the UGS Grijpskerk was transitioned into a (seasonal) storage site for high-caloric gas ("industry gas") from small gas fields, excluding Groningen. Located approximately 3400 meters below the surface, it has been in operation for years. As of 2022, the UGS Grijpskerk has been repurposed to store low-caloric natural gas ("consumer gas") from Groningen, following the cessation of production at the Groningen gas field. The UGS now accommodates natural gas from alternative sources, blended with nitrogen to produce low-caloric consumer gas. Positioned amidst other small gas fields, the UGS Grijpskerk falls within the influence area of induced seismicity originating from the Groningen field. (see Figure 1).

Gas extraction in the northern Netherlands induced seismic events causing damage to structures. In addition, the compressive forces causing geological layers to compact following gas extraction results in subsidence at the surface, directly and indirectly impacting buildings, objects, and the surface water infrastructure. Gas storage in some fields further contributes to seasonal variations in subsidence and heave, as a result of gas extraction in winter and injection in summer, respectively. Salt mining and the associated salt creep leads primarily to subsidence. The interplay of these various mass removal activities in the deep subsurface may lead to combined effects at the surface. This implies that also during yearly actions of storage and recovery, permanent changes occur and accumulate. In Figure 2 a schematisation is given of the possible processes, interactions, and effects at play in the deep but also the shallow subsurface in the North of The Netherlands including the Grijpskerk area. This schematisation, although exaggerated in scale, shows that a potentially complex system of processes and interactions takes place.

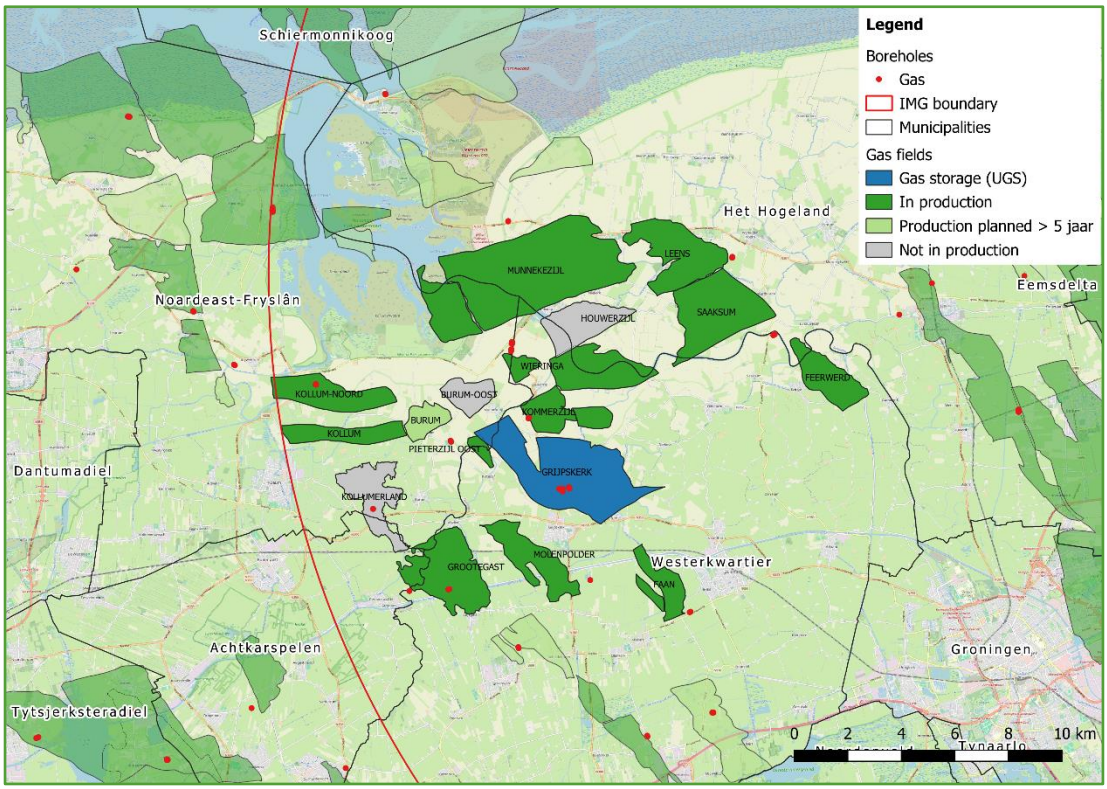

* Some fields, like Kommerzijl and Pieterzijl Oost, are still in production, while others, such as Burum-East, are no longer in operation, and some, like Burum, are not yet in production. Most gas fields use multiple wells (red dots), that crosscut many geological formations and thus potentially forming leakage pathways for fluids and gases from one horizon to another. It is important to note that a single field may produce from multiple reservoir layers, such as the Rotliegendes, Zechstein 2C, and Vlieland formations, either simultaneously or in sequence. This can be incorporated in the modelling. The red line is the border of the IMG mandate area, i.e. the "Huizinge circle" (IMG boundary in the Legend).

Figure 1. illustration of on-going and past deep subsurface activities in the study area, with UGS Grijpskerk in blue, alongside surrounding active, inactive, and temporarily abandoned natural gas fields (source: NLOG.nl).

1.2 Introduction to the concerns around UGS Grijpskerk

The Underground Gas Storage (UGS) Grijpskerk (depicted in blue in Figure 1) is surrounded by various gas fields, including Kommerzijl, Saaksum, Pieterzijl, Kollum, Molenpolder, Wieringa, Burum, Burum-East, and Grootegast. The location of the UGS and surrounding gas fields includes part of the Westerkwartier and the Het Hogeland municipalities in the Province of Groningen and the Noardeast-Fryslân municipality in the province of Fryslân. The area is rural and characterised by a polder landscape with scattered historically important villages. The area is largely below sea level, partly reclaimed from tidal flats and the Lauwers estuary and partly a terp, dike and salt marsh landscape and peat landscapes further south (see also chapter 7). Until the recent past, the Lauwers estuary formed an open connection to the Wadden Sea. The older villages are often centred around ancient man-made terps (dwelling mounds) that served as refuge during flooding. The regular flooding deposited silt and clay, which generated soil that is very fertile. Therefore, farming has been and still is an important economic activity here. In 1969 the Lauwers estuary closed off with a dike from the Wadden Sea (see also section 7.7.2). The water boards Wetterskip Fryslân and Noorderzijlvest are jointly responsible for the water management and water safety in the area.

Over the years, locals have experienced ground motion events and witnessed the development of damage to houses that raised questions about the individual and combined impacts of these activities on their homes, farmland, groundwater, and the overall environment. Citizens in the vicinity of UGS Grijpskerk are concerned about how the UGS operations might affect and interact with other ongoing

or completed gas extraction activities. Adding complexity to the situation is the fact that the area was put under the mandate of the Institute for Mining Damage Groningen (IMG), which handles mining damage due to the influence of the Huizinge earthquake in 2012 (see Figure 1).

While citizens are directed to the IMG for damage claims, it is important to note that the IMG has, until now, only examined the impact of the Groningen field and UGS Norg, specifically focusing on the seismic effects originating from that field. Other potential local effects, which residents are concerned about, have not been considered so far. Because of these concerns the Netherlands Ministry of Economic Affairs and Climate Affairs (currently: Ministry of Climate and Green Growth) has formulated this research project together with the citizens. This research will be executed under the KEM programme. The project's main research question and its objectives are explained in section 1.3.

1.3 Objectives

The objective of this KEM-48 assignment is to define and clarify the possible interactions between different subsurface activities in the Northern part of the Netherlands with a focus on subsidence and seismicity. As explained in the previous section, this research project has been defined with the assistance of citizens in the Northern part of the Netherlands who are concerned about the number of activities in their neighbourhood and the consequences of possible interaction between these activities in the shallow and deep subsurface. The research question aims to provide a fact-based, independent answer to these concerns. The main concern is formulated in the research question:

"What are the cumulative effects and interactions of the different mining activities around the Lauwers Sea trough and the interaction of the UGS Grijpskerk, the surrounding small gas fields and the Groningen gas field?"

This project aims to answer the main research question by defining the possible and probable interactions between various activities in the subsurface. The research is divided into Phase I and Phase II.

I. In Phase I an overview of the possible interactions between different subsurface activities is obtained through a general literature study and first data analysis.

II In Phase II the region close to the gas storage Grijpskerk (in the so-called general "Lauwers Sea trough" area) will be studied in more detail concerning these possible interactions, including the specific geology of the Lauwers Sea region, both shallow and deep, with old riverbeds, sand from the Wadden Sea, its geological history, production locations of small gas fields, the Groningen field and gas storage operations in the region.

1.4 Scope of Phase I: general cumulative effects

1.4.1 Research questions

For Phase I the following sub-research questions have been formulated:

1. What information is available about interactions between different adjacent underground (man-made) activities, natural processes, and about the cumulative mutual effect, divided into the following topics:
    a. Subsidence (see chapter 2)
    b. Induced seismicity (see chapter 3)
    c. Leakage (see chapter 4)
    d. Other (see section 9.1)[1]

[1] Instead of a separate chapter for other effects, we have listed all potential additional processes deserving attention in Phase II (besides subsidence, induced seismicity, and leakage). This is based on feedback from local stakeholders, the bicycle tour, and our Hazid-like session. We've incorporated this discussion into the recommendations chapter (section 9.1).

2. In what way are buildings affected by processes and interactions? (see chapter 5) [2].
3. What is the distance (both in depth as lateral) which would exclude cumulative effects between mining activities for subsidence, induced seismicity, leakage, other? (see chapter 6)
4. What can be studied in more detail in Phase II for the Grijpskerk area? (The answer to this question is formulated in the form of recommendation in chapter 9. Its related plan of action are in an integral way described in Part II, see chapters 7[3], 8 and 9).

1.4.2 Deliverables

The deliverables provided at the end of Phase I:

- Deliverable 1: A literature study focussing on the possible mechanisms of interactions among various subsurface activities, including worldwide experiences.
- Deliverable 2: A general report on Phase I (research questions 1, 2, 3 and 4), with clear conclusions and recommendations.
- Deliverable 3: A Dutch summary of the main findings of Phase I which answers the research question in a clear and non-technical way.

1.5 Structure of this report

This report follows closely the structure and research questions as they were laid out in the request for proposal (MEA, 2023). The report clearly makes a distinction between the literature study on the one hand and the feasibility and the real situation of concern and the methodology for Phase II on the other hand.

This report covers Phase I of the project and consists of the following parts:

- Part 1. Literature study. This answers the research questions 1 and 2 that is described in section 1.4.1 and is the deliverable 1 described in Section 1.4.2. The literature study comprises the chapters 2 to 6 of this report.
- Part 2. Project plan Phase II. This answers research question 4 described in section 1.4.1 in yielding a project plan for Phase II. The project plan for Phase II contains describes the study area, a feasibility study and gives recommendations for the modelling and analysis for Phase II (chapters 7 to 9 of this report). An inventory of possible other topics (research question 1d) is provided in section 9.1 (part of the recommendations for further study)
- General Report Phase I: Taken together, part 1 and 2 combined form deliverable 2, which is this report.
- The Dutch summary of the main findings of Phase I form deliverable 3. The summary can be found at the front of this report and forms an integral part of this report. An English summary is also provided.

1.5.1 Context of the project

The KEM-48 project team consists of experts from the companies CRUX, Cohere Consultants, Q-Con and Geodelta. The project team has combined expertise in geohydrology, geotechnics, geology, mining, reservoir technology, seismology, and geodesy. For the scientific quality control scientists from the TU Delft have been attached to the project as an advisory group. The advisory group acts as a participatory review panel and can also be consulted by the project team for questions about the modelling and reporting. In addition, there is an external peer review panel, consisting of four experts

[2] This is an additional research question we have incorporated due to our interpretation that the subject matter is intricately linked with research questions 1a and 1b. In our assessment, the topic deserved coverage in a separate chapter for clarity.
[3] Chapter 7 provides an overview of the research area, offering an initial delineation of the study zone. While it is part of phase II, we found it essential to incorporate it into this phase to review the feasibility and recommendations in the context of the area of investigation.

in the fields of (1) regional geology and geography; (2) geodesy; (3) geohydrology; and (4) induced seismicity and reservoir modelling.

The KEM guidance group is regularly informed on the progress of this project. This group consists of the representative of a local advocacy group and their advisor, the representative from the Dutch Ministry of Climate and Green Growth and other members of the KEM panel. They are regularly informed on the progress of the project. Ministry of Climate and Green Growth is the client for the project its representative in the guidance group is the main point of contact for this project. The entire KEM panel are also informed on the progress during the project at a lower frequency than the guidance group. Next to the client, the Ministry of Climate and Green Growth, the KEM panel plays an important role in monitoring the overall scientific quality and relevance of the outcomes of this project to the KEM programme.

1.6 Existing studies and research programmes

Mainly triggered by concerns and damage following the induced seismicity in the Groningen field, several research programmes have been initiated by public and private (NAM) funding agencies. Because the outcomes of the different programmes are relevant to this project we summarise the main components below.

1.6.1 KEM studies

The Dutch Minister of Economic Affairs initiated the Knowledge Programme on Effects of Mining (KEM) to address recommendations from the Dutch Research Council for Safety. KEM aims to accelerate knowledge development on mining effects and risks, promote multidisciplinary collaboration, and create independent tools for assessment. The program includes a research framework, agenda, projects, knowledge exchange platforms, and a scientific expert panel to ensure quality and independence.

About 25 KEM research projects have been (partially) carried out up till now. Together, they cover a wide range of topics related to mining effects, mainly to hydrocarbon extraction, geothermal energy recovery and salt solution mining. Most relevant to this KEM-48 project are projects covering topics on induced seismicity caused by gas storage and gas extraction in small gas fields, as well as projects covering subsidence, and leakage. These projects are listed below:

KEM-01: Geomechanical factors determining fault criticality during pressure cycling of underground gas storage in reservoirs. The objective of this study was to re-assess the basic geomechanical causes of seismicity, specific risk factors, and safe operational bandwidths for reservoir storage conditions, that have not been addressed in previous studies. (*completed*)

KEM-07: Geomechanical analysis for investigating the occurrence of induced seismicity in small gas fields in the Netherlands. The objective of this research question was to explore the feasibilities of a physics based, numerical (geomechanical) analysis of the causes of induced seismicity in the small gas fields in The Netherlands. (*completed*)

KEM-16: Part toolbox subsidence. The objective was to research in several pilots how current Dutch subsidence hazard models can be integrated and improved to become a high-quality generic tool for onshore subsidence hazard analysis; and later be extended to a full subsidence hazard and risk instrument (*finished*). Another aspect of KEM-16 was its research on indirect effects of deep subsidence. (*on-going*).

KEM-17: Over-pressured salt solution mining caverns and possible leakage mechanisms. The specific goals for this KEM project were to improve knowledge on the processes that occur when brine pressure in the cavern (locally) exceeds the minimum stress in the cavern roof or wall. Currently two end-member processes and an intermediate process are described in the literature and discussed during conferences: permeation, hydraulic fracturing, and preferential fingering. (*completed*)

KEM-19: Long term fluid migration, leakage risks and monitoring strategies. The specific objective of this research was to define the regional hazard and risk assessment method and practices, considering post abandonment vertical and horizontal pressure (re-)distribution and migration of fluids (gases and formation water) through aquifers, faults, and existing abandoned wells (*completed*)

In this context we will consider findings from recent geomechanical studies indicating that the stabilizing effect of depletion tends to dominate over poro-elastic stress load. Consequently, earthquake activity might occur predominantly on fault sections, which are not hydraulically connected to a depleting reservoir, e.g., in the over-burden (Smith et al., 2022; Baisch et al., 2023).

KEM-39: Geomechanical and geochemical factors determining fault criticality during pressure (non) cycling of underground CO2, H2, N2 storage. The objective of the research question is to re-assess the causes of seismicity, specific risk factors including chemical processes in the reservoir, and safe operational bandwidths for reservoir storage conditions during pressure (non) cycling of underground storage of CO2, H2, and N2 in depleted gas fields. (*completed*)

1.6.2 DeepNL research – funded by NWO, NAM and RVO

The aim of DeepNL (DeepNL, 2024) is to contribute to a better understanding of how the deep subsurface behaves under the influence of human interventions. In addition, the programme also aims to strengthen the research community in the Netherlands around this theme and to increase the coherency within the field. DeepNL research programme defines three clusters: (from: DeepNL Annual report 2022):

Cluster 1: Analysis of processes and conditions that lead to seismicity and subsidence. Can we understand and model how the processes at depth are translated through the subsurface to an effect at the Earth's surface? Status: 3 research projects – *on-going*.

Cluster 2: Analysis of processes and conditions that lead to seismicity and subsidence. Can we understand and model the conditions and processes in the deep subsurface that can ultimately lead to earthquakes and subsidence? Status: 5 research projects – *on-going*

Cluster 3: Monitoring of conditions and forecasting. How can we monitor the subsurface conditions that could lead to earthquakes, and can we forecast the occurrence of earthquakes? Status: 10 Research projects – *on-going*.

In all these 3 research clusters there are aspects that can be useful for this KEM project. In our literature study we checked first the publications and presentations from DeepNL. Since TU Delft is strongly involved in DeepNL andour advisory group, TU Delft quickly guided us to the most relevant studies.

The project "Monitoring and Modelling the Groningen Subsurface based on integrated Geodesy and Geophysics: improving the space-time dimension", with PI Ramon Hanssen and co-PI Femke Vossepoel (both in the advisory group) investigates how to optimally integrate improved observational and modelling methods to understand shallow and deep causes of subsidence using satellite and in-situ observations and data assimilation.

The project "InFocus: An Integrated Approach to Estimating Fault Slip Occurrence" with PI Femke Vossepoel (member of advisory group) takes a physics-based, data-driven approach to better understand the causes of induced seismicity through data assimilation into advanced seismo-mechanical models.

Other DeepNL projects, in particular the projects Science4Steer (A scientific basis for production and reinjection strategies to minimize induced seismicity in Dutch gas fields) and SOFTTOP (Investigating heterogeneous soft topsoils for wave propagation, cyclic degradation and liquefaction potential) are also relevant for this study.

1.6.3 IMG-funded research

Ground movement due to gas extraction in the Groningen field and the gas storage facilities in Norg and Grijpskerk has impacted many residents of Groningen and Drenthe. This has eroded the residents' trust in the NAM and the government. Therefore, since July 1, 2020, the Mining Damage Institute Groningen (IMG) has been established (incorporating the *Tijdelijke Commissie Mijnbouwschade Groningen*, TCMG). It serves as an independent governmental body to handle all damages caused by earthquakes, subsidence, and ground heave (IMG, 2023). Below are the relevant research projects that are on-going:

GEMMA: Gecombineerde Effecten van Meervoudige Mijnbouw Activiteiten (Combined Effects of Multiple Mining Activities). This research was initiated, formulated, and guided by a panel consisting of IMG experts and Committee Mining damage (CM) members, including external experts.

IEDB: Indirecte Effecten van Diepe Bodemdaling (Indirect Effects of Deep Subsidence). This research was initiated and funded by IMG and focusses on the groundwater level changes caused by deep subsidence and its impact on consolidation, peat oxidation and swelling and shrinking of clays.

1.6.4 Ministerial/SodM funded studies.

- Study of effects of shale gas (W+B, Fugro, Arcadis) (Witteveen+Bos, 2013)
- Lagging effects of coal mining in The Netherlands (IHS, W+B) (IHS, 2016)

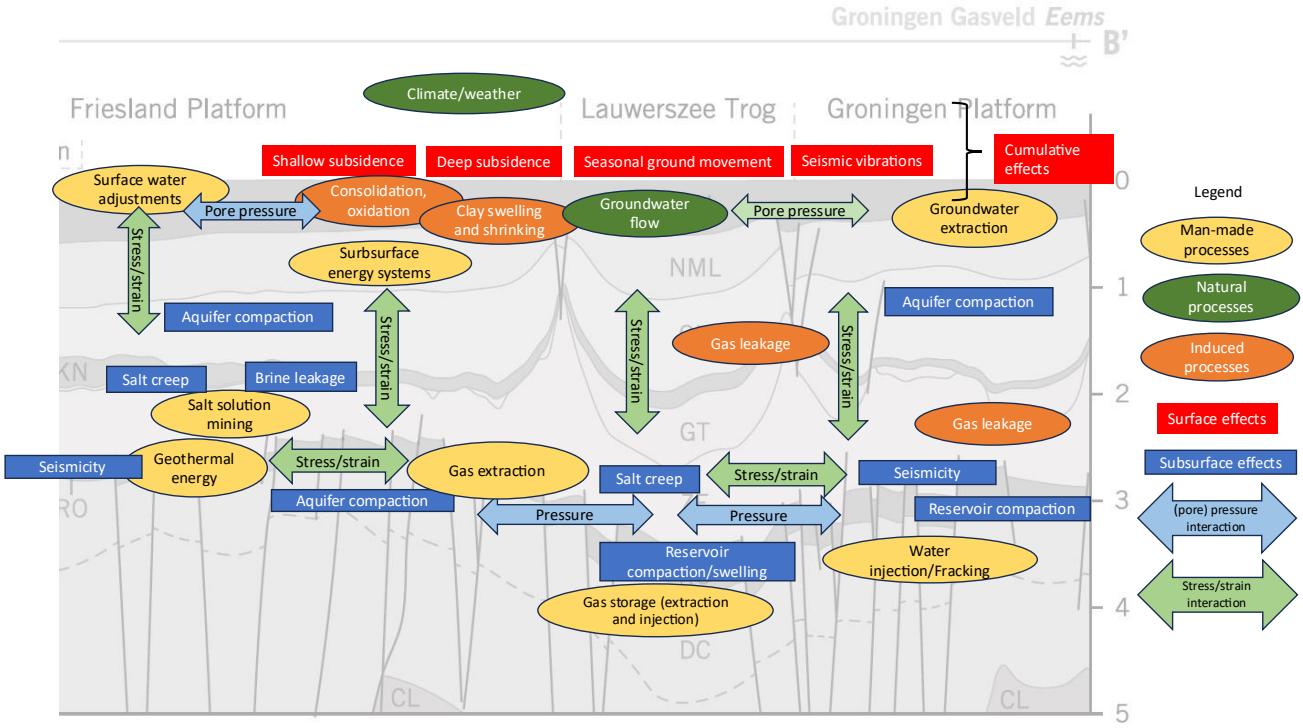

*Salt solution mining and geothermal energy utilisation is not present near Grijpskerk, but forms part of the scope for the general review in Phase I.

Figure 2. Schematisation of the possible processes, interactions, and effects at play in the shallow and deep subsurface in the North of The Netherlands and partly in the Grijpskerk area.

PART 1: LITERATURE STUDY

2

SUBSIDENCE

2.1 Summary and conclusions

This chapter gives an answer to the following research question as defined in section 1.4.1

1. What information is available about interactions between different adjacent underground (man-made) activities, natural processes, and about the cumulative mutual effect? This chapter covers the answer in the context of topic **a) subsidence**

Subsidence at the earth surface is the sum of different processes in the subsurface. In this chapter we identify various processes that take place at different depths, different rates and magnitudes that eventually result in a measurable subsidence at surface level.

Natural subsidence in the Netherlands is driven by long-term processes like natural compaction, postglacial isostasy, and tectonics, resulting in regional lithospheric tilting and gradual subsidence at rates less than 1 mm per year in the northern part of the Netherlands. Anthropogenic subsidence is categorized into shallow, intermediate, and deep mechanisms. Shallow subsidence arises from peat oxidation plus clay and peat compaction due to lowered groundwater tables. Intermediate subsidence, at 20 to 200 meters, results from groundwater extraction. Deep subsidence involves gas, oil, and salt extraction causing direct and indirect effect at the surface.

Factors contributing to shallow subsidence include geotechnical response (compaction, consolidation, and creep), and for example, long term effects of cyclic loading paths. Different compaction models like Koppejan's and isotache models are discussed in this chapter, along with the impact of low-frequency noise. Peat compaction and oxidation, clay compaction, swelling and shrinking, and hydrogeological factors are explained, emphasizing their significance. Subsidence from groundwater extraction globally, especially in coastal areas, is highlighted. In the Netherlands, large-scale new or increased groundwater extraction may cause subsidence, requiring Environmental Impact Assessments. The rise of Aquifer Thermal Energy Storage (ATES) and High/Medium ATES systems are discussed, with emphasis on potential subsidence differences affecting building and infrastructure. The amount of subsidence caused by extraction of natural gas, depends on factors like pressure drop and reservoir characteristics. Mining of salt by dissolving it, as practised in the Netherlands, leads to subsidence with both gradual and possibly sudden effects in case of cavern roof collapse, which have to be managed by Good Salt Mining Practice. Table 2 (section 2.9) gives an overview of subsidence values based on various references, distinguishing between natural and anthropogenic causes.

Subsidence can be modelled for different scenarios. Gas extraction involves approximations using poroelasticity, Geertsma's (1973) model and its modifications. Compaction coefficient limitations and nonlinear behaviour lead to differences in approaches and therefore differences between subsidence models. Salt solution mining induces subsidence through creep and gradual cavern closure, which is approached by employing semi-analytical and numerical methods. Gas storage in reservoirs considers

elastic deformation. Shallow subsidence estimation uses geotechnical models, addressing spatial variabilities. Groundwater extraction is modelled conventionally and with recent trends in data assimilation for large-scale predictions.

Monitoring of deep subsidence is done traditionally using geodetic measurements. Advancements in technology, such as InSAR, GPS and LiDAR, provide semi-continuous large-scale monitoring. These new technologies add much more detailed information in space and time but need to be interpreted cautiously and need to be used complementary to the conventional methods.

In the northern part of The Netherlands these are the maximum subsidence rates that can be expected

- Natural subsidence: <1 mm/year
- Shallow anthropogenic subsidence: 12 mm/year
- Deep anthropogenic subsidence:
  - Gas extraction: 6 mm/year
  - Gas storage: 20 mm/year
  - Salt mining: 14 mm/year

Intermediate subsidence due to groundwater extraction is considered negligible compared to the other sources of subsidence. However, in other countries, especially in densely populated cities, groundwater extraction is often a major contributor to subsidence.

2.2 Samenvatting en conclusies (NL)

Dit hoofdstuk geeft antwoord op de volgende onderzoeksvraag zoals gedefinieerd in sectie 1.4.1:

1. Welke informatie is beschikbaar over interacties tussen verschillende aangrenzende ondergrondse (door de mens gemaakte) activiteiten, natuurlijke processen, en over het cumulatieve wederzijdse effect? Dit hoofdstuk behandelt het antwoord in de context van het onderwerp **a) bodemdaling**

Bodemdaling aan het aardoppervlak is de som van verschillende processen in de ondergrond. In dit hoofdstuk identificeren we verschillende processen die plaatsvinden op verschillende dieptes, met verschillende snelheden en groottes, die uiteindelijk resulteren in meetbare bodemdaling aan het maaiveld.

De natuurlijke bodemdaling in Nederland wordt veroorzaakt door langetermijnprocessen zoals natuurlijke inklinking, postglaciale isostasie en tektoniek, resulterend in regionale lithosferische kanteling en geleidelijke bodemdaling van maximaal 1 mm per jaar in het noordelijke deel van Nederland. Antropogene-, door mensen veroorzaakte bodemdaling wordt onderverdeeld in ondiepe, tussenliggende en diepe mechanismen. Ondiepe antropogene bodemdaling ontstaat vaak door oxidatie van veen en zettingen in klei en veen als gevolg van veranderende grondwaterstanden. Tussenliggende bodemdaling, op 20 tot 200 meter diepte, is het gevolg van grondwaterwinning. Diepe bodemdaling omvat gas-, olie- en zoutwinning, met directe en indirecte effecten aan het oppervlak.

Factoren die bijdragen aan ondiepe bodemdaling zijn geotechnische effecten (zettingen, consolidatie en kruip) en bijvoorbeeld lange-termijn effecten van cyclische belasting. Verschillende inklinkingsmodellen zoals die van Koppejan en isotache-modellen worden besproken, samen met de impact van laagfrequent geluid. Zettingen en oxidatie van veen, zettingen in klei, zwel- en krimp van klei, en hydrogeologische factoren worden uitgelegd, waarbij hun belang wordt benadrukt. Bodemdaling door grondwaterwinning wereldwijd, vooral in kustgebieden, wordt belicht. In Nederland kan nieuwe en toenemende grondwaterwinning bodemdaling veroorzaken, wat een milieueffect rapportage (MER) vereist. De opkomst van Aquifer Thermal Energy Storage (ATES) en High/Medium ATES-systemen wordt besproken, met nadruk op mogelijke verschillen in bodemdaling. Diepe bodemdaling door gaswinning hangt af van factoren zoals drukverlaging en

reservoirkenmerken. Zoutwinning in Nederland leidt ook tot diepe bodemdaling met geleidelijke en mogelijk plotselinge effecten door het bezwijken van het dak van een caverne. In Tabel 2 (paragraaf 2.9) is een overzicht gegeven van orde-grootte bodemdalingswaarden, snelheden en invloedsbereik op basis van verschillende bronnen, onderscheid makend tussen natuurlijke en antropogene oorzaken.

Bodemdaling kan worden gemodelleerd voor verschillende scenario's. Gaswinning omvat een benadering van bodemdaling met behulp van poro-elasticiteit, modelaanpassingen van Geertsma's (1973) oorspronkelijke model en modificaties hierop. Onzekerheden over de compactie coëfficiënt en niet-lineair gedrag leiden tot de belangrijkste variaties in bodemdalingmodellen. Bodemdaling door zoutwinning ontstaat door kruip en krimp van de cavernes, waarvoor semi-analytische en Eindige Element Modellering worden toegepast. Opslag van gas in reservoirs houdt rekening met elastische vervorming. Schatting van ondiepe bodemdaling maakt gebruik van geotechnische modellen, waarbij de ruimtelijke variabiliteit bepalend is. Bodemdaling door grondwaterwinning wordt op een traditionele manier gemodelleerd en met recente ontwikkelingen in data-assimilatie kan dit ook worden toegepast op grote gebieden.

Monitoring van diepe bodemdaling gebeurt traditioneel met geodetische metingen. Vooruitgang in technologie, zoals InSAR, GPS en LiDAR, biedt kansen voor semi-continue grootschalige monitoring. Deze nieuwe technieken leveren veel aanvullende informatie in ruimte en tijd, maar de interpretatie moet zorgvuldig gebeuren en in aanvulling op de traditionele geodetische metingen.

In het noordelijk deel van Nederland zijn dit de maximale bodemdalingssnelheden die verwacht kunnen worden:

- Natuurlijke bodemdaling: < 1 mm/jaar
- Ondiepe (antropogene) bodemdaling: 12 mm/jaar
- Diepe antropogene bodemdaling:
  - Gaswinning: 6 mm/jaar
  - Gasopslag: 20 mm/jaar
  - Zoutwinning: 14 mm/jaar

Bodemdaling door grondwaterwinning wordt hier als verwaarloosbaar beschouwd in vergelijking met de andere mechanismen. In andere landen, met name in dichtbevolkte steden, is grondwaterwinning echter vaak de belangrijkste oorzaak van bodemdaling.

2.3 Introduction

Subsidence is a phenomenon marked by settling or sinking of the Earth's surface. It can occur due to various natural and human-induced (anthropogenic) causes. Subsidence is usually a combined manifestation of different mechanisms, of which some mechanisms are locally more dominant than others.

In this project, we also consider ground heave, which is associated with underground gas storage facilities, were seasonal injection and extraction of gas leads to alternating and seasonal heave and subsidence. This seasonal (cyclic) subsidence is different from the long-term on-going subsidence that is irreversible.

Seasonal swelling and shrinking of clays due to changes in groundwater level can also lead to alternating ground heave and subsidence. In the south of the Netherlands in the former coal mining area, there is regional ground heave due to an increase in groundwater level. Since our focus is on the northern Netherlands, however, the ground heave such as in Limburg is outside the scope of this project. The general trend in the Northern part of the Netherlands is towards subsidence and not ground heave. Therefore, throughout the report we will use the term subsidence mostly to describe ground movement, unless ground heave is the dominating phenomenon.

This chapter provides an overview of the different mechanisms that can act in the subsurface in the Northern part of the Netherlands that can lead to subsidence and ground heave. This chapter focuses on the interaction between drivers of subsidence and interacting with other phenomena and processes in the subsurface.

We make a distinction between natural and anthropogenic causes and between deep, intermediate, and shallow subsidence. The overlap in the terminologies is addressed by the clarification in Table 1.

Table 1. Classification of different subsidence or heave mechanisms.

Depths	Mechanism	
	Anthropogenic (man-made)	**Natural**
Shallow subsidence (Holocene) 0-20 m depth **Most effects in first 2-3 m.**	- Compaction clay and peat (2.6.1) * - Oxidation of peat (2.6.3) - Swelling and shrinking of clay (2.6.4) cause: active c water table changes caused by water management, or drainage (in top 2 to 3 meters below surface)	- Compaction clay and peat (2.6.1) - Oxidation of peat (2.6.3) - Swelling and shrinking of clay (2.6.4) cause: phreatic water level change by climate, seasonal or land use change
Intermediate subsidence (Pleistocene-Paleocene) 20-500/1000m	- Groundwater extraction (2.7.1) - Groundwater extraction and injection for subsurface energy systems (2.7.2) Depth range: 20-200 meters	- Compaction (sediments) (2.4.1) Depth range 20-500/1000 meters
Deep subsidence (Cretaceous and older) 500/1000m and deeper	- Gas/oil extraction (2.8.1) - Gas storage (see 2.8.1) - Salt solution mining (2.8.2)	- Postglacial isostacy (2.4.2) - Tectonics (2.4.3)

* Referral to the sections in this chapter where this mechanism is explained in further detail.

This chapter also describes in general terms the effects ground movement can have on infrastructure, buildings, and the environment. It further addresses the available techniques to model and monitor ground movement. The challenge in understanding ground movement is to disentangle the mechanisms at play in the subsurface and subsequently to point out the dominating cause or combination of causes of occurring subsidence or heave; this challenge varies between geographic areas.

Chapter 6 analyses the influence of mechanisms on each other and the area affected by individual mechanisms, forming the basis for the disentanglement.

2.4 Natural subsidence

Natural subsidence encompasses long-term movements, with three significant contributors that operate over millennia: natural compaction, postglacial isostasy, and tectonics (Kooi et al., 1998). When assessing surface movements, the combined effects of these contributors become evident. In the Netherlands, 20th-century measurements of vertical land movement indicate a regional gradual tilting of the lithosphere, occurring in a NNW–SSW direction (Figure 3). Figure 4 illustrates the disentanglement of long-term surface movement into the three constituents since the Quaternary, (Kooi et al., 1998). In the Northern part of The Netherlands, a gradual, natural subsidence with anticipated velocity of less than 1 mm per year (Kiden et al., 2002) has been estimated to persist to the present day.

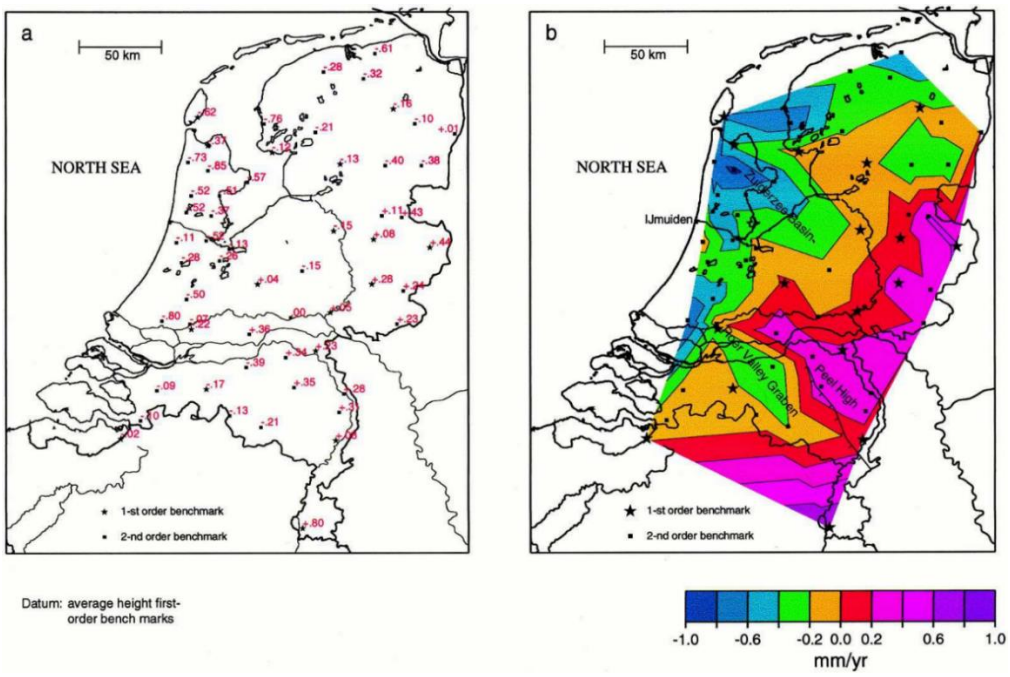

* (a) Inferred rates of individual benchmarks. (b) Contour map of inferred rates. Minus sign denotes subsidence. Standard deviations vary between 0.1 and 0.3 mm/yr. (From: Kooi et al., 1998).

Figure 3. Regional vertical land movement (mm/yr) of the top of the Pleistocene in the Netherlands obtained by least-squares kinematic adjustment of first- and second-order underground benchmarks.

2.4.1 Natural compaction

Geographically situated at the southeast of the North Sea basin and at the estuaries of major rivers, the Netherlands has accumulated sedimentary deposits since the Paleocene (65 Ma), leading to natural compaction of lower-lying strata. Natural compaction or auto-compaction is a mechanical process occurring caused by continued natural loading by ongoing sedimentation, in which younger deposits settle on older deposits. In deeper, less permeable clay deposits, the increasing weight of these younger deposits squeezes out pore water, leading to increasing effective stresses (σ') causing compaction in deeper soil layers, resulting in a subsidence that is observable at the ground level. This phenomenon occurs at considerable depths, typically exceeding 300 meters according to Van Asselen et al. (2020). The rate of natural compaction in deltas typically ranges between 0.7 and 2.2 mm/yr and is naturally compensated for by a continuous sedimentation supply (Nicholls et al., 2021; Syvitski, 2008). The compaction is caused by sedimentation, and the compaction itself causes sedimentation in turn. So, this is a feed-back loop. Even when the sediment supply is reduced or even halted because of human constructions such as flood defences like dikes and upstream dams, the delta is out of balance and will still subside at a rate similar to that of natural compaction (Ericson et al., 2006; Syvitski et al., 2009; Tessler et al., 2018). Erosion has the opposite effect, but it does not occur in the northern part of the Netherlands.

2.4.2 Postglacial isostacy

Postglacial isostasy denotes the surface response ensuing from the diminishing load resulting from the melting of land ice. In the Netherlands, the impact of glacial melting in Scandinavia and Scotland has gradually diminished over the past 10,000 years (Lambeck & Chappell, 2001; Kiden et al., 2002; Peltier et al., 2002).

The deep mechanism that is also a cause of subsidence is isostatic rebound of the Earth's crust, which is the result of the gradual retreat of glaciers covering the northern parts of Europe and Scandinavia. The retreat started between 20,000 and lasted until 12,000 years ago, which was the start of the

current warmer period, the Holocene. Until today, the Scandinavian shield is undergoing an isostatic upward rebound. The rebound hinges in the deep crust north of the Netherlands and as a result the Netherlands still undergoes regional subsidence (less than 1 mm per year).

2.4.3 Tectonics

Tectonics predominantly influence the Roerdal graben rift system in the southern part of the country (Van Wees et al., 2014). The process was exemplified by the Mw = 5.8 earthquake in Roermond on April 13, 1992 (Van Eck & Davenport, 1994). However, tectonic seismicity and associated tectonic movement are not relevant in the northern part of The Netherlands (section 7.8.2 and Figure 42). These effects do neither occur as a signal in our current geodetic data nor in the InSAR data. To detect tectonic movement, six permanent gravity measurement stations are operating spread over the Netherlands (Reudink and Klees, 20017). These instruments are best suited to detect very small but large-scale movements.

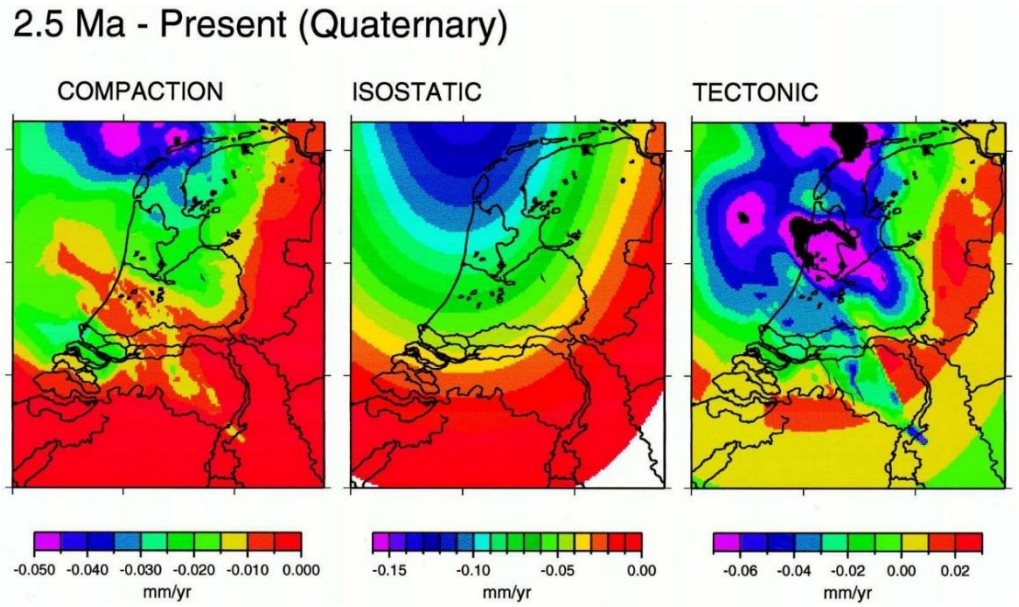

Figure 4. Separation of compaction, isostatic and tectonic contributions to vertical land movement for Quaternary (2.5 Ma–Present) constructed by 3-dimensional back stripping of Cenozoic stratigraphy of the Netherlands and the southern North Sea basin (From: Kooi et al., 1998)

2.5 Anthropogenic causes of subsidence

For the anthropogenic causes of subsidence, it is also important to introduce a division into different mechanisms that act at different depths. First, however, one needs to provide definitions of shallow, intermediate, and deep subsidence. Throughout this report this definition is used to differentiate between mechanisms, depths and causes behind the shallow and deep subsidence.

2.5.1 Shallow subsidence

Shallow subsidence in the Netherlands we define here as the sinking of the ground surface due to compaction of mainly unconsolidated (Holocene) clay and peat layers down to a depth of **20 m**. The compaction is usually caused by lowering of the water table, causing a decrease in pore pressure and an increase in effective stress. This results in consolidation or compaction of these soft layers, i.e. in shallow subsidence. Since the water tables variations usually takes place in the first 2-3 m meters below the surface (especially in the northern part of The Netherlands) the effects take also place in the upper 2-3 meter. The shallow subsidence is usually irreversible, which means that the soil layers

will not rebound to its original volume when the water table returns to its previous higher (section 2.6.1). Lowering of the subsurface water table, also exposes peat layers to oxygen. Peat oxidation sets in, meaning that the organic components of the soil gradually disappear. This also leads to shallow subsidence (section 2.6.3). Holocene sand layers are usually not sensitive to consolidation. However, loosely packed sand layers can settle if subjected to a lowered water table or vibrations such as those occurring to traffic or earthquakes (section 2.6.2). The shallow subsidence can be human-induced or natural. Some types of clay exhibit also swelling and shrinking under varying water content induced by shallow ground water level changes or changes in land use. Swelling and shrinking of clay takes place at shallow depths, around the varying water table. This is explained further in Section 2.6.4.

2.5.2 Intermediate subsidence

Intermediate subsidence refers to ground surface settling resulting from extracting groundwater from aquifers at depths ranging from **20 to 200** meters. These aquifers include both shallow (Pleistocene-aged) sand layers and deeper Miocene-aged layers. Intermediate subsidence due to groundwater extraction is further discussed in section 2.7.1.

The subsurface plays a crucial role in the energy transition, serving both for energy storage and production. However, subsurface utilization carries environmental risks. Generally, when deployed at depths of less than 200 m, energy storage systems involving groundwater circulation result in smaller, more localized subsidence when compared to processes at greater depths like natural gas extraction, which may also extract associated fluids. As subsurface usage increases, cumulative effects emerge, including those related to subsurface energy storage systems. This is discussed further in section 2.7.2.

Natural compaction, or auto-compaction, is a natural mechanical process driven by sedimentation. Younger deposits settling on older ones, especially in deep, less permeable clay, increase effective stresses, causing compaction and observable subsidence (section 2.4.1).

2.5.3 Deep subsidence

Deep subsidence is defined here as the settling of the ground surface due to extraction of gas, fluids, or material from the ‘deeper subsurface’. ‘Deeper subsurface’ in the northern part of the Netherlands means dealing with geological formations older than the intermediate sediments (Cretaceous age and older). Mining takes place at depths larger than **500 m**. The Netherlands’ mining law is also applicable from depths larger than 500 m.

In the northern part of the Netherlands deep subsidence is mainly associated with natural gas extraction and salt solution salt mining and to a smaller degree to oil- and groundwater extraction. In this definition deep subsidence is thus a mainly a human-induced phenomenon. Onshore oil and natural gas extraction occurs usually from reservoirs at depths between 500 and 4000 m; salt solution mining from 700 to 3000 m. The mechanisms behind deep (anthropogenic) subsidence are further explained in Section 2.7. The largest and more pronounced deep subsidence takes place around the salt solution mining operations near Veendam and Harlingen. Natural gas extraction from the Groningen field has a less prominent effect compared to salt solution mining. However, owing to the extensive geographic dimensions of the Groningen field and the associated large extent of its subsidence bowl, it has a broader impact area and intersects with the subsidence bowls of both salt solution mining and smaller natural gas fields.

2.6 **Shallow subsidence**

2.6.1 Compaction of clay and peat

The terminology for compaction varies greatly between different branches of science. In the geotechnical literature compaction is often referred to as settlement.

Subsurface compaction results from an increase in effective stress within the soil, either due to an increase in surface loading (due to an embankment or foundation) or a decrease in groundwater levels. Terzaghi (1925) realised that the total stress (σ) in the subsurface is the sum of effective stress (σ') and pore pressure (u):

$\sigma = \sigma' + u$ (see also Figure 5)

Due to a surface load, total stress will increase when the water between the pores cannot escape. This is the case in fine grained soils (clay) and in layers with hydraulic resistance against vertical flow. The moment the pore pressure dissipates (drains), it results locally in a lower pore pressure and therefore an increasing in effective stress and thus compaction.

Conversely, lowering the groundwater head maintains total stress in the soil but reduces pore pressure, resulting in increased effective stresses. Compaction is a time-dependent process and consists of primary compaction during the consolidation period, and secondary compaction known as creep. The compaction is only time-dependent if the water cannot escape, i.e. in clay layers.

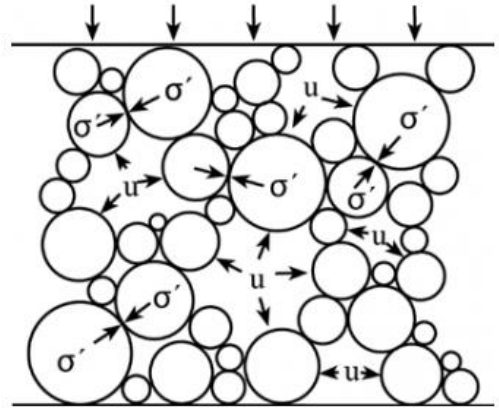

Figure 5. Total stress as a sum of the effective stress (σ') and pore pressure (u). (Source: Van Asselen et al., 2020)

Consolidation

Consolidation refers to the process where soil particles are rearranged, because of water moving out of the soil voids. The consolidation period, sometimes referred to as the hydrodynamic period, is defined as the period required for the pore pressure (and therefore the effective stress) to reach an equilibrium, i.e. no more water is driven out of the soil voids. Consequently, the consolidation period depends greatly on the soil permeability. Permeable soils like sand and gravel undergo primary compaction, which is virtually immediate, compared to less permeable types such as silt, clay, and peat. Beyond permeability, the propagation of pore pressure variations within a soil layer relies on the duration and magnitude of these variations. Hydrodynamically, it is established that high-amplitude, high-frequency pore pressure signals attenuate more swiftly in a soil layer than low-amplitude, low-frequency signals (Hanckmann et al., 2022).

An important aspect of compaction lies in its path dependency. In the past, higher than the current effective stresses may have prevailed in the soil, for instance due to a pre-load due to the presence of glaciers in the Saale ice age (as in the centre of Groningen city) or a lower groundwater level. But also ageing or leaching can play a role (Bjerrum, 1967). Higher effective stresses experienced by a soil in the past, i.e. pre-consolidation stresses, cause soils to behave stiffer to effective stress changes below the pre-consolidation stress, and their compression to remain elastic and, therefore, reversible.

Creep

Upon completion of the consolidation period where primary compaction has taken place and effective stress has reached equilibrium, compaction does not cease. Instead, secondary compaction, known as

creep, starts to become dominant. One of the primary mechanisms driving creep is the breakdown of interparticle bonds like van der Waals forces. These bonds can disintegrate under constant effective stress, leading to the rearrangement of soil particles and subsequent compaction (Mesri, 1973; Le et al., 2012; Bosmans, 2021). Creep predominantly manifests in peat and clay soils, often causing significant residual settlement in these soil types. Additionally, the presence of humic substances in clay plays a crucial role, as soils rich in humic content tend to be more susceptible to creep than non-humic soils.

In the Netherlands, the compaction model of Koppejan (Koppejan, 1948) is frequently employed, alongside more sophisticated models such as the a, b, c isotache model (Den Haan, 1992, 1994) or the NEN-Bjerrum model (Bjerrum, 1967). These compaction models include the effects of creep and are often integrated with consolidation models based on Terzaghi, or Darcy principles such as D-settlement where the reduction of the soil permeability due to compaction is accounted for (Visschedijk et al., 2016).

2.6.2 Compaction of sand by cyclic loading

Compaction due to cyclic loading is a special form of compaction based on Terzaghi principles and is commonly associated with granular materials like gravel or sand. In geotechnical engineering soil layers are often treated as homogeneous layers where it is assumed that the effective stress applied to the soil matrix is uniformly distributed. However, in practice the effective stress has preferential pathways on the grain size scale, leading to high contact stresses between some soil particles while others bear minimal loads (Youd, 1977). These preferential loads can change continuously over time under cyclic stress conditions driven by e.g. wind, wave, tidal and ice loads (Kim et al., 2015). In addition, vibrations, which represent a rapid cyclic loading process, can create fluctuating shear stresses within the soil matrix (Sawicki and Swidzinski, 1989; Negro et al., 2000).

When cyclic loading is applied, whether this is slow or rapid, the sand skeleton deforms to accommodate the changing effective stress conditions, resulting in continuous deformation of the soil matrix (see Figure 6). As a result, the soil matrix continuously adopts new packing configurations and potentially a new bulk density as long as the cyclic loading persists. However, as time progresses, grains tend to settle into more stable positions, leading to a reduced compaction potential. Therefore, the sensitivity of a soil matrix to cyclic loading largely depends on the initial packing conditions, often referred to as pre-shearing conditions, with loosely packed sands being the most susceptible. This phenomenon associated with rapid cycling is commonly known as liquefaction.

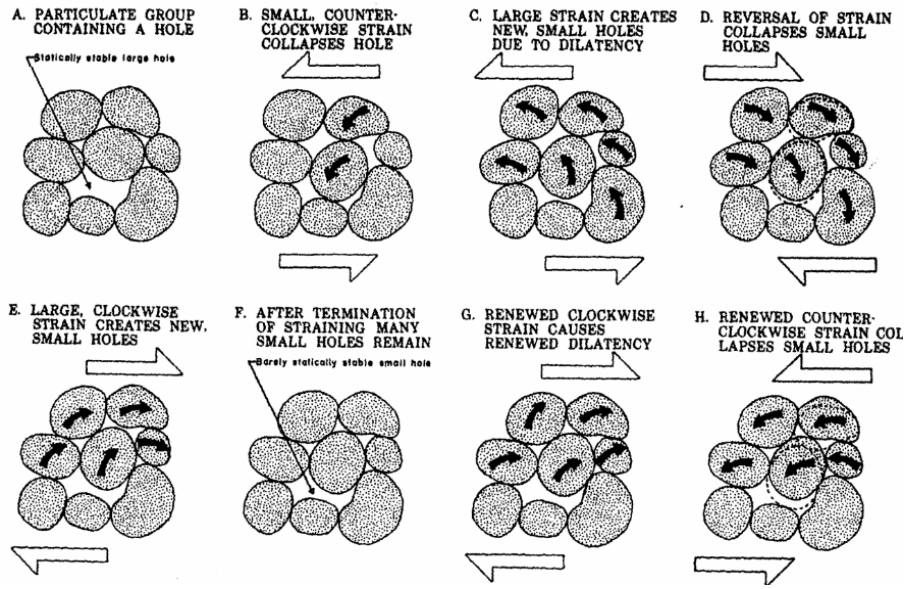

Figure 6. A schematic overview on the change in packing for a group of soil particles during cyclic loading (Source: Youd, 1977)

The impact of cyclic loading on the soil matrix diminishes with depth. This is a direct consequence of the increasing influence of normal stress by overburden of overlying soils, superseding the stress induced by cyclic loading. In case the soil matrix is saturated with water, the stress induced by cyclic loading results in increasing and decreasing pore pressures. If the (suddenly) induced stresses alternate rapidly (e.g. at rates between 1-10 Hz) or when the compaction of the granular material is large enough, excess pore pressure may not have the chance to flow away, leading to minimal changes in total volume. Consequently, the effective stresses exerting on the soil particles decreases, and in extreme cases, it may nearly vanish, causing the soil to behave as a viscous fluid (i.e. liquefaction) (Meijers, 2007).

Vibration induced cyclic loading

Vibration-induced damage on (infra)structures is a known issue in geotechnical engineering, arising from various sources such as traffic (Hanazato et al., 1991; Crispino and D'Apuzzo, 2001; Hunaidi, 2000; Auersch, 2005; Gupta et al., 2008), pile driving (Svinkin, 2008; Massarsch et al., 2015), and vibrational sheet piling installation (Athanasopoulos and Pelekis, 2000; Meijers, 2007). Figure 8 shows an overview of magnitude and affected area, based on expert knowledge.

In the Netherlands, the assessment and monitoring of vibrations are conducted based on the Dutch Vibration Guideline (SBR-A, 2017) where a distinction is made between direct vibrational damage on structures and indirect damage caused by differential compaction induced by vibrational cyclic loading. Predicted construction vibrations using e.g. the Dutch manual on sheet piling (CUR 166, 2012), and the Dutch manual for piling (organisation of Dutch Pile Manufacturers-PREPAL, 1992) can be assessed against the SBR-A threshold values. The threshold value for vibrational induced compaction is set at the acceleration amplitude of 1.0 m/s^2, which corresponds to an exceedance probability of 1% (see Figure 7). When this threshold is exceeded, the theoretical risk of building damage induced by differential compaction is more than 1%. The absolute compaction is then not determined. For traffic and demolition vibrations, no clear predictive models are available; these are typically measured and assessed in practice.

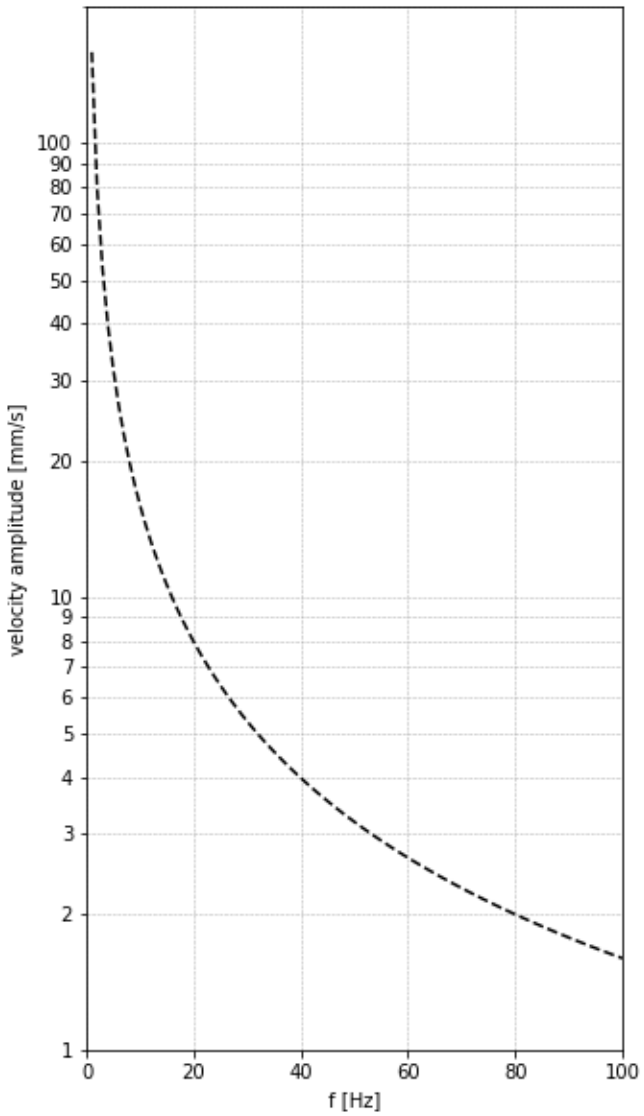

* The velocity amplitude (v) corresponds to the acceleration amplitude (a) of 1 m/s2 via the following formula: a = 2π*f*v. With f is the frequency (Hz).

Figure 7. The SBR A threshold value corresponding to an exceedance probability of 1% for damage by vibrational induced compaction (Source: SBR, 2017).

The absolute vibration induced compaction is approximated using the Hergarden model, which takes the following into account: the velocity, acceleration, amplitude, and frequency of the vibration (i.e. number of cyclic loads per unit time), and the relative density of the granular soil (Hergarden, 2000; Hergarden and Tol, 2001). The zone of influence is often predicted using the Barkan model for wave attenuation (Barkan, 1962). Although many combinations of the aforementioned factors exist, and the effect of wave refraction within the subsurface is poorly understood in terms of predictions, in practice, vibration induced compaction of granular soils typically ranges from millimetre to decimetre scale (Drabkin et al., 1996) with an area of influence up to a maximum of around 10 meters.

Low Frequency Noise

Besides the conventional construction vibration sources, there is a concern on the effect of Low Frequency Noise (LFN) emitted by for instance gas transport infrastructure (pipelines or pumps) and how it may induce cyclic loading. Also wind turbines, traffic, heavy machinery and heat-exchangers are sources of low frequency noise (LFG, 2024). Krylov (1995) showed that gas flow through pipelines can potentially generate LFN at amplitudes high enough to cause vibrations in the subsurface to be

noticeable by people, with the potential to lead to annoyance. However, they have never been able to confirm these findings in the field (Krylov, 1997). A recent study in The Netherlands showed that a spatial correlation exists between observed LFN and underground gas infrastructure (Van Vught, 2018; KEM-31 report).

In the context of cyclic loading, a foreign case study by Liu et al., (2020,2021) investigated the abnormal vibrations of pipelines at the Yongchang natural gas compressor station as a result of unstable operations of the compressor equipment. The study concluded that maximum amplitude velocities up to 2.9 mm/s were observed and modelled with frequency signatures between 4-62 Hz. However, numerical simulations indicated that amplitude velocities up to 117 mm/s were possible within the frequency range of 0-7.5 Hz, posing a risk to the pipeline transportation system. However, the latter example is an exceptional case, which is an above-ground situation at a compressor station. This allows for engineered measures and can be mitigated with appropriate design and construction, whereas low frequency noise from underground infrastructure is more difficult to mitigate.

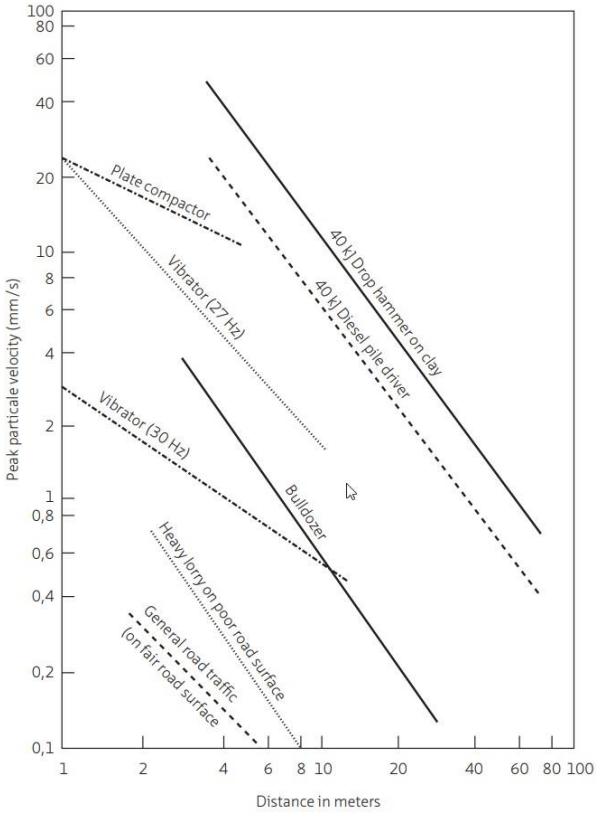

Figure 8. Indication of traffic and construction induced vibrations and their influence distances. (Source: COB F530)

Earthquake induced cyclic loading resulting in liquefaction

Earthquakes are known to induce compaction in both dry and saturated sandy soils in a process often referred to as densification or liquefaction (Tokimatsu & Seed, 1987; Seed & Idriss, 1971). Liquefaction occurring beneath buildings and other structures can cause major damage during earthquakes. It is generally believed that liquefaction can only be induced by earthquakes with a magnitude M 5.0 or higher (Ambraseys, 1988; Rodriguez et al., 1999). However, cases have been reported where liquefaction occurred in saturated unconsolidated sediments near the epicentre at magnitudes as low as M 4.5 (Holzer et al., 2010; DuRoss, 2011). In The Netherlands only a single case of an earthquake induced liquefaction event has been observed. This was during the 1992 Roermond earthquake with a magnitude of M 5.3 (Nieuwenhuis, 1994). It should be noted that the correlation between liquefaction and earthquake magnitude is purely an empirical correlation from sites across the globe

and does not include location-specific effects that may increase the acceleration (i.e. vibration level) at ground level (i.e. site and basin effects, Van Ginkel et al., 2022).

In the Netherlands, liquefaction as a result of induced seismicity has not been observed so far. A study by Deltares, (2016) showed that the subsurface in the northern Netherlands (prone to induced seismicity with recorded induced earthquakes of magnitudes up to M 3.6) contains large portions of loosely packed sands of tidal origin that is sensitive to liquefaction. In a later (KEM) study, an attempt was made to quantify the risk of liquefaction in relation to building damage. The results indicate the effect of liquefaction due to man induced earthquake is limited (KEM-14, 2021). This is why liquefaction is not part of the schematic depicted in Figure 2.

2.6.3 Oxidation of peat and/or organic clays

In a large part of the Grijpskerk area the shallow subsurface contain layers of peat and organic clays (see chapter 7).

Oxidation is an irreversible process that breaks down organic matter, commonly occurring when an organic-rich layer like peat is no longer fully saturated thus exposing it to oxygen. In general terms, the process results in the transformation of organic matter into carbon dioxide (CO_2), which escapes into the atmosphere.

Moreover, oxidation can occur even in water-saturated zones within the soil. In such cases, oxygen is acquired from oxidizers like dissolved oxygen, nitrate and sulphate, which are partly integrated into biomass. However, over the long term, decomposition driven by oxygen from air is the primary factor contributing to soil subsidence.

The rate of oxidation predominantly hinges on the availability of oxygen, particularly the amount that can penetrate from the atmosphere into the depth of the peat layer. Furthermore, the quantity and composition of organic matter in the soil profile significantly affect the rate of oxidation. This rate diminishes over time, as easily degradable components of the peat decompose first, leaving behind more oxidation resistant components. The process therefore only occurs in near-surface peat or organic soils.

To quantify peat oxidation and forecast its effects, Fokker et al. (2019) developed a straightforward analytical model. In this model, an organic-rich layer was conceptualized as a single stratum divided by the water table into wet and dry segments. The oxidation model proposed by Fokker et al. (2019) effectively captured observed subsidence in the Almere area, Netherlands (Verberne et al., 2023):

$$\Delta h_{ox} = (1 - e^{-V_{ox}\Delta t})(h(t) - h_{wet} - R_{ox}[h_0 - h_{wet}])$$

Here, Δh_{ox} represents the reduction in layer thickness due to oxidation, V_{ox} the oxidation rate, Δt the time step, $h(t)$ the organic layer thickness, h_0 the initial layer thickness, h_{wet} the saturated thickness, and R_{ox} the fraction of organic matter. A fraction of 0 implies a layer composed entirely of organic matter.

2.6.4 Swelling and shrinking of clay

The partial drying of clay layers and an increase in soil suction stresses can induce shrinkage. Layers like sand and gravel are not prone to this phenomenon. Not all clay minerals are equally susceptible to swelling and shrinking. Clay minerals that are particularly susceptible include montmorillonite, vermiculite, smectite, and bentonite. Smectite is a clay mineral that occurs in the marine clays in Groningen (Breeuwsma, 1985). Dehydration can be triggered by various factors, such as a drop in the water table, evaporation, and water absorption by vegetation and tree roots. Roots have the potential to desiccate the soil, leading to considerable shrinkage.

Clay layers undergoing partial drying experience soil compression, resulting in a decrease in volume (shrinkage) and the formation of cracks within the layers. Shrinkage can be divided into two components: irreversible and reversible shrinkage. Irreversible shrinkage occurs when the soil dries out completely and does not' rehydrate, marking the concluding stage of soil maturation (Barciela Rial, 2019; van Asselen et al., 2020). The reversible part, on the other hand, refers to the shrinkage that can be reversed when the soil regains moisture. When the soil becomes wet again, it expands to the same extent as the shrinkage induced by drought. Measured soil subsidence due to shrinkage ranges from several millimetres to centimetres and can even exceed 10cm (van Asselen et al., 2020).

An analytical model that accounts for the time-dependent nature of clay shrinkage was developed by Fokker et al. (2019) and effectively applied by Verberne et al. (2023). This model employs a methodology like the oxidation model discussed earlier in paragraph 2.6.3:

$$\Delta h_{sh} = (1 - e^{-V_{sh}\Delta t})(h(t) - h_{wet} - R_{sh}[h_0 - h_{sh}])$$

Here, Δh_{sh} represents the reduction in layer thickness due to shrinkage, V_{sh} the shrinkage rate, Δt the time step, $h(t)$ the clay thickness, h_0 the initial layer thickness, h_{wet} the saturated thickness, and h_{sh} the fraction of clay above the groundwater table that is still susceptible to shrinkage.

At many locations in the northern part of the Netherlands seasonal heave and subsidence in the order of ± 8 to ±12 mm can be observed in the InSAR data. This is a trend that can be seen at various locations, some less pronounced than others. The trend in heave and subsidence appears to be related to the dry series of summers between 2018 and 2022 (EGMS, 2024, KNMI, 2024). An example of a well pronounced seasonal subsidence and heave signal is given in Figure 9. The heave appears to be related to the winter period and the subsidence with the summer period. Only 2021 was not an extremely dry summer (KNMI, 2024), which is also reflected in the less pronounced 'dip' in the subsidence data. See Annex VIII for an overview of the annual drought data that shows the annual rainfall shortage caused by the dry summers of 2018, 2019, 2020 and 2022. Data from 2023 is missing, but that summer was notably wet.

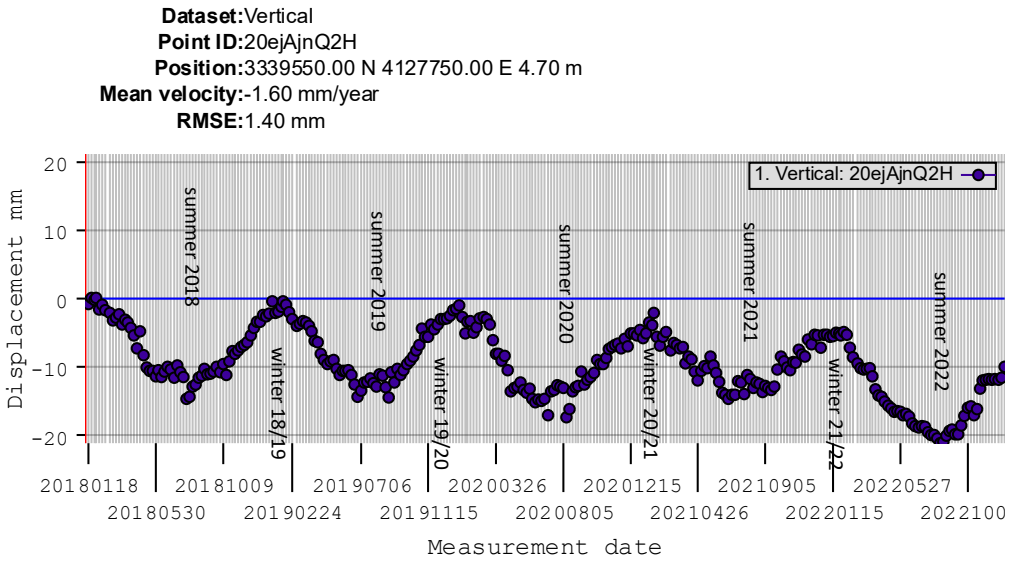

Figure 9. Example of a location in Eastern Groningen (Winschoten) where seasonal heave and subsidence in the order of ± 12 mm can be observed, which appears to be related to the dry series of summers between 2018 and 2022 (EGMS, 2024).

2.6.5 Hydrogeology

Although compaction can occur by a top load such as the placement of buildings or large infrastructure on the soil, the sections 2.6.1 to 2.6.4 describe that hydrogeology can be an important driver for

shallow subsidence. Fluctuations of the water table drives peat oxidation, shrinking/swelling of clays and can induce compaction related stress changes in the subsurface. In the following paragraphs, the effects of different hydrogeological processes are discussed.

Groundwater regime

As previously discussed in section 2.6.1, the sensitivity of a cohesive (clayey and peaty) soil for compaction strongly relies on its pre-consolidation stress. For example, in the Northern Netherlands shallow Holocene have not experienced pre-loading by glacial ice, so that their pre-consolidation stress is mainly determined by historical groundwater levels.

Ideally, understanding the historical trends of groundwater fluctuations helps to predict soil responses to new stresses. Yet, historic groundwater level fluctuations are typically not known. And so, a representative low value of the groundwater level has to be based on past measured groundwater levels. In The Netherlands, various methods are applied to base a representative low value from measured groundwater levels. For example, the 5th percentile of a groundwater level time series is sometimes used. An alternative is to determine a representative low value on an occurrence within a given time span (e.g. the value occurring once a year), or by means of some formal definition of representative values (WUR, 2024). Van Dalen et al. (2022) recommended that a representative groundwater series should be measured at least monthly for a minimum of three consecutive hydrological years (April 1st – March 31st).

Temporal drainage to serve activities

In the Netherlands, various subsurface activities like constructing or maintaining foundation structures, basements, pipelines, or cables often need localized drainage measures. These drainage measures are temporary, varying from a few days for pipeline/cable maintenance to several years for large infrastructure projects.

Temporal drainage activities result in local groundwater drawdowns ranging from decimetres to meters with a radius of influence extending from a few meters up to a few kilometres. Depending on the local geological conditions, the duration and depth of dewatering with respect to the natural groundwater conditions, resulting subsidence from these activities may attain up to a few decimetres (CRUX, expert knowledge). However, precautionary actions are often taken when subsidence is expected to exceed 15mm in the proximity of nearby properties (Geldof et al., 1998).

Water management

Worldwide demographic, economic, and technological trends have accelerated our ability to change the environment including the hydrological system, knowingly and unknowingly, by changing land use and human water consumption (Cosgrove and Loucks, 2015). The desire to feed the increasing human population has led to a major global extension and growth of irrigation practices, which in the year 2000, accounted for around 70% of the global freshwater withdrawal and about 90% of the total human water consumption (Döll et al., 2012). Especially irrigation has led in some areas to groundwater depletion when fed by groundwater at a rate exceeding the natural recharge (Taylor et al., 2011). Besides irrigation, land use has extended by means of land reclamation over the past decades (Wang et al., 2014; Martin-Anton et al., 2016; Sengupta et al., 2018), requiring active water management by lowering the water table to approximately a few decimetres below the ground surface inducing shallow subsidence. Depending on how land reclamation is executed, secondary effects can occur such as loss of surface water buffer area, the loss of unsaturated subsurface that used to absorb rainstorms and land erosion (Søndergaard and Jeppesen, 2007; He et al., 2014; Numbere and Camilo, 2017; Bhunia et al., 2021). These secondary effects change the capability of the land to hold water, and the response of the land to storm events, flooding and droughts

In the Netherlands the regional and local surface water levels are managed through a complex network of ditches, watercourses, weirs, and pumping stations that have been created over the course of

centuries (Hoeksema, 2007). The responsible governmental entities are the regional Water Boards or Water Authority's (NL: *Waterschappen*). Water Boards govern the water system within their area of jurisdiction through a democratic process that is designed to accommodate as many, sometimes conflicting, interests as possible. Examples of conflicting interests include the drainage of agricultural and urban areas versus the wetting and moistening of nature reserves. The latter serves as a buffer zone during dry periods or to mitigate issues like subsidence and peat oxidation (Erkens et al., 2016). At the end of this democratic process there is an agreement called "peilbesluit" that regulates the exact management of weirs and pumping stations in the area.

The "peilbesluit" determines what **water level** will be maintained in the water courses. However, for land use and soil subsidence, the drainage in the subsurface between the water courses is essential. Water levels in water courses differ from the **groundwater level** fluctuation, which vary due to precipitation, evapotranspiration, and seepage (Figure 10). Due to net evapotranspiration in dry periods, groundwater levels in fields may well fall below the level in the water courses. These fluctuations increase with distance from the nearest drain. As a result, land consolidation, a process where land is exchanged to obtain larger parcels (NL: *ruilverkaveling*), may result in a significant increase in groundwater fluctuations at the parcel centre. This effect is further elaborated upon in section 6.4.1.

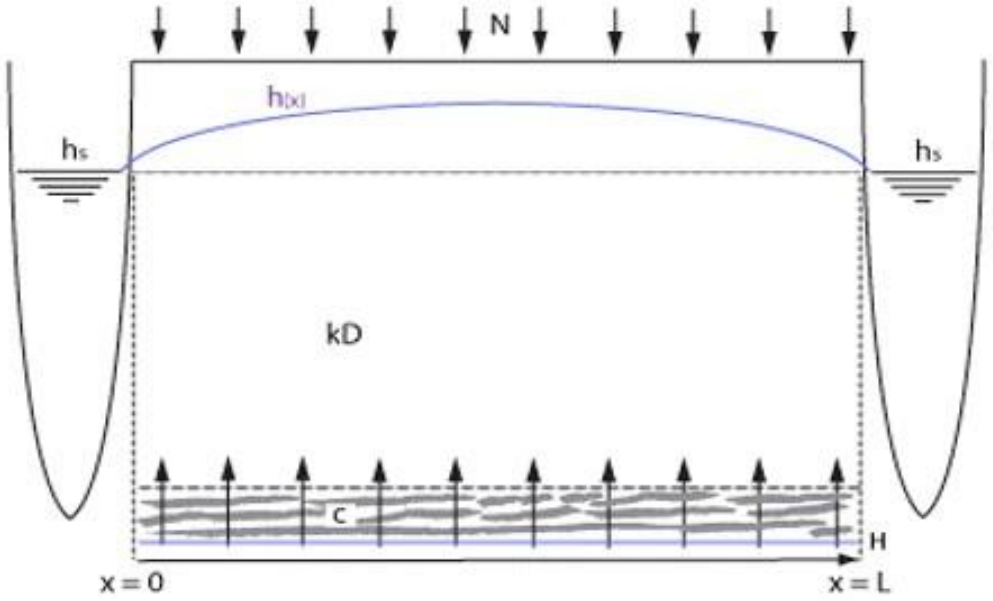

* The groundwater table h(x) depends on the net precipitation N (difference between precipitation and evapotranspiration), seepage from and towards underlying confined aquifers through an aquitard with hydraulic resistance c, the hydraulic transmissivity kD of the phreatic aquifer, the surface water level h_s, and the distance from the surface level.

Figure 10. An illustration of the processes affecting the groundwater table in between two waterways. (Source: From Grondwaterformules.nl based on Wesseling and Wesseling, 1984)

Climatological extremes

Climate and land use primarily determine the water exchange between the atmosphere and the earth surface, whereas the underlying soil and geology dictate the amount of water that can be transmitted and stored in the subsurface (Taylor et al., 2013a). The potential impact of climate change in the hydrological cycle is significant as water exchange between the atmosphere and the earth surface is estimated to be the equivalent of ~30% of the world's renewable freshwater resources (Döll, 2009). The net recharge, which is precipitation minus evapotranspiration, is strongly influenced by climate variability including climate extremes such as droughts and floods (Taylor et al., 2013b; Gurdak et al., 2011). The consensus among climate scientists is that climate change leads to a greater temporal variability in precipitation extremes (Allan and Soden, 2008; O'Gorman, 2015; Dai et al., 2018),

resulting in increasing fluctuations in the global groundwater system (Jasechko et al., 2024), and consequently resulting droughts and floods being more severe. In the context of subsidence, the increasing magnitude of groundwater fluctuations affects the susceptibility of the subsurface to shrinkage and swelling of clays, whereas the lower extremes induced by droughts are highly relevant in the context of permanent subsidence through compaction or peat oxidation.

In recent years the Netherlands have faced major drought events (2018-2020, 2022) and the expectation is that droughts will last longer and will be more severe (Bartholomeus et al., 2023). These mentioned droughts have temporarily led to a significant regression of the groundwater table in the order of decimetres throughout the country. Although water boards start to take measures to retain water in wet periods for use in dry periods, it is expected that our experience with weather and climate from the past no longer applies to the future. Hence the 5th percentile of a groundwater series, a benchmark for soil compaction analysis, may be subject to change.

Vegetation

Trees are known to cause significant local depressions in the groundwater table. Tree roots extract moisture from the soil, and if they grow in soils prone to shrinkage such as peat and clay, settlement can occur. In times of increased rainfall, like autumn, winter, and early spring, the soil tends to expand due to the influx of moisture. However, when roots draw moisture from the soil beneath the foundations of buildings or other structures, soil shrinkage can lead to subsidence and potential damage (Mercer et al., 2011). Particularly in prolonged dry periods, roots tend to absorb moisture from the surrounding soil, exacerbating the issue.

In the Netherlands, a 1995 report by the DLO-Staring Centrum (Bakker et al., 1995) investigated cracks and subsidence in rural roads near trees. Based on five cases, the report concludes that in poorly permeable soil, such as peat and heavy clay, the roots' absorption of moisture surpasses the groundwater flow to the roots. Consequently, the pore pressure near the tree experiences a significant local drop. This phenomenon exposes soil layers to increased shrinkage at greater depths, leading to localized subsidence. Within the radius equal to the height of the tree, an increase in subsidence of 5cm was observed (Bakker et al., 1995). The area of influence was typically marked by a deep, sometimes wide crack. Given the scope of this research, this is a local effect and not relevant to be considered. However, for specific building damage cases, it may very well be relevant.

2.7 Intermediate subsidence, anthropogenic cause

2.7.1 Subsidence due to groundwater extraction

Globally, the usage of surface water is impeded by increasing pollution, salinization, and climate change effects such as flooding and storm surges. In search for alternatives, groundwater at intermediate depths has become an increasingly important resource since the 1990s. However, groundwater usage by means of groundwater extraction (i.e. pumping) results in land subsidence, which has been observed around the world (e.g., Poland, 1984; Galloway and Burbey, 2011, Erban et al., 2014).

Over-exploitation of groundwater can lead to significant subsidence rates. Famous examples of pumping induced subsidence in coastal areas are Venice, Tokyo, Jakarta, and Bangkok, where subsidence rates have been observed of, 1.4 cm/year (Tosi et al, 2002), 4 cm/year (Hayashi et al., 2009), 8,4 cm/year (Djaja et al., 2004) and 12 cm/year (Phien-wej et al., 2006), respectively. Moreover, an inland example is Beijng, which experiences subsidence rates of 14 cm/year (Chen et al., 2020).

Drinking water companies, alike industries, in the Netherlands have been extracting large quantities of groundwater from (semi) confined aquifers (see chapter 10 for definition) since the 19th century, mostly from depths between 20 and 200m. These aquifers are often protected by aquitards (see chapter 10 for definition), sometimes formed during the Holocene, consisting of clay and peat layers

shielding the confined aquifers from human induced shallow soil pollution like spreading of dung, over-fertilization, and use of pesicides. Besides drinking water companies and industries, groundwater fed irrigation has increased over the last 70 years, especially in sandy areas.

Groundwater extraction leads to reduced water pressures within the aquifers surrounding the wells. Given the long-standing history of most drinking water extractions in The Netherlands, the fact that most extraction sites are pumping stable quantities of water, and the typical pressure redistribution time of approximately a few decades (e.g. Deltares, 2020), it can be assumed that most of the pumping induced subsidence has already taken place due to consolidation at the older extraction sites.

The risk of subsidence associated with future extensions of drinking- or industrial water extractions is addressed in the obligatory Environmental Impact Assessment ("*m.e.r. beoordeling*"). Large water extractors in the Netherlands are forced to extract groundwater sustainably, which is to be proven a priori using a steady state hydrogeological model calibrated for dry periods with the maximum requested water extraction for the specific site. The predicted land subsidence is assessed for negative effects on the environment. Any expansion of the drinking water sites needs to be revised by studying its effects on the environment, including subsidence. A recent study on the expansion of a small pumping site for drinking water near Hammerflier (Overijssel Province in The Netherlands) reported a total modelled subsidence of 1.8 cm (Aveco de Bondt, 2023). This outcome has led the province and the drinking water company to look for mitigating measures before initiating the expansion of the groundwater extraction. Shallow groundwater in phreatic aquifers (see chapter 10 for definitions) generally interacts with groundwater in lower semi-confined aquifer, because the confining layers are seldom fully impervieous. Therefore, extraction below confining layers genrerally affects the water table and may lead to compaction and possibly oxidation of softer layers such as peat and clay, i.e. to subsidence.

In the study area around Grijpskerk there are no drinking water extraction areas. The nearest is in Nietap, in Drenthe Province between Leek and Roden. There are however shallow groundwater extraction wells and shallow ATES systems (see section 2.7.2). The information on shallow groundwater extractions wells is in The Netherlands not complete, since there are many illegal or unregistered groundwater wells. The registered wells and ATES in and near the study area are shown in Figure 12.

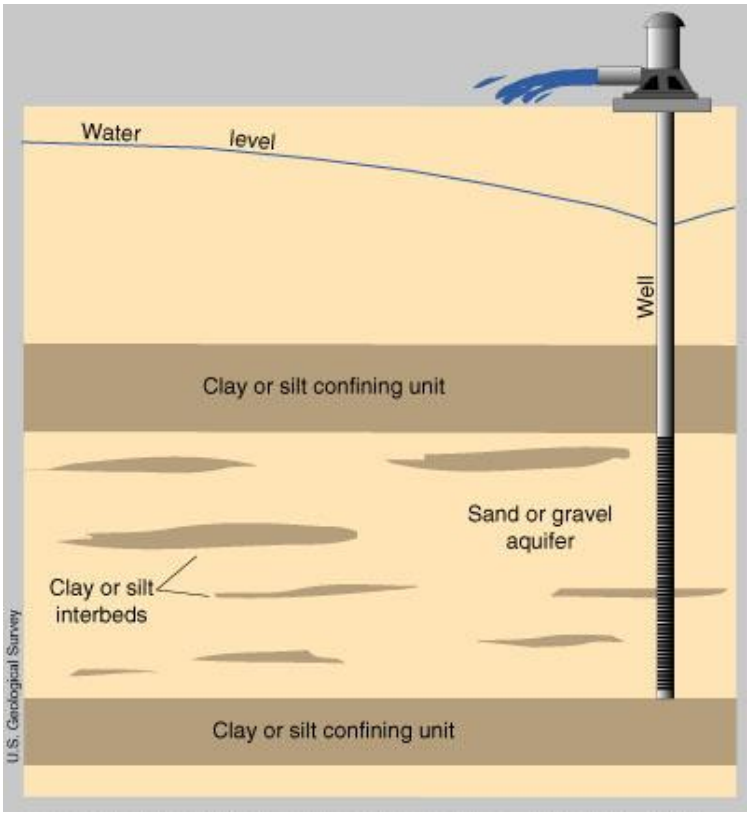

Figure 11. Sketch of groundwater extraction at intermediate depths (source US Geological Survey).

2.7.2 Subsidence due to groundwater extraction and injection for subsurface energy systems

Over a depth range from 20 to 500/1000 m., the subsurface has and will have an important role to play in the energy transition, for both energy storage and energy supply. Subsurface usage has inherently an environmental risk. In general, energy storage systems that circulate groundwater will yield smaller and more localized subsidence as one would expect from a single extraction well given the same extraction rate. Due to the increasing usage of the subsurface, accumulation of effects will occur, thus also for subsurface energy storage systems. Therefore, a summary of relevant developments is given below.

Aquifer Thermal Energy Storage (ATES) systems

The number of ATES (Aquifer Thermal Energy Storage) systems has significantly increased in recent years in the Netherlands, with a continuous increase in installations (CBS, 2021). At the moment of writing this report well over 2,000 ATES systems are active (source NPLW). These systems operate at depths down to hundreds of meters, and, more specifically for Groningen between 50 and 70m below the ground surface. They typically have a maximum drawdown in the well of several meters, and an influence radius of typically a few hundred meters by setting the minimal relevance level at 5cm change in hydraulic head (Deltares, 2010).

Local drawdowns cause an increase in effective stress within the aquifer, with subsequently compacting effects. Typically, subsidence in the order of centimetres in the vicinity of the well can occur within the first few seasons (Erkens & Kooi in 2018.). To mitigate induced compaction, ATES systems are often installed as deep as possible, i.e. far from the Holocene confining layers. For an overview of shallow ATES systems in the study area, see Figure 12.

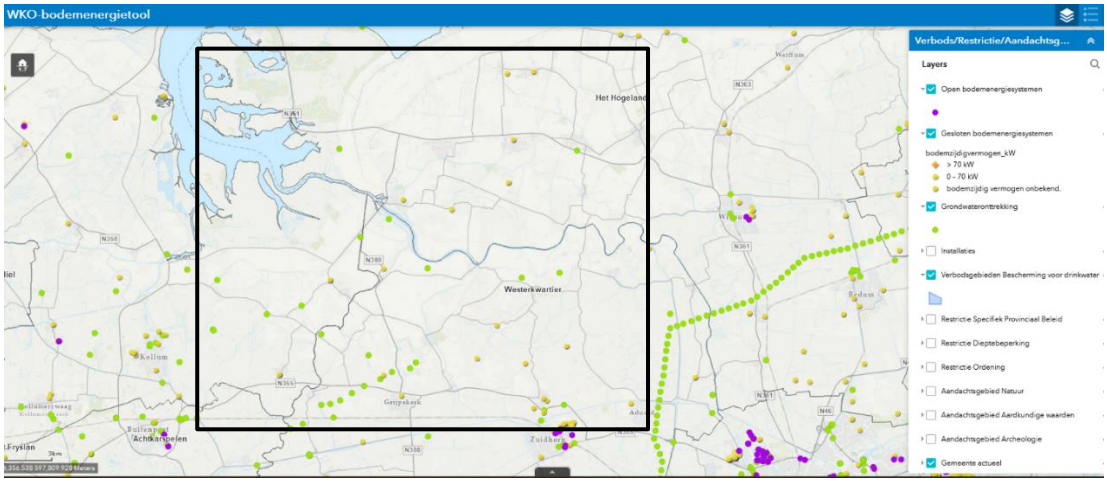

* There are no drinking water extraction locations in the project area. The nearest drinking water area are between Leek and Roden, near Burgum and in Glimmen (SE of Groningen City). See also Annex V, Figure 99 for a larger map. (Source: WKOTool, 2024).

Figure 12. Map of the study area (black square) with open (purple) en closed (yellow/orange) ATES systems and the permitted and registered groundwater extraction locations (green).

High/Medium Temperature Aquifer Thermal Energy Storage (HT/MT-ATES)

The HT/MT-ATES systems use greater temperature difference than ATES systems to enable more energy storage per unit volume. The maximum temperature for HT-ATES systems reaches 90°C, whereas for MT-ATES systems, it is 50°C. Due to these higher temperatures, HT/MT-ATES systems are specifically designed to operate at depths from hundred's to a 1000m beneath the surface. Several provinces in the Netherlands have recognized HTS/MTS systems as crucial elements in transitioning towards a fossil-free future (Provincie Groningen, 2020).

The HT/MT-ATES systems are predominantly in an experimental stage and no significant safety concerns have yet been brought forward (Van Gessel et al., 2021). HT/MT-ATES systems are anticipated to cause less subsidence than ATES systems because they operate at greater depths, primarily within consolidated, rigid deposits that are less susceptible to compaction in contrast to the younger, unconsolidated Holocene peat and clays found in the shallow subsurface. Hypothetically, there could be a thermo-elastic deformation effect due to the heating and cooling in the reservoir. In a study by Stricker et al. (2024) the subsidence and heave as a result of thermo-elastic deformation experienced at the surface is less than 1 mm. Within the HT/MT ATES reservoir the deformation is in the order of mm's. This effect is even overstated since thermal stresses decay much more rapidly than is assumed in the study. Deformation due to HT/MT-ATES can thus be considered negligible.

Geothermal Energy

Geothermal energy is in this report classified under activities below 1000-1500m. In The Netherlands, a distinction is made between deep geothermal energy (1500-4000m depth), and ultra-deep geothermal energy (>4000m depth). Geothermal energy systems function similar to an ATES system, but with the difference that geothermal energy systems operate one way, i.e. flow between the extraction and injection wells is not seasonally reversed. The extraction and injection wells are usually situated around 1500m apart to reduce thermal interference. Hot water, ranging from 70°C (in deep geothermal) to 120°C (in ultra-deep geothermal), is extracted from the extraction well and utilized to harness energy. Once the heat is extracted from the water, the cooled water is re-injected into the original subsurface layer through the injection well, thus maintaining a pressure balance. The risks associated with induced deep subsidence are therefore considered minimal, also due to the reasons mentioned for HT/MT-ATES systems. In the northern Netherlands, geothermal energy is not yet in use, and ultra-deep geothermal energy has not been deployed anywhere in the country, making it

irrelevant for the scope of this study. However, it is likely that geothermal energy will be introduced in the northern Netherlands in the future.

2.8 Deep subsidence, anthropogenic cause

2.8.1 Subsidence due to natural gas extraction

Subsidence due to natural gas or oil extraction is a phenomenon associated with the removal of gas and liquid from reservoir rock, resulting in a reduction of pore pressure. The pore pressure also supports the weight of overlying rocks, and a reduction can lead to increased effective stresses in the rocks. The load of overlying rock and soil layers may then cause the matrix of the reservoir rock to undergo compaction (Geertsma, 1973; de Waal et al, 2012 and Doornhof et al., 2006). This compaction is a volume reduction in the subsurface, ultimately leading to surface subsidence. The degree of compaction depends among other things on:

- the pressure drop in the pores of the rock (increase in effective stress in the rock matrix);
- the thickness of the reservoir rock; and
- the geomechanical characteristics of the rock.

The nominal effect of subsidence at the surface is independent of the depth of the reservoir. The compaction that takes place in the reservoir at depth, manifests itself ultimately completely at the surface. However, the subsidence bowl that develops depends on the geometry of the reservoir and, the deeper the reservoir, the larger the area undergoing subsidence. The latter is a result of the geometry of the subsidence bowl, which laterally expands from the edge of the gas reservoir toward the surface (section 6.4.3). Gas may also be extracted from different reservoirs at different depths, e.g. from the Rotliegendes, Zechstein 2C and Vlieland Formations in the Grijpskerk area. These combined effects can be incorporated in the subsidence models.

The compaction in gas reservoirs is often larger than in oil reservoirs due to the difference in compressibility between natural gas and oil. During gas extraction, the reservoir experiences a more rapid reduction in pore pressure compared to oil extraction.

Deformation of reservoir rock consists of various components, namely (Geertsma, 1973; Settari, 2002):

- Elastic (reversible) deformation, which can be time-independent or time-dependent.
- Inelastic (irreversible) deformation (plastic deformation), which can be time-independent or time-dependent.

Several theories describe elastic and inelastic deformation and the failure behaviour of rock in relation to pressure changes. In rock mechanics, the Mohr-Coulomb, Griffith, and Hoek-Brown failure criteria (Jaeger et al, 2007; Hoek, 1990) are the most often used. If a fault moves then a part next to the fault can move downward, which in theory can be translated to subsidence at the surface. The effect is however very small in the magnitudes that we have observed so far and negligible compared to the compaction due to the pressure reductions.

The key point to emphasize here is that (reservoir) rock at depth can exhibit complex behaviour. This complex behaviour involves a combination of elastic and inelastic deformation and time-independent and time-dependent deformation. Changes in pore pressure can translate to different loading conditions for the rocks, which may lead to deformation of the reservoir rock. This in turn can have consequences for effects that are observed at the surface, such as subsidence and induced seismicity (see chapter 3).

In low lying coastal areas like the Netherlands, even small amount of surface subsidence can have pronounced impact that affects the hydrological regime of a large area. Because of the large gas production over long periods subsidence, especially above the Groningen gas field, has thus gained

much scientific attention in the Netherlands. Geertsma (1973a, 1973b) was one of the firsts to develop a computer model with which he could predict the subsidence from the Groningen field. The basis of his model is still used today. The current focus in subsidence research is on minimising the uncertainty of the modelled predictions into the future. The uncertainty on surface effects of subsidence is still relatively large, despite the large amount of data that is available (Thienen-Visser and Fokker, 2017; Schouten and de Waal, 2020; Candela et al., 2022).

There are immediate, time-independent, effects from pressure changes, but to predict the future effects it is important to also quantify the time-dependent effects. Time-dependent, inelastic, deformation (creep) is a phenomenon where deformation in the rock occurs even after the pressure change has stopped. This phenomenon results in relatively small increments of deformations (compared to inelastic and elastic deformations) but over a long period. This makes it a significant component of uncertainty. On the topic of time-dependent deformation experimental work has been done by for example Pijnenburg and Spiers (2020) and numerical modelling based on microphysics by Mehranpour et al. (2021).

The modelling aspects are further covered in Section 2.10.1. The lateral extent of deep subsidence is covered in Section 6.4.3.

2.8.2 Subsidence due to salt solution mining

Up to 1000 m thick upper Permian Zechstein deposits can be found in the subsurface in the northern Netherlands (Geluk, 2007, Figure 112). These layers deposited by evaporation of sea water between 265 to 252 million years BP, consist of rocks like halite, anhydrite, polyhalites, and magnesium salts. Salt domes, halokinetic deformations, caused salt to rise from depths of several km to shallower depth of maximum ca. 400 m below ground surface. (Geluk, 2007; Duin et al., 2006). The Zechstein layers play an essential role in petroleum systems both as a seal and by forming structural traps for oil and gas (Pletch et al., 2010).

In the north and east of the Netherlands, salt domes are mined via solution mining, creating caverns, and causing gradual subsidence due to convergence and salt creep causing the dissolved caverns to close over time. Globally, and in the Netherlands impermeable salt caverns are used for underground storage, including of natural gas and nitrogen. Future scenarios suggest potential development for hydrogen storage (Larré et al., 2019). Currently, no policy exists for optimizing the capacity of the underground caverns for storage of different gases and fluids, compressed air, wastewater, nuclear waste or even heat. Research in the Netherlands on the future use of abandoned caverns is expected to increase in the context of the energy transition (SodM, 2018).

In Groningen near Winschoten and Zuidwending, the Zechstein salt layer forms a salt dome (salt diapir) between depths of 500 to 1600 m, allowing the dissolution of tall caverns with volumes ranging from 0.6 to 4 million cubic meters each. Winschoten has 12 caverns for salt extraction, with one used by Gasunie for nitrogen storage. Zuidwending has 16 salt caverns, including 7 for natural gas storage (SodM, 2018). Zuidwending will be the location of The Netherlands' first hydrogen storage facility (Hystock, 2024).

Near Veendam, magnesium salt (bischofite) is extracted from layers a few tens of meters thick, forming interconnected caverns with an estimated total volume of 5 to 10 million cubic meters. Privately held Nedmag BV uses the 'squeeze method' to extract magnesium salt without the creation of caverns (Nedmag, 2023), which means there are no caverns left after salt extraction ends.

The halite layer in Harlingen ranges from 2500 to 3000 m, with onshore cylindrical caverns having volumes of 0.2 to 1.0 million cubic meters each. Recently, the salt solution mining operations had to shifte offshore due to unexpected subsidence onshore interacting with natural gas extraction as interpreted by de Waal et al., 2016.

Industry (Frisia, Nobian, and Nedmag BV) operates at varying depths, forming caverns with distinct dimensions and shapes. Figure 91 in Annex IV provides an overview of salt cavern dimensions and depths. Figure 94 in Annex V provides a map with the locations of the salt mining operations. Subsidence due to salt solution mining exhibits a more localized, deeper, and curved shape compared to gas extraction. Two types of subsidence are recognized: gradual and sudden (SodM, 2018).

Gradual subsidence is inherent in salt mining, with predictions ranging from centimeters to almost one meter. For instance, in Veendam, in the assessment of the extraction plan, the permit considers a maximum subsidence of 95 cm due to salt extraction as the worst-case scenario (Nedmag, 2018). Salt creep continues post-mining, causing gradual cavern collapse and subsidence over time, continuing over possibly thousands of years. Scientific consensus on the long-term effects is lacking, introducing uncertainty for post-mining risk assessment (SodM, 2018). The lateral extent of the subsidence areas due to salt mining is discussed in section 6.4.3.

Sudden subsidence leads to sinkholes, often caused by the partial or complete collapse of unstable caverns. Due to the instability of a cavern in Twente in 1991, a sudden event subsidence resulted in a sinkhole. It had a diameter of 30 meters and a depth of 4.5 meters. The sinkhole formed beneath a road but there were no casualties. This was the first and until now the last time a sinkhole was recorded in the Netherlands because of salt mining. This incident led to a new guideline, the Good Salt Mining Practise (GSMP), which was developed between 1991 and 2004. This guideline led to the closure of some caverns and has the objective to ensure a safe and sustainable salt extraction, minimizing ground subsidence and preventing sinkholes during production. The guideline Imposes restrictions on cavern size and provides instructions on cavern shape, depth, and distances between caverns.

Solution mining starts with injecting fresh water into underground salt deposits. This water dissolves the salt, forming caverns. The growth of these caverns is a fundamental aspect of the solution mining process. On the other hand, the “squeeze method” as employed by Nedmag in Veendam, does not lead to the creation of large caverns. The subsidence is immediate since the bischofite layer is squeezed into a smaller solution cavern where the bischofite is dissolved into the brine and immediately extracted.

Convergence comes into play as the dissolution of salt in the caverns reduces support to the overlying rock layers. The surrounding salt and overlying rock start to converge toward the voids created by the solution mining process. This convergence of overlying rock layers is a critical factor in the overall subsidence process.

In time, the created salt cavern becomes smaller due to convergence. This convergence is caused by time-dependent deformation (creep) of the rock salt. This time-dependent deformation is different from the time-dependent deformation in gas reservoirs discussed in section 2.8.1., due to the very different mechanical properties of salt.

In Annex IV some illustrations can be found of different cavern configurations in the Netherlands. The modelling aspects are further covered in Section 2.10.2. The lateral extent of deep subsidence is covered in section 6.4.3.

2.9 Magnitudes of subsidence

The amount of subsidence ranges widely (Table 2). This non-exhaustive table gives an overview, based on various national and international references, including observations from InSAR over 4 years (2018-2022) as well as expert judgement. The table provides a first insight into the order of magnitude of the subsidence rates and values of the different mechanisms that can be expected in the study area and comparison with other rates and values in other countries or outside the study area. We have made a distinction between maximum observed values over larger periods and subsidence rates (mm/year). For the subsidence rates we made a distinction between international references and for

the typical values expected or observed in the northern part of the Netherlands for anthropogenic causes of subsidence due to mining.

Table 2. Non-exhaustive overview of expected values of subsidence due to various mechanisms.

	Global maximum observed values (mm)	Global ranges in observed/modelled velocity (mm/year) (min-max)	Observed/modelled velocity (mm/year) (min-max) in northern Netherlands	Lateral extent in northern Netherlands
Shallow subsidence				
Compaction of clay and peat	1,600	1-30 [2]	1-6 [15]	1 m – ± 30 km
Oxidation of peat and organic soils	5,000	1-100 [1,2]	1-6 [15]	1 m – ± 30 km
Swelling and shrinking of clay	300	1-6 [4,5] 1-10 [16]	5- 12 (also heave) [15]	1 m – ± 30 km
Intermediate subsidence				
Natural compaction	60	1-2 [3]	0.01-0.03 [7]	>> 10 km
Groundwater extraction	8,500 [17]	1–500 [6, 18]	n.a.	100-200 m
Deep subsidence				
Gas extraction	260 [11]	-	2-6 [10,11]	1- 8 km (from edge of GWC)
Gas storage	20	-	5-20 [14,13] (also heave)	1- 6 km [13]
Salt mining	650 [12]	-	11-14 [12]	1.5-5 km [12]
Natural subsidence				
Postglacial Isostacy	-	-	0.02-0.10 [7]	>> 10 km
Tectonics	-	-	0.01-0.04 [7]	>> 100 km

References:

1. Galloway, D. L., Jones, D. R., & Ingebritsen, S. E. (Eds.). (1999). Land subsidence in the United States (Vol. 1182). Geological Survey (USGS).
2. van Asselen, S., Erkens, G., Stouthamer, E., Woolderink, H. A., Geeraert, R. E., & Hefting, M. M. (2018). The relative contribution of peat compaction and oxidation to subsidence in built-up areas in the Rhine-Meuse delta, The Netherlands. Science of the Total Environment, 636, 177-191.
3. Nicholls, R. J., Lincke, D., Hinkel, J., Brown, S., Vafeidis, A. T., Meyssignac, B., Hanson, S.E., Merkens, J.L., & Fang, J. (2021). A global analysis of subsidence, relative sea-level change, and coastal flood exposure. Nature Climate Change, 11(4), 338-342.
4. Burnol, A., Foumelis, M., Gourdier, S., Deparis, J., & Raucoules, D. (2021). Monitoring of expansive clays over drought-rewetting cycles using satellite remote sensing. Atmosphere, 12(10), 1262.
5. Verberne, M., Koster, K., Lourens, A., Gunnink, J., Candela, T., & Fokker, P. A. (2023). Disentangling shallow subsidence sources by data assimilation in a reclaimed urbanized coastal plain, South Flevoland polder, the Netherlands. Journal of Geophysical Research: Earth Surface, 128(7), e2022JF007031.
6. Chen, B., Gong, H., Chen, Y., Li, X., Zhou, C., Lei, K., ... & Zhao, X. (2020). Land subsidence and its relation with groundwater aquifers in Beijing Plain of China. Science of the Total Environment, 735, 139111.
7. Kooi, H., Johnston, P., Lambeck, K., Smither, C. & Molendijk, R. (1998). Geological causes of recent (~100 yr) vertical land movement in the Netherlands. Tectonophysics 299: 297–316.
8. NAM (2014) Winningplan Grootegast 2014: 3.3 mm/year (10 cm 1978-2008)
9. NAM (2012) Winningsplan Grijpskerk-Noord 2012: 4.3 to 5.3 mm/year (6-8 cm 1993-2008)
10. NAM (2017) Winningplan Grijpskerk-Zuid 2017: 1.7 mm/year (8 cm 1975-2023)
11. NAM (2017) Winningsplan Groningen: 5.6 mm/year (26 cm 1964-2010)
12. NEDMAG (2018) Winningsplan Veendam: 11.2 – 13.9 mm/year (46 cm 1977-2018 measured – 95 cm 1977-2045)
13. NAM (2016) Opslagplan UGS Norg (subsidence/heave per year: +/- 2 cm)
14. NAM (2021) Opslagplan UGS Grijpskerk (subsidence/heave per year: +/- 0.5 cm)
15. EGMS (2024) European Ground Motion Service. Website: https://egms.land.copernicus.eu/ (Last accessed 21-02-2024)
16. Asselen, S. van, H. Kooi, J.J.H. van den Akker (2020), STOWA Deltafact Bodemdaling, versie 3.1
17. USGS (2018) Land Subsidence in the San Joaquin Valley (California). https://www.usgs.gov/centers/land-subsidence-in-california/science/land-subsidence-san-joaquin-valley (Last accessed 09-05-2024)
18. EOS (2021) O'Hanlon, L. (2021), The looming crisis of sinking ground in Mexico City, Eos, 102

2.10 Modelling of subsidence

Several techniques have been employed to model the magnitude and shape of subsidence bowls due to depleting reservoirs, storage facilities and mining areas, which are described in the following

sections 2.10.1 to 2.10.4. An overview of the different modelling approaches for subsidence due to depleting reservoirs is also provided by van Thienen-Visser & Fokker (2017).

2.10.1 Modelling of subsidence due to natural gas extraction

An early approximation for subsidence in the context of hydrocarbon production combines the theory of poroelasticity and the nucleus-of-strain concept (Geertsma, 1973a; Geertsma, 1973b). With this approach, a so-called compaction coefficient and the related subsidence is approximated for reservoirs of arbitrary 3-dimensional shapes. The approach by Geertsma (1973a, 1973b) was later modified to model general axisymmetric pressure distributions (Segall, 1992) and to incorporate the influence of a rigid basement (van Opstal, 1974). Finite element modelling (FEM) is an alternative for modelling complex geometries, in heterogeneous conditions.

Van Thienen-Visser & Fokker (2017) outline two limitations regarding the compaction coefficient, which is physically defined to relate the pressure depletion in the reservoir to the volumetric strain. First, the compaction coefficient is only determined from the elastic moduli within the framework of linear poroelasticity. Secondly, the compaction coefficient depends on the compressibility of the porous medium, which is influenced by the stress path. Hence, direct extrapolations of this parameter from laboratory results need to be treated with caution (Hettema et al., 2000; Schutjens et al., 2004).

Experimental studies demonstrate that processes other than linear elastic behaviour are relevant to model reservoir compaction and associated subsidence (e.g. Brantut et al., 2013; Brzesowsky et al., 2014; Hol et al., 2015; Niemeijer et al., 2002; Schutjens, 1991). Some approaches capture the nonlinearity of compaction behaviour with a rate-dependent compaction coefficient, which depends on the time, depletion magnitude and depletion rate (e.g. De Waal, 1986; Pruiksma et al., 2015).

Subsidence modelling has employed various time-dependent approaches, as outlined by van Thienen-Visser and Fokker (2017). Firstly, the time decay model (Mossop, 2012) accounts for a delayed subsidence increase after production has ceased, suggesting a temporal lag in development. In contrast, the linear isotach model (Den Haan, 1994) and the rate-type compaction model (rTiCM, De Waal, 1986; Pruiksma et al., 2015) respond to pressure changes and pressure rates, exhibiting both instantaneous and delayed strain responses. Consequently, subsidence predictions differ among these compaction models, with variations exceeding 10 cm, as illustrated in Figure 1 of the work by Thienen-Visser and Fokker (2017).

2.10.2 Modelling of subsidence due to salt-solution mining

Rock salt deforms at low deviatoric stresses leading to the risk of cavern closure due to creep (e.g. Habibi 2018). This difference in the volume due to successive closure (‘convergence”) is considered as the cause of subsidence in the context of salt solution mining (e.g. Xu et al., 2014). Consequently, the produced salt volume dV controls the subsidence level for stationary conditions.

Subsidence models for non-stationary subsidence caused by salt solution mining include the same semi-analytical approaches or FEM-modelling as described in section 2.10.1. Analogous to the necessity for compaction models to constrain the subsidence above depleting reservoirs, convergence models for the temporal evolution of the volume shrinkage of the salt cavern(s) are required here. Convergence models include physical approaches and statistical models (see Babaryka & Benndorf, 2023 for a summary).

For subsidence modelling of the salt mining operations in the northern part of the Netherlands (Figure 94, Annex V), one is referred to the following references:

- Nedmag: SGS (2018), Antea (2021), Deltares (2018)
- Heiligerlee/Winschoten and Zuidwending: BGR (1999, 2006, 2007)
- Barradeel/Havenmond: WEP (2010, 2012)

2.10.3 Modelling of the time-dependent deformation of salt (creep)

The modelling of salt creep involves at least an understanding of its temperature and pressure dependent deformation mechanism to changes in stress.

Quantification of salt deformation is in general well constrained using a thermodynamic approach. This shows that different thermodynamics and associated parameters apply depending on depth, temperature, water content, grain size and composition (e.g. Carter et al., 1993; Spiers et al., 1990; Hunsche & Hampel, 1999 and Berest, 2023). Therefore, the resulting thermodynamic rate laws can only be implemented in numerical models, valid for each specific location.

In practical applications it is important to consider that salt creep has been observed to delay subsidence development in salt layers overlying depleting gas reservoirs (Marketos et al. 2016), see also section 6.6. In the context of underground storage, the effects of low stresses and pressure cycling are to this point not yet fully understood (SodM, Ingeokring Salt symposium). Also, other processes as recrystallisation at large strains and transient creep need further investigations (TNO presentation, salt workshop IMG)

2.10.4 Modelling of subsidence and heave due to gas storage in gas reservoirs

Targeted storage locations for depleted gas reservoirs (in particular in the Groningen and Fryslân regions) are sandstone reservoir rocks with either salt or clay caprock. Gas (usually methane) storage in depleted reservoirs has from a mechanical perspective the advantage that there is data available about the composition and pressure behaviour during the exploration and production history.

Once a depleted gas reservoir is turned into an underground gas storage UGS site, cyclic storage operations are usually performed in a pressure range where elastic deformation dominates (NAM, 2016). In theory, when only elastic deformation occurs, if the pressure would return to its original value (e.g., by re-injection) the deformation will revert to the initial situation, in other words: the rock elastically and smoothly moves back to its original thickness. Given the increasing importance of energy storage in the energy transition, , research looking into the validity of this assumption will be important, especially when the gas type is changed, for instance to CO_2: Carbon Capture and Storage (CCS) or to H_2: Underground Hydrogen Storage (UHS). Subsidence and heave associated with cyclic storage operations are usually be modelled with the same approaches as outlined in section 2.10.1 .

2.10.5 Modelling of shallow subsidence

In geotechnical engineering, shallow subsidence is often estimated using state-of-the-art commercially available numerical models such as Plaxis[4] or dSettlement[5]. The outcome is often compared to monitoring data. Both models consider soil properties, pressure changes in time and applied stresses to calculate subsidence around construction sites such as dikes, buildings, and infra structural objects.

When modelling larger areas, shallow subsidence presents a challenge due the large spatial variabilities of the soil stratigraphy, properties, and hydrogeological conditions. For example: the spatial resolution of observations of soil properties is low compared to its spatial variation. In recent years different modelling strategies were developed to understand and predict shallow subsidence, when dealing with the spatial heterogeneities. Physics based models have been developed to predict subsidence (e.g. Koster et al., 2018; Mayoral et al., 2017; Nusantara et al., 2018; Schothorst, 1982; Van Asselen et al., 2018). These models use input parameters based on field- and laboratory observations. However, the users decisions on closed-form equations and input parameters profoundly influences

[4] Geotechnical Engineering Software | Bentley Systems
[5] D-Settlement | Deltares

the outcome. Closed-form equations are analytical mathematical expressions that provide a direct and efficient solution for calculating subsidence without resorting to numerical simulations.

On the other hand, history matching is an approach that optimizes the parameter values based on the measurement. It optimizes the alignment between the subsidence model and field observations, by means of trial-and-error, correlation, or data assimilation methods. Data assimilation method is becoming increasingly popular as it combines model and field observations effectively (Evensen, 2009; Evensen et al., 2022; Candela & Koster, 2022). Successful applications of data assimilation to model subsidence include studies by Muntendam-Bos et al., 2009; Fokker et al., 2019; and Verberne et al., 2023. However, data assimilation is reliant on field observations, often utilizing InSAR data due to its spatial continuity and high precision. Nevertheless, interpreting InSAR data can be challenging in itself as it captures all surface movements. In regions affected by deep subsidence, unravelling individual components of total subsidence via data assimilation becomes notably complex as multiple combinations of physical parameters and processes can yield the same subsidence.

Another approach is the use of stochastic models to gain insights into shallow subsidence in areas lacking observational data. In investigating the indirect effects of deep subsidence near the Groningen gas field in the Netherlands, Van Dalen et al. (2022) utilized a stochastic approach, employing 1-dimensional analytical approximations for compaction, oxidation, and clay shrinkage/swelling. In this method, input parameters are stochastic variables with predefined ranges and distributions.

2.10.6 Modelling of subsidence due to groundwater extraction

The classical approach of modelling pumping induced subsidence is by modelling the influence area of pore pressure depletion. Depending in the complexity of the geology, both analytical (e.g. Bear and Corapcioglu, 1981a,b; Corapcioglu and Bear, 1983) and numerical approaches may suffice. In case drainage systems are within the area of influence, which is often the case for large scale pumping wells, one has to turn towards numerical modelling. Popular software packages to model groundwater flow are MODFLOW (Langevin et al., 2017) and FEFLOW (Diersch, 2013). Once the extent of a groundwater extraction is known, the resulting subsidence can be estimated using similar geotechnical tools as mentioned in section 2.10.5.

In recent years, the method of modelling large scale pumping induced subsidence has shifted towards data assimilation approaches (Teatini et al., 2006; Erban et al., 2014; Calderhead et al., 2011; Smith and Majumdar, 2020). In this approach both groundwater data measuring pumping induced drawdown, and satellite data measuring subsidence, are combined to deduce compaction coefficients of the specific subsurface; thus, allowing large-scale subsidence predictions with an accuracy that is hard to match when compared to classical numerical models.

2.10.7 Modelling the interaction between different mechanisms

Until here, the approaches to subsurface modelling presented consider the deformation associated with a single source of compaction, i.e., a single geotechnical facility. These methods imply hydro-mechanically coupled (poro-elastic) simulations.

In the current context, the back-coupling from stress-changes to changes of the reservoir pressure is currently assumed to be a secondary effect. When ignoring this effect, the super-position principle of stresses holds. Thus, it is implied that the deformation signals of different sources of compaction can be superimposed, and the combined deformation signal from multiple sources can be modelled using the same approach, e.g., as implemented in KEM-16. This assumption needs be validated in Phase II, otherwise the super-position principle does not hold in all cases.

This is the core of the proposed study in phase II, as explained in Part II of this report, see for instance section 9.8, where the modelling strategy is elaborated.

2.11 Monitoring of subsidence

This section is about geodetic monitoring of soil and subsoil movements in the north of the Netherlands. This monitoring is based on geodetic measurements, which can be terrestrial-based like GPS/GNSS, levelling or via remote sensing methods like drones, airplanes, and satellites, and can cover extensive areas. An overview is given in the Annex I Geodetic Measuring Techniques.

Geodetic monitoring is the repeated collection of geodetic measurements, and the analysis of these repeated measurements to make inductions about changes in position and form of objects (often subsidence), like houses, constructions, roads, and the Earth itself, and, by extension, of any object under, on and above the Earth's surface. Monitoring geodesists are concerned with the continuous effort to distinguish the real changes in position and form of the objects concerned. This encompasses dealing with measurement noise, modelling discrepancies, and autonomous movements of objects across, above, and beneath the Earth. Inevitably, errors, whether from the geodesists or others, contribute to a small percentage of the challenges in this continuous effort. Moreover, geodetic monitoring is about distinguishing the causes of movements, for which a close collaboration with other specialists (geo-physicists, geo-technicians etc.) is necessary. Annex III (Geometry Models for Deformation Analysis) provides a comprehensive treatment of models used, whereas section 2.11.1 gives an overview of models used in geodesy and geo-mechanics.

Geodetic monitoring in the Netherlands, and in the north especially, has, in its history, developed sophisticated analytical models (Annex III). Models, combined with the contemporary computing power for analysis and interpretation, make it feasible to improve and extend the estimates of subsidence in the Netherlands (cf. section 2.11.2).

The quality of deformation analysis is influenced by seasonal effects and long-term effects, which are difficult to capture, when monitoring time series are too short or not well planned (section 2.11.2). Future trends in monitoring are addressed in section 2.11.3.

2.11.1 Symbiosis of Geodesy and Geo-mechanics

The quality of geodetic measurements depends on two types of geodetic models:

1. Measurement Models: These models detail the processes of how measurements are conducted, for instance, how a laser distance meter measures distance. They define the starting point of measurement within the instrument, the speed of the laser beam (affected by air density and humidity), its path (straight or curved, based on the changes in the air's refractive index), and the exact point of reflection. The result is a simple numerical value representing the measured distance.

2. Geometry Models: These models establish the relationship between geodetic measurements and the geometry of the measured objects. For example, in measuring the heights of levelling bolts, these models help interpret the measurements in the context of among other things, the Earth's curvature, the Normalized Amsterdam Level (NAP, a reference for elevation), and local variations in mass density of the Earth. A geometry model is needed as well to assess subsidence. If that same bolts are assumed to be subject to deformation, and the deformation is assumed to be linearly downward, the subsidence rate can be estimated. The assumed linear trend is a geometry model, which is based on assumptions on the deformation process. However, a quite different subsidence rate might result, if another geometric model is applied, for example a linear trend with a trend break, caused by a certain event, for example an earthquake.

This means that a third type of models is important for geodetic deformation analysis.

3. Geomechanical Models: geodetic descriptions and estimates are based on geomechanical Models of the movements of the soil and subsoil (see section 2.8.1 and 2.10.5). Inputs and outputs of such models often have greater standard deviations than those in the measurement and geometry models.

Careful consideration must always be given to whether the measurement models, the geometry models, and the geomechanical models are well aligned. Measurement models usually have high precision, geomechanical models low precision, and geometry models are in between. The geometry models, however, play a crucial role. Seemingly small changes in these models can have far-reaching consequences for the conclusions drawn about movements.

Geodetic calculations involve not only the instruments' standard deviations but also the noise of the geometry model and mathematical descriptions of geometry changes. An important part of the noise is the temporal noise, which refers to continuous, unpredictable small movements of measurement points in time, which are not related to subsidence.

Models, both geodetic and geomechanical, play a crucial role in predicting soil movements. The importance of integrating both geodetic and geo-mechanical models to assess soil movement is emphasized.

Validation and cyclic process

Geodetic measurements are often considered as definitive data on actual movements. Many believe that geodetic measurement data can easily validate geomechanical models, with the thought that geodetic centimetres should be ample for verifying geomechanical meters. However, the situation is more complex. The measurement models are usually fine, but the geometry models and the geomechanical models often have deviations from reality that can both be considerable.

Therefore, geodetic and geomechanical models are developed iteratively; geodetic measurements lead to adjustments in the geomechanical models, and geomechanical insights lead to adjustments in the geodetic models. Phase II of this project, such a cyclic process will be completed between the geodetic and geophysical specialists in the consortium. Details about the feasibility study are included chapter 8.

2.11.2 Deformation patterns

Seasonal effects

Seasonal effects play a crucial role in influencing subsidence patterns, primarily driven by variations in groundwater extraction, soil moisture, and vegetation cycles, but also by fluctuations in mining quantities of oil, gas, and salt. Seasonal shifts can cause reversible ground movements, which makes it challenging to differentiate between transient and permanent subsidence. In geodetic models, these effects can be accounted for by integrating time-series data that capture seasonal variations. Advanced techniques like InSAR provide high temporal resolution data, enabling the modelling of these seasonal influences (see also Figure 9 in section 2.6.4). By incorporating such data, geodetic models can more accurately represent the cyclical nature of subsidence, improving predictions and aiding in distinguishing between short-term and long-term ground movements.

Long-Term Monitoring

Long-term monitoring is essential in geodetic studies to capture the full spectrum of deformation processes, from immediate responses to slow, gradual changes. Continuous or periodic monitoring over years or decades provides invaluable data to identify trends, assess stability or progressive deformation, and understand the life cycle of various geophysical phenomena. In the north of the Netherlands, we have spirit levelling measurements spanning several decades.

Different Sources of Deformation

Deformation arises from a multitude of sources. Natural causes include tectonic movements, landslides, changes in water levels of rivers and the sea, and isostatic adjustments. Human-induced factors encompass mining, groundwater extraction, and urban development. Each source has distinct characteristics and implications, necessitating tailored monitoring and analysis strategies.

Geodetic monitoring (levelling) and GNSS measurements in the Netherlands typically involve the use of markers positioned on structures with a rigid foundation. The underlying assumption is that deformation observed in these well-founded markers is predominantly due to intermediate and/or deep subsidence, with shallow subsidence deemed insignificant. A robust foundation typically refers to piled foundations resting on a more rigid (Pleistocene) sand layer. When dealing with older buildings featuring shallow foundations, it is commonly assumed that the majority of settlement has already taken place, and the foundation can also be regarded as rigid.

InSAR satellite deformation measurements do not differentiate between objects or structures with deep or shallow foundations. Consequently, additional analyses are necessary to discern between objects with rigid foundations solely affected by intermediate and deep subsidence and those with shallow or no foundations, which are also influenced by shallow subsidence.

2.11.3 Future of monitoring

In geodetic deformation analysis, the ongoing development of new techniques, the refinement of models, and the persistence of uncertainty form a dynamic triad that drives progress and challenges.

New Techniques

Advancements in technology have significantly enhanced geodetic measurement capabilities. Techniques such as GNNS (Global Navigation Satellite System), GPS (Global Positioning Systems), InSAR (Interferometric Synthetic Aperture Radar), and LiDAR (Light Detection and Ranging) provide high-resolution spatial data. These methods have revolutionized our ability to monitor and analyse earth deformations with greater precision, accuracy, and over broader areas. The deployment of satellite-based technologies enables continuous, large-scale monitoring, capturing subtle movements that were previously undetectable. It is without doubt that the development and innovations of these techniques will continue, and that completely new techniques will be added to the existing ones.

Better Models

With the influx of rich data from advanced techniques, the development of more sophisticated models has been a natural progression. These models are crucial for interpreting geodetic data, allowing us to understand underlying geophysical processes better. They integrate various data types, account for different scales of observation, and incorporate complex physical phenomena. However, the challenge lies in accurately translating vast data sets into models that realistically represent the complexities of earth deformations.

Persistent Uncertainty

Despite technological advancements and improved models, uncertainty remains a significant factor in geodetic deformation analysis. This uncertainty arises from various sources, including measurement errors, limitations in data processing techniques, and the inherent unpredictability of geophysical processes. The challenge is to quantify and reduce these uncertainties for more reliable predictions and interpretations.

Overall, while new techniques and better models offer enhanced insights into deformation processes in the north of the Netherlands, the persistent uncertainty underscores the need for continuous innovation and cautious interpretation in geodetic research.

3

INDUCED SEISMICITY

3.1 Summary and conclusions

This chapter gives an answer to the following research question as defined in section 1.4.1

1. What information is available about interactions between different adjacent underground (man-made) activities, natural processes, and about the cumulative mutual effect? This chapter covers the answer in the context of topic **b) Induced seismicity.**

The root cause for induced earthquakes are stress changes in the subsurface caused by anthropogenic activities that lead to rock failure. Different technologies can be associated with induced earthquakes. In the northern part of the Netherlands, earthquakes have been associated with gas production, gas storage, geothermal exploitation, and fluid disposal.

The sensitivity at which earthquakes can be detected and the accuracy at which they can be located depend on the number and on the geometrical configuration of monitoring stations. If anthropogenic subsurface activities are densely spaced, like in the Netherlands, it may not always be possible to unequivocally relate an observed earthquake to a specific subsurface activity.

3.2 Samenvatting en conclusies (NL)

Dit hoofdstuk geeft antwoord op de volgende onderzoeksvraag zoals gedefinieerd in sectie 1.4.1

1. Welke informatie is beschikbaar over interacties tussen verschillende aangrenzende ondergrondse (door de mens gemaakte) activiteiten, natuurlijke processen, en over het cumulatieve wederzijdse effect? Dit hoofdstuk behandelt het antwoord in de context van onderwerp **b) Geïnduceerde seismische activiteit.**

De hoofdoorzaak van geïnduceerde aardbevingen zijn spanningsveranderingen in de ondergrond veroorzaakt door antropogene activiteiten. Verschillende technologieën kunnen in verband worden gebracht met geïnduceerde aardbevingen. In Noord-Nederland zijn aardbevingen veroorzaakt door gaswinning, gasopslag, geothermische winning en waterinjectie.

De gevoeligheid waarmee aardbevingen kunnen worden gedetecteerd en de nauwkeurigheid waarmee ze kunnen worden gelokaliseerd, hangt af van het aantal en de geometrische configuratie van meetstations. Als antropogene activiteiten in de ondergrond dicht bij elkaar liggen, zoals in Nederland, is het niet altijd mogelijk om een waargenomen aardbeving eenduidig in verband te brengen met een specifieke activiteit in de ondergrond.

3.3 Introduction

Triggered and induced seismicity are the earth response to transient non-tectonic phenomena (Cesca et al., 2013). Transients which can induce, or trigger seismicity can either be of natural or

anthropogenic origin. Throughout this report, we use the terminology “induced seismicity” solely for earthquakes, which are caused by human underground activities. Following Grünthal (2014) we do not differentiate between “induced” and “triggered seismic events“ and use these terminologies synonymously.

Different energy technologies such as mining, hydrocarbon exploitation, and geothermal production can be associated with induced seismicity (National Research Council, 2013). On a global scale, human-induced earthquakes have become an important topic of political and scientific discussion, owing to the concern that these events may be responsible for widespread damage and an overall increase in seismicity (Ellsworth, 2013).

In the Netherlands, induced earthquakes up to magnitude ML=3.6 have occurred (Figure 13). Despite their moderate magnitude level, some of these earthquakes caused significant damage (van der Voort & Vanclay, 2015) due to their shallow origin. In October 2023, the large Groningen gas field was shut down due to induced seismicity concerns. Moreover, two geothermal doublets in the Roer-Valley Graben were suspended after the occurrence of an ML=1.7 earthquake (Muntendam-Bos et al., 2022).

3.4 Mechanics of induced seismicity

Ultimately, the root cause for induced seismicity are stress changes in the subsurface caused by anthropogenic activities. This can be related to the changes in pore fluid pressure, or changes to the local stress field due to ongoing deformation. Induced earthquakes usually occur on a pre-existing plane of weakness, i.e. a geological fault. As with rock failure, when a pre-existing fracture or fault is loaded beyond its capacity (i.e. the frictional resistance), it will fail. The failure process can be seismic (associated with earthquakes) or aseismic (not associated with earthquakes), depending on how the instability evolves.

For practical applications, some simple phenomenological approaches exist for shear stresses exceeding the fracture strength of a rock. The most commonly used approaches are derivations of the Mohr-Coulomb failure criterion for stresses (Scholz, 2002):

Let τ and σ_n denote the shear and normal stress resolved on a fracture plane, p_{fl} the in-situ fluid pressure, μ the coefficient of friction and c_0 cohesion, then shear slippage occurs on the fracture if:

$$\tau \geq \mu \cdot (\sigma_n - P_{fl}) + c_0.$$

If the left-hand side of this equation equals the right-hand side, the stress state is commonly referred to as the “critical stress” or “stress criticality”.

Stress perturbations on an idealised, cohesionless fracture can be described by Coulomb stress changes ΔCS, which can be defined as:

$$\Delta CS = \Delta\tau - \mu \cdot (\Delta\sigma_n - \Delta p_{fl}), \quad \text{(Scholz, 2002)}$$

with $\Delta\tau$, $\Delta\sigma_n$, and Δp_{fl} denoting changes of shear stress, normal stress, and fluid pressure acting on the fracture. Positive ΔCS values increase the tendency to failure of the fracture.

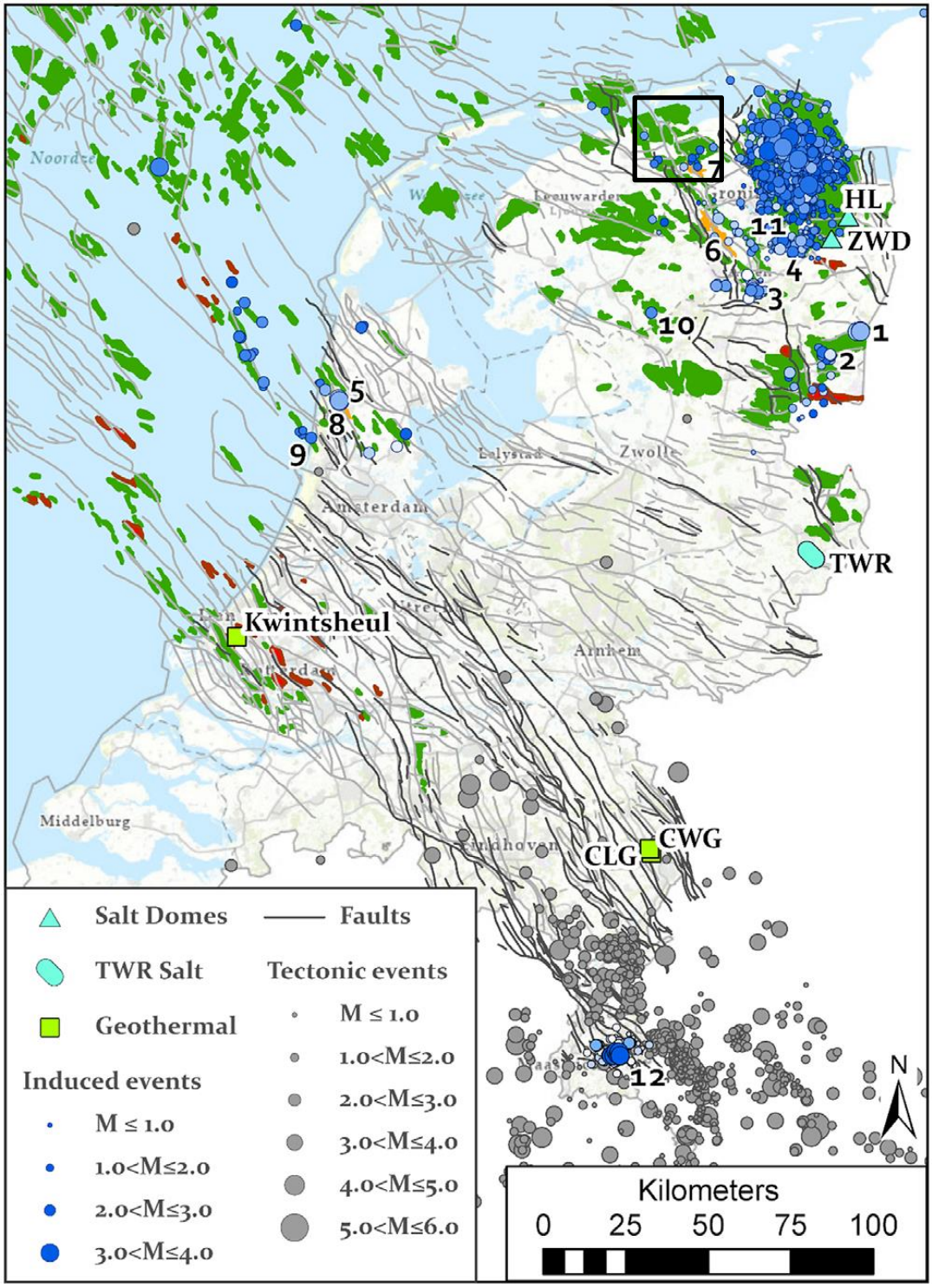

* The natural seismicity is indicated by grey circles, induced seismicity by blue circles. Grey lines indicate faults. Oil and gas fields are denoted in red and dark green, respectively; the underground gas storage (UGS) gas fields in orange. For abbreviations and numbering see Muntendam-Bos et al. (2022). Geothermal doublets associated with seismicity are shown as bright green squares, salt domes with large solution mining caverns by cyan triangles, and the shallow solution mining area of Twente-Rijn by a cyan ellipse. The approximate location of the Grijpskerk study area indicated with a black box.

Figure 13. Overview of seismicity in the Netherlands (Source: Muntendam-Bos et al. (2022).

3.5 Monitoring of induced seismicity

Earthquakes radiate seismic waves which attenuate with increasing distance from the hypocentre. The amplitude of the seismic signal scales with the earthquake magnitude. If the earthquake signal exhibits a sufficient signal-to-noise ratio, it can be detected, for example, in the ground vibration recordings of seismic monitoring stations.

For discriminating earthquake signals from other sources of ground vibrations and for locating the origin (hypocentre) of an earthquake, a minimum number of 3 monitoring stations is required. The lowest magnitude level at which an earthquake can be detected and the accuracy at which its hypocentre can be determined depend on the number and on the geometrical configuration of monitoring stations that are recording the earthquake signal.

In the Netherlands, earthquake activity is monitored by the KNMI. The capability for detecting earthquakes with the KNMI seismic monitoring network varies over the Netherlands and has improved over time as new monitoring stations were deployed. Figure 14 shows the lowest magnitude level at which earthquakes (occurring at 3 km depth) can be detected with the KNMI network as of the year 2021. For comparison, the lowest magnitude level at which an earthquake occurring at 3 km depth can be felt near its epicenter is about M_L=1.5 (Dost et al., 2004). In the Netherlands, a M_L=3 earthquake at a depth of 3 km can cause damage in the epicentral region and can be felt at up to several tens of kilometers.

The accuracy at which the epicenter of an earthquake (with a fixed depth at 3 km) can be determined varies from the order of 100 m (1-σ confidence level) in densely instrumented regions to the order of several kilometers in regions with a low instrumentation density (Ruigrok et al., 2023). Historically, the number of monitoring stations in the Netherlands was much smaller, implying larger location uncertainties and reduced detection capabilities (Dost et al., 2012).

In the Netherlands, regions exist where subsurface activities are densely spaced. An epicenter location error in the order of several kilometers implies that an earthquake may not be unambiguously associated with a specific geotechnical activity.

In KEM-07 (Vörös & Baisch, 2018), a classification scheme was introduced that accounts for the uncertainty in earthquake associations (Figure 15). This classification scheme proved to be valuable for testing geomechanical models and will be used in phase II of the current study.

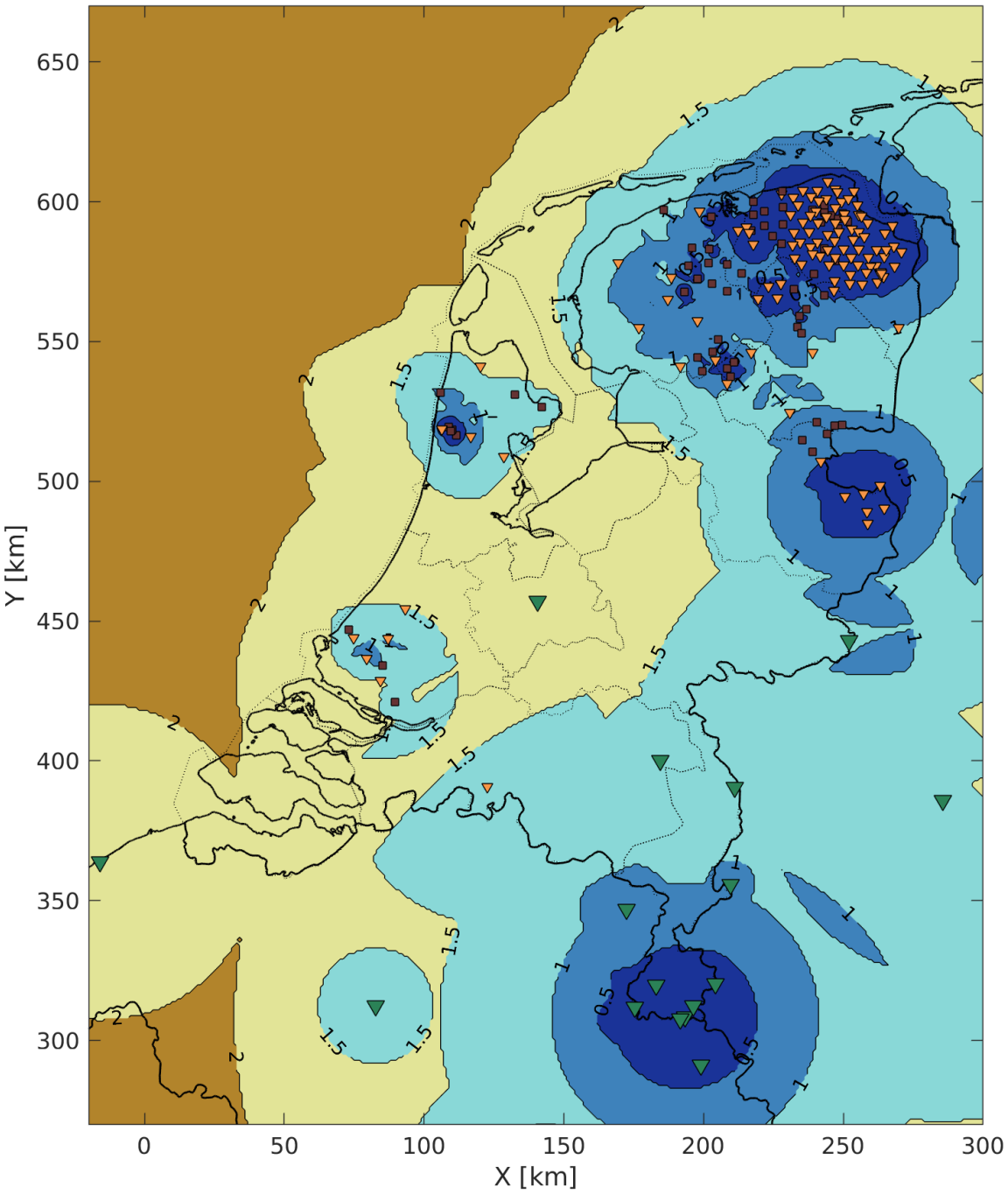
Y [km]
650
600
550
500
450
400
350
300
0
50
100
150
200
250
300
X [km]

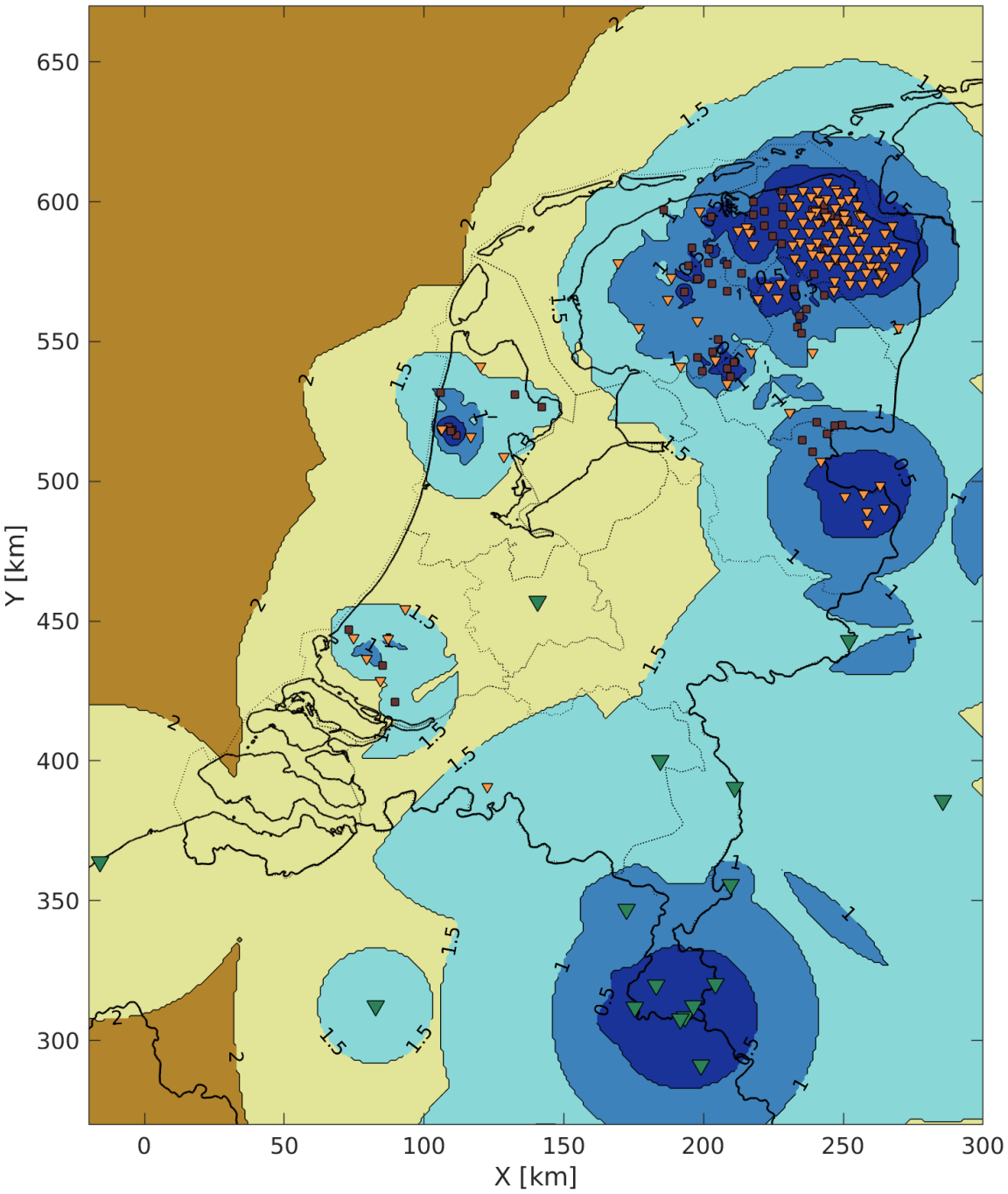

* For model assumptions see Ruigrok et al. (2023). Blue colours (from dark to light) indicate regions with MoC<0.5, MoC<1 and MoC <1.5. Yellow indicates MoC < 2, brown MoC > 2. More recent data can be downloaded from the KNMI data platform (KNMI, 2024)

Figure 14. Magnitude of completeness (MoC) over the Netherlands as of 2021, requiring a minimum number of 3 positive detections (Source: KNMI TR405 - Ruigrok et al., 2023).

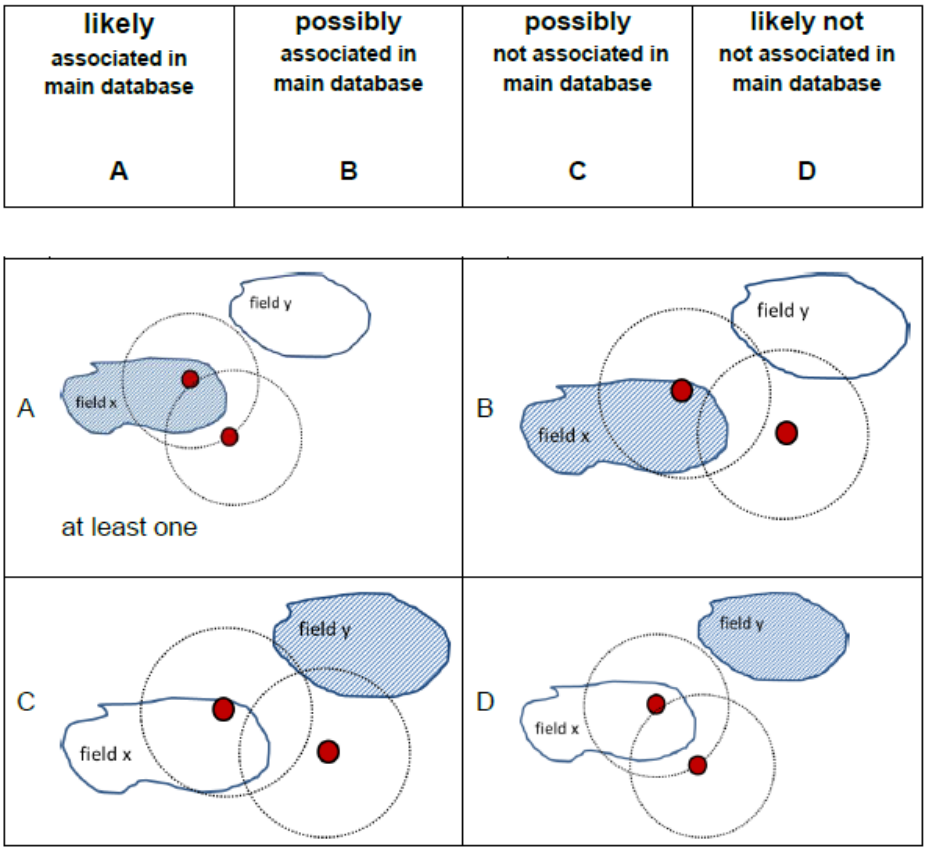

* Based on the epicentres of observed earthquakes (red dots) and their location uncertainty (dotted circles), a gas field (shaded area) falls into one of the following four categories: A) It is likely that the field hosted at least 1 earthquake. B), C) It is possible that the field hosted at least 1 earthquake. D) It is unlikely that the field hosted any earthquake.

Figure 15. Classification scheme developed in KEM-07 (Vörös & Baisch, 2018).

3.6 Induced seismicity due to natural gas extraction

The geomechanical processes leading to induced seismicity during gas production have been investigated in numerous studies (see Kühn et al., 2022 for an overview). It is well-understood that earthquakes are caused by poro-elastic stresses resulting from gas extraction and associated reservoir compaction. Seismicity can occur on internal and on boundary faults of a reservoir. Compaction induced Coulomb stress changes (compare with section 3.3) are largest at the contact area between reservoir and over-/underburden (Van den Bogert, 2015). Stabilizing, negative Coulomb stress changes tend to prevail on those reservoir faults, which are hydraulically connected to the depleting reservoir (Baisch et al., 2023; Smith et al., 2022)

Foulger et al., 2018 provide a global overview of show cases, where gas extraction has been associated with seismicity. Despite the enormously large number of gas production wells, they report only 3 dozen gas fields with seismic activity. Most of these fields with reportable data are in the Netherlands and in Northern Germany, indicating that gas-production related earthquakes occur only under very specific geological conditions. The figures reported by Foulger et al. (2018), however, are arguably subject of an observational bias. Many gas fields are not monitored by a local seismological network, and only a small subset makes available or publishes comprehensive datasets. Consequently, the lower level at which earthquakes in a gas field can be detected, e.g., by a national earthquake monitoring network, varies strongly. Furthermore, earthquakes detected by national networks may not routinely be checked for a correlation with gas production activities.

A detailed national summary for gas production induced seismicity in the Netherlands is presented by Muntendam-Bos et al. (2022). Thirty-eight gas fields in the Netherlands are associated with induced seismicity. While most of the events are small in magnitude ($M_L < 2.5$), several larger earthquakes have occurred. So far, earthquakes with $M_L>3$ occurred in the gas fields Bergermeer (up to $M_L=3.5$), Groningen (up to $M_L=3.6$), and Roswinkel (up to $M_L=3.4$).

3.7 Induced seismicity due to gas storage

Depleted gas fields can be used for underground gas storage (UGS). During the initial gas production phase, earthquakes can be caused by poro-elastic stresses related to reservoir compaction (see previous section). The seismic deformation is an irreversible (non-elastic or inelastic) process. For example, consider a case where an earthquake has occurred during initial gas production. Immediately after the earthquake has occurred, the stress-state on the hosting fault will be at most reduced by the amount of the coseismic stress-drop below stress criticality (e.g., Candela et al., 2021). In the Netherlands it is assumed that the coseismic stress-drop is generally smaller than 5 MPa (Staatstoezicht op de Mijnen, 2016), implying that seismically active faults would remain within a few MPa close to stress criticality after an earthquake has occurred.

Once turned into an UGS with injection and withdrawal cycles, earthquakes can be caused by poro-elastic stresses during re-filling (KEM-01, Ferronato et al., 2018). Using numerical simulations, KEM-01 and KEM-39 (Isotton et al., 2022) investigate under which conditions seismicity may occur during gas production and subsequent cyclic gas storage operations. KEM-01 considers inelastic deformation mechanisms that may lead to irreversible stress paths during cyclic storage operations. KEM-39 additionally considers geo-chemical effects that may alter the frictional behaviour of faults. Findings of the two studies consistently indicate that previously seismically active faults during initial gas production are most prone to seismicity during subsequent re-filling. This is consistent with the concept of a near-critical stress-state after an earthquake has occurred (see above). Furthermore, critical conditions during re-filling are reached only near the end of subsequent injection stages when the reservoir pressure reaches the virgin, pre-production pressure level (Figure 16).

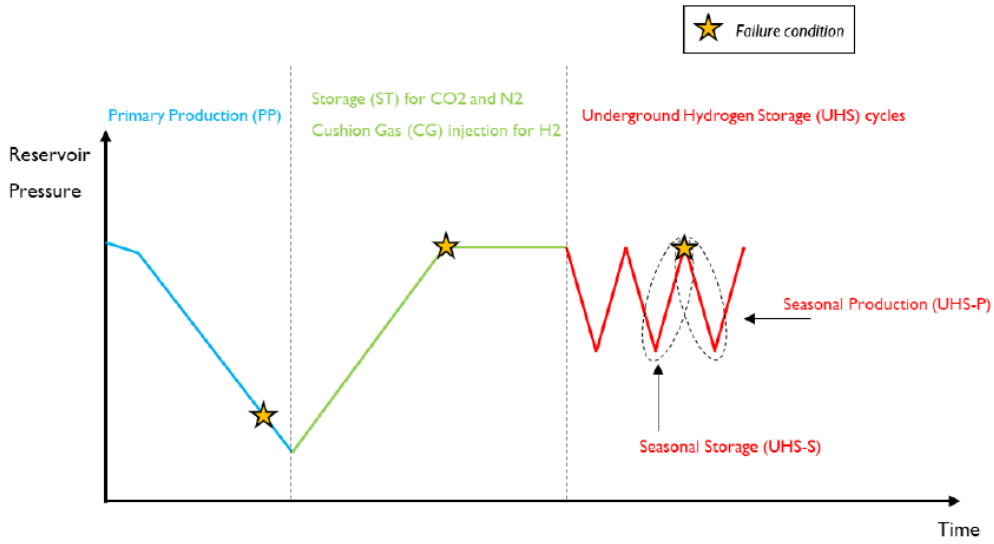

* Yellow stars indicate failure conditions according to geomechanical modelling in KEM-01 and KEM-39. Figure from KEM-39 (Isotton et al., 2022). Note that the geomechanical models cannot explain the occurrence of seismicity during an early phase of cushion gas injection.

Figure 16. Sketch showing the pressure evolution in a gas reservoir during initial production (blue), cushion gas injection (green) and seasonal production (red).

We note that loss of pore space through inelastic deformation during compaction is a relevant process (e.g. Hol et al., 2018, Pijnenburg and Spiers, 2020), which is not accounted for in the KEM-01/KEM-39 studies, where the reservoir is treated as a linearly elastic medium. Conceptually, reducing pore space could explain the occurrence of seismicity also at an early stage of the initial refill as observed in several UGS (see further in this section).

A geomechanical analysis by NAM (2016) indicates that stress paths remain (virtually) the same under depletion and re-pressurisation at the Norg UGS (the Netherlands), exhibiting little potential for seismicity occurring at a late stage of cyclic operations.

On a global scale, earthquakes exceeding M=3.5 are reported for two UGS. Three earthquakes in the range Mw=4.1 to Mw=4.3 are associated with the initial cushion gas injection into the Castor, Spain, UGS (Cesca et al., 2014). At the Hutubi, China, UGS, earthquakes up to ML=3.6 occurred during the first filling period (Tang et al., 2018).

The Netherlands have four operating UGS systems which utilise former natural gas reservoirs: Norg, Grijpskerk, Bergermeer and Alkmaar. Only the latter was not associated with seismicity during production. After Norg was converted into an UGS, a single additional event of M_L=1.1 occurred at the end of its initial injection to full capacity (Muntendam-Bos et al., 2022). Fifteen years after conversion and start of UGS operation at Grijpskerk, a single M_L=1.5 was recorded during cyclic operation (Muntendam-Bos et al., 2022). It should be noted, however, that the location accuracy and the associated possibility that the earthquake could have occurred in a neighbouring gas field have not yet been investigated (Grijpskerk was excluded from the earthquake-reservoir association performed in KEM-07, Vörös & Baisch, 2018). At the UGS Bergermeer, seismicity was closely monitored with a downhole geophone array allowing to detect reservoir earthquakes at the level of M_L=−1.5. The intensity of micro-seismic activity (M_L<1) during refill was strongest during the cushion gas injection, suggesting that previously critically stressed areas of the fault were re-activated by refill (Fenix, 2018).

3.8 Induced seismicity due to fluid disposal

Disposal of wastewater (e.g., co-produced fluid, stimulation fluids) in deep wells is a common technology associated with hydrocarbon production. By raising the fluid pressure, existing faults/fractures are destabilised when the ratio between shear to effective normal stress exceeds their frictional resistance (compare with Section 3.3). This is the most common mechanism to explain seismicity caused by wastewater disposal (National Research Council, 2013; Schoenball et al., 2018). Numerous cases of earthquakes caused by wastewater disposal are reported in the scientific literature (Foulger et al., 2018; Keranen et al., 2014), the largest of them exhibiting magnitude M_w=5.8 (Schultz et al., 2020).

There is a single recorded case in the Netherlands, where an earthquake has been attributed to wastewater disposal (M 2.8 at De Hoeve, Weststellingwerf; TNO, 2015).

3.9 Induced seismicity due to oil extraction

In principle, the same geomechanical processes leading to gas production induced seismicity (section 3.4) may apply to seismicity induced by oil production. Foulger et al. (2018) note, however, that “in many oilfields multiple processes are underway simultaneously including oil and gas extraction, waste-water disposal, water injection to aid oil recovery and hydrofracturing”. Associating observed earthquakes to one or the other mechanism therefore is a challenging task. Despite the enormous number of producing oil wells worldwide, Foulger et al. (2018) report only 8 cases where earthquakes are possibly associated with oil extraction. None of these cases is in the Netherlands.

3.10 Induced seismicity due to salt mining

The seismicity inducing mechanisms associated with salt solution mining have not been completely understood, yet. For smaller seismic events with M<1, small slip events due to stress equilibration in the proximity of salt caverns (Muntendam-Bos et al., 2022) and shear and rock fall events due to cavern closure (Bosq et al., 2020; Dyagilev et al., 2013) have been proposed. Other proposed mechanisms include hydrofracturing, enhanced mass removal without sufficient compensation by salt creep (Foulger et al., 2018) and fault slippage due to a water injection related elevated pore pressure (Wang et al., 2020).

The global data base "HiQuake" contains eight cases of seismicity postulated to be associated with solution mining (Foulger et al., 2016). These include small magnitude earthquakes as well as earthquakes to the level of M_L=5 (Nicholson & Wesson, 1992). Another M_L 4.6 earthquake occurred in 1985 in association with solution mining of salt from depths of 800–1800 m at the Zigong salt mine, Sichuan Province (Li et al., 2007). More recently, a seismic sequence consisting of an M=6 earthquake, followed by another four M>5 events were observed in the Sichuan province in 2019. These events were attributed to water injection for local salt solution mining (Wang et al., 2020).

Muntendam-Bos et al. (2022) present two case examples for induced seismicity associated with salt solution mining in the Netherlands. In the region of Twente, salt extraction is conducted around the cities of Hengelo and Enschede at a depth of approximately 400-500 m. From 2016-2022, the network recorded 59 small events between M_L of -2.8 and 0. In the Heiligerlee salt dome, brine is leached from twelve caverns located at a depth of 700-1600 m. Until 2020, 60 events with local magnitudes between -1.2 and 0.7 were recorded.

3.11 Induced seismicity due to geothermal exploitation

The geothermal systems considered in this study consist of production and injection wells. Hot fluid is produced through one or more production wells. After extracting heat, the cooled fluid is re-injected into the geothermal reservoir through one or more injection wells. Frequently, seismicity in this type of reservoir is thought to be caused by the hydraulic overpressure applied for re-injecting fluids: By raising the in-situ fluid pressure, fractures are destabilised when the ratio between shear to effective normal stress exceeds their frictional resistance (KEM-06, A'Campo et al., 2020; Evans et al., 2012; Ge & Saar, 2022; Zang et al., 2014). Additional mechanisms were discussed that could be relevant for the occurrence of earthquakes in geothermal reservoirs. These include chemical changes of fault properties (Buijze et al., 2019) as well as poro- and thermo-elastic stresses associated with fluid injection (Buijze et al., 2019; Jeanne et al., 2017; Rozhko, 2010) or unbalanced production (Fialko & Simons, 2000). Poro-elastic effects can reach further in a short timescale but decay rapidly with distance. During long-term injection, changes in temperature cause volumetric strain of the rock mass, which leads to stress changes within and around the volume experiencing a temperature change. Stresses caused by cooling accumulate over time and may become the dominating effect for long-term injections. The relevance of poro-thermo-elastic mechanisms, however, remains unclear as it is difficult to relate observed earthquakes to a specific mechanism.

There is a single case in the Netherlands, where earthquakes have been attributed to geothermal production. Several earthquakes with magnitude up to M_L=1.7 occurred in the "Californië" geothermal system (labelled CWG/CLG in Figure 13). These earthquakes were interpreted to be caused by cooling stresses (Vörös & Baisch, 2022).

In the neighbouring geothermal technologies ATES and HT-ATES (section 2.7.2) hot water is injected for seasonal storage and produced during times of heat demand (Stricker et al., 2020). As of 2018, about 2800 ATES systems were in operation, mostly in the Netherlands, Sweden, Denmark, and Belgium (Fleuchaus et al., 2018). In principle, ATES/HT-ATES could cause seismicity due to the same mechanisms discussed above. Conceptually, however, the relative proximity to surface of ATES

schemes and their host rock lithology (porous sedimentary rocks) precludes the build-up of sufficiently high stresses and hence a sufficiently large seismic energy release when failure occurs.

Our literature study has indicated that neither ATES nor HT-ATES were associated with induced seismicity yet.

3.12 Induced seismicity due to hydraulic fracturing

Hydraulic fracturing ("fracking") is a technology to improve the inflow performance of a well in a reservoir. By forcing a fluid under very high pressure into a rock formation, cracks are artificially created and enhanced (Detournay, 2016). To generate a seismic signal, the speed of the crack opening must be in the range of seismic wave speeds, i.e. in the order of kilometres per second (Aki & Richards, 2002). The mechanical opening of a pure tensile crack is controlled by the injected fluid volume. As a result, the crack opening velocity is orders of magnitude lower than the seismic wave velocities and the pure tensile crack does not generate a measurable seismic signal (Keppler et al., 1988). Induced seismicity only occurs when stress changes lead to abrupt shear failure on an existing fault. Different concepts have been proposed to describe the occurrence of induced seismicity as a secondary phenomenon of tensile rupture propagation (for an overview see Eisner & Staněk, 2018).

On a global scale, hydraulic fracturing induced earthquakes are predominantly observed in shale-gas reservoirs, where the strongest earthquakes exceed magnitude 5 (Schultz et al., 2020). The largest magnitude earthquakes occurred during multi-stage fracturing, invoking large fluid volumes. In the Netherlands, hydraulic fracturing operations were performed in the porous (soft) sandstones using much smaller fluid volumes (EBN, 2014). In The Netherlands, based on available data, there is no evidence that hydraulic fracturing in the Netherlands has caused measurable induced earthquakes. For operations before 1986 and for very small earthquakes below the detection threshold, it cannot be ruled out that undetected seismicity occurred (TNO, 2018).

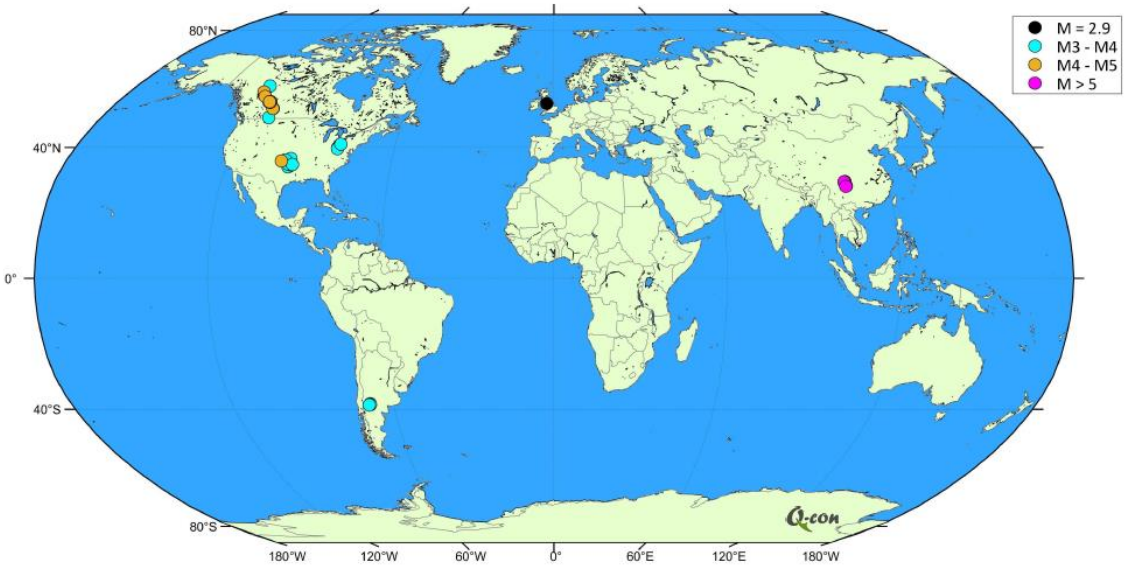

Figure 17. Global overview of the strongest earthquakes associated with fracking in unconventional reservoirs. Figure from Baisch et al. (2021).

3.13 Static and dynamic triggering of seismicity

Earthquakes can be triggered by static and dynamic stress transfer. For example, static stress transfer from large natural earthquakes can have an impact on the aftershock activity (King et al., 1994; Stein, 1999). Similarly, small magnitude earthquakes transfer stresses to their surroundings. In the context of fluid injection induced seismicity, stress transfer of many earthquakes occurring on the same fault

can constructively superimpose, leading to pronounced stress concentration at the periphery of seismic activity (Baisch et al., 2015). These locations can be very close to stress criticality and become susceptible to another process called dynamic or remote triggering: Long period surface wave trains of natural earthquakes can cause elastic stress changes sufficiently large for remotely triggering earthquakes (Hill, 2008). Such remote triggering of seismicity has been observed especially in geothermal areas (e.g., Baisch et al., 2006; Prejean, 2004), although the underlying physical mechanisms are not yet fully understood (Hough, 2005).

4

LEAKAGE

4.1 Summary and conclusions

This chapter gives an answer to the following research question as defined in section 1.4.1

1. What information is available about interactions between different adjacent underground (man-made) activities, natural processes, and about the cumulative mutual effect? This chapter covers the answer in the context of topic **c) leakage**

Methane leakage along damaged wellbores after decommissioning is a well-known risk within the oil and gas industry. Factors like poor cement design, shrinkage, and chemical degradation of cement can contribute significantly to wellbore integrity failures. International experiences show varying rates of well leakage, influenced by factors like well type, age and depth, geographical and geological conditions, and the well plugging status. While methane seepage through natural faults is recognized, it is not considered a primary concern compared to wellbore integrity issues. Understanding aquifer pressure redistribution and long-term fluid migration after reservoir decommission can give valuable information on the leakage potential. For the Groningen Gas field this occurs on the timescale of centuries. The cumulative effects of small neighbouring gas fields remain undiscovered (KEM-19 (2022); KEM-19b).

4.2 Samenvatting en conclusies (NL)

Dit hoofdstuk geeft antwoord op de volgende onderzoeksvraag zoals gedefinieerd in sectie 1.4.1

1. Welke informatie is beschikbaar over interacties tussen verschillende aangrenzende ondergrondse (door de mens gemaakte) activiteiten, natuurlijke processen, en over het cumulatieve wederzijdse effect? Dit hoofdstuk behandelt het antwoord in de context van onderwerp **c) lekkage.**

Methaanlekkage langs beschadigde olie en gasputten na buitenbedrijfstelling is een bekend risico in de olie- en gasindustrie. Factoren zoals slecht cementontwerp, krimp en chemische degradatie van cement kunnen aanzienlijk bijdragen aan het falen van de putintegriteit. Internationale ervaringen laten variabele percentages putlekken zien, die worden beïnvloed door het type, de leeftijd, diepte en plugstatus van de put, en de geografische en geologische omstandigheden. Hoewel methaanlekkage via natuurlijke breuklijnen wordt erkend, wordt dit niet beschouwd als een primair probleem in vergelijking met putlekkage. Inzicht in de herverdeling van druk in reservoirs na de buitenbedrijfstelling, en de daarmee geassocieerde lange termijn vloeistofmigratie kan waardevolle informatie opleveren over het lekkagepotentieel. Voor het Groningengasveld gebeurt dit op de tijdsschaal van eeuwen, waarbij de invloed van cumulatieve effecten met kleine naburige gasvelden niet bekend is (KEM-19 (2022); KEM-19b).

4.3 Introduction

Climate change owing to greenhouse gas emissions is widely acknowledged by scientists as the primary threat to humanity (Holechek et al., 2022). Consequently, unabated oil and natural gas production will decline, and thus even more fields that shut in for economic reasons, are going to be decommissioned. Leakage of methane in the energy sector in particular, and that of other greenhouse gases have received a lot of attention by industry, the research community and policy makers (cf. Methane Abatement - Energy System - IEA)

An essential part of decommissioning is the restoration of geological barriers that prevent vertical fluid migration. One crucial concern of decommissioned gas fields is the potential leakage of deep thermogenic methane into shallow aquifers, a recognized issue within the oil and gas industry for many years (Erno and Schmitz, 1996; Harrison, 1983; Schout, 2020). Methane found in shallow aquifers can lead to groundwater contamination, greenhouse gas emissions, and, in substantial quantities, pose an explosion hazard for groundwater users, who sometimes even find their drinking water to be explosive. It should be noted that methane occurs commonly and naturally in shallow aquifers, which is usually due to local methanogenesis, a process where microbial bacteria break down organic matter into biogenic methane (Whiticar, 1999). Distinction between naturally occurring biogenic methane from deep thermogenic source can be achieved through isotope analysis (Schout, 2020).

4.4 Wellbore leakages

Oil and gas wells are constructed to prevent the escape of fluids into shallow aquifers. However, in practice, this can prove challenging, particularly in the period following the abandonment of the gas field (Brufatto et al., 2003; van Gessel, 2019; LeMay et al., 2019; Moghadam et al., 2023). In the Netherlands, wells are sealed by means of a well plug, which does not seal the entire wellbore but only plugs the well around the boundaries of permeable formations (see Figure 19). The work procedure is known as plugging and abandonment (P&A) following the Dutch Mining Decree (NOGEPA, 2019). Figure 18 illustrates in detail which potential leakage pathways exist around a segment of a wellbore. When leakage can occur along these pathways, it is referred to as a well barrier failure (Davies et al., 2014).

For deep thermogenic methane to migrate vertically to the surface, multiple successive well barrier failures must occur, establishing a pathway for leakage from reservoir depth towards the atmosphere. This scenario is also known as a type of well integrity failure. Multiple factors affect wellbore integrity, most importantly the quality of cement design, and the susceptibility of cement to shrink and chemically degrade (Yousouf et al., 2021).

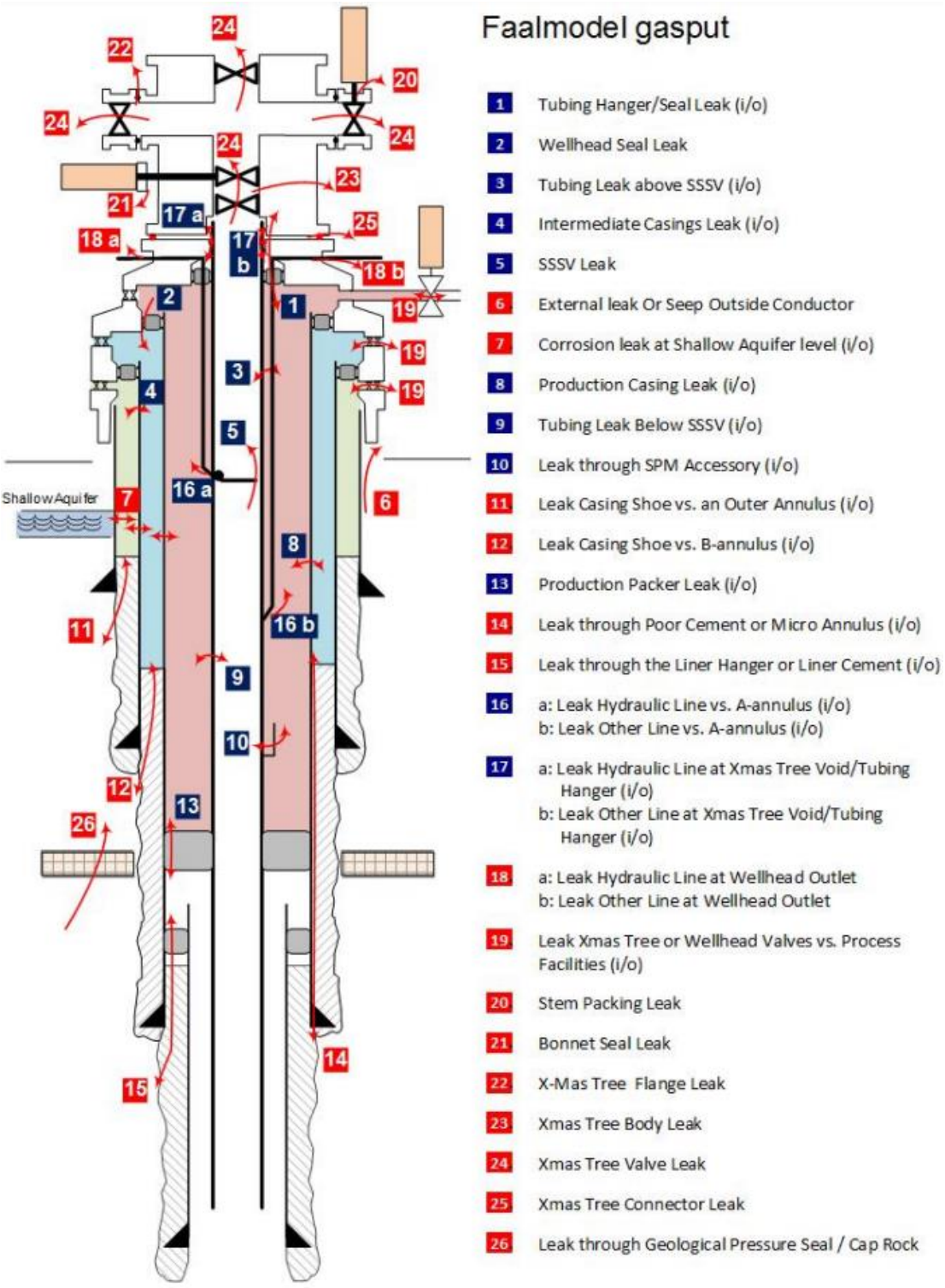

Figure 18. A schematization of the possible gas leakage pathways leading to well integrity failure (Source: SodM, 2019). Note that the figure does not show leakage between the cement sheath and surrounding caprock, and between the borehole casing and the cement sheath.

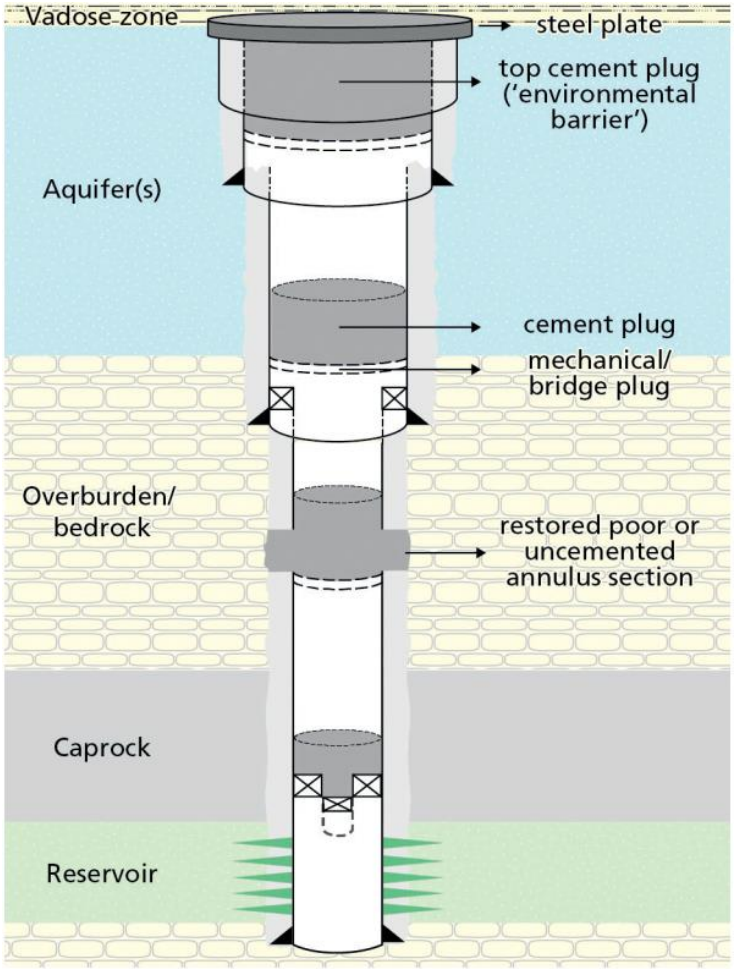

Figure 19 Typical design of an onshore Dutch gas well after decommissioning following the Dutch Mining Decree (NOGEPA, 2019). (Source: Schout, 2020)

4.4.1 Poor cement design

Well plugs contain cement as part of their concrete construction. Various types of cement can be used, depending on the required properties and uses. A poor choice of cement design leads to cement sheath degradation and thus to potential wellbore integrity failure (Turley, 2014; Visser, 2011; Garg and Gokavarapu, 2012; Wilcox et al., 2016). The quality and applicability of the cement depends mainly on its rheological properties determining the flowability and stability of the cement (Lootens et al., 2004), and mechanical properties such as the compressive and tensile strength (Yousouf et al., 2021; Thiercelin et al., 1998; Goodwin and Crook, 1992) to withstand the natural and induced mining stresses that occur in the subsurface. Nevertheless, the durability of cement in well bores Is finite and thus after a long period they still might lose their integrity; however, this phenomenon is poorly reported in literature and understood.

4.4.2 Cement shrinkage

Shrinkage of cement sheaths at the cement-caprock interface is a known hazard in the oil and gas industry that involves the removal of free water from the cement mixture into the cement matrix through a process called hydration of the cement matrix. If the cement cannot absorb sufficient water from the surrounding caprock to compensate the hydration process of the cement matrix, the cement will reduce in volume (Chenevert and Shrestha, 1991; Dusseault et al., 2000; Kosmatka and Wilson, 2011; Sasaki et al., 2018). As a result of cement shrinkage, the contact stress between the cement sheath and the neighbouring caprock can fall below the local pore pressure, allowing gas flow along

the cement-caprock interface, also referred to as the well bore annulus. Experimental setups on a laboratory scale indicate that the expected shrinkage rate of various types of cement can range between 0.6 and 6 volume percentage (Yousouf et al., 2021). However, the measured bulk shrinkage volumes in the lab may not be representative under wellbore conditions (Sasaki et al., 2018).

4.4.3 Chemical degradation

Chemical reactions in the subsurface affects the in-situ cement sheath quality of wellbores. Cement sheaths degrade chemically when in contact with aggressive acidic fluids, such as carbonic acid, sulphuric acid and hydrochloric acid; all of which can occur naturally in oil and gas fields, (Omosebi et al., 2017a,b). A common reactant with cement is CO_2 which can occur naturally both in gas and liquid phase. By exposing cement to dry CO_2 gas, the calcium hydroxide of the cement is carbonated to form calcium carbonate. Given the molar volume of calcium carbonate is higher compared to the original carbon hydroxide, the total volume increases, making the cement stronger and less permeable (Neville, 1995; Hartmann et al., 1999).

When the cement is exposed to wet or dissolved CO_2 instead of dry CO_2, the reaction chemistry with the cement changes drastically, because CO_2 in water creates carbonic acid (H_2CO_3) which reacts and corrodes with different components of the cement and casing steel (Cailly et al., 2005; Barlet-Gouedard, 2006; Scherer et al., 2015). Carey et al. (2007) and Crow et al. (2010) found evidence of chemical degradation of cement sheaths in wells by investigating multiple core samples including casing, cement and caprock from 30-year-old production wells in the United States. In those wells, oil was extracted using CO_2 injection as a pressure driver. Permeability analysis showed that the sealing well plug remained largely intact, preventing significant flow of CO_2. However, CO_2 migration along the casing-cement and cement-caprock interfaces was substantiated by the presence of CO_2 requiring carbonate precipitates. This implies that the casing-cement interfaces are the highest risk component regarding performance of wellbore integrity.

Most studies on chemical degradation of cement are carried out for situations with high CO_2 concentrations such as Carbon Capture and Storage (CCS), or sites where oil recovery is enhanced by injecting CO_2. Many natural gas reservoirs such as the Groningen Gas field contain much lower CO_2 concentrations of around 1 volume percentage (De Graaf et al., 2011), significantly reducing the cement degrading potential due to chemical reactions.

4.4.4 International experience with gas leakage

As discussed before, well integrity failure can result in upward migration of gasses through the annular space and reach the wellhead. When the wellhead is shut in, gas will accumulate and experience increasing pressures, which is referred to as Sustained Casing Pressure (SCP). When the wellhead is not sealed, the gas is allowed to vent to the atmosphere and is referred to as Surface Casing Vent Flow (SCVF). Both SCP and SCVF are relatively easy to measure as long as the well head is present. However, in case a well is decommissioned or does not have an intact well head, detection is only possible via soil gas flux measurements (Kang et al., 2014), or by monitoring the methane concentrations in the shallow aquifers (Van Stempelvoort and Jaworski, 1995; Schout, 2020).

The amount of reported well leakage varies greatly worldwide ranging from 1.9% to up to 75% of the registered wells, depending on the study area (Davies et al., 2014; Yousouf et al., 2021). Factors that contribute to this variability are the well type, age and depth (Watson and Bachu, 2009; Ingraffea et al., 2014), geographical and geological conditions, and plugging status (Van der Kuip et al., 2011; Kang et al., 2016). Especially well age seems to be important since the regulations and techniques of well plugging and abandonment have improved over time (Brufatto et al., 2003; Schout, 2020). An extensive Dutch study on integrity failure in 28 abandoned gas wells and 1 oil well which have been plugged, cut and buried below the ground surface, showed that of these 28 wells only 1 well was proven to leak gas from a thermogenic, i.e. deep origin source (Schout, 2020).

4.5 Leakage along faults

Methane leakage through naturally occurring faults and fractures is widespread phenomenon and has been observed in all continents (Etiope, 2015; Hovland, 2012). In fact, these natural seeps are the oldest tools to estimate the quantity of oil and gas resources (KEM-19, 2022). However, such natural macro-seeps are only observed for a relatively small subset of oil and gas reservoirs (Etiope et al., 2009).

Besides natural leakage, the possibilities for gas leakage along faults have been studied to evaluate the potential of Carbon Capture and Storage (CCS) in depleted gas fields (Rutqvist, 2012; Moritz, 2015), and to identify leakage rates from natural CO_2 reservoirs (Miocic et al., 2019). Although the risk associated with methane leakage along faults is acknowledged, it has not been identified as a major risk. If faults were leaking during the reservoir history at a rate that is considered harmful near the surface, gas is not likely to have accumulated to form a reservoir. Moreover, as opposed to CCS sites, depleted gas reservoirs after abandonment will have lower pore pressures than the initial pressure, which is known to reduce the permeability of fractures (Wiprut and Zoback, 2002).

Reactivation of faults and fractures can enhance bulk permeability, as observed in Enhanced Geothermal Systems (EGS) (Olasolo et al., 2016; Zimmerman et al., 2011). Predicting changes in fault permeability upon reactivation is challenging, particularly in sedimentary rocks (Zoback and Gorelick, 2012; Jeanne et al., 2018). Besides the changing permeability, fault activation can result in episodic release of hydrocarbons from the hydrostatic deep subsurface through a process referred to as fault-valve behaviour (Sibson, 1990). Since depletion of a gas reservoir can potentially cause reactivation of faults (Candela et al., 2019), the main risk for fault leakage would be associated with potential increased fault permeability during periods of fault reactivation.

Other pathways for gas leakage are faults associated with salt diapirs piercing through the overlying caprock (Niemann et al., 2005). Given the presence of both salt diapirs and gas fields in the Groningen area, this could be relevant. However, the gas first needs to escape from the reservoir through the sealing layers, which is unlikely given the impermeable nature of the Zechstein salt formation, while active faults in the region tend to heal fast due to its ductility (Ten Veen et al., 2012; Hunfeld et al., 2020).

4.6 Long-term fluid migration

Wildenborg et al. (2022) conducted a numerical study on the long-term fluid migration in abandoned wellbores within the Groningen gas field. The research suggests that methane leakage from depleted gas reservoirs poses minimal risk, as it is more likely for fluids to infiltrate the depleted reservoir instead. However, in the case of small gas reservoirs with active water-drive, the influx of water could re-pressurize the gas, potentially leading to continued leakage.

The primary factors that contribute to methane leakage over a hundred-year period after abandonment were investigated by means of sensitivity analysis. Where the cement sheath suffers severe damage (investigated by applying an average permeability of 100 mD for the cement), the model predicts significant gas leakage at a rate of 4200 kg/year through the damaged well bore entering the shallow aquifer and the atmosphere, which aligns with field observations of Schout et al. (2019). However, these rates are achievable only when both the reservoir and cap rock are at hydrostatic pressure. For this worst-case scenario, it was found that a methane plume in a shallow aquifer could extend up to several hundred meters around the leakage source.

The mentioned study also examined the impact of a relatively shallow methane source in the Breda formation, located 50–200 meters below the shallow aquifer system. This investigation revealed significant leakage rates of up to 330 kg/year through the damaged well bore. It can be concluded that besides monitoring the reservoir pressure, knowledge of shallow methane sources is equally important. Especially when considering that the section of a wellbore that needs to be damaged to

facilitate methane leakage is directly proportional to the distance between the methane source and the shallow subsurface.

4.7 Aquifer pressure redistribution

Fluid migration is common phenomenon in the oil and gas industry. It occurs both during and after the production of an oil or gas field. The production of oil and gas results in depletion of the reservoir causing fluids from adjacent formations to migrate towards the reservoir. After abandonment of a reservoir this fluid migration continues, resulting in long term regional aquifer pressure redistribution. Fluid migration has been observed in many field sites in the north of The Netherlands (van der Molen et al., 2019; Kole et al. 2020).

In the Netherlands the reservoir pressure redistribution has been extensively studied for the Groningen gas field and its neighbouring regions (Wildenborg et al. 2022). To assess the pressure redistribution, a simplified, 3D-regional, two-component numerical fluid flow model was employed for a 500-year timeframe following abandonment. The findings indicated that aquifer pressure redistributions happen on a timescale of centuries. However, the model solely addressed the impact of Groningen gas field depletion on the surrounding area. It did not consider the influence of pressure interaction with smaller neighbouring gas fields due to limitations in the model's resolution, leaving this aspect undisclosed. Consequently, the overall understanding of aquifer activity and connectivity on a regional scale remains incomplete. The effect of smaller gas fields on the regional scale is currently being explored in the KEM-19b study.

5

EFFECTS

5.1 Summary and conclusions

This chapter gives an answer to the following research question as defined in section 1.4.1

2. In what way are buildings affected by processes and interactions?

This chapter introduces the impact of subsidence and induced seismicity on buildings. Most of the research on the effects of vibrations from induced seismicity happened after the M 3.6 Huizinge earthquake of 16 August 2012. The focus was on the use of models to calculate peak ground velocity based on magnitude and distance to the hypocentre. A so-called Empirical Ground Motion Model for induced seismicity from the Groningen field is used for damage assessment. KNMI developed a specific model for smaller earthquakes in gas fields outside Groningen.

Deep or shallow subsidence results in horizontal extension and angular distortion in buildings, and this can lead to damage. Mining-induced subsidence can have direct effects, resulting in horizontal strains, and it can indirectly affect the groundwater level, leading to differential settlement and angular distortion in a building. Different aspects of subsidence, such as sagging and hogging, can occur at different scales with different impacts on buildings. Lower bound criteria for damage are provided based on the damage indicators horizontal strain and angular distortion. Different methods exist for determining horizontal strain and angular distortion due to deep subsidence.

5.2 Samenvatting en conclusies (NL)

Dit hoofdstuk geeft antwoord op de volgende onderzoeksvraag zoals gedefinieerd in sectie 1.4.1

2. Op welke manier worden gebouwen beïnvloed door processen en interacties?

Dit hoofdstuk beschrijft de impact van diepe en ondiepe bodemdaling en trillingen door geïnduceerde aardbevingen op gebouwen. Het meeste onderzoek naar de effecten van trillingen door geïnduceerde aardbevingen op gebouwen is gedaan na de M 3,6 aardbeving bij Huizinge van 16 augustus 2012. De focus lag op het gebruik van modellen om de piekgrondsnelheid te berekenen op basis van magnitude en afstand tot het hypocentrum. Een zogenaamd Empirisch Ground Motion Model voor geïnduceerde aardbevingen uit het Groningen-veld wordt gebruikt voor schadebeoordeling. KNMI heeft een specifiek model ontwikkeld voor aardbevingen uit de kleine gasvelden buiten Groningen.

Bodemdaling als gevolg van diepe of ondiepe bodemdaling resulteert in horizontale rek en hoekverdraaiing in gebouwen, en dit kan leiden tot schade. Door mijnbouw veroorzaakte bodemdaling heeft directe effecten resulterend in horizontale rek. Het kan ook indirecte effecten hebben op het grondwaterpeil, wat leidt tot differentiële zettingen en hoekverdraaiing in een gebouw. Verschillende aspecten van bodemdaling, zoals convexe en concave bolling, kunnen op verschillende schaal voorkomen en met verschillend effect op gebouwen. Ondergrenzen voor schade worden gegeven op

basis van de belangrijkste schade-indicatoren horizontale rek en hoekvervorming. Er zijn verschillende methoden om horizontale vervorming en relatieve rotatie als gevolg van diepe bodemdaling te bepalen.

5.3 Introduction

The previous chapters describe processes occurring in the subsurface that have impact at ground surface. These processes are both natural and man-made or man-induced. Chapter 6 describes interactions between the different processes; it also focuses on influence distances. People living in the Grijpskerk area are mainly worried about how these processes and interactions affect buildings and their foundation.

This chapter specifically explores how subsidence and induced seismicity affect buildings. For this, the processes that can cause damage are discussed. The discussion is bases on current knowledge and addresses gaps in our understanding. As a consequence of the damage to buildings in Groningen province, most research used is to focus on its impacts. Subsidence got less attention; it was regarded a minor factor in causing damage in the Groningen area. The attention was laid on the impact of mining-induced subsidence on the safety of dikes and water-management systems under the jurisdiction of the waterboards.

The recent shift in attention towards subsidence results from awareness of the cumulative effects of mining on the outskirts of the Groningen earthquake-affected area, especially in regions with active salt mining. On top of this, there is a growing concern regarding groundwater-caused foundation damage throughout The Netherlands (Rli, 2024 [6]). This is triggered by a series of dry summers related to climate change. This increased awareness highlights the importance of understanding the impact of subsidence on structures.

5.4 Effects of vibrations due to induced seismicity on buildings

5.4.1 Models for induced seismicity

A considerable amount of research has been carried out to understand the impacts of induced seismicity in the Groningen area. The research gained momentum following the occurrence of the M 3.6 Huizinge earthquake on August 16, 2012. This significant seismic event led to the creation of an organization dedicated to settling damage claims, and it is currently managed by the IMG due to the substantial number of claims. Outside the Groningen field and UGS Norg, the CM advises on damage due to induced seismicity in small gas fields. Additionally, this event heightened awareness about the increased risk that induced seismicity poses to the people of Groningen, surpassing that of other regions in The Netherlands. Consequently, a program aimed at reinforcing buildings was initiated, and it is presently under the management of the NCG.

Because of the risk concerns, much of the research was focused on the impact of induced seismicity on the structural integrity of buildings. This research dealt with modelling the impact of different risk scenarios and involved the development of large-scale laboratory tests where one-to-one scale buildings were subjected to earthquake vibrations on shake tables. The research culminated in an operational approach where buildings in the high-risk areas of Groningen where individually analysed on structural integrity and later through a typology approach developed by TNO. The typology approach allows for a faster and simpler evaluation of the safety, because the evaluation can be done on groups of buildings instead of individual buildings.

For calculating the vibrations at any location resulting from induced earthquakes, models are utilized, based on scientific research and observations from the KNMI sensor network.

[6] https://www.rli.nl/pers/2024/help-huiseigenaren-en-huurders-bij-funderingsschade

The focus has been on creating a model for risk assessment for Groningen, particularly predicting ground acceleration for larger events (magnitude M=4 to M=5 and above). Several reports document the development of Ground Motion Prediction Models (GMM). GMM version 6 was used in the 2021/2022 hazard and risk assessment (Bommer et al., 2019), while GMM version 7 will be applied in future assessments (Bommer et al., 2021).

An Empirical Ground Motion Model (EGM) was also developed for smaller earthquakes (M=1.8 to M=3.6), specifically for building damage. The model covers peak ground acceleration, peak ground velocity, and Vtop, crucial for building damage assessment and compliance with SBR Guidelines (SBR, 2017). The Empirical Ground Motion Model, last updated in 2019, incorporates records from 2018 earthquakes and recalibrations based on the KNMI seismic monitoring network data (Bommer et al., 2019). For determining the effects of induced seismicity of the smaller gas fields outside the Groningen gas field, a model is used that is developed by KNMI, largely based on the Bommer model but adjusted to recorded earthquakes from small gas fields (Ruigrok and Dost, 2020), see also section 6.5.

With these models a Peak Ground Velocity is calculated (in mm/s) as a function of magnitude and distance to the hypocentre. The uncertainties inherent in the sensor recordings and the computational models are considered as margins in the model outcomes. Currently, the amplification effects of the shallow subsurface is not yet incorporated in the Empirical Ground Motion Model, contrary to the GMM, where the shallow ground amplification effects are implicitly modelled.

5.4.2 Damage indicators and thresholds

The Commissie Mijnbouwschade (CM) and Instituut Mijnbouwschade Groningen (IMG) use an exclusion limit of 2 mm/s for vibrations caused by an earthquake, calculated with a 1% probability of exceeding. This criterion is identical for induced earthquakes from the Groningen area and from all the other induced earthquakes from small gas fields.

When evaluating a causal relationship in the case of vibrations from induced earthquakes, the CM and IMG adheres to the SBR Vibration Guideline A as the norm (SBR, 2017). The threshold value provided in this guideline implies that if the vibration values are below this threshold, the likelihood of damage due to vibrations (thus also vibrations from earthquakes) is assumed to be less than 1%. It is thus a conservative standard.

Much practical experience has been gained with the application of the SBR Vibration Guideline Part A. The guideline was assessed for the 2017 revision based on documented practical cases. Furthermore, after the publication of this version, additional scientific research has been conducted in the form of model-based determination of the probability of damage to masonry buildings, confirming the mentioned likelihood of damage (Korswagen et al., 2022).

The model-determined vibrations are compared against the thresholds from the SBR Vibration Guideline A. If these thresholds are not exceeded, it is reasonably assumed that there is no causal relationship between the vibrations and damage to a building. If the threshold is exceeded, further site-specific damage assessment has to take place to assess the causal relationship between damage and mining-induced earthquakes.

5.5 Effects of subsidence on buildings

Buildings can deform due to many causes, such as self-weight, changes in temperature, changes in moisture content, or foundation movements. All of the above may lead to a strain in the building which in turn may lead to damage. This section focuses on the strain in induced in a building due to deep subsidence and shallow subsidence.

The relevant indicator to determine the likelihood of damage due to settlements is the horizontal strain in the masonry. This horizontal strain can be transferred directly by the horizontal strain on the foundation (the building can be horizontally stretched or compressed), as well as by a curvature or a

differential displacement of the foundation. As a result, the building will deform, causing the horizontal strains in the masonry. The total strain in the masonry is the sum of the horizontal strain in the foundation and the strain due to the angular distortion of the foundation. Tilt in buildings is an indicator that is considered less relevant for the development of damage.

The angular distortion is determined by the curvature and any differential displacement of the foundation. Therefore, the criterion for the occurrence of damage is a combination of horizontal strain and relative rotation at the foundation level. Horizontal strain is explained further in section 5.5.3 and angular distortion is explained further in section 5.5.4.

5.5.1 Effect of deep subsidence

Deep subsidence leads to a movement of the ground level, which, in addition to settlements, results in rotations and curvatures of the ground level, which can have an impact on the foundation of a building (TNO, 2021). Due to the gradual shape and thus small curvature of the subsidence bowl the building usually does not experience a significant angular distortion. Due to the curvature, the subsurface does experience horizontal strain, either due to 'hogging' leading to extension or due to 'sagging', leading to compression, depending on the location of the building respective of subsidence bowl (Figure 20). Only a portion of this horizontal strain will actually be transferred to the building, depending on the character of the foundation.

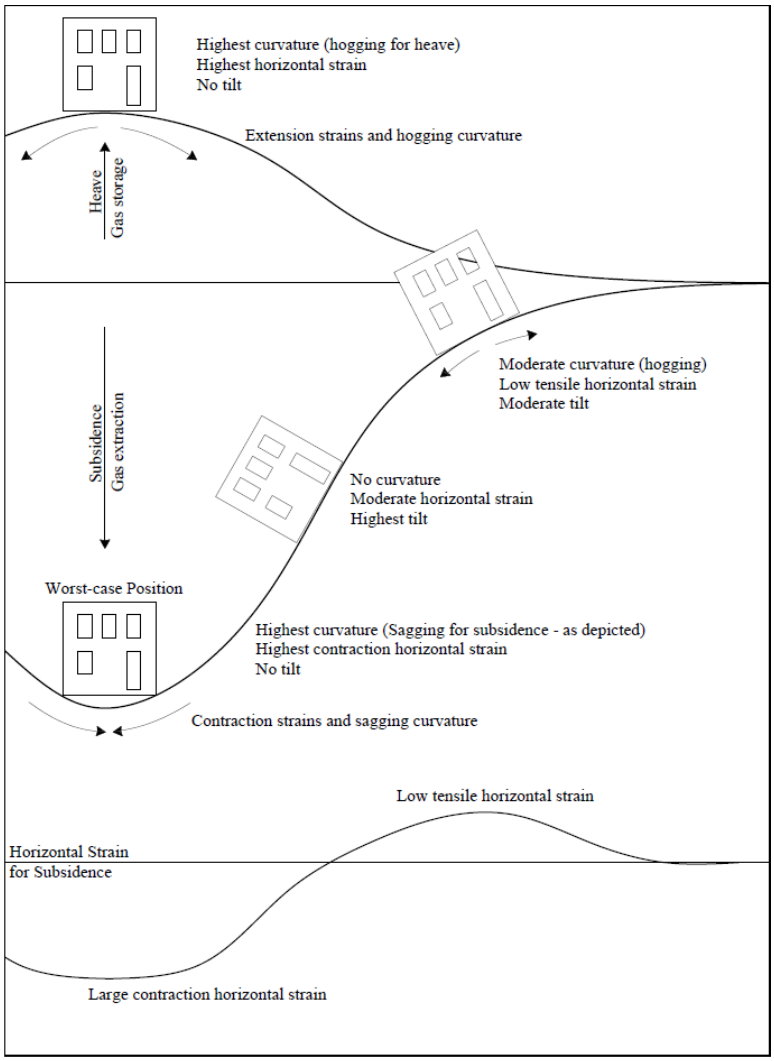

Figure 20. Comparison of a building placed at different locations in the subsidence bowl. The sketch is extremely amplified. (After: TU Delft, 2021)

5.5.2 Effect of shallow subsidence

Shallow subsidence that is not uniform can result in differential settlement underneath a building. This can result in strains in a building due to relative rotations. Here there are also two modes, 'hogging' and 'sagging'. It should be emphasised that this hogging and sagging is different in scale and character as the hogging and sagging modes that occurs in a deep subsidence bowl explained in section 5.5.1. Hogging related to differential settlement is the mode where the sides of the building settle more than the average, whereas in sagging the centrepiece of the building settles most (Figure 22, Korff, 2009). Differential settlements add to the strain as shown in Figure 23. This figure is based on the Eurocode (2007) that provide limit values for relative rotation.

Since the terminologies hogging, sagging and strains are used interchangeably, it can create some confusion. Table 3 summarises the differences between the mechanisms and modes that could lead to damage for deep and shallow subsidence.

Table 3. Summary of the mechanisms and modes with the terminologies used in the text that can lead to damage in masonry buildings.

Deep subsidence		**Shallow subsidence**		mechanisms leading to damage
Curvature of subsidence bowls		Differential settlement		
Hogging of surface	Sagging of surface	Hogging of building	Sagging of building	
Horizontal extension (tensile) strain in subsurface	Horizontal compression (contraction) strain in subsurface	Angular distortion (main mechanism)		
Horizontal strain transferred to building. (main mechanism)				
extensional strain in building	compression strain in building	extensional strain in building	compression strain in building	
strain in masonry due to deep subsidence		strain in masonry due to shallow subsidence		
Total strain in masonry possibly leading to damage				

* The terminologies in this table connect to Figure 20, Figure 23 and Figure 24.

The extent to which a building is capable of accommodating such movements or deformations has been determined by Boscardin and Cording (1989) and Son and Cording (2005). The combination or the individual components strain, and angular distortion can lead to different levels of damage, based on various cases from Boscardin and Cording (1989). They developed a graph (Figure 21), that is widely used and accepted in engineering practice. Different damage levels can be derived by plotting the horizontal strain and angular distortion.

The classification by Boscardin and Cording is mostly based on subsidence cases from shallow underground mining and tunnelling and appears therefore less applicable for assessing the likelihood of damage due to deep mining. The horizontal strains and angular distortions measured in gas and salt subsidence bowls are very small and usually plot in the lower left corner of the Boscardin and Cording classification, classifying everything as negligible damage. To establish a more precise damage threshold TNO (2021) has carried out a comprehensive literature review. This is explained in section 5.5.5. Section 5.5.6 explains how to derive values of horizontal strain and angular distortion from deep subsidence measurements.

The TU Delft is currently working on a model-based approach, in combination with laboratory tests on masonry walls, to develop more sophisticated vulnerability curves to determine probability of different degrees on damage based on horizontal strain and angular distortion. The additional effect of vibrations due to induced earthquakes is also examined in the GEMMA[7] program. results are expected in Q2 2024.

[7] GEMMA: *Gecombineerde Effecten Meerdere Mijnbouw Activiteiten*: Combined Effects of Multiple Mining Activities. A joint research program defined by CM and IMG executed by NEO, TNO and TU Delft.

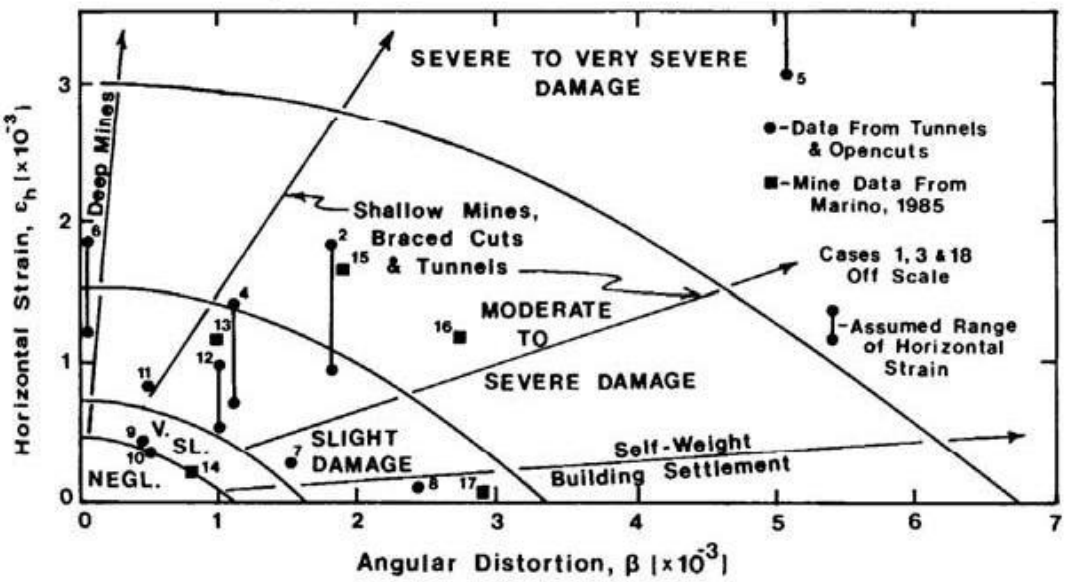

Figure 21. Relationship of damage to angular distortion and horizontal strain (extension) (Source: Boscardin and Cording, 1989)

5.5.3 Horizontal strain

The curvature, i.e. large-scale sagging or hogging within a subsidence bowl can lead to the development of horizontal strains in the subsurface (Figure 20). Large-scale sagging result in compression and hogging results in extension. Buildings are especially vulnerable to the transfer of extension from the subsurface via the foundation to the walls and other structural element of a building. This effect is illustrated in Figure 24. Buildings are less vulnerable to compression. Only a small portion of the horizontal strain in the subsurface is usually transferred via the foundation directly into the building. In engineering practice, a 6% transfer rate is used, but in poor foundations, a larger portion of the horizontal strain may be transferred into the building.

Additionally, the buildings may experience varying degrees of tilt and angular distortion, based on their location relative to the subsidence bowl. In cases of heave, the subsidence bowl's configuration is inverted. In the centre, buildings undergo hogging, while towards the edge, they experience sagging. Figure 20 depicts, in a stylized sketch, the way the location of a building in relation to the subsidence- or heave bowl influences the strains and tilts experienced by the building. Especially the combination of horizontal strain and angular distortion can lead to damage to buildings in masonry structures. These damage indicators are explained in section 5.5.5.

5.5.4 Angular distortion

Angular distortion is caused by sagging or hogging, but then at the scale of the building rather than the sagging and hogging in a regional subsidence bowl where the scale is much larger than the dimension of the building. Angular distortion due to deep subsidence also occurs, but this is usually negligibly small due to the small curvature of the subsidence bowl. Angular distortion is mostly caused by local differential settlement underneath the foundation of a building (see Figure 23). This can be caused indirectly by mining due to the effects of changes in groundwater level (section 6.7.1)

Differential settlement due to shallow subsidence, particularly variations across a building, can lead to various types of damage, notably the hogging mode (sideways settling more than average) and the sagging mode (centre settling the most). Figure 23 outlines the strain characteristics due to hogging, including potential damage mechanisms in brittle materials (Boscardin & Cording, 1989). The hogging

mode poses a potential threat as it induces horizontal extensional strains in a structure. Figure 22 illustrates hogging and sagging in relation to a shallow subsidence trough due to tunnelling or shallow excavations. Although it is incomparable to the scale of a typical deep subsidence bowl it illustrates the difference between sagging and hogging. Masonry buildings, which make up most of the building inventory, are especially vulnerable to these horizontal extensional strains. While sagging also results in horizontal strains, these are compressional in nature, and masonry is more adept at handling compression than tension. Building deformations involve multiple modes, such as shear, bending, elongation, and shortening, often occurring simultaneously. Definitions used in this study are provided by Korff (2009) and Giardina (2013), visualized in Figure 23 (Giardina, 2013). In the list below the parameters and symbols from in Figure 23 are explained.

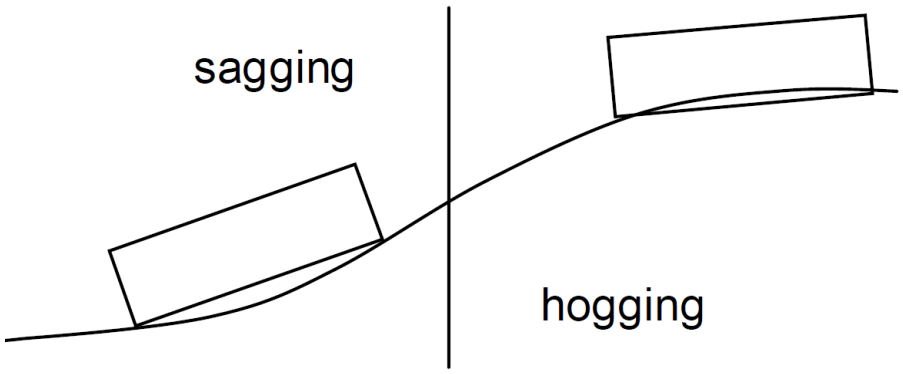

* It should be well (!) noted that the scale of a subsidence trough due to tunnelling or construction is much different from the subsidence bowl caused by deep subsidence as defined in this study.

Figure 22. Sagging and hogging deformation modes in relation to a shallow subsidence trough of building pits and tunnelling (Source: Korff, 2009)

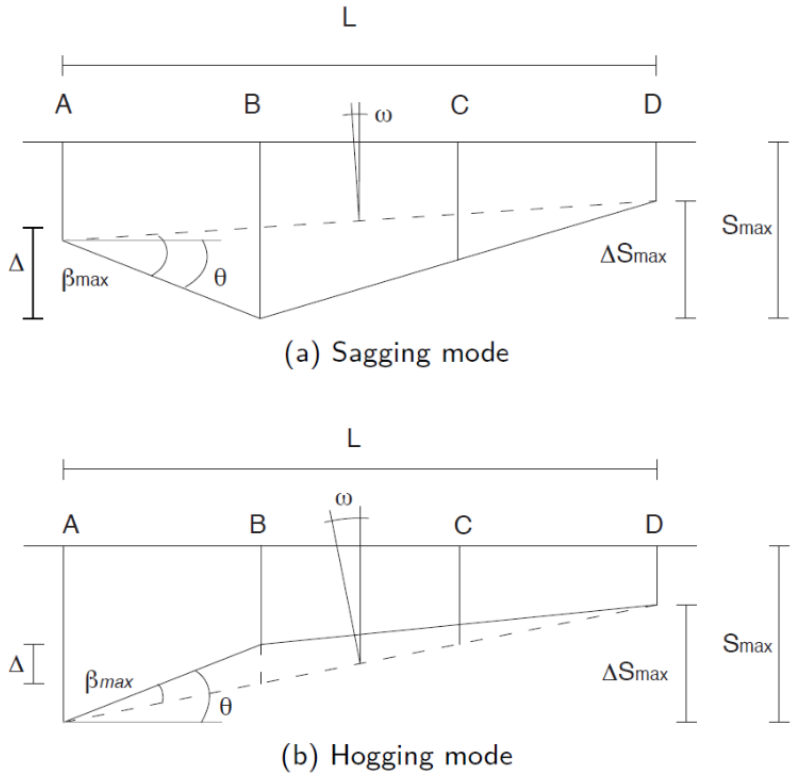

Figure 23. Deformation parameters (Source: Giardina, 2013, modified after Eurocode, 2007).

Parameters:

- S: **Settlement** is the vertical displacement of a point;
- δS or ΔS: **Relative settlement or differential settlement** is the difference between the settlements of two points;
- Δ: **Relative deflection** is the maximum vertical displacement relative to the straight line connecting two reference points;
- Δ/L: **Deflection ratio** is the ratio of the relative deflection between two points to the length, L between them;
- θ : **Rotation** is the gradient of a straight line (relative to horizontal) connecting two points or slope of a settlement curve;
- ω: **Tilt** is the rigid body rotation of the entire structure. Rigid body rotation can be assessed in three dimensions, and it should be made clear if and in what way tilt is considered (e.g. horizontal, vertical);
- β: **Angular distortion** (or relative rotation) is the rotation of the straight line connecting two reference points relative to their tilt at the foundation level;
- ε: The change in length (ΔL) of the structure due to the applied horizontal displacements results in a **horizontal strain** (ε=ΔL/L).

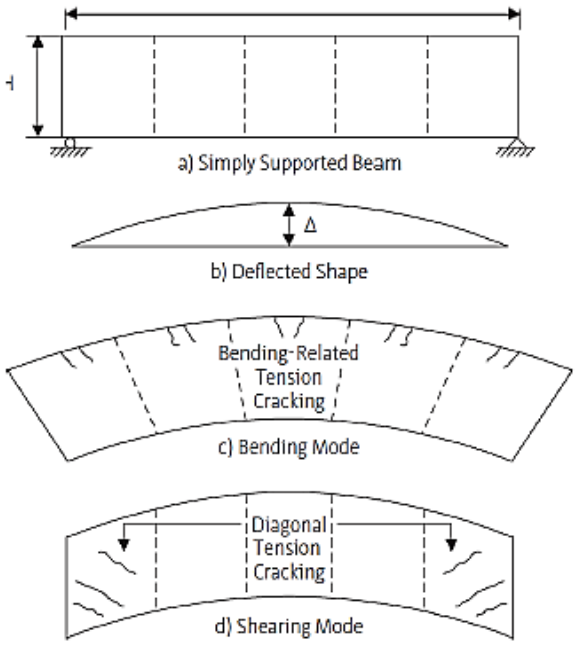

Figure 24. Overview of deformations in buildings and related damage for the most damaging hogging mode (Source: Boscardin & Cording, 1989).

5.5.5 Damage indicators and thresholds

TNO (2020) carried out a review of over 25 scientific studies for foundation movement-induced damage and identifies angular distortion (also called: relative rotation) (β) and horizontal strain (ε) as the damage indicators. The internationally accepted approach by Boscardin and Cording (1989), refined by Son and Cording (2005), is widely used and accepted in engineering practice to assess damage to masonry buildings from such movements. It was also concluded that masonry structures tolerate smaller distortions than frame structures (concrete, steel, timber) before visible cracks occur.

To establish a lower bound criterion in TNO (2020) an allowable strain is proposed, which is lower than the boundary defined by Boscardin and Cording (1989) and Son and Cording (2005). This value, result in negligible damage, considers buildings with a higher percentage of openings, making it suitable for

the Groningen building stock. Figure 25 illustrates the chosen lower bound criterion, indicating that if the combination of horizontal strain and angular distortion falls above the dotted line, damage to buildings can be expected.

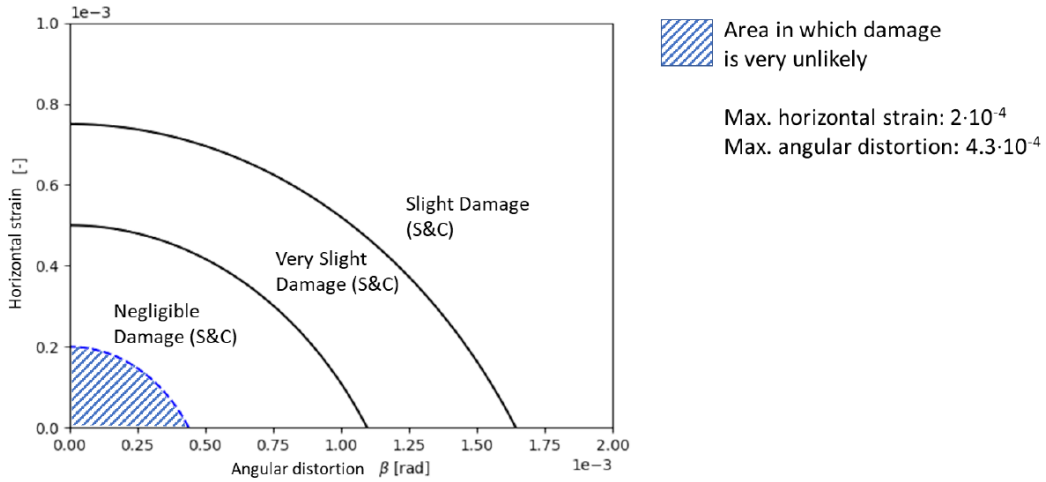

Figure 25. Illustration of area in which damage is very unlikely (represented by dashed area) for the combination of horizontal strain and angular distortion (Source: TNO, 2020: adapted from Boscardin and Cording, 1989; Son and Cording, 2005).

5.5.6 Determining horizontal strain due to deep subsidence

There are three methods to determine horizontal strain and relative rotation due to mining-induced deep subsidence:

1. Calculation by subsidence modelling
2. Derivation based on interpolated measured deep subsidence.
3. Use of InSAR satellite deformation measurements.

The calculation by subsidence modelling is based on the principles explained in section 2.10. Subsidence modelling can be approached through various methods, including purely analytical or numerical methods, or a semi-analytical approach like the one applied by Fokker and Orlic (2006). The latter approach is employed in a software known as AESubs, which combines elements of analytical and numerical methods. This software tool, utilized in the TNO study for IMG, is instrumental in determining vertical and horizontal ground surface displacements and strain profiles, commonly referred to as influence functions (TNO, 2021). The model directly computes horizontal strain, and based on the displacements, tilt and curvature can be derived. It should be possible to also derive angular distortions (or relative rotations) from the displacement profile, but in TNO (2021) this was not described, probably because the expected values are negligibly small.

Analytical derivation of horizontal strain and angular distortion from vertical geodetic deep subsidence measurements can be performed, with or without InSAR measurements. Deltares (2018) conducted analyses for NEDMAG's salt mining operations around Veendam. These analytical calculations rely on contour lines of equal deep subsidence, generated by interpolating vertical geodetic measurements. The horizontal strain is computed using a semi-empirical approach initially applied in tunnelling (O'Reilly and New, 1982), while the relative rotation is simply determined based on the distance between two consecutive contour lines, assuming a building length of 20 meters.

InSAR satellite deformation measurements have the potential to directly determine the horizontal component of deep subsidence. InSAR satellites use a radar beam emitted at a specific angle, measuring the phase difference between the emitted and reflected signals. This allows for accurate displacement measurements over small time intervals (in the order of days), ensuring high spatial and

temporal precision. Due to the radar beam angle, both vertical and horizontal components of ground movement can be derived. However, InSAR satellites move in either ascending (south-north) or descending (north-south) orbits, limiting the horizontal components to East-West or West-East orientations. Notably, there is a lack of published studies using InSAR data to derive horizontal strain from deep subsidence. Usually, InSAR is utilized to display ground movement using the vertical component, as demonstrated on the publicly available Dutch Bodemdalingskaart 2.0 website. However, the European Ground Motion Services (EGMS) website offers the same satellite data with the added benefit of providing the horizontal component as well.

6

INTERACTIONS AND INFLUENCE DISTANCES

6.1 Summary and conclusions

This chapter gives an answer to the following research question as defined in section 1.4.1

3. What is the distance (both in depth as lateral) which would exclude cumulative effects between mining activities for subsidence, induced seismicity, leakage, other?

The extent of processes in the subsurface and their significance for the environment varies widely from one location to another. Attempting a comprehensive literature review of these processes and interactions thereof, without specifying a case study area, leads to a somewhat philosophical exercise and requires a perfect understanding of the subsurface, which we arguably will never have. Therefore, the consortium has chosen a pragmatic approach, prioritizing the description of the most prevalent interactions divided in the shallow intermediate and deep subsurface. The assessment of the cumulative effects could then be done for specific sites where more information on the subsurface and specific processes is available.

Influence area

Shallow subsidence is influenced by factors like top loading, vibration-induced cyclic loading, and hydrogeological shifts, with varying extents of impact determined by geological, hydrogeological, and human-induced factors. For example, top loading typically affects the subsurface by inducing stress under an angle of 45 degrees. Given that the top layer rarely consists of cohesive soils exceeding 20 meters depth, the lateral influence distance is often limited to 20 meters as well. When using the SBR engineering standards for vibration-induced compaction the influence distance is typically limited to approximately 10 meters when induced by infrastructural work, but this can extend to the kilometer scale for seismic events. For hydrogeological processes the 5cm threshold limit form the SIKB is used as a formal definition of the impact area. Depending on the hydrogeological driver, the influence area can vary from a few meters for temporal drainage activities to hundreds of meters for water management, and all the way up to sub-continental regions when considering climatological events such as droughts.

Intermediate subsidence is primarily driven by groundwater extraction for consumption and subsurface energy systems, affecting areas from hundreds of meters to the kilometer scale. Deep subsurface processes, such as oil/gas extraction and salt mining, have specific influence rules, with impacts extending about twice the depth of the gas-water or oil-water contact for oil/gas extraction and around mined caverns for salt mining.

Seismicity can be triggered by any subsurface activity that causes stress changes. Defining stress change thresholds triggering earthquakes is complex and depends on subsurface faults' conditions. Seismic events generate waves that attenuate through the subsurface to the surface, with models predicting Peak Ground Velocity (PGV) to delineate influence areas and assess potential damage. The

influence zone of an induced seismic event is strongly influenced by its magnitude. For magnitudes above 2.0, the affected area can extend for several kilometres from the epicentre, and this distance grows exponentially with larger magnitudes.

Vertical fluid migration, influenced by factors like lithology and subsurface activities affecting pore pressure, can significantly affect the lateral extent of hydrogeological processes. This vertical fluid migration, controlled by pressure communication between subsurface layers, can lead to phenomena such as seepage through aquitards and salinization from deeper aquifers. In the shallow to intermediate subsurface, vertical fluid migration is a recognized issue in environmental hydrogeology, where groundwater extraction can impact regional flow patterns, depending locally on the well penetration depth. Conversely, significant pressure communication between layers in the intermediate to deep subsurface is possible. However, in regions like the Northern Netherlands, characterized by numerous low-permeability aquitards, large-scale seepage between layers is generally considered insignificant.

Type of interactions

The process of subsidence and heave interacts closely with changes in the hydrogeological system, creating a dynamic feedback loop. Subsidence not only alters local geology but also impacts the topography of the area. Conversely, hydrogeological processes, influenced by various factors such as topography, geology, and climate, can act as significant drivers for shallow subsidence. Human activities, including groundwater extraction and land use changes, further exacerbate these processes.

For instance, changes in surface water levels can influence ground surface movement through phenomena like shallow subsidence and clay swelling. Moreover, regional groundwater flow patterns are influenced by factors such as subsidence induced relative sea-level rise, which in turn can have consequences on subsidence rates and groundwater quality. This impact is proportional to the local subsidence gradient. Therefore, the relationship between the size of the subsidence bowl and the drainage system plays a critical role in understanding the impact of subsidence on groundwater levels and surface water management.

Additionally, the interaction between drought events and increased water demand can exacerbate subsidence. Agricultural water demand generally rises during dry periods, increasing the risk of overuse of water resources that can lead to accelerated subsidence rates.

In the deep subsurface mining activities such as oil and gas extraction induce compaction, affecting surface subsidence over time. Subsurface modelling that considers these compaction sources need to consider the impact of creep-induced subsidence in salt caprocks and lateral fluid migration. Long-term fluid exchange between gas reservoirs and aquifers influences subsurface dynamics, which, if not modelled, can lead to unexpected subsidence events in the future.

International examples showcase interactions between earthquakes, subsidence, and mining activities. In the Netherlands, cases like salt solution mining and gas extraction in Fryslân illustrate unexpected subsidence. Induced seismicity from water injection in De Hoeve and combined effects in the Veendam area demonstrate complex and sometimes unexpected interactions between various mining activities.

6.2 Samenvatting en conclusies (NL)

Dit hoofdstuk geeft antwoord op de volgende onderzoeksvraag zoals gedefinieerd in sectie 1.4.1

3. Wat is de afstand (zowel in diepte als lateraal) die cumulatieve effecten tussen mijnactiviteiten voor bodemdaling, geïnduceerde seismische activiteit, lekkage en andere uitsluit?

De reikwijdte van processen in de ondergrond en de impact op de omgeving varieert sterk van de ene locatie tot de andere. Het uitvoeren van een uitgebreide literatuurstudie op deze processen en hun

interacties, zonder gebruik te maken van een specifiek casusgebied, leidt tot een vrij filosofische exercitie en vereist een perfect begrip van de ondergrond, iets wat we waarschijnlijk nooit volledig zullen hebben. Daarom heeft het consortium gekozen voor een pragmatische benadering, waarbij prioriteit wordt gegeven aan de beschrijving van de meest voorkomende interacties, verdeeld over de ondiepe, tussenliggend en diepe ondergrond. De beoordeling van de cumulatieve effecten kan vervolgens worden gedaan voor specifieke locaties waar meer informatie over de ondergrond en specifieke processen beschikbaar is.

Invloedsgebied

Ondiepe bodemdaling wordt beïnvloed door factoren zoals bovenbelasting, trillingen door cyclische belasting en hydrogeologische veranderingen, met variërende mate van impact bepaald door geologische, hydrogeologische en door de mens veroorzaakte factoren. Bijvoorbeeld, bovenbelasting beïnvloedt de bodem tot 20 meter diepte, terwijl trillingen verdichting kan veroorzaken tot 10 meter van de bron reikt maar kilometers kan bereiken bij geïnduceerde aardbevingen. Hydrogeologische processen kunnen gebieden van enkele meters tot sub continentale regio's beïnvloeden, afhankelijk van waterbeheer en klimatologische omstandigheden. Tussenliggende bodemdaling wordt voornamelijk gedreven door grondwaterwinning en ondergrondse energiesystemen, wat gebieden van enkele kilometers tot meerdere kilometers beïnvloeden. Diepe ondergrondse processen, zoals olie/gaswinning en zoutwinning, hebben specifieke invloedsgebieden, met impact tot van een- tot ongeveer tweemaal de diepte van het gas-water contact voor gaswinning en rond zoutcavernes.

Seismische activiteit kan worden veroorzaakt door elke activiteit die spanningsveranderingen in de ondergrond veroorzaakt. Het definiëren van de grenswaarden voor spanningsverandering die aardbevingen veroorzaken is complex en hangt af van de condities van ondergrondse breuken. Seismische activiteit genereert golven die via de ondergrond het oppervlak bereiken. De energie (amplitude) neemt daarbij met de afstand af. Er zijn modellen die de Piekgrondsnelheid (PGV) voorspellen om invloedsgebieden af te bakenen en potentiële schade te kunnen beoordelen. Het invloedsgebied van een geïnduceerde beving wordt sterk beïnvloed door de magnitude. Voor magnitudes boven de 2,0 kan invloedsgebied zich over meerdere kilometers vanaf het epicentrum uitstrekken, en deze afstand wordt exponentieel groter bij grotere magnitudes.

Vloeistofmigratie wordt gecontroleerd door drukcommunicatie tussen ondergrondse lagen en factoren die verticale migratie beïnvloeden. Factoren zoals lithologie en ondergrondse activiteiten beïnvloeden de poriedruk, wat leidt tot fenomenen zoals kwel en wegzijging door waterremmende lagen en verzilting vanuit diepere aquifers. Grondwaterwinning beïnvloedt regionale stromingspatronen, waarbij de diepte van de invloed afhankelijk is van de penetratiediepte van putten en de permeabiliteit van het aquifer. Aan de andere kant is aanzienlijke drukcommunicatie tussen lagen in de intermediaire tot diepe ondergrond mogelijk. Echter, in noordelijk Nederland, gekenmerkt door talrijke aquitards met lage permeabiliteit, wordt grootschalige lekkage tussen lagen als niet realistisch beschouwd.

Type interactie

Het proces van bodemdaling en -stijging hangt nauw samen met veranderingen in het hydrogeologische systeem, wat een dynamische terugkoppeling creëert. Bodemdaling verandert niet alleen de lokale geologie, maar heeft ook invloed op de topografie van het gebied. Omgekeerd kunnen hydrogeologische processen, beïnvloed door verschillende factoren zoals topografie, geologie en klimaat, belangrijke drijvende mechanismes voor ondiepe bodemdaling zijn. Menselijke activiteiten, waaronder (ondiepe) grondwaterwinning en veranderingen in landgebruik, verergeren deze processen verder.

Zo kunnen veranderingen in oppervlaktewaterniveaus de bodembeweging veroorzaken door zettingen, oxidatie en krimp- en zwel van klei. Bovendien worden regionale grondwaterstromingspatronen beïnvloed door factoren zoals relatieve zeespiegelstijging (door de

bodemdaling), wat op zijn beurt gevolgen kan hebben voor bodemdaling snelheden en grondwaterkwaliteit. Deze impact is ook gerelateerd aan de lokale bodemdalingsgradiënt. Daarom speelt de relatie tussen de omvang van de bodemdalingskom en het afwateringssysteem een belangrijke rol bij het begrijpen van de impact hiervan op de grondwaterniveaus en het oppervlaktewaterbeheer.

Daarnaast kan de interactie tussen droogte en waterbehoefte ondiepe bodemdaling verergeren. In de landbouw neemt de vraag naar water voor irrigatie doorgaans toe tijdens droge perioden, wat het risico op overmatig gebruik van grondwater vergroot. Dit kan weer kan leiden tot grotere (verschil) zettingen in de ondiepe ondergrond.

Gaswinning veroorzaakt compactie en dit veroorzaakt in verloop van tijd diepe bodemdaling. De compactie modellering zou ook de impact op de afsluitende zoutlaag moeten beschouwen en de laterale vloeistofmigratie. Langdurige vloeistofmigratie tussen gasreservoirs en aquifers beïnvloedt de ondergrondse dynamiek, wat mogelijk ook weer leidt tot diepe bodemdaling of -stijging.

Internationale voorbeelden tonen interacties tussen aardbevingen, bodemdaling en mijnbouwactiviteiten. In Nederland zijn er gevallen zoals gecombineerde zoutwinning en gaswinning in Fryslân wat leidde tot onverwacht grote diepe bodemdaling. Geïnduceerde seismische activiteit door waterinjectie in De Hoeve en gecombineerde effecten in het Veendam-gebied zijn andere voorbeelden van complexe interacties tussen de verschillende mijnbouwactiviteiten.

6.3 Introduction

The extent of processes in the subsurface and their significance for the environment varies widely from one location to another. Attempting a comprehensive literature review of these processes and interactions thereof, without specifying a case study area, leads to a somewhat philosophical exercise and requires a perfect understanding of the subsurface, which we arguably will never have.

Therefore, the consortium has chosen a pragmatic approach, prioritizing the description of the most prevalent interactions.

Furthermore, several case studies are included to exemplify interactions that the consortium or local stakeholders deem relevant to the study area around Grijpskerk. Some examples are cited when believed they can aid in understand the underlying process.

In this chapter, we will discuss various interconnected topics related to subsurface phenomena. First, we will explore the influence area of different subsidence drivers, starting with shallow subsidence (section 6.4.1), followed by intermediate subsidence (section 6.4.2), and deep subsidence (section 6.4.3). Next, we will investigate induced seismicity, discussing influence area of stress conditions responsible for triggering of induced seismicity (section 6.5.1) and attenuation of the trigged seismic waves (section 6.5.2). We will then shift our focus to vertical fluid migration, examining its occurrence in the shallow-intermediate subsurface (section 6.6.1) and intermediate-deep subsurface (section 6.6.2). Finally, we will analyse various interaction types, including the hydrogeological feedback system, regional groundwater flow, and the interplay between water management and subsidence, and how droughts and water demand interact with subsidence (section 6.7.1). Additionally, we will describe the modelling of interactions in the intermediate - deep subsurface, and the interactions related to lateral fluid migration. We will conclude this chapter by examining international and national case studies (section 6.7.2).

6.4 Area of influence

6.4.1 Shallow subsidence

Compared to the intermediate and deep subsurface, the shallow subsurface experiences a great variety of stress-inducing processes, with each process acting on a different scale depending on the nature of the process and the local geology. Since shallow subsidence is notoriously difficult to quantify in a generic manner due to the large dependence on the specific geological, hydrogeological, and anthropogenic conditions, it was opted to describe the area of influence in terms of subsidence drivers and their order of magnitude. The shallow subsidence drivers are classified in three major components, namely: (i) applying a surface load, (ii) vibrational induced cyclic loading, and (iii) changes in the hydrogeological system (section 2.6.5). A summary of their radial extent is listed in Table 4.

When a load is applied on the ground surface, e.g. by constructing a building or large infrastructural objects, the associated stress in the soil below, diminishes by spreading out with depth under an angle of around 45-degrees (Poulos and Davis, 1974). The associated shallow subsidence is dominated by the occurrence, and spatial distribution, of cohesive soil layers like peat or clay, which makes its lateral extent, given the 45-degree angle, directly proportional to their thickness, which typically does not exceed 20m in the Dutch Holocene deposits.

We observe that vibration induced compaction is typically limited to an area up to 10 meter from the vibration source (by comparing Figure 8 and Figure 7 in section 2.6.2). However, if vibrations originate from sensible induced seismicity (as low as, but very rarely at M 1.5, typically felt by many people with M 3.0 and higher), the area of influence is in the order of kilometres, but that is highly dependent on magnitude, depth, subsurface geology and soil characteristics (section 6.5). Large natural seismicity can be felt even up to hundreds of kilometres away, while the actual impact area, in terms of damage, also depends highly on the magnitude, depths, types of earthquake and soil conditions.

The hydrogeological system is highly variable in both space and time. On a regional scale the subsurface exhibits heterogeneity, including e.g. delta, river, glacial and Aeolian deposits, resulting in variability in groundwater flow and hydraulic head. Additionally, groundwater levels are significantly influenced by both natural processes and human activities such as e.g. water management and climatological droughts (section 2.6.5). Depending on these factors, the influence area of hydrogeological processes can range from just a few meters due to minor drainage activities up to entire sub-continental regions during prolonged drought events. **In the Netherlands, a 5 cm threshold is typically used for temporary groundwater level reductions as the lower limit for an impact area** (SIKB, 2017). Therefore, we use this threshold to determine hydrogeological influence areas. However, in cases of peat oxidation and pile rot, defining a threshold is much more challenging and must be considered on a case-by-case basis.

Table 4. Influence area of shallow subsidence drivers

Shallow subsurface driver	**Area of influence**
Top load	< 20m (thickness underlying weak layer)
Vibrational induced cyclic loading (section 2.6.2) • Infrastructural • Earthquakes	 • < 10m • < kilometre scale
Hydrogeology (section 2.6.5) • Water management • Temporal drainage activities • Vegetation / root water uptake • Natural groundwater fluctuations • Droughts	 • < kilometre scale • < 1 – 2 km • < 100m (proportional to the height of the concerning vegetation) • Regional (shrinking and swelling of clays) • Sub-continental

6.4.2 Intermediate subsidence

The intermediate subsidence is predominantly induced by groundwater extractions with the purpose of consumption or subsurface energy systems. The influence area is generally constrained to up to a few kilometres for large scale groundwater extractions, e.g. for drinking water purposes. Section 2.7.1 describes that excess groundwater extractions lead to entire deltas or regions to subside as a result of the cumulative effect of many groundwater extractions in the region. However, this is not an issue in the Northern Netherlands as groundwater is sustainably extracted in much smaller quantities (Section 2.7.1). The effect of intermediate subsidence at the ground surface that is associated to these groundwater extractions depend on the lithological buildup of the subsurface and the shape of the compaction source and is similar to deep subsidence due to the development of a relatives gentle and smooth subsidence bowls (Fokker and Osinga, 2018; section 5.5). For determining the lateral influence area at the intermediate depth where groundwater extractions take place, the same threshold of 5 cm hydraulic head is used (section 6.4.1).

Table 5. Influence area of intermediate subsidence drivers

Intermediate subsurface driver	**Area of influence**
Groundwater extraction (section 2.7.1)	< kilometre scale
Subsurface energy systems (section 2.7.2) • ATES • HT/MT-ATES • Geothermal Energy	 • < 500m • < 1500m • Several kilometres
Natural compaction (section 2.4.1)	Regional watershed scale

6.4.3 Deep subsidence

To establish an area of influence for deep subsurface processes, a minimum level of subsidence is required to define where stress changes are considered relevant. In the context of this study, it is reasonable to set the lowest level for subsidence at 1 mm, which is the resolution limit (accuracy) of the main observation data (i.e. Dutch reference level *NAP*). The mining operators and the regulator in The Netherlands generally use an accuracy threshold of 20 mm for the lowest level of mining-induced subsidence. With this definition, an area of influence can be modelled field specific. On the other hand, there are general rules and observations to determine what the area of influence is of the subsidence bowl of oil/gas extraction and salt mining. These are summarised below.

As a general rule of thumb, it is considered that the primary subsidence area above a gas or oil field extends to an area equal to 1 time the depth of the field beyond the perimeter of the gas or oil field. Here, the perimeter is the mapped gas-water or oil-water contact (GWC/OWC) in the reservoir since that is the zone of pressure drop within the reservoir. This contact is typically a horizontal plane at a generally in the reservoir rock. The depth of the gas-water- or oil-water contact is used as a measure for the lowest depth of the reservoir at which the compaction occurs. This is schematically depicted in Figure 26. In Schouten and de Waal (2019), model-based relationships are provided between the width and depth of the subsidence bowl to the depth of small gas fields (see Figure 27). From this graph, it can be inferred that at a distance/depth ratio of 1.0 to 2.0, subsidence is minimal. This implies that for a typical small gas field (with a GWC at 3 kilometres), the deep subsidence becomes minimal at a distance of 3 to 6 kilometres from the gas field boundary. To exclude potential horizontal strain phenomena that may occur right at the border of the subsidence bowl, a distance/depth ratio of 2 is a conservative assumption as the limit for the assessment area. The area between 1 time and 2 times the depth can be referred to as the secondary subsidence area (also see Figure 26). In reality, subsidence maps in this area usually no longer display measured or model-based deep subsidence.

For salt mining, a similar rule-of-thumb can be used as in oil or gas extraction. In that case the origin from which to draw the boundary is the point-source from which the salt is mined, mostly the centre of the cavern or the location of the salt extraction well. In the case of multiple caverns, the total area of influence is determined by the envelope of the overlapping areas of influence of individual caverns.

In salt mining the depth of the top of the caverns or, in case of Veendam, the depth of the (magnesium) salt layer that is mined is used. Table 6 a summary is given of the approximate influence areas for the deep subsidence drivers.

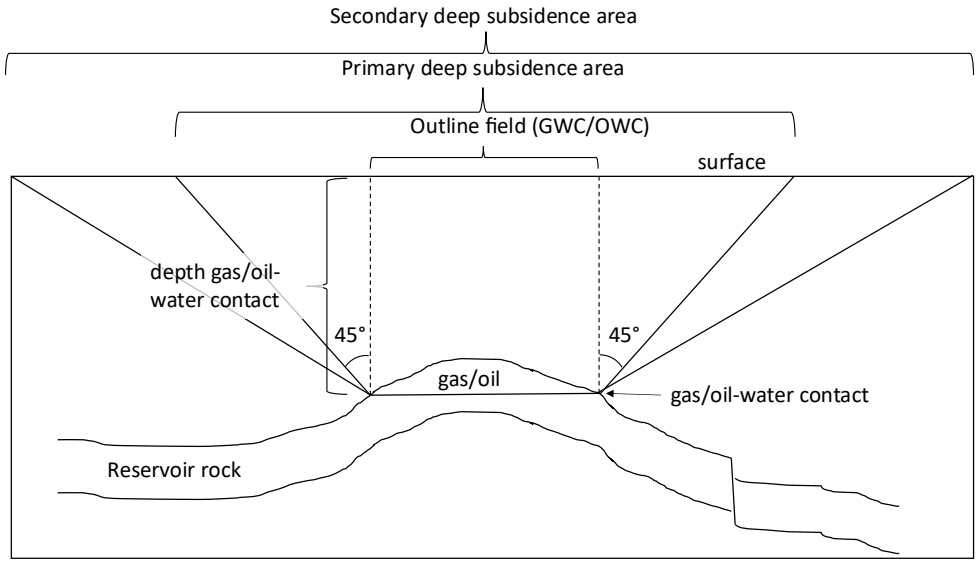

Figure 26. Illustration of the area of influence of deep subsidence due to gas (or oil) extraction.

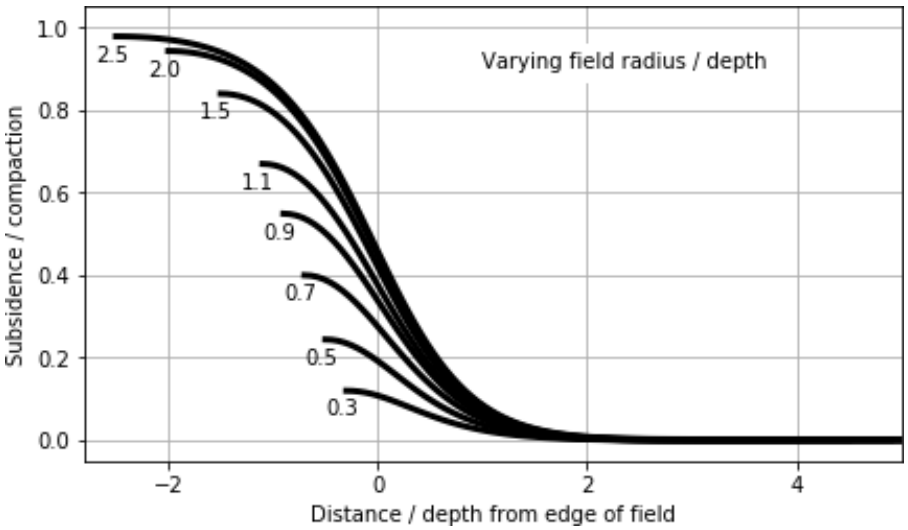

Figure 27. Relationship between the normalized parameters distance/depth and subsidence/compaction for various (gas) field sizes (field radius/depth) (Source: Schouten and de Waal, 2019).

Table 6. Influence area of deep subsidence drivers

deep subsurface driver	**Area of influence**
Oil/Gas extraction (see section 2.8.1)	Depends on depth of GWC/OWC. On average the depth of GWC of small fields is about 3 km, thus the maximum area of influence is buffer of 6 km around the mapped outline of GWC. For each oil/gas field the GWC/OWC outline en depths is known.
Salt mining (see section 2.8.2 • Veendam • Winschoten • Zuidwending	Approximately: • 4-5 km from centre • 1.5-2.5 km from cavern field • 2.0-2.5 km from cavern field

6.5 Induced seismicity

Consideration is given to two aspects of interactions and influence area in this context. The first involves examining the area at which subsurface activities might trigger earthquakes from a stress perspective (section 6.5.1). The second aspect entails reviewing the area at which induced earthquakes have effects (section 6.5.2).

6.5.1 Influence area based on stress conditions

Defining a lower limit of stress changes at which these become irrelevant for triggering earthquakes is not straightforward. This lower limit depends on the (background) stress-strength conditions of subsurface faults. In the Roer-Valley Graben, faults may be closer to stress-criticality than elsewhere in the Netherlands. Therefore, the area of influence of a subsurface activity will be larger in the Roer-Valley Graben than e.g. in the Netherlands. Despite this location dependency, first order estimates of the area of influence for gas/oil/salt are proposed in Mijnlieff et al. (2023). It should be noted that subsurface activities bring a fault closer to stress-criticality. Even after subsurface activities have stopped, the higher level of stress criticality may persist. Due to a combined effect, subsequent subsurface activities could trigger earthquakes already at a comparably low level of stress changes.

6.5.2 Influence area based on the attenuation of seismic waves

When a seismic event, either natural or induced, occurs, seismic waves emanate from the source (hypocentre) and traverse through the subsurface to the Earth's surface. The resulting seismic energy manifests as detectable vibrations, measurable at the surface. As distance from the seismic source increases, the seismic energy attenuates, and the vibrations become smaller until they become undetectable. Using soil and rock properties, NAM and KNMI develop Ground Motion Prediction Equations (GMPE) based on KNMI measurements of induced seismic events and general seismic attenuation models. In the Groningen region, these equations are commonly known as Ground Motion Models (GMM) or Empirical Ground Motion Models (EGMM), as explained in section 5.4.1.

Figure 28 illustrates various models showing the relationship between Peak Ground Velocity (PGV) and distance for a Magnitude 3.0 earthquake. The graph highlights the attenuation of PGV with increasing distance from the source. For comparison, the red line indicates the vibration amplitude above which damage at ordinary buildings cannot be excluded according to the engineering standards (e.g. SBR, 2017).

To avoid unjust exclusion of damage claimants from compensation, IMG and CM employ a conservative approach in their damage assessment practices, which incorporates greater uncertainties than indicated by Figure 28. KNMI develops an EGMM specifically for assessing damage caused by induced seismicity in gas fields outside the Groningen field, as outlined by Ruigrok and Dost (2020). This EGMM considers magnitude, depth, confidence limits (uncertainty), and the damage level (PGV) threshold to delineate areas of influence. Figure 29 provides examples where the choice of confidence interval (90% vs. 99%) and PGV threshold values significantly impact the identified area. IMG and CM use a conservative P99 confidence interval with a 2 mm/s threshold value to determine the exclusion zone for potential damage.

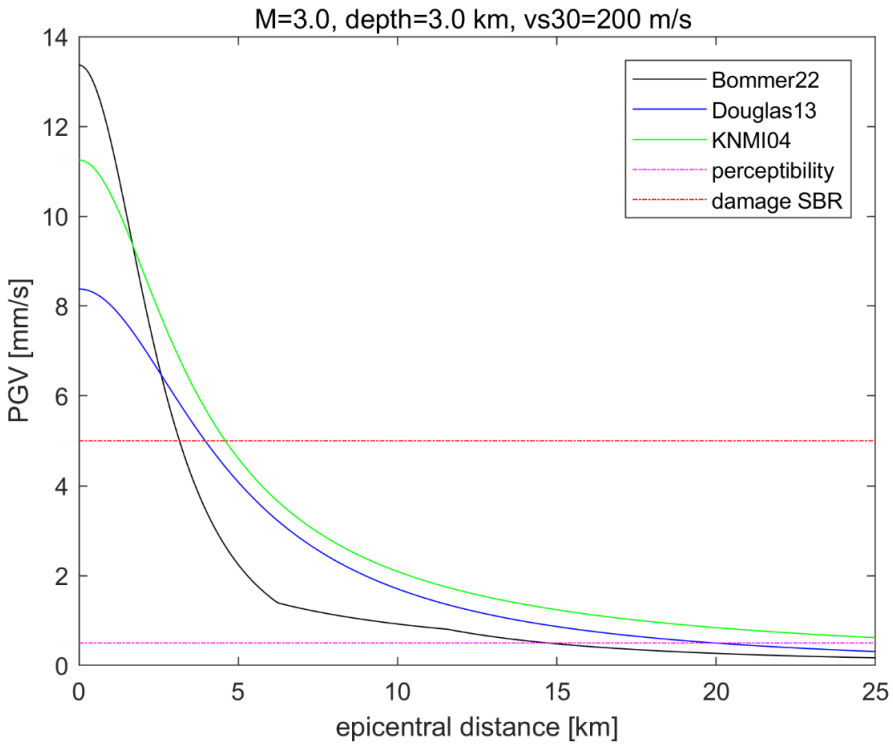

* Bommer22: mean model by (Bommer et al., 2022); Douglas13: mean model by (Douglas et al., 2013) with amplification factors by (Poggi et al., 2011); KNMI04: mean model by (Dost et al., 2004). Model parameters as indicated in the title.

Figure 28: Modelled peak ground vibration (PGV) as a function of epicentral distance using different ground motion prediction equations (GMPEs).

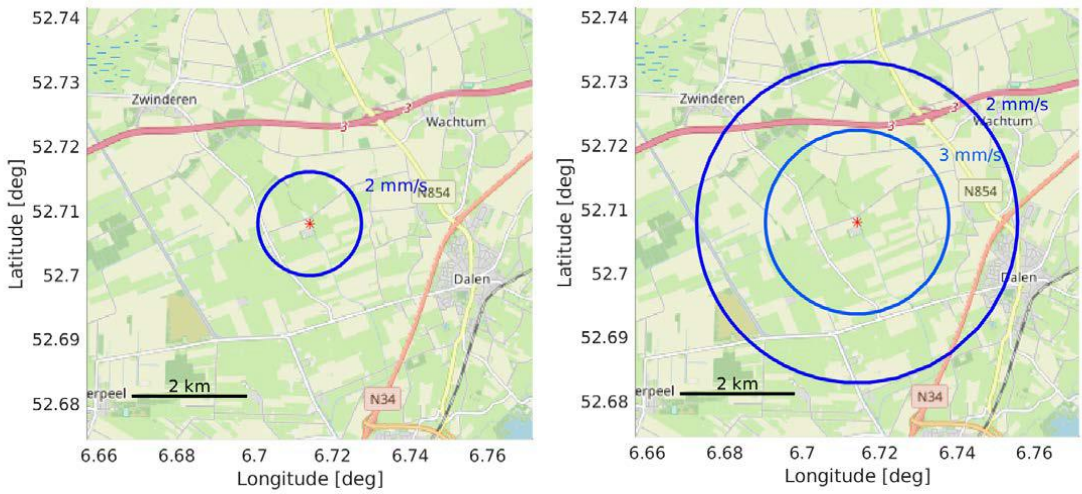

* Left: Circle depicting the bounding line of the 2 mm/s PGV threshold region for the P90 model, and the updated epicentre (red star). Right: Circle depicting the bounding line of the 2 mm/s and 3 mm/s PGV threshold regions for the P99 model. The 2 mm/s threshold value for the P99 model is for instance used by IMG to outline the “Huizinge circle” that determines the maximum area of influence for the Huizinge earthquake of 2012.

Figure 29. Example of different areas of influence of the M 2.0 Dalen event (17-7-2018) for different uncertainty model. (Source: Ruigrok and Dost, 2020)

6.6 Vertical fluid migration

Besides the influential area, the depth of influence is important to understand. When active pressure communication takes place between the shallow, intermediate, and deep subsidence, models may no

longer be able to accurately conceptualize the process for which they are developed. This can lead to significant discrepancies between the observed and modelled data, or, even worse, a fitted model that may not be able to accurately predict as it does not encapsulate the process for which it was developed.

6.6.1 Shallow – intermediate subsurface

Pressure communication between the shallow, intermediate, and deep subsurface may alter regional flow patterns. This largely depends on the lithological buildup including the presence and effectiveness of aquitards and sealing salt layers that delineate the subsurface regions, along with subsurface activities affecting the local pore pressure. The phenomenon of vertical fluid migration due to local and regional differences in pore pressure between the shallow and intermediate subsurface is well-documented in the Environmental Hydrogeology literature (Hantush, 1960; Neuman and Witherspoon, 1969; Christensen et al., 2009). In many Dutch polders, for instance, it is recognized that the local water table is influenced by seepage through Holocene aquitards (Bear, 1972; Wesseling and Wesseling, 1984). Moreover, salinization issues in various polders often stem from upward seepage originating from deeper saline aquifers (De Louw et al., 2010). Apart from seepage itself, the difference in pore pressure between the shallow and intermediate subsurface layers depends on various factors. These include precipitation and evapotranspiration-driven recharge, surface water levels, and localized drainage activities in the shallow subsurface. For the intermediate subsurface factors such as hydraulic heads in the hinterland, surface water levels intersecting aquitards between the shallow and intermediate subsurface layers (e.g., the sea), and groundwater extractions, play a significant role. Due to the interconnectedness of the shallow and intermediate subsurface layers, Dutch Water Boards require parties seeking a license for drainage activities to evaluate the impact of seepage in their studies whenever it is deemed relevant (SIKB, 2017). In case of large-scale groundwater withdrawal in the intermediate subsurface, e.g. for drinking water purposes, the effects on the phreatic water table and quality are assessed through an Environmental Impact Assessment (“m.e.r. beoordeling”).

The vertical influence area of groundwater extraction in the intermediate subsurface relies on the extent to which the local aquifer is penetrated by the groundwater well. In case of a fully penetrating well, the vertical influence area becomes nearly absolute throughout the vertical extent of the aquifer. Conversely, when water is extracted from a partially penetrating well, the induced flow becomes radial, significantly reducing the vertical influence area (Kruseman and De Ridder, 1970). However, considering the minimum relevance threshold of 5 cm established for the horizontal influence area in section 6.4.1, the vertical influence area will in practice often cover the entire depth of the aquifer.

6.6.2 Intermediate – deep subsurface

Similar to the shallow-intermediate subsurface interface, vertical pressure communication between the intermediate and deep subsurface relies heavily on the spatial distribution and hydraulic properties of flow-resisting layers, or aquitards. A sensitivity study by Birkholzer et al., (2009) shows that for perfect stratified systems that significant pressure communication between the intermediate and deep subsurface is possible when the average aquitard permeability exceeds 1.0×10^{-18} m^2 (about 1.0×10^{-6} m/d), assuming a sequence of 4 aquitards of each 100m thick. Given that the stratigraphy in the Northern Netherlands consists of a sequence of many low permeable aquitards between the deep and intermediate subsurface (Annex VII. Stratigraphic units), it is generally assumed that seepage between the intermediate and deep subsurface is insignificant (KEM-19, 2022). The vertical fluid migration associated with buoyant hydrocarbons is described in section 4.5.

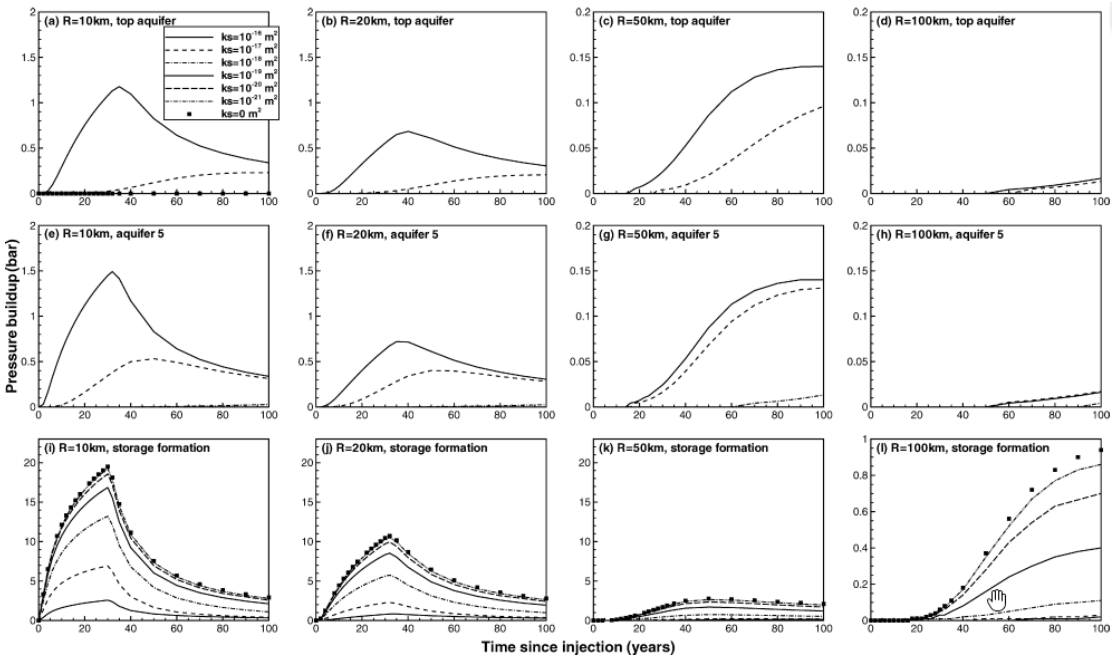

* Pressure results are plotted at different radial locations and in different aquifers, starting with the deep storage formation (bottom row), Aquifer 5 is located 700m above storage formation (middle row), and the top aquifer is located 1200m above the storage formation (top row). Aquifers 5 and 8 are separated from the storage formation by 4 and 7 aquitards respectively. Each aquitard is 100m thick with ks as the aquitard permeability. The permeability of the intermediate aquifers was held constant at 1.0 x 10-13 m2.

Figure 30. Sensitivity of pressure evolution to seal permeability of intermediate aquitards (Source: Birkholzer et al., 2009)

6.7 Type of Interactions

6.7.1 Shallow to intermediate subsurface

The hydrogeological feedback system on subsidence

The process of subsidence and heave is strongly coupled to changes in the hydrogeological system, even to the extreme that subsidence has a feedback loop through the hydrogeological system. In general, subsidence actively affects both the local geology, i.e. changing porosity, permeability, and thickness of hydrogeologic units, and topography, whereas hydrogeological processes are an important driver for shallow subsidence, driven by three natural factors: topography, geology, and climate (Tóth, 1999).

Thus, the strongly coupled system that hydrogeology and subsidence have is a feedback system, which is expected to be highly nonlinear considering the nonlinear equations governing the phreatic water levels and the compaction processes. The feedback system is schematized in Figure 31 and includes *human activities*, which, although not strictly speaking natural, is considered as the fourth major driver on the hydrogeological system (Cosgrove and Loucks, 2015).

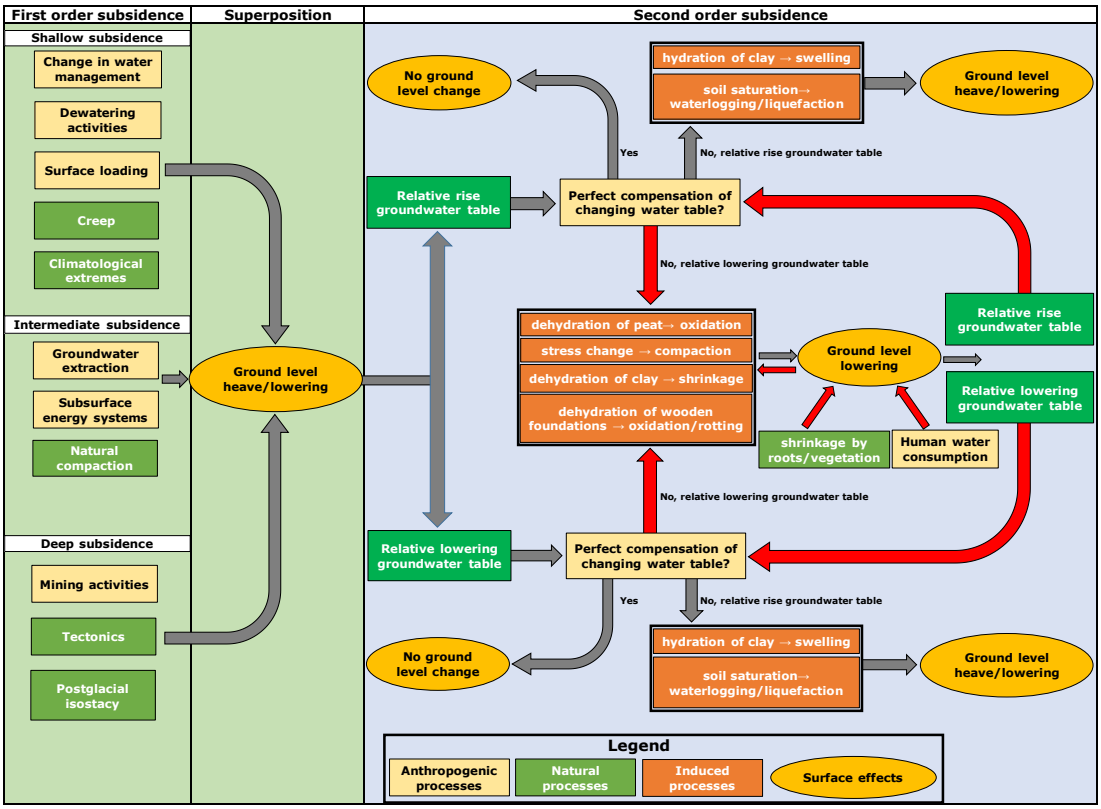

Figure 31. Reinforcing feedback loops affecting heave/subsidence

A first-order subsidence or heave effect is a change in local topography by means of accumulation of various anthropogenic and natural processes (Figure 31) The first-order effect of subsidence/heave contributes to a reinforcing feedback loop. Topography determines the magnitude and direction of groundwater flow, as groundwater flows from high potential to low potential areas (i.e. potential energy, is spatially distributed and varies). In other words, when first-order subsidence/heave increases the elevation differences at the surface (i.e. topography), groundwater flow will redirect and increase in magnitude towards lower lying drainage basins such as rivers, lakes, sea, or anthropogenic drainage systems like ditches and canals. By redirecting and increasing groundwater flow to lower areas, the groundwater table will decrease in higher areas (i.e. higher areas are more drained) and increase in lower areas (i.e. lower areas get wetter) assuming a constant recharge and seepage fluxes. When subsidence occurs in an area initially at higher elevation compared to its surrounding, (unlikely for shallow subsidence events as these areas tend to be more compaction resilient, which is precisely why these areas are elevated) first order subsidence will decrease groundwater flow towards the drainage basins, causing the groundwater table rise in higher areas, and lower in lower areas. Finally, there is a scenario where first order subsidence changes the direction of the topographic gradient, i.e. uphill terrain becomes downhill terrain with respect to the drainage system. In such cases, the direction of groundwater flow is reversed resulting in a relative rise of the water table in the former uphill terrain, and to lower in the former downhill terrain.

On the other hand, geology and diagenetic history determine the permeability of hydrogeologic units in the subsurface as well as the storage capacity of water in the subsurface. Processes such as compaction, shrinking/swelling of clays and peat oxidation change the local geometry and properties of hydrogeologic units, and therefore the capacity of the subsurface to conduct and store groundwater (Benson and Trast, 1995; Whalley et al., 2012). Together with topography, geological properties determine where and how much groundwater is stored in the subsurface and at what rates and patterns the groundwater flows (Tóth, 1999).

The effect of anthropogenic induced changes in geology on the shallow hydrogeological system proves to be a challenging subject for experts in numerical modelling, as back-coupling from geotechnical

models to hydrogeological models results in large computation times and uncertainties (Schmid et al., 2014). Hence, research often only focuses on the forward coupling from hydrogeology to subsidence, in terms of geology as well as topography, but generally does not include quantitative case studies on the back-coupling from subsidence to hydrogeology.

From a broader perspective, the size and gradient of the cumulative subsidence depression (i.e. bowl) in relation to the size and distribution of the drainage basin greatly determines to what extent the hydrogeological system will change on a local and regional scale. For instance, when the subsidence bowl surpasses the size of the drainage basin, which is often the case for subsidence with a deep origin, the entire drainage basin, and its surroundings experience subsidence (Figure 32). This results in large absolute changes in topography, but relatively minor changes in topographic gradient, causing a much smaller impact on groundwater levels with respect to the ground surface than one would expect based on the absolute subsidence observed (Kooij et al., 2021; Deltares, 2023).

Shallow subsidence often results in smaller and more irregular subsidence bowls compared to deep subsidence, resulting in higher degrees of curvature and topographic relief. This phenomenon is primarily attributed to a greater variability in soil compressibility within shallow unconsolidated sediments compared to deep consolidated sediments. Additionally, subsurface stresses responsible for changing the position of the ground surface during subsidence tend to disperse over a wider area as the distance between the subsidence event and the ground surface increases. The result is much gentler curvatures, and thus topographic relief, when subsidence has a deeper origin.

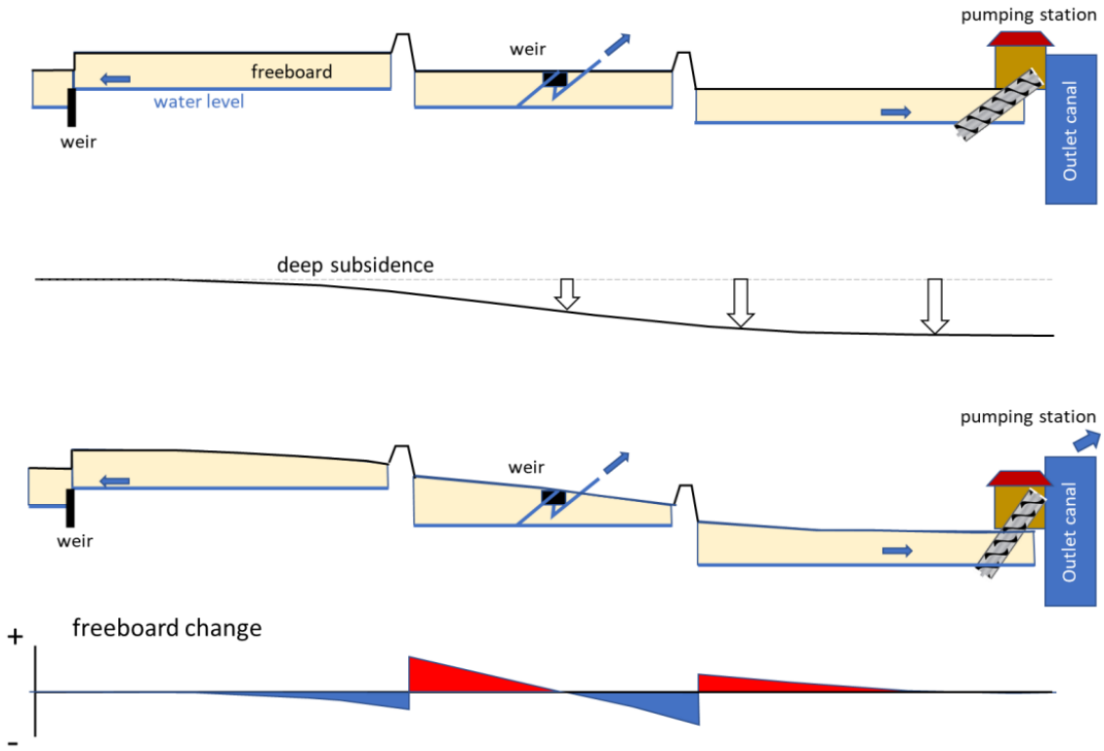

* Top panel: situation before deep subsidence, showing three areas with each a distinct water level maintained by controlling infrastructure (weirs and pumping stations). At the middle area, the discharge at the weir occurs at the middle of the profile in an out-of-profile direction. The other panels respectively show the deep subsidence, the impact on ground surface, water level and freeboard, and the freeboard change (red = increase of freeboard, blue = decrease of freeboard). In the sketch is it assumed that the water level at the drainage outlet canal to the right is maintained at the original level

Figure 32. Schematic illustration of the effect of deep subsidence on freeboard, i.e. the difference between land surface elevation and surface water levels of a fixed water level area (NL: *drooglegging*) (Source: Deltares, 2023).

Regional groundwater flow

Besides the local topography, geology and water management, the groundwater table in the phreatic aquifer is also linked to the regional groundwater system, i.e. regional topology, geology, and water management, through seepage from and towards the underlying aquifers (Figure 33). These regional hydrogeological feedback systems are slow to respond, and, depending on the hydraulic resistance of the Holocene aquitards, need changes in the order of decimetres to significantly change the regional seepage fluxes.

An example of changing regional water levels is the relative sea-level rise which is globally around 2.6 mm yr^{-1}, and near coastal plains up to four times faster at 7.8 to 9.9 mm yr^{-1} due to subsidence (Nicholls et al., 2021). For the Northern Netherlands an average sea-level rise of 6,3 mm yr^{-1} over the period 2018-2100 is projected, with a high estimate of 9,3 mm yr^{-1} (Vermeersen et al., 2018).

Major concerns regarding relative sea-level rise are the vulnerability of coastal lands to storm surges and floods (Nichols et al., 1999), and salinization of the coastal groundwater system (Oude Essink et al., 2010; De Louw et al., 2010; Colombani et al., 2015) leading to an overall deterioration of ground- and surface water quality. Especially when seawater intrusion can seep through the Holocene aquitards towards the phreatic aquifers, causing harm to, for example crop growth. However, the processes behind, the distribution of fresh and saltwater interfaces is rather complex due to its historic and site dependency.

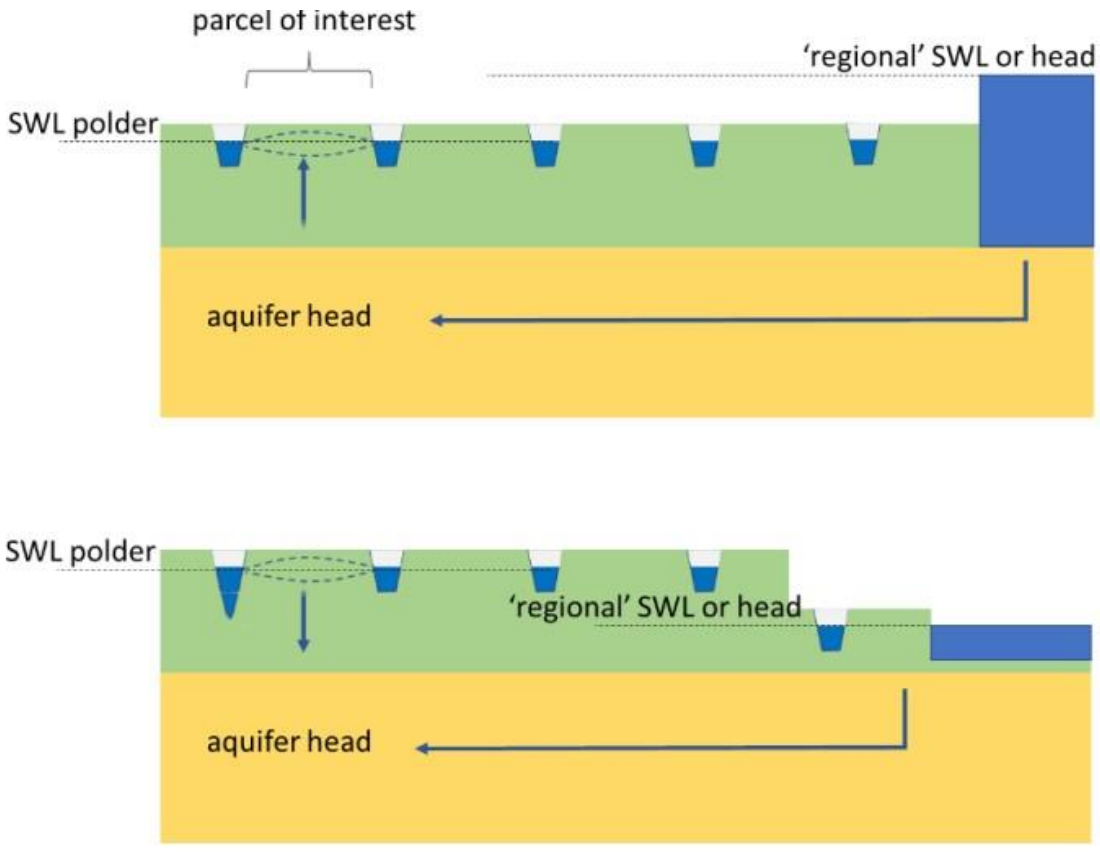

* Above the effect of high polder levels in the region or a relative sea-level rise. When significant, this will lead to an upward seepage flux at the parcel of interest, pushing up the local water table. Below the effect of a low polder level in the region. When significant, this will lead to downward seepage at the parcel of interest, pulling down its water table.

Figure 33. A schematic drawing of the influence of the regional groundwater system on the local seepage flux at the parcel of interest. (Source: Deltares, 2023).

Interplay of water management and subsidence

In the previous sections, we explained how an initial subsidence or heave event affects the hydrogeological system by changing the local topography and geology, resulting in local changes of water levels with respect to the ground surface. As also discussed before, the hydrogeological system is affected by human interferences. When a relative rise or regression of the water table is expected to cause societal repercussions, such as desiccation or waterlogging affecting agricultural production systems and natural areas, local governments and water boards generally opt to counteract them by adjusting the surface water levels to adjust the (ground)water table.

This adjustment is meant to compensate changes in the hydrogeological system underwent. However, the effectiveness of human water management is constrained by the spatial configuration of the available water management (drainage) system, leaving the intermediate areas between regulated waterways susceptible to fluctuations as a result of precipitation, evapotranspiration, seepage fluxes between the phreatic and confined aquifers, and properties of the entry resistance of the drainage system (Bear, 2012). These fluctuations are minimal near open waterways but peak at the centre of the (un)regulated parcels, which is the point furthest away from the waterways (Figure 34).

When parcels increase in size, for example as a consequence of land consolidation (NL: “ruilverkaveling”), larger drainage depths are needed at the waterways to maintain “dry feet” at the parcel centre, causing a net lowering of the groundwater table close to the waterways. However, land consolidation often goes hand in hand with drainage optimization, involving the installation of a network of drainage pipes across the enlarged parcel. Depending on their depth of connection to nearby waterways, and the hydraulic head difference between the (ground)water table and surrounding surface water levels, these pipes can both drain groundwater and supply surface water.

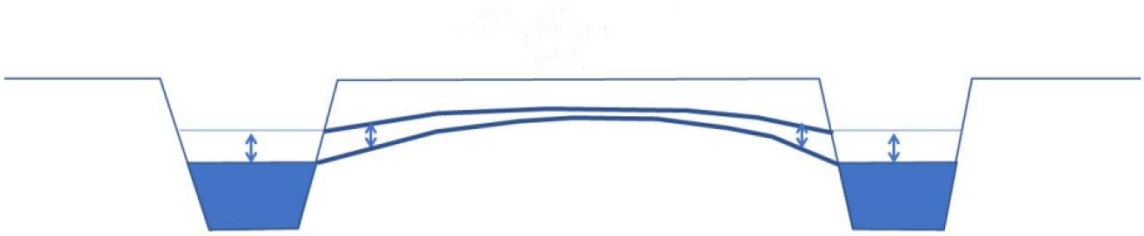

Figure 34. Sketch on how groundwater on a parcel can be regulated by changing the waterway levels. Due to the nonlinearity of the phreatic groundwater system, the groundwater levels closer to the waterways are more sensitive for changes in water management compared to the groundwater table at the parcel centre (Source: Kooij et al., 2019).

Section 2.6 describes how changes in surface water levels cause ground surface movement through shallow subsidence and clay swelling. Especially when the lithology around the changing water table consists of clay or peat, the resulting subsidence can amplify or damp the initial first order subsidence. This amplification or damping can be regarded as a second-order effect resulting from the initial, first-order subsidence.

When Water Boards keep mitigating the effects of second order subsidence by adapting surface water levels, a positive feedback loop can inadvertently be created (Erkens et al., 2016). Notable instances of such feedback loops are observed in clayey and peaty soils such as in New Orleans (Snowden et al., 1980) and the western Netherlands (Schothorst, 1977; Dufour, 1998), where land was reclaimed and drained at a constant level with respect to the ground surface. Figure 31 implies that the only solution to stop the reinforcing feedback loop is to restore the groundwater table as close as possible to its original position with respect to the ground surface (Erkens et al., 2016).

Theoretically, deep, and intermediate subsidence could potentially trigger a vicious subsidence cycle similar to the aforementioned case studies on land reclamation. However, the impact of deep subsidence on the regression of the relative groundwater table is in the order of centimetres (Kooij et al., 2019). When compared to the water table change required for land reclamation, which is in the

order of meters, this effect is very small. Consequently, the second-order subsidence resulting from deep subsidence is so small that it raises questions about whether water boards will intervene actively to mitigate the effects of the associated second-order subsidence. Given that waterboards typically operate with an operational accuracy in the order of decimetres, it's evident that active adjustments could potentially escalate the situation.

Interplay droughts and water demand on subsidence

Another important cause of subsidence through the hydrogeological system is the interplay between receding water tables, due to climate induced droughts, and increase in water demand. Especially agricultural water demand grows in a drying climate. Human water consumption, e.g., for irrigation, industry, and households, is known to intensify climatological droughts (Wada et al., 2013). An illustration of how the synergy between drought and water usage increases subsidence is evidenced in the Dutch province of Drenthe. Here, subsidence was locally accelerated to 10 mm/year during the droughts of 2018 and 2019. A distinct contrast to the typical subsidence rate of around 2 mm/year in the region (Heikes et al., 2021). A hydrogeological study revealed that the volume of water utilized for irrigation exceeded initial estimations and it was found that water levels had been overestimated by 10 to 30 centimetres, resulting in an underestimation of subsidence (Gielen et al., 2023). A more extreme case on how droughts and increase in water demand can accelerate subsidence is the San Joaquin Valley, USA, where subsidence rates up to 0.5 m yr^{-1} have been observed (Faunt et al., 2016),

6.7.2 Intermediate to deep subsurface

Subsidence

The approaches to subsurface modelling presented in section 2.10 consider the deformation associated with a single source of compaction, i.e., a single geotechnical facility. These methods imply hydro-mechanically coupled (poro-elastic) simulations.

In those calculations, the back-coupling from stress-changes to changes of the reservoir pressure is considered as a secondary effect. When ignoring this effect, the super-position principle of stresses holds. Thus, it is implied that the deformation signals of different sources of compaction can be superimposed, and the combined deformation signal from multiple sources can be modelled using the same approach, e.g., as implemented in KEM-16.

This is the core of the proposed study in phase II, as explained in Part II of this report, see for instance section 9.8.1, where the modelling strategy is elaborated.

Effect of gas extraction on salt caprock

Hydrocarbon reservoirs often have rock salt caprocks that undergo creep when exposed to shear stress. The pumping process induces compaction and shear stresses in rock salt, resulting in time-dependent ground deformations and surface subsidence. Finite Element models for medium-sized rock salt-capped reservoirs reveal that creep-induced subsidence is a significant factor, requiring meticulous modelling of rock salt caprocks (Marketos et al., 2016). The discussion addresses uncertainties in low-stress creep behaviour, various constitutive models for rock salt creep, and the spatial distribution of rock salt physical properties. This includes uncertainties in grain-size and chemical composition, influencing the overall subsidence response. Engineers tasked with predicting subsidence must consider these uncertainties and calculate response bounds based on multiple scenarios for rock salt body behaviour (Marketos et al., 2016).

Lateral fluid migration

The long-term (i.e. century scale) effects of fluid exchange and pressure redistribution between the Groningen gas reservoir and its surrounding aquifers are already investigated in KEM-19. (2022) and KEM-19b. The literature review in this study shows that the subsurface acts as a hydrodynamic system

and a long-term fluid exchange between post-production gas reservoirs and their surrounding aquifers is therefore considered likely (Verweij et al., 2012; Muggeridge and Mamode, 2012).

During oil or gas extraction from a reservoir, fluids are often drawn from nearby aquifers. The extent to which this occurs is described as “water drive”. The influx fluids into the reservoir actively restrains the pressure drop within the reservoir, while simultaneously causing a decrease in pore pressure in the nearby aquifers. Conversely, the pore pressure in the nearby aquifers decreases. However, upon abandonment of the reservoir, fluid migration persists, resulting in increased pore pressures within the depleted reservoir and further reduction of the pore pressure in the nearby aquifers.

Studies conducted at a Carbon Capture and Storage (CCS) site in Algeria have shown that the changes in pore pressures resulting from lateral fluid migration can lead to local subsidence or heave at the ground surface (Vasco et al.; Zoccarato et al, 2016, Békési et al, 2020). In the Northern Netherlands subsidence has been observed above aquifers connected to gas fields (Fokker et al., 2016; Fokker et al., 2018; KEM-19., 2022) and for the Groningen gas field pressure depletion in surrounding aquifers has been confirmed by means of numerical simulations (KEM-19, 2022).

In addition to the potential for subsidence and heave, the rise in pore pressure within the reservoir due to lateral fluid migration may theoretically trigger induced seismic activity along faults within the reservoir and its boundary faults (section 3.6). Moreover, findings from a modelling study by Moghadam et al., (2023) suggest that increased pore pressure could heighten the risk of hydrocarbon leakage along compromised wellbores, thereby increasing the likelihood of contamination in shallow aquifers. However, the KEM-19 study highlights that due to the significantly greater compressibility of gas compared to water, the pressure increase within a gas reservoir is relatively minimal in comparison to the pressure decrease within the aquifers during equilibration. This distinction, however, does not hold for depleted oil fields.

The numerical simulations conducted in the KEM-19 study, which explored various scenarios with unconstrained model parameters, align with the aforementioned range of hypotheses. It was modelled that a pressure depletion of 30 to 50% relative to the pre-production level would occur within the surrounding aquifers over the next 500 years, including the aquifer in the Lauwerszee trough region. However, this relative depletion of the aquifer in the Lauwerszee Trough is not anticipated to reach the Grijpskerk area within the next 100 years. Regarding the risk of induced seismicity, the elevated pore pressures within the reservoir of only a few bars were considered too small to activate intra-reservoir faults. However, such elevation in pore pressure could potentially induce seismicity on boundary faults.

The uncertainty in their numerical simulations often stemmed from unknown parameters related to aquifer properties, such as connectivity, pore pressures, and actual size. Furthermore, the potential influence of small gas fields near Groningen was not considered in this study but will be addressed in the following KEM-19b study.

Examples of international case studies on interactions

In this section we list international showcases for interactions between earthquakes and subsidence as well as for earthquake-earthquake interactions. These showcases stem from different geological and operational settings, which are not directly transferrable to the situation in the Netherlands. Some of the underlying geomechanical processes, however, may also be relevant for the analysis conducted in Part II of this study.

- Hejmanowski et al. (2019) investigate subsidence caused by two mining-induced earthquakes (M4.7 and M4.8) in Poland. Using InSAR data these authors identified local dynamic subsidence troughs of a regular shape and an aerial extent of about 2 km, which correlate with the epicenter location and time of the earthquakes. The maximum vertical displacement in these areas reached 116 mm. Subsequently, Witkowski et al. (2024) expanded the study by Hejmanowski et al. (2019) and identified further examples in Poland, where mining induced earthquakes (M>3) correlate with

local subsidence troughs. For all examples, these authors infer a shallow "collapse" depth of several hundred meters below the surface. The authors infer a substantial aseismic contribution to the observed subsidence, although the exact processes have not finally been resolved.

- Surface elevation changes in the order of several meters have been observed following great earthquakes (e.g., Wells & Coppersmith, 1994). Hughes et al. (2015) report major topographic changes caused by a sequence of M_W 6–7 earthquakes at Christchurch, New Zealand. Here, liquefaction in susceptible soils with high water tables was manifested at the ground surface in earthquakes as low as M_W 5.0.

- The Lorca area (Spain) has undergone one of the highest subsidence rates (16 cm/yr) in Europe as a direct consequence of long-term groundwater extraction (Fernandez et al., 2018). Gonzales et al. (2012) suggest that associated unloading stresses influenced the occurrence of a magnitude Mw 5.1 earthquake.

- Remote triggering (compare section 3.13 and 6.5.1) is observed in several geothermal reservoirs. For example, Baisch et al. (2006) report an earthquake exceeding magnitude ML=3 that occurred minutes after strong teleseismic wavetrains passed the geothermal reservoir. These observations indicate that remote triggering can occur even ~1 year after the termination of anthropogenic activities.

Interaction case studies from The Netherlands

In this section we discuss a few (non-exhaustive) cases where interaction between different mining activities play a role in northern part of The Netherlands.

- Lateral interactions between salt solution mining and gas extraction: In the western Fryslân province of the Netherlands, both halite solution mining and natural gas production caused subsidence exceeding original predictions. By 2015, the salt subsidence bowl experienced 33 cm, compared to the 7 cm forecasted in 1995. Above the Harlingen gas field, subsidence reached 33 cm in 2015, exceeding the 10 cm prediction for 2003. Accelerating subsidence led to a project reassessment in 2008. Higher-than-estimated cavern convergence rates explained salt mining discrepancies, while gas field subsidence resulted from pore-collapse in the reservoir chalk. Corrections made in 1998 improved salt mining predictions and understanding loading rate impact on pore-collapse stress levels enhanced alignment with field behaviour in gas production, emphasizing the need for such considerations in subsidence forecasts (de Waal et al., 2016).

- De Hoeve induced seismicity due to water injection: On the 26th of November 2009 a seismic event of M 2.8 occurred near the village De Hoeve in Fryslân. At first it was not clear whether this was related to gas extractions since no gas extraction activities took place in this area at the time. Also, the KNMI did at first not contribute this event to gas extraction. There was however a well present from Vermilion that was used for water injection at the time. After some analysis it was concluded by the operator that this event was probably related to the water injection (TCBB, 2018)

- Combined effects in the Veendam area: The Veendam area in Groningen is an area that is influenced by the combined effects of multiple mining activities. The gas extraction from the Groningen fields causes induced seismicity and subsidence, the influence of which overlaps with the salt mining activity in Veendam, and the salt mining and gas storage in Winschoten/Heiligerlee and Zuidwending. The ceased gas extraction south of Veendam from the Annerveen gas field has over the years also had overlapping influence areas. Currently, IMG and CM are collaboratively investigating the combined effects of these overlapping mining activities and working to distinguish their individual contributions. The findings of this research, called the GEMMA program, have not been published yet.

.

PART 2: PROJECT PLAN PHASE II

7

CASE STUDY AREA

7.1 Summary and conclusions

This chapter describes the Grijpskerk area from various perspectives. The landscape is diverse, including sea clay and peat extraction landscapes with distinct characteristics and historical influences. Regional subdivisions like De Marne, Lauwers, Middag-Humsterland, Reitdiep, Westerkwartier, and Oostergo are detailed. A field excursion provided insights into the geography and stakeholder concerns related to mining activities.

Deep geological features of the UGS Grijpskerk and surrounding gas fields in the Lower Rotliegend sandstone reservoir rock within the Lauwerszee Trough sub-basin are described. The geological map reveals the Lauwerszee Trough's formation during the Caledonian orogeny, influencing sedimentation and creating fault systems. Evidence of fault activity is observed in formations above the Permian, with long-lived geological activity.

The Pleistocene witnessed three glacial periods, influencing sediment deposits, and forming distinctive features. The Eemian interglacial period led to a significant sea-level rise, while the Weichselian period created a tundra-like environment with sand deposits. The Holocene saw sea-level rise, shaping the current landscape. Human activities, such as peat exploitation, formation of dwelling mounds, dewatering and dike construction, played a crucial role in landscape formation.

The hydrogeological system is divided into shallow, intermediate, and deep sections. The shallow geology is influenced by factors like polder water management, precipitation, and seepage. Intermediate hydrogeology focuses on Quaternary sandy units, while deep hydrogeology comprises marine deposits with limited influence on shallower systems.

The geomorphology is primarily tidal dominated, featuring tidal inlets, creek channels, and levees with thick clay deposits. Pleistocene sand ridges and ground moraines contribute to landscape diversity. Buildings generally have shallow foundations. Water management is overseen by two water boards, and the freeboard concept plays a crucial role in regulating surface water levels.

7.2 Samenvatting en conclusies (NL)

Dit hoofdstuk beschrijft het gebied Grijpskerk vanuit verschillende perspectieven. Het landschap is divers, met onder andere zee klei- en veenwinningslandschappen met kenmerkende eigenschappen en historische invloeden. Regionale onderverdelingen zoals De Marne, Lauwers, Middag-Humsterland, Reitdiep, Westerkwartier en Oostergo worden gedetailleerd. Een excursie bood inzicht in de geografie en de zorgen van belanghebbenden met betrekking tot mijnbouwactiviteiten.

De geologische kenmerken van het UGS Grijpskerk en omliggende gasvelden in het reservoirgesteente van het Lower Rotliegend-zandsteen binnen het subbekken van de Lauwerszee Trog worden beschreven. Diverse geologische bronnen laten de vorming van de Lauwerszee Trog tijdens de Caledonische orogenese, zien met invloed op sedimentatie en de vorming van breuksystemen. Bewijs van breukactiviteit is zichtbaar in formaties boven het Perm.

Het Pleistoceen kende drie ijstijden, met invloed op sedimentafzettingen en het vormen van kenmerkende kenmerken. Het Eemien-interglaciaal leidde tot een significante stijging van de zeespiegel, terwijl het Weichselien een toendra-achtige omgeving met zandafzettingen creëerde. Het Holoceen zag een stijging van de zeespiegel, wat het huidige landschap vormgaf. Menselijke activiteiten, zoals veenontginning, bewoning op terpen en wierden, afwatering van polders en maken van bedijkingen, speelden een cruciale rol in de vorming van het landschap.

Het hydrogeologische systeem is verdeeld in ondiepe, tussenliggende en diepe secties. De ondiepe geologie wordt beïnvloed door factoren zoals polderwaterbeheer, neerslag en kwel. De tussenliggende hydrogeologie heeft zandige eenheden uit het Kwartair, terwijl de diepe hydrogeologie mariene afzettingen omvat met beperkte invloed op ondiepere systemen.

De geomorfologie wordt voornamelijk getij gedomineerd, met getijdeninlaten, kreekkanalen en dijken met dikke klei afzettingen. Pleistocene zandruggen en grondmorenes dragen bij aan de diversiteit van het landschap. Gebouwen hebben over het algemeen ondiepe funderingen. Waterbeheer wordt overzien door twee waterschappen, en het concept van de drooglegging speelt een cruciale rol bij het reguleren van het waterpeil.

7.3 Introduction

Based on the problem definition and research questions, the decision was made to delineate the region centred around the UGS Grijpskerk. The adjacent small gas field area is also within the scope but limited to the gas fields in the immediate vicinity and within the geological constraints of the Lauwerszee Trough. Gas fields in the Wadden Sea and further south towards the UGS Norg are not included in the scope. The general outline is illustrated by the black box (Figure 35), with a specific focus area outlined in the red box. It is important to note that the approach employed in this study is data-driven, meaning that data outside the study area may be incorporated if necessary. Therefore, the outline should not be viewed as a boundary for input but rather as a constraint for output in the analysis. It is also important to emphasize that if an effect is detected or potentially extends beyond the project outline, it will still be considered, particularly in cases involving indirect effects on groundwater or hydrology. This impact may extend beyond the defined area due to the irregular nature of the waterboard's water management zones.

A significant portion of the terminology employed in the subsequent sections is derived from typical Dutch concepts and terminology associated with the local soil conditions and the longstanding traditions of land reclamation and water management. Some of the terms are challenging to translate, and as such, the original Dutch words or terminology are retained. In chapter 10 names and terminologies can be looked up for their definition and explanation.

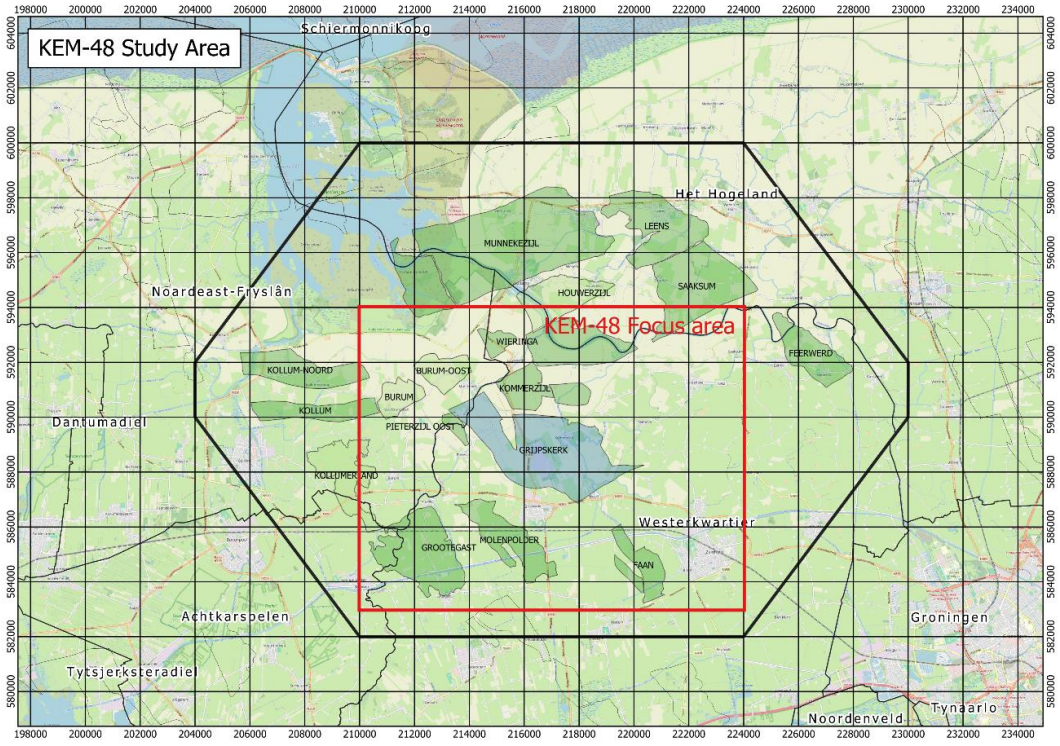

Figure 35. Overview map of the case study area. With the general outline of the scope area (in black) and focus area (in red). The outline of the relevant gas-fields is provided with their names.

7.4 Experiences from the fieldwork/bicycle tour

On Tuesday, October 31st 2023, a bicycle tour took place around the Grijpskerk area, organized by two members of the KEM-48 team, Siefko Slob (Cohere Consultants) and Wout Hanckman (Crux). The purpose of the field visit was to gain insight into the landscape, land use, land cover, hydrology, geomorphological elements, and their connection to geology and the shallow subsurface.

Erik Meijles from the University of Groningen, the external reviewer of the KEM-48 project with specific geographic knowledge of the area, led the tour. The client (MEA) representative and member of the KEM panel, also participated. Stakeholders Grietje Zijlstra, Frans Talstra, and Wridzer Bakker were present as well to provide the local content.

The field visit commenced at the Grijpskerk station, following the route outlined in Figure 93, passing through UGS Grijpskerk and visiting villages such as Kommerzijl, Pieterzijl (for a coffee stop), Warfstermolen, Munnekezijl, Zoutkamp, Lauwerzijl, Pieterzijl (for lunch), Visvliet, crossing the Van Starkenborghkanaal, Lutjegast, Grootegast, Sebaldeburen, and again crossing the Van Starkenborghkanaal back to Grijpskerk.

The tour encompassed various NAM locations, including Munnekezijl-1, Krabburen-1, Lauwerzijl, and Grootegast-100, as indicated on the route map in Figure 93. The site visit covered a significant portion of the KEM-48 Focus area. The eastern part of the focus area (Zuidhorn/Noordhorn, Niehove, Oldehove and Saaksum was because of time constraints not covered.

Items that were identified during the field visit (the photos are shown in Annex VI):

- NAM UGS complex Grijpskerk (see Figure 100)
- Geodetic marker on house north of Niezijl (see Figure 101)
- Damage at farmhouse along Hogeweg (Kommerzijl)
- Old sluice in Kommerzijlsterriet river at Kommerzijl (See Figure 104)
- Old valley structure visible in landscape, currently followed by the Kommerzijlsterriet river.

- Remnant of dike structure (Ooster-Waarddijk) (see Figure 106)
- Crossing of Lauwers river in Pieterzijl into Fryslân
- Sluice complex near Zoutkamp (Friesche sluis) where the Lauwers rivers empties into the Lauwersmeer (see Figure 104)
- Pass by NAM complex Munnekezijl-1 and Krabburen-1 where geodetic markers are attached to utility buildings.
- Pass by NAM location Kommerzijl (Figure 105)
- Near Eibersburen view on old Farmhouse with clear visible damage which has a geodetic marker. Near the NAM location Grootegast-100 (Grootegast gas field) (see Figure 108)
- Around Lutjegast and Grootegast change to a different landscape and landuse, i.e. smaller agricultural plots, mainly for grazing, less open landscape with more trees, which has a clear relation with the subsurface. In the area further north, the soil is mainly sea clay and around Lutjegast and Grootegast the soil becomes sandier and with more relief variation (see Figure 110 and Figure 111)
- From Sebaldeburen on the way back to Grijpskerk different landscapes were crossed.

The time was not sufficient to cover all areas and all aspects, but the field visit was useful to get a general view of the focus area. The coffee- and lunchbreak at the community centre in Pieterzijl was useful to talk in-depth with the stakeholders. The general impression is that the area is characterized by a mix of rural landscapes, villages, and water features. Here are some general features of the area around Grijpskerk:

Agricultural landscape: The region is predominantly rural, with vast expanses of agricultural fields, including farmlands for crops and pastures for livestock.

Villages and settlements: Grijpskerk itself is one of the larger villages within this landscape, and there are other smaller villages and settlements scattered throughout the area. Grijpskerk has a train station, high school, industrial area, supermarket, sport fields, nursing home, library, and other facilities.

Building stock: the building stock is varied. The village centres primarily feature older detached or semi-detached houses, while the rural areas outside the villages showcase scattered farmhouses accompanied by their stables and utility buildings. Additionally, many villages include relatively new terraced or detached houses. Stakeholders highlight that a significant portion of the building stock in the region has experienced varying degrees of damage, with some instances believed to be associated with gas production and/or storage activities.

Water features: The presence of canals, rivers, dikes, and sluices. The waterways are playing an important role in transportation (industrial and recreational), the local hydrology and landscape (see also Figure 97 in Annex V.

Gas fields: there are various industrial gas locations, all operated by NAM. These are infrastructures for gas well maintenance, gas extraction, storage, and distribution. The NAM location for UGS Grijpskerk is one of the larger locations.

Cultural and Historical Elements: The area also has cultural and historical elements, such as historic buildings, farmhouses, churches, bridges, dikes, sluices and man-made dwelling features and other structures that contribute to the region's heritage.

Scenic beauty: While the terrain is generally flat, the openness of the landscape, the historic villages and man-made dwelling mounts and the presence of water contributes to the scenic views. The Lauwersmeer is a national park and the area Middag-Humsterland has been designated as National Landscape (Nationaal Landschap.)

7.5 Geographical Description and Landscape Types

The project area has a diverse cultural, geographical, and geological history. The region has been extensively described and studied, providing a wealth of sources and data. The Dutch Cultural Heritage Agency (Rijksdienst voor Cultureel Erfgoed) has divided the Dutch landscape into 78 regions in Panorama Landschap (Raap et al., 2022). These regional descriptions serve as brief landscape biographies, forming the basis for further research into the landscape history of each region. This initiative aligns with Histland, a nationwide classification system for historical cultural landscapes in the Netherlands developed by Wageningen UR. Histland distinguishes 45 landscape types and 11 main types (Dirkx and Nieuwenhuizen, 2013; Barends 2010), establishing connections between the historical landscape of a specific area, the processes leading to that landscape, the current landscape forms, and the extent of landscape changes since 1850, the benchmark year (de Bont, 2004; Dirkx and Nieuwenhuizen, 2013).

Furthermore, the landscape can be described from a geomorphological perspective, connecting to the description of shallow geology (see section 7.11.1).

In this section, we broadly follow the descriptions per region based on '*Panorama Landschap'*. Each region is systematically described at two levels, and this information for each region can be accessed through the interactive online map viewer (RCE, 2024a).

The **first level** involves a description based on the so-called "structure carriers" Structure carriers are significant structures and elements organized according to their landscape-forming function. In broad strokes, the research area can be characterized as the Northern Netherlands sea clay landscape. The southern part of the project area represents a typical North Dutch peat extraction landscape (see Figure 36).

The **second level** provides a description based on the classification according to Histland (RCE, 2024b), offering a perspective on the historical development. The Main Landscape Types are given in Figure 37. Below in section 7.5.1 and 7.5.2, the various Main Landscape Types present in the project area are described.

The **third level** involves a description and classification based on landscape characteristics (Regions) (RCE, 2024b), as further elaborated in section 7.7 and shown in Figure 38.

7.5.1 Northern Netherlands Marine Clay Landscape (Het Noord-Nederlandse zeekleilandschap)

The Northern Netherlands sea clay landscape is known for its open character with elevated mounds (*terpen* in Fryslân, *wierden* in Groningen) on salt marsh ridges. After 1840, many mounds were excavated for terp soil, resulting in steep edges. The area included livestock farming on lower salt marshes, agriculture on salt marsh ridges, and radial plot division from the mounds. Salt marshes exhibited irregular block parcelling due to the use of existing channels, while younger polders had a more regular pattern. Extra-dike drinking wells (NL: *dobben*) were constructed for livestock.

Ring dikes were built from the 10th century, followed by core- or mother polders (Frisian terminology) and the reclamation of areas such as De Marne. Monasteries played a significant role in this process. Regular dike breaches resulted in water basins (NL: kolken). Locks (NL: *zijlen*), later supplemented with mills and pumping stations, were used for drainage. Villages sometimes emerged along zijlen, and canals were dug to connect villages. A micro- or surficial drainage network system was created to feed into the main canals.

Stinsen/stinswieren, dating back to the 13th century, were originally elevated stone towers with moats and earthen walls. From the 16th century, they lost their original function and were converted into country houses, such as *states* in Fryslân and *borgen* in Groningen.

Main Landscape Types:

- Old marine clay polders: Polders formed by diking inhabited salt marsh areas. Old sea clay polders are often referred to as old land polders. They are also known as salt marsh ridge and/or *knikklei* reclamations. These polders were usually constructed before the 13th century from a salt marsh ridge, sandbar, or other natural elevation. Often, the young sea clay polders are arranged around the old sea clay polders.
- Young marine clay polders: Polders formed by embanking sea incursions and new accretion. Young sea clay polders are often referred to as newly reclaimed lands. These polders were typically developed after the 13th century through the systematic construction of dams or dikes. Polders created in the 19th and 20th centuries can also be classified as young sea clay polders.
- Natural vegetated ('untouched') landscapes: Often areas outside dikes or recently reclaimed areas, such as salt marsh areas not yet suitable for agriculture. The outer dike area around the current Lauwersmeer and the outer dike Wadden Sea area north of De Marne are examples within and in the vicinity of the project area. These areas are still dominated by a dense network of anthropogenic ditches. These areas are of high natural value.

7.5.2 North Dutch Peat Extraction and Reclamation Landscape (Noord-Nederlands veenontginningslandschap)

A water-rich landscape with many small towns that originated at the intersections of trade routes and waterways. The ribbon villages are small, and in Fryslân, simple churches with bell towers are common. Outside the cities and villages lies a flat, open landscape with elongated, strip-shaped plots. During peat extraction, there was no strong feudal authority, giving rise to the irregular patches and differences in size and shape of the reclamation blocks. Although the peat is virtually gone, the peat reclamation history is still visible in the area. The land is intersected by many waterways. To protect the area, dikes, embankments, locks, mills, and pumping stations were constructed. In many places, villages were relocated after some time (sometimes multiple times) due to the land becoming too wet from subsidence. The peat polders in Fryslân are redeveloped former peat extraction areas, often based on the old landscape structure.

Main Landscape Type (according to Histland):

- Peat extraction/reclamation landscapes: The peat extraction or reclamation landscape in Groningen originated in the Middle Ages (Zomer, 2016). The landscape resulted from draining the peat areas by digging ditches and canals. This led to rectangular plots suitable for peat extraction and agriculture. The landscape is characterized by straight waterways, roads, and elongated farms. The enduring influence of historical reclamation is clearly visible in the form and structure of the peat extraction/reclamation landscape.

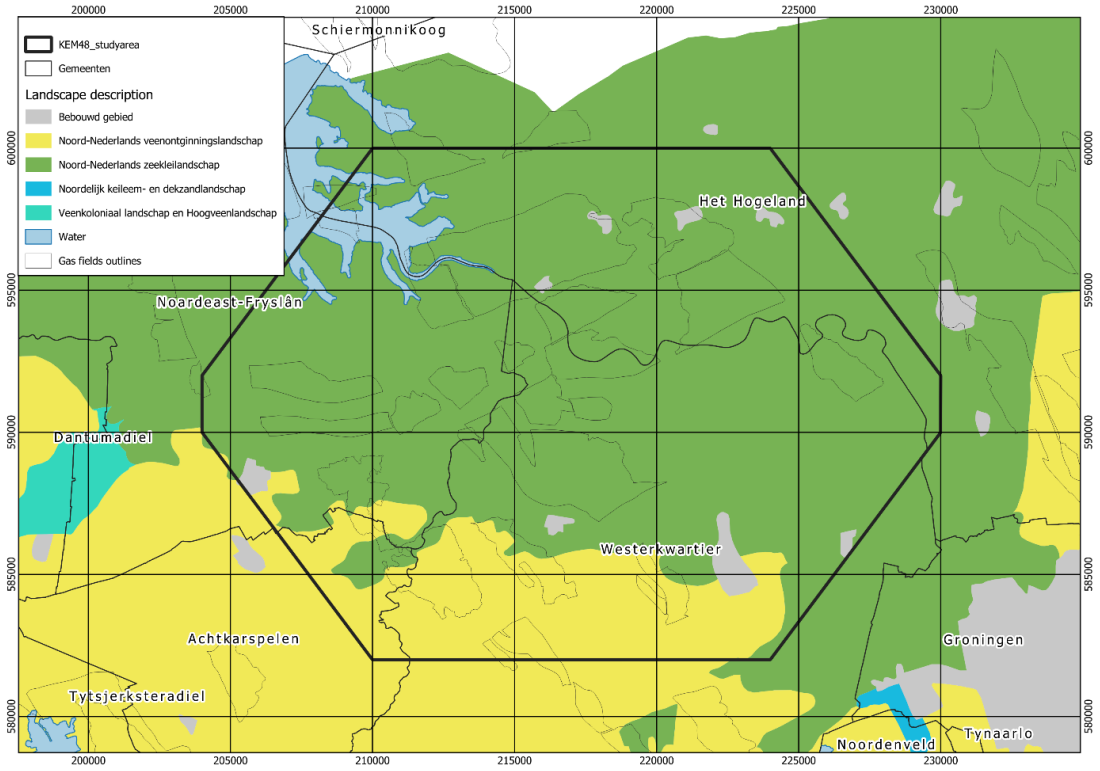

Figure 36. Map of the case study area with the (first level) Panorama landscape region (RCE, 2024a).

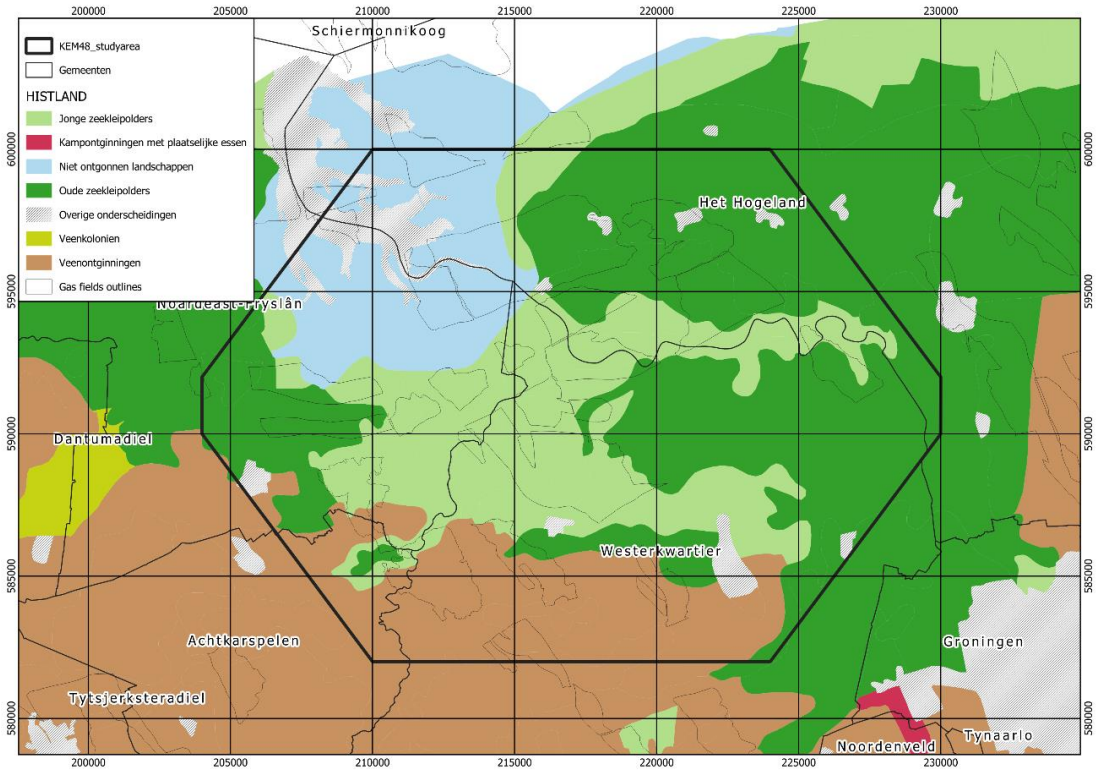

Figure 37. Map of the case study area with the main landscape types (second level) according to the classification of Histland (RCE, 2024b)

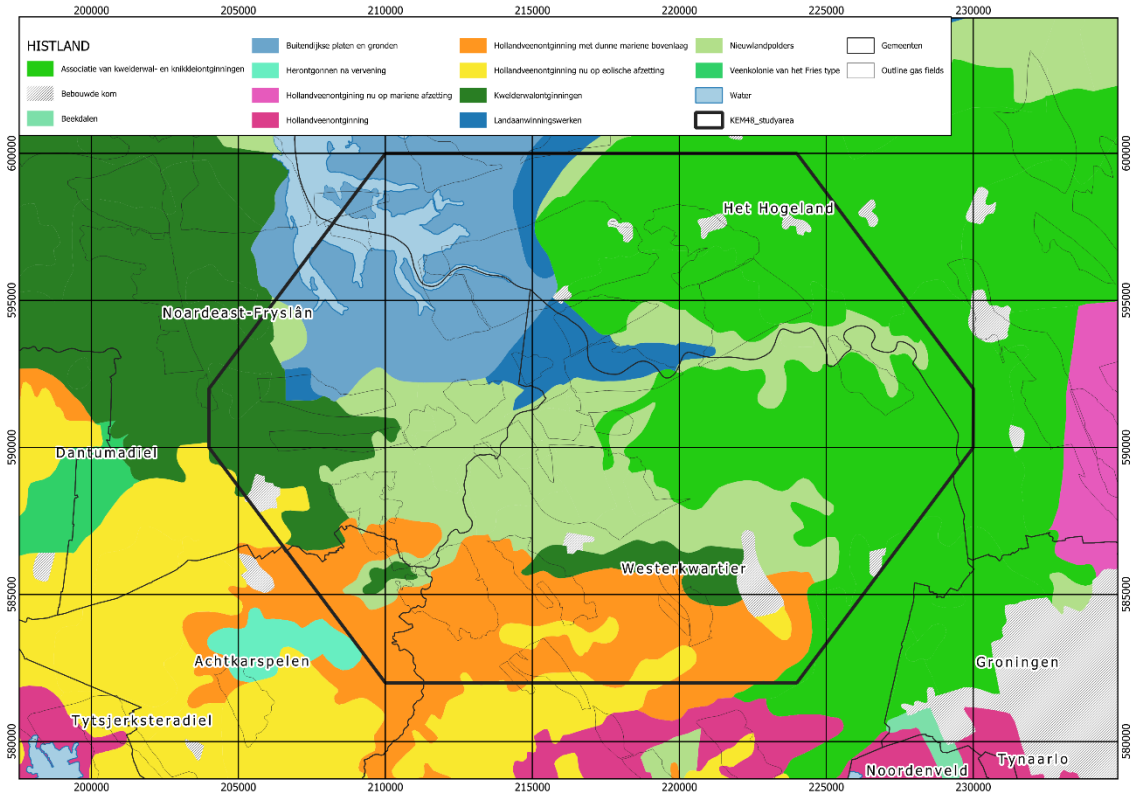

Figure 38. Histland-based (third level) classification of the landscape. (RCE, 2024b)

7.6 Landscape history of the area

The northern part of the research area is a region that has been strongly influenced by rising sea levels since the end of the last ice age (about 12,000 years ago). It is an area characterized by faults, tidal areas, salt marshes, and salt marsh ridges. Deep valleys in the landscape, such as the ancient Hunze Valley carved out by glacial ice in previous ice ages, were natural depressions where the sea could easily intrude. The advancing sea eventually covered the Hunze Valley with clay, transforming the original sand-dominated landscapes.

Sand ridges north of the Wadden Islands formed an open coastline with an intertidal area, which is now the Wadden Sea. During periods of sea level rise, the coastline shifted inland, but after 5000 BCE, the land began to grow again. At the mouth of the (then) Hunze River, a tidal basin of mudflats and salt marshes, the Hunze Basin, formed. The Hunze Basin roughly extended between Groningen and Dokkum. It was a Pleistocene system of erosional valleys bordered on the east by the Winsum High and on the west by the Oostergo High (Zomer, 2016 cf. Figure 39).

Salt marsh ridges formed at the edge of this basin through sediment deposition during floods, while bank ridges formed along inland watercourses. The relief of salt marsh and bank ridges influenced the hinterland, resulting in a landscape of higher sandy soils and lower salt marsh basins with heavy clay soils (Westerhuis et al., 2023 and references therein).

The first settlements in the salt marsh area (from 600 BCE) were established on *wierden* and *terpen*, artificial mounds built to stay dry during high tides. Villages on artificial dwelling mounds were formed, often on slightly higher bank ridges of the Hunze river. In addition to village mounds, house mounds can also be found, elevated dwelling areas for usually one farm. These dwelling mounds are usually somewhat younger (11^{tht}-12^{th} century). The village terps and house terps can still be easily identified on the geomorphological map and the AHN (lidar-based height model of The Netherlands) (see Figure 95 and Figure 96).

A breakthrough of the Lauwers Sea in the northeast created a connection with the Hunze Basin, creating an east-west connection. Around 800 AD, the Hunze River began to follow this connection, creating the Reitdiep. The origin of the Reitdiep, whether natural or artificial, is unclear, but human influence is suspected. Until the 12th century, the sea had free reign in the Reitdiep watershed. This led to floods and the retreat of salt marsh inhabitants.

The salt marsh landscape gradually lost ground to the sea. Agricultural peat extraction and associated land subsidence made the landscape more vulnerable to floods, especially during storm surges (Nieuwhof and Vos, 2007). Due to a southern incursion of the Lauwers Sea, a channel was formed in the first millennium that separated Middag and Humsterland (Westerink, 2022).

From the 12th century, dikes were constructed on a larger scale to protect the hinterland from floods. The first dikes were built along the banks of rivers and channels running through the area. These dikes were often not sufficient, and house terps were still being made until 1300 to be safe from floods. Especially the Marne area still experienced strong influence from the Lauwers Sea. In the 13th century, the Zuiderdijk or Zuurdijk was constructed, following a straight path due to the absence of natural elevations. In 1287, this dike was destroyed during the St. Lucia flood, leading to the construction of a new dike about one kilometre south of the original dike. This new dike ran along Houwerzijl and Ewer to Barnegaten.

In the 14th century, various dikes were built along the Reitdiep from Schillingeham to Groningen, especially after the floods in 1361. These dikes can still be clearly recognized in the landscape (Westerhuis et al., 2023). In the Westerkwartier, the Wester Waarddijk and its extension, the Oosterwaarddijk (from Munnikezijl to Kommerzijl), can still be clearly identified. These dikes have no official protected standing, which is why in some places, these dikes are still partially excavated by landowners today.

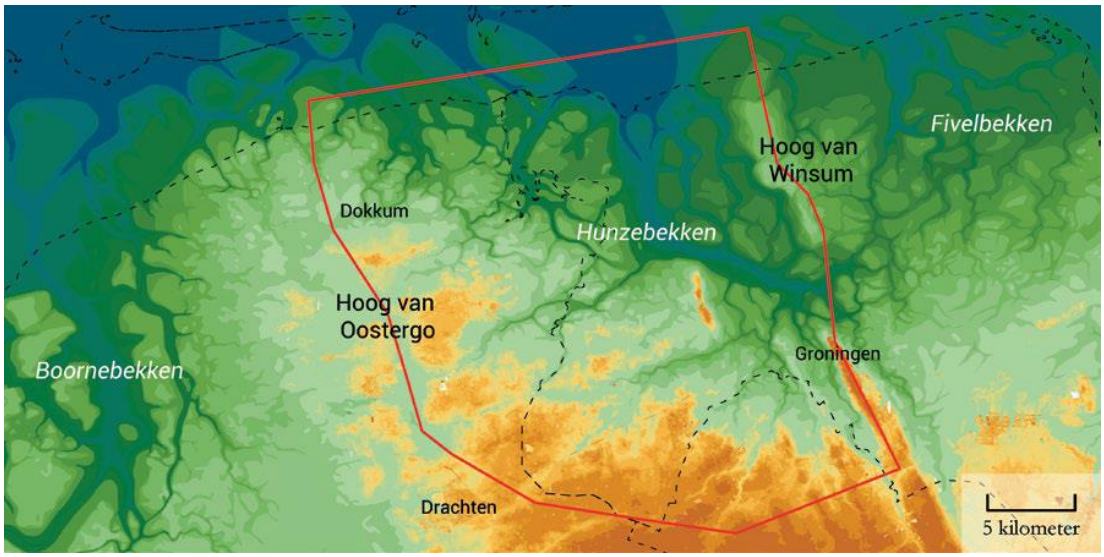

Figure 39. The Pleistocene depth map of the Hunze basin (NL: Hunzebekken) and surroundings (Zomer, 2016)

7.7 Regions

The research area can be roughly divided into the following regions, according to the RCE system (Raap et al., 2022), also see Figure 38:

- De Marne: De Marne is a large, open clay soil area with terps on salt marsh ridges. In the project area, this is the region north of the Reitdiep, covering the western part of what is now the current municipality of Het Hogeland. It includes, among others, the villages Zoutkamp, Ulrum, Leens, and Eenrum.

- Lauwers: The area northeast of Kollum in Fryslân, including the watershed of the Lauwers and the area of the Lauwersmeer National Park. It includes the most eastern part of the municipality of Noardeast-Fryslân, the northwestern part of the current municipality of Westerkwartier, and the western part of the municipality of Het Hogeland in the province of Groningen. It includes, among others, the villages Visvliet, Lauwerzijl, Kommerzijl, Pieterzijl, Munnekezijl, Burum, Warfstermolen, and Kollummerpomp.
- Middag-Humsterland and Reitdiep: The area south and west of the Reitdiep and east of the Lauwers River, covering the northeastern part of the current municipality of Westerkwartier. It includes the historical sub-areas Humsterland and Langewold. It includes, among others, the villages Grijpskerk, Niezijl, Noordhorn, Niehove, Oldehove, Ezinge, Feerwerd, Garnwerd, and Aduard.
- Westerkwartier: Part of a typical peat extraction/reclamation landscape. The northern part of Westerkwartier is formed by the transition from the keileat plateau to the clay area. This part of the region originated under the influence of the Lauwerszee and the Reitdiep. The area includes the southern part (south of the Van Starkenborgh Canal) of the current municipality of Westerkwartier and includes, among others, the villages Lutjegast, Niekerk, and Zuidhorn.
- Oostergo: Oostergo is an open Frisian terp landscape with old sea clay polders. This region covers a relatively small area in the extreme southwest of the project area. It is an area in Fryslân with the villages Kollum and Gerkesklooster, respectively in the municipalities of Noardeast-Fryslân and Achtkarspelen.

7.7.1 De Marne

Characteristic of the De Marne region is an agricultural landscape consisting of old, open areas that are slightly higher and surrounded by the former sea basin of the Hunze. The core area of De Marne includes a *wierde* landscape consisting of successive salt marsh ridges, separated by older tidal flat depositsand salt marsh planes. Along the coast are un-diked salt marshes. Further out are the tidal flats that are part of the Wadden Sea, which is a protected nature reserve. The salt marshes have been formed through systematic land reclamation works.

The southern part has characteristics of the original tidal landscape, with a 13th-century sea dike (near the village of Zuurdijk) that resisted the influences of the Lauwerszee at that time. The southern part of De Marne has a more small-scale character with *wierde* villages and grasslands with irregular plots, mainly as arable land.

Moving northward, the land is more regularly divided, arising from 18th- and 19th-century accretions, with farms along dikes and scattered settlements in the form of road or dike villages. Due to drainage and land consolidations, the landscape has acquired a more uniform character than in the south. Around the older arable land lies a dike landscape, reclaimed in the nineteenth century. Unprotected salt marshes and mudflats are part of the saltwater tidal landscape of the Wadden Sea (RUG, 2024).

7.7.2 Lauwers

The Lauwers area includes marine clay polders in the watershed of the Lauwers River and the former Lauwerszee. It comprises both old sea clay polders and newly developed ones. The landscape bears traces of the former sea basin gradually reclaimed after its maximum expansion. The area features polders, former sea dikes, and natural waterways with locks that flow into the current Lauwersmeer. Here, dikes and old dike tracings with breach basins characterize the landscape. Along these dikes lie villages such as Kollumerpomp, Warfstermolen, and Munnekezijl, which are old *zijl* villages. *Zijl* means sluice or lock and these villages originated around these structures (LNV, 2009). The southern part, around Burum, is part of the *wierde* landscape.

The Lauwers is a small river that partially forms the border between the provinces of Groningen and Fryslân. North of Visvliet, the Lauwers splits into the Olde Lauwers and the Lauwers, rejoining after

Pieterzijl to become the Lauwers again. North of Munnekezijl, the river is diverted through the Munnikezijlsterried to Lauwerzijl, then passes through Zoutkamp beyond the Friesche Sluis (means Frisian Sluice but is actually located in Groningen) into the Lauwersmeer, eventually flowing through the Zoutkamperril channel. This channel is the continuation of both the Lauwers and the Reitdiep. The Alddiep and the Dokkumer Grutdjip also traverse the area, flowing into the Lauwersmeer through the Willem Lorésluis and downstream, the Dokkumer diep.

Most of the area is occupied by the embanked Lauwerszee (Lauwers Sea), the current Lauwersmeer (Lauwers Lake), north of Kollumerpomp and Krabbeburen, and west of Zoutkamp. The Lauwersmeer was an estuary, the Lauwerszee, in open connection with the tidal-dominated Wadden Sea until 1969. To mitigate the risk of flooding, the Lauwerszee was closed off with a dam in 1969.

After the closure, the mudflats became partially exposed and were developed into a nature reserve. The former salt marshes along the old coastline were transformed into agricultural land. Due to the closure and the constant inflow from the Reitdiep, Lauwers, and Dokkumerdiep, the water changed from salty to brackish and ultimately to freshwater. The Lauwersmeer is now a National Park, used for recreation, and a portion in the northeast is a military training ground.

7.7.3 Middag-Humsterland and Reitdiep

Middag-Humsterland and the Reitdiep area form a very old reclaimed marine clay landscape along the Reitdiep, characterized by *wierdes* and dikes. Humsterland and Middag were originally mudflats or islands within the bend the Reitdiep makes towards Groningen City. Irregular block cultivation along *maren* (creeks) and well-preserved terp villages are typical. This area, formed by deposits from the Lauwerszee and the Hunze/Reitdiep, shows traces of seawater invasion through channels and creeks, as evidenced by numerous dike remnants, terps, and sluice villages.

The Reitdiep is a waterway running from the city of Groningen (Noorderhaven) to the Lauwersmeer. The Reitdiep has been largely canalized and dammed, but the original meandering structures of the ancient river are still visible in the landscape. Formerly called the Hunze, the Reitdiep was the only and most important connection from Groningen City to the sea via the then Lauwerszee before the excavation of the Eemskanaal. With an open connection to the sea, it was a strongly meandering tidal river. The current upstream part of the river Hunze, now also known as the Drentse Aa, runs in Drenthe east of the Hondsrug ridge through the Hunzedal. The historical region name Hunsingo, of which De Marne and Het Hogeland are part, refers to the old name of this river.

Around 600 B.C., the accumulating salt marshes became inhabitable, and the partially canalized Reitdiep played a crucial role in the formation of this landscape. The old *wierden* on both banks of this river serve as the core of the current villages in the area. The high dikes and often kilometres-wide outer dike grounds of the Reitdiep contribute to the character of this small-scale landscape. Meandering watercourses and ditches also contribute to the structure of the area.

This landscape, one of the oldest intact cultural landscapes in the Netherlands, has been well-preserved, and the contiguous Middag-Humsterland area was designated a National Landscape in 2005 (Middaghumsterland, 2024). Except for a small northern area used for agriculture, livestock farming predominates in this region.

7.7.4 Westerkwartier

The Westerkwartier region (roughly the southern part of the current municipality of Westerkwartier, which is much larger than the region) is a largely redesigned landscape where peat was extracted. The Westerkwartier region houses several *keileem* (boulder clay) and sand ridges or ‘gast’ with valley-shaped lowlands in between. A *gast* is a term for a natural sand ridge or elevation in the landscape originally used for habitation. Settlements on the *gasten* are concentrated in regional villages, with

the building line following the course of the ridge. Some place names (Grootegast, Lutjegast) are reminders of this.

The church villages Noordhorn and Zuidhorn are situated on an isolated 5 m high *keileem* ridge formed during the penultimate ice age. This is also referred to as a *gast*, and contrary to the other sand ridges, it runs northwest to southeast and is the northernmost recognizable parallel extension of the Hondsrug structure.

The land parcels are usually long strips perpendicular to the cultivation axis (an accessible linear structure like a road or riverbank). Original surface forms have often been altered by cultivation and drainage, excavation for road construction, and land consolidations. The sand ridges of the Westerkwartier are currently considered 'megaflutes' (section 7.9.1), comparable to the Hondsrug ridge, but much smaller (pers. comment Erik Meijles).

Large parts of the area were covered with peat, which was excavated for peat extraction between 1700 and 1900. The peaty lowlands between the *gasten* were used as common pasture (*heemschar* or *hamrik*) or meadow. The extensive open lowlands distinguish themselves from the *gasten*, which, through buildings, orchards, and hedgerows, have a small-scale and enclosed character.

The part of the Westerkwartier region within the project area is formed by the transition from the *keileem* plateau to the clay area. This part of the region originated under the influence of the Lauwerszee and the Reitdiep. The land use in the region is predominantly livestock farming. The formerly common alder belt landscape has decreased in surface area after land consolidations.

The name Westerkwartier traditionally refers to one of the *Ommelanden* to the west of the city of Groningen, consisting of the old regional names Humsterland, Middag, Langewold, and Vredewold (Ligterink, 1968). *Ommelanden* is the old, originally medieval, term for the areas in the current Dutch province of Groningen lying outside the city of Groningen. The *Ommelanden* Hunzingo and Westerkwartier largely correspond to the current municipalities Het Hogeland and Westerkwartier, respectively. The *Ommeland* Westerkwartier originated in the 16th century through the merging of the *Ommelanden* Langewold and Vredewold. The regions Langewold and Vredewold are defined by ribbon development following the east-west sand ridges.

7.7.5 Oostergo

As the Oostergo region covers only a small part of the project area, here is a concise description. The region in the project area includes the villages Kollum and Gerkesklooster in an open Frisian terp landscape with old marine clay polders. This region covers a relatively small area in the extreme southwest of the project area. It is an area in Fryslân with the villages Kollum and Gerkesklooster. To the south, the region is bordered by the Prinses Margriet canal, which continues in Groningen as the Van Starkenborgh canal. The village of Kollum is situated on the transition to the landscape of the Southern Frisian Forests. The core of the village has retained a medieval structure, originating at the crossing of a watercourse and the oldest sea dike. Kollum has a protected village view. In East-Kollum, the original irregular block-shaped cultivation (recognizable by curved ditches and roads and remnants of old channels) has been well-preserved (RUG, 2024).

7.8 Geology

7.8.1 General description and sources of information

The extent of the study area is largely defined by the scope of this research and outlines the Underground Gas Storage (UGS) Grijpskerk and its surrounding gas fields. These fields are all situated in the Lower Rotliegend (Late Permian) sandstone reservoir rock and are constrained within the Lauwerszee Trough sub-basin. Geological research in the area has mainly focussed on hydrocarbon exploration. Therefore, most of the information is on the Rotliegend gas reservoirs and it geological

traps, i.e. faults and the Zechtstein top salt seal. While the Carboniferous and Devonian rocks underlying this area remain less understood, the geological formations between Permian and present times have also received limited exploration due to less interest from a hydrocarbon-exploration standpoint. Nonetheless, the subsurface in the Netherlands is comprehensively mapped, offering a clear overview up to a depth of 5000 meters. Accessible through online platforms like TNO's DINOloket and via freely available GIS layers through NLOG, 3D models provide valuable insights. These platforms, including DINOloket, enable the creation of 1D virtual boreholes or 2D sections, with original geophysical data and borehole logs, which also form the basis for the 3D models. The presence of carbonate platform in the lower carboniferous has received more attention the last couple of years as a possible source for (ultra-deep) geothermal energy.

The recently released geological map of the Kingdom of the Netherlands (TNO, 2023) contains a detailed geological cross-section within the research area (Figure 40). The illustration reveals a nearly complete geological sequence extending from the upper Carboniferous, except for the Jurassic groups. Consequently, an unconformity is observed where the Lower Cretaceous overlays the Upper Germanic Trias group. Notably, on both the adjacent Fryslân and Groningen platforms, the Trias groups are either virtually absent or significantly thinner. Moreover, there are signs suggesting that the Early Carboniferous formations in the Fryslân and Groningen Platforms consist of carbonate reefs (Hoornveld, 2013), presenting potential opportunities for geothermal energy exploration. Annex VII provide an overview of all the stratigraphic units that are encountered in the deep subsurface, including the stratigraphic columns of the Netherlands (Figure 112).

The collaborative SCAN program, led by EBN and TNO and funded by the Ministry of Climate and Green Growth, addresses knowledge gaps in the Dutch subsurface for geothermal exploration. These gaps arise from limited geophysical or borehole data in areas with minimal hydrocarbon exploration opportunities. SCAN focuses on completing the overall subsurface description of the Dutch subsurface for geothermal applications, both in the deep and in the ultra-deep, the latter focussing on the Dinantian. As part of SCAN, a project reinterpreted geophysical and borehole data to extract more information from the carboniferous and basement rocks (SCAN, 2019). The resulting sections, including a central section intersecting the study area (Figure 41), revealed greater detail in the deeper (Carboniferous) subsurface, offering enhanced information on faults compared to Figure 40.

7.8.2 Structural elements

In the deep subsurface of the research area, a notable structural feature is the Lauwerszee Trough, which was a sub-basin trending to the Northwest within the larger Southern Permian Basin. The Lauwerszee Trough separates the Fryslân Platform in the West from the Groningen Platform or Groningen High in the East.

This division is clearly visible in the cross sections provided in Figure 40 to Figure 44, which are primarily made from the perspective of hydrocarbon exploration. The Groningen gas field lies in its entirety in the Groningen Platform. The gas fields in Fryslân like Marum and Opeinde are situated in the Fryslân Platform. The Lauwerszee Trough forms the Lower Permian Rotliegend gas play, characterized by the productive Slochteren Formation sandstones in tilted fault blocks, sourced from the Carboniferous below. The Rotliegend Ten Boer Claystone and Upper Permian Zechstein evaporitic rocks act as top and lateral seals for the fault system (Corona, 2003).

The Lauwerszee Trough, situated at the base of the Rotliegend (Permian) and the top of the Carboniferous, is a few hundred meters deeper than the adjacent Fryslân Platform and Groningen High, making it not a very significant basin in terms of depth. However, it is a distinct and long-lived geological feature (Jager, 2007).

All the gas fields in the study area including the UGS Grijpskerk are situated in this Lauwerszee Trough system. The Lauwerszee Trough trends roughly NW-SE (Figure 42) with the western boundary running along the line Nes (Ameland)-Dokkum-Kollum-Leek-Assen and the eastern boundary (less well

constrained) running roughly along the line Schiermonnikoog-Winsum-Groningen Stad-Zuidlaren. An important fault system constraining the western boundary of the Trough is the Hantum fault zone.

All the NW-SE striking faults currently observed in the Netherlands trace back to the Caledonian orogeny that lasted from the Cambrian to the Devonian (Figure 16). There is limited knowledge regarding the exact timing and formation factors of the Lauwerszee Trough (Hoornveld, 2013) There are three theories, but the most likely explanation according to Hoornveld (2013) is that extension during the (Early) Carboniferous (Dinantian) reactivated the existing NW-SE trending zones of weakness (Hoornveld, 2013 and Kombrink, 2008). This could have formed the (asymmetric) Lauwerszee graben structure with the (reactivated) Hantum fault zone at its western margin.

The Hantum fault zone is a complex system consisting of several distinct parts. The southernmost part of the Hantum Fault was active during the Rotliegend deposition and caused syn-tectonic thickening of the sediments within the Lauwerszee Trough (EBN, 2023). The Early Permian and Middle to Late Jurassic extensional tectonic regimes were synchronous with magmatism activities and thermal events (Van Bergen and Sissingh, 2007) that are related to the Variscan Pangaea assembly (Van Hulten, 2012).

There is also evidence of movement in younger sediment above the Zechtstein salt, resulting in deposition of the combined Lower and Upper Germanic Trias group sediment within the Lauwerszee trough, which are significantly thinner to virtually absent towards the West on the edge of the Fryslân platform, and which are also thinner or absent on the eastern side on the Groningen platform. However, de Jager (2007) states that the long-lived geological activity is evidenced by the subcrop patterns and increased thicknesses of Rotliegend, Lower Cretaceous, and Paleogene deposits although he also mentions that the increased thickness of the post Permian formations may be influenced by the withdrawal of Zechstein salt into flanking salt walls that started in the Triassic and possibly continued during the Early Cretaceous and Tertiary periods (de Jager, 2007). Kombrink et al. (2012) state on the other hand that The Mesozoic and Cenozoic successions of the Lauwerszee Trough do not differ markedly in thickness from the adjacent Fryslân and Groningen Platforms, i.e. that the bounding faults have not been extensively reactivated.

Nevertheless, the occurrence of normal fault movement resulted in the formation of sealing faults in the Rotliegend formations on either side of the Lauwerszee Trough. This led to the Rotliegend acquiring gas-bearing properties, establishing an autonomous Gas-Water Contact (GWC) in relation to the Groningen Platform (De Jager & Geluk, 2007). Continued fault movement is also depicted clearly on the long section of the most recent geological map of the Netherlands (see Figure 40). It appears that the more recent fault movement in the formations above the Permian (Triassic and younger) is more likely caused by the movement of the flanking Zechstein salt walls that follow the older geological (tectonic) fault zones on either side of the Lauwerszee Trough, see Figure 46.

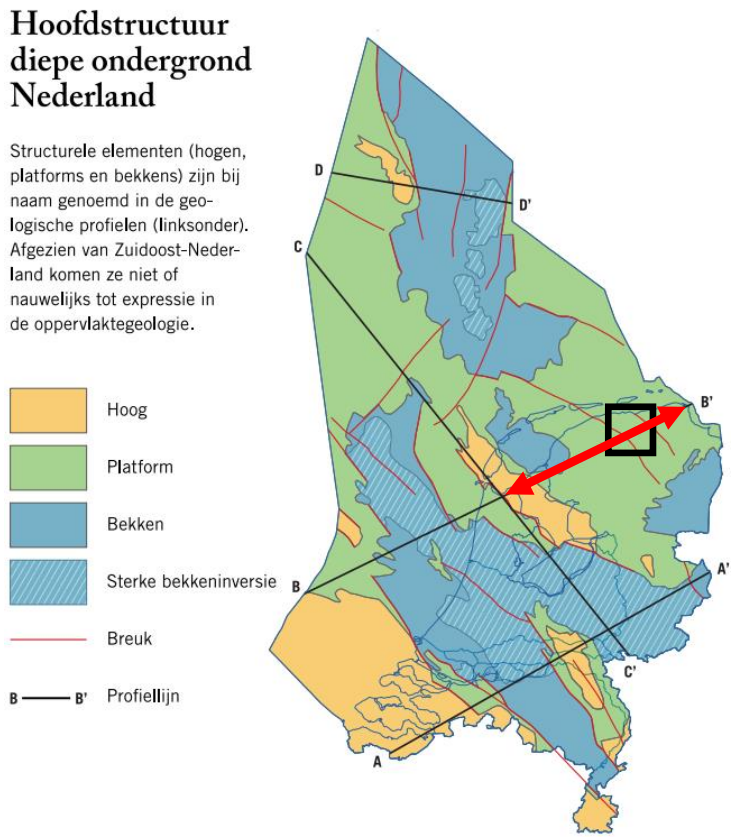

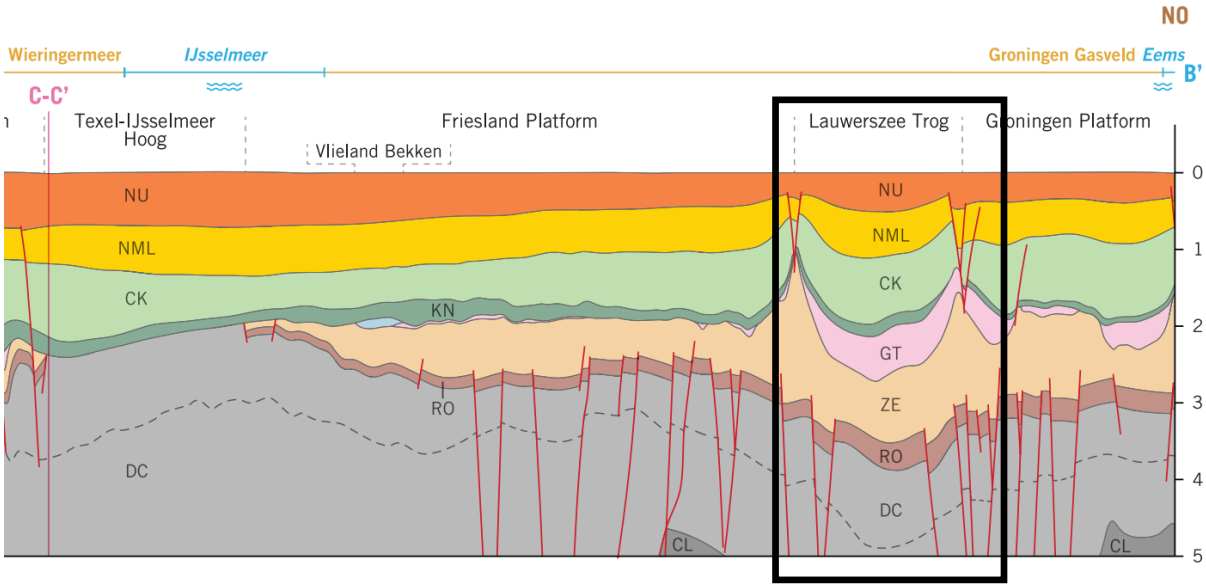

* The part of the section is indicated on the map above as a red arrow. In the section above and the overview map the approximate location of the Grijpskerk study area is highlighted with a black box. Note that the vertical scale is highly exaggerated. Legend–- NU: Upper North Sea Groupp; NML: Middle and Lower North Sea Group; CK: Chalk Group; KN: Rijnland Group; GT: German Triassic Group; ZE: Zechstein Group (Salt); RO: Upper Rotliegend Group (Sandstone gas reservoir rock); DC: Limburg Group. For further explanation of the units, see Annex VII.

Figure 40. Geological long section from the tip of North Holland (SWW Wieringermeer) to the Eems delta (NEE Groningen) (Source: Geologische kaart van het Koninkrijk der Nederlanden, TNO, 2023).

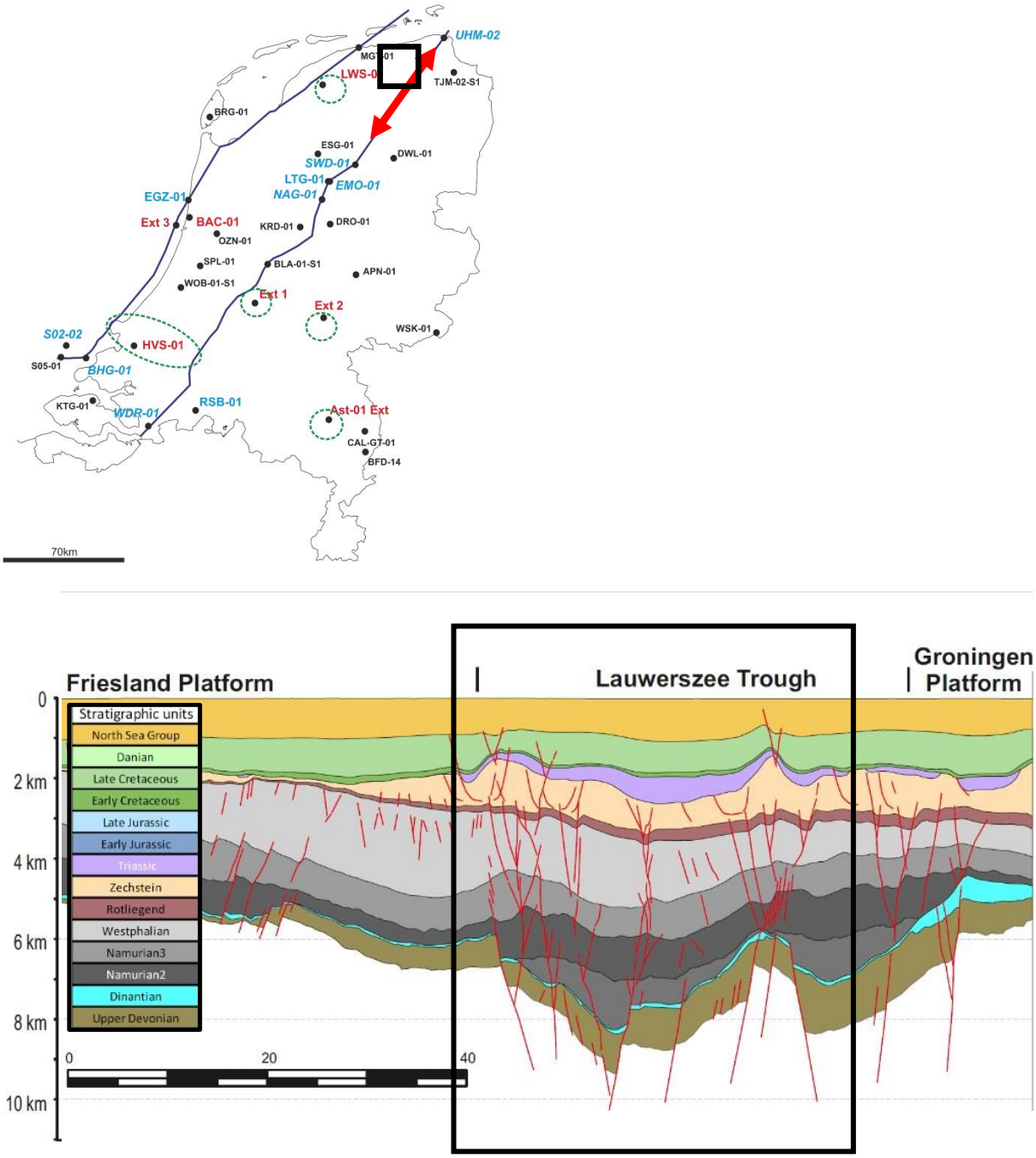

Figure 41. A segment of the Central Section through the Netherlands has been established through the reinterpretation of existing geophysical data and bore logs (SCAN, 2019).

Interestingly, the section shown in Figure 41 conveniently intersects the study area, as illustrated by the black box. Upon comparison with Figure 40, it is evident that there is greater detail in the deeper (Carboniferous) subsurface and providing enhanced information on faults. The approximate location of the section is given by the red arrow in the map above.

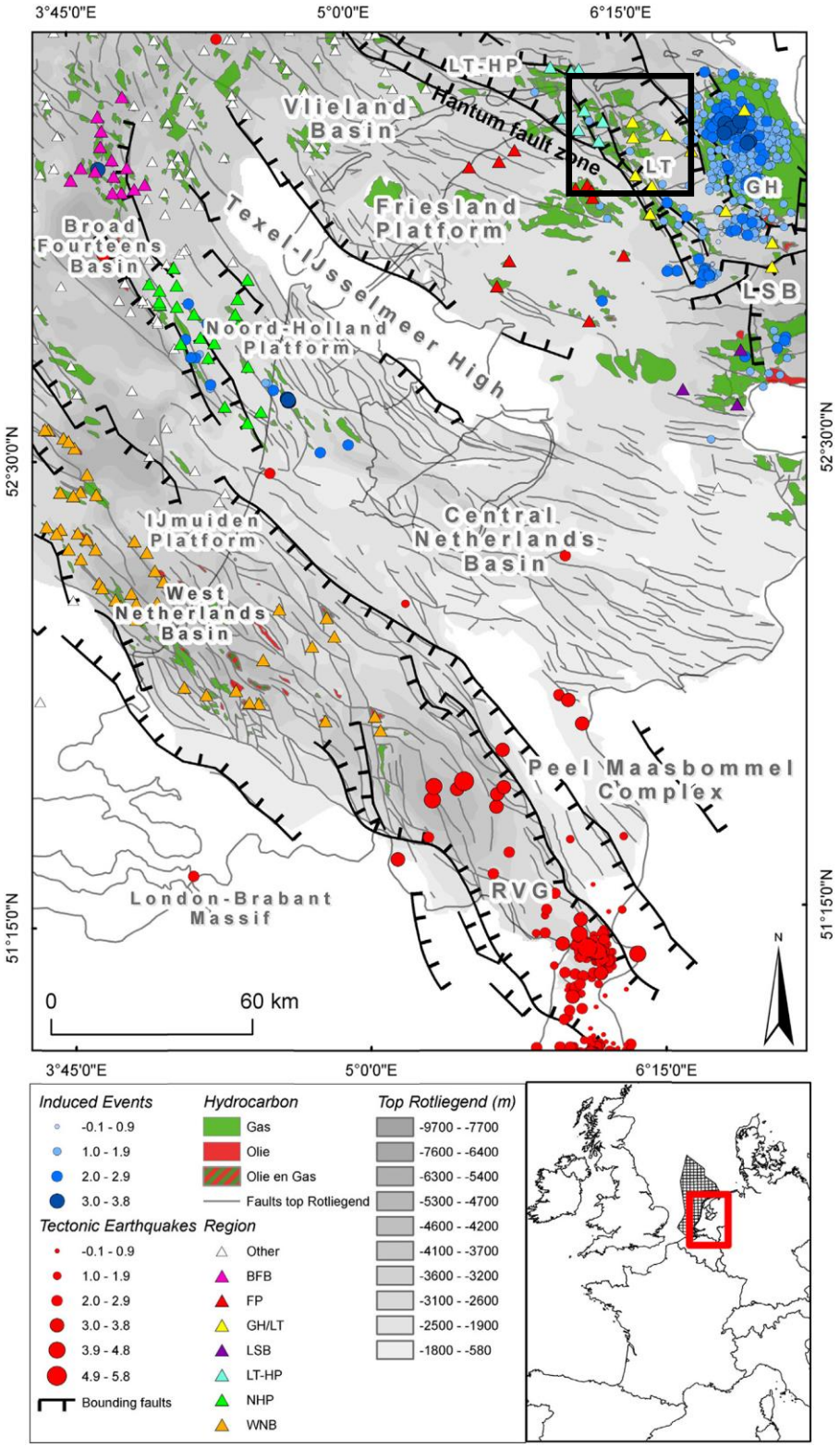

* Regional location of the main map is shown in the lower right panel. Red circles: natural seismicity; blue circles: induced seismicity; green: gas reservoirs; red: oil reservoirs; solid lines: major fault zones; triangles: where leak-off tests have been performed. BFB = Broad Fourteen Basin, FP =Fryslân Platform, GH/LT =Groningen High/Lauwerszee Trough, LSB =Lower Saxony Basin, LT-HP =Lauwerszee trough-Hantum Platform, NHP =Noord Holland Platform, WNB = West Netherlands Basin, RVG =Roer Valley Graben, PB= Peelrand Block, EL= Ems Low.

Figure 42. Tectonic map, seismicity, and hydrocarbon reservoirs in the Netherlands (Source: Van Wees et al. ,2014).

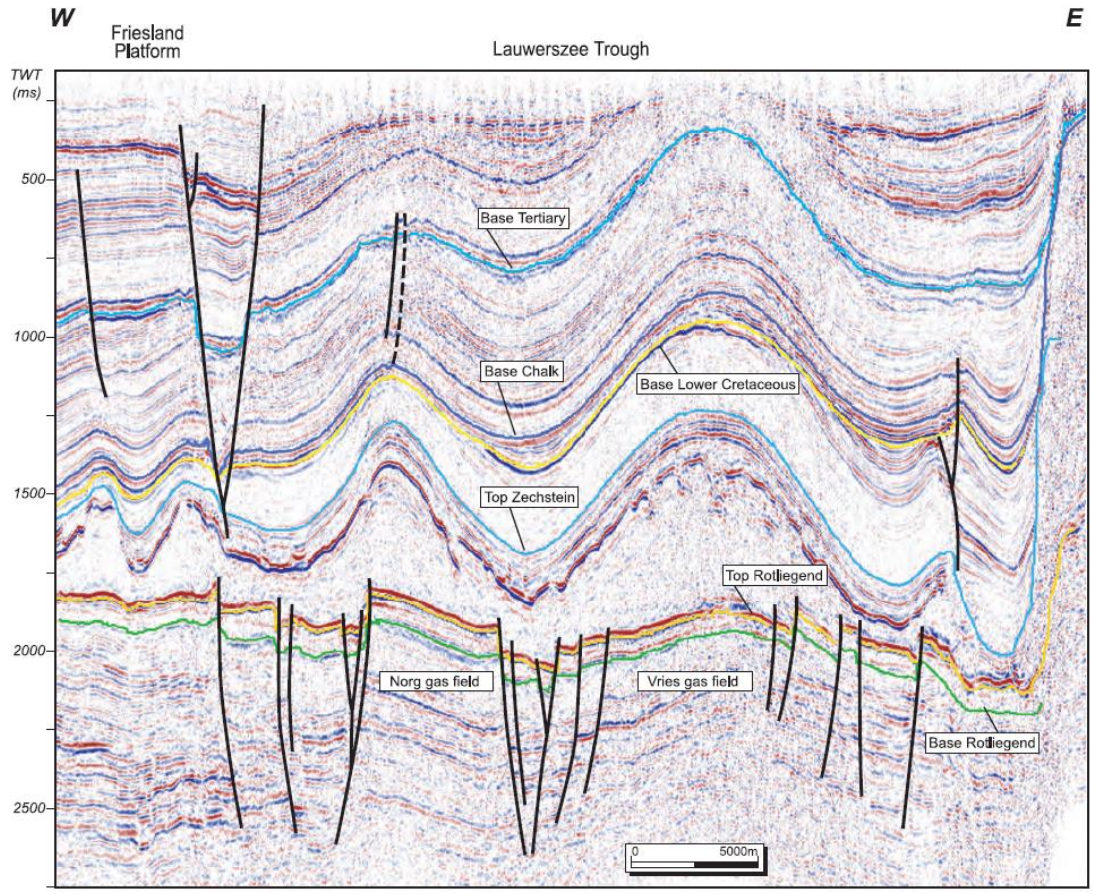

Figure 43. Seismic line in the north-east Netherlands (Fryslân Platform to Lauwerszee Trough) showing gas fields in fault blocks at Rotliegend level. Southernmost part of the Lauwerszee Trough, outside of the study area, but showing similar fault blocks as present in the Grijpskerk area. From: Jager and Geluk (2007).

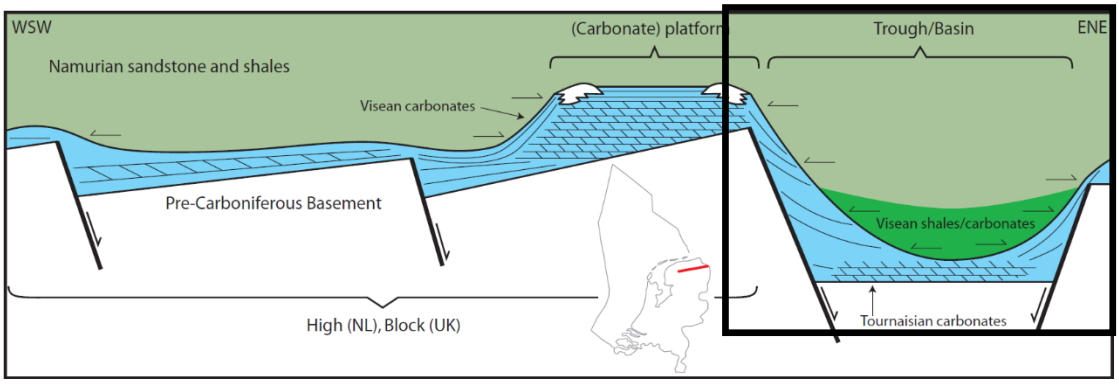

Figure 44. Schematic cross-section showing the structural and stratigraphical setting of the deeper geology in the study area in the Lower Carboniferous (Dinantian: Tournaisian and Visean) and Upper Carboniferous (Namurian). The Lauwerszee Trough is clearly visible already as a structural feature. On the West side on the Fryslân platform a carbonate platform is believed to be present, based on interpretation of geophysical data. From: Kombrink (2008).

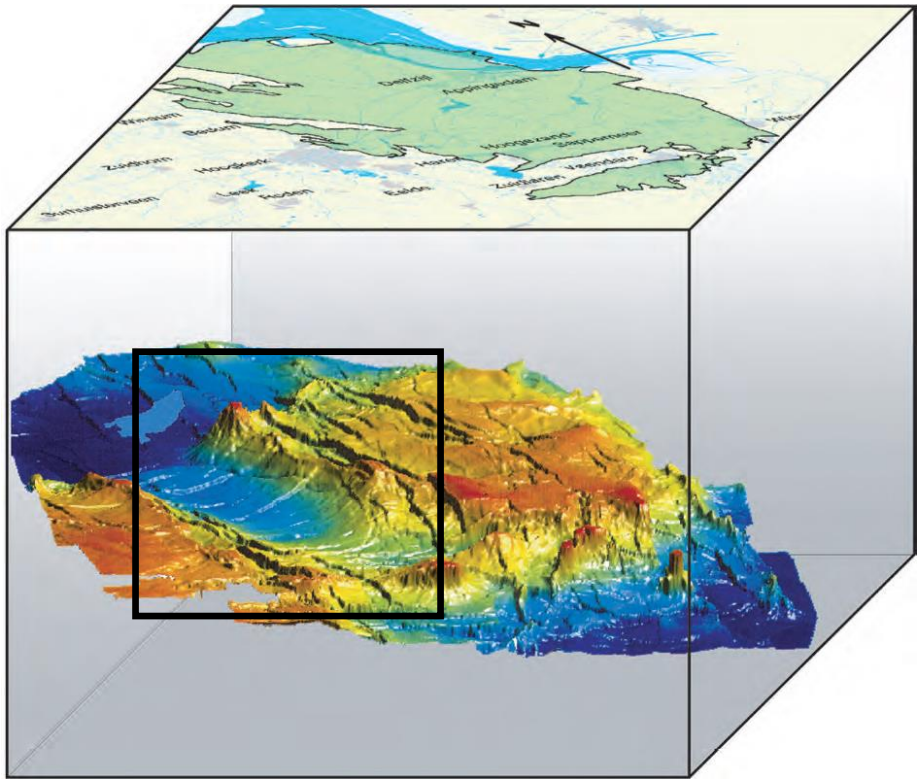

Figure 45. 3D view of the Groningen field, with to the west of the Groningen field, the depression of the Lauwerszee Trough shows up in blue colours, with the Fryslân Platform further to the west in yellow to reddish colours (de Jager and Geluk, 2007). The black box outlines approximately the Grijpskerk area.

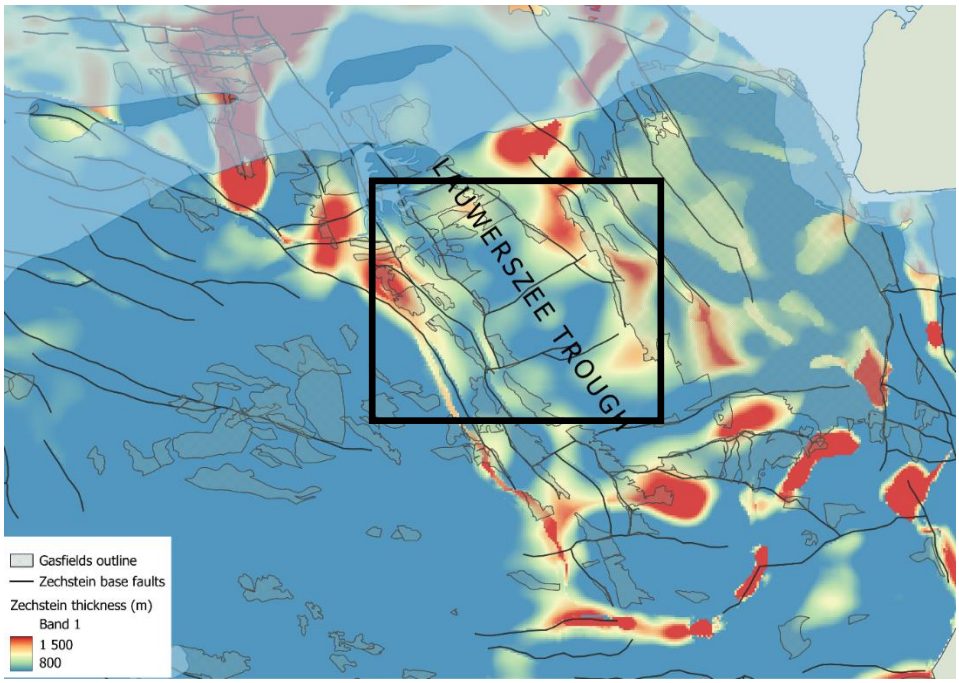

Figure 46. Overview maps with the thickness of the Zechstein shown, exaggerated to show the locations of salt diapirs, pillows and salt walls. The onshore geographic extent of the Lauwerszee Trough is bounded west by the clearly visible salt wall and the Hantum Fault zone. The eastern boundary of the Lauwerszee trough is less well constrained, especially further to the south. Data source: NLOG. The black box outlines approximately the Grijpskerk area.

7.9 Pleistocene and Holocene

The epochs Pleistocene (2.6 million BP to 11,700 BP) and Holocene (11,700 BP to present) are part of the geological period Quaternary. The lower boundary of the Quaternary deposits varies in depth (see Figure 47). In the northwest of the Netherlands, the deepest lower boundary is located at approximately 500 m NAP. In the east and south of the Netherlands, older deposits can be found close to the surface. In the Grijpskerk area, the lower boundary is located between 200m and 250m below the ground surface (Keijer, 2015).

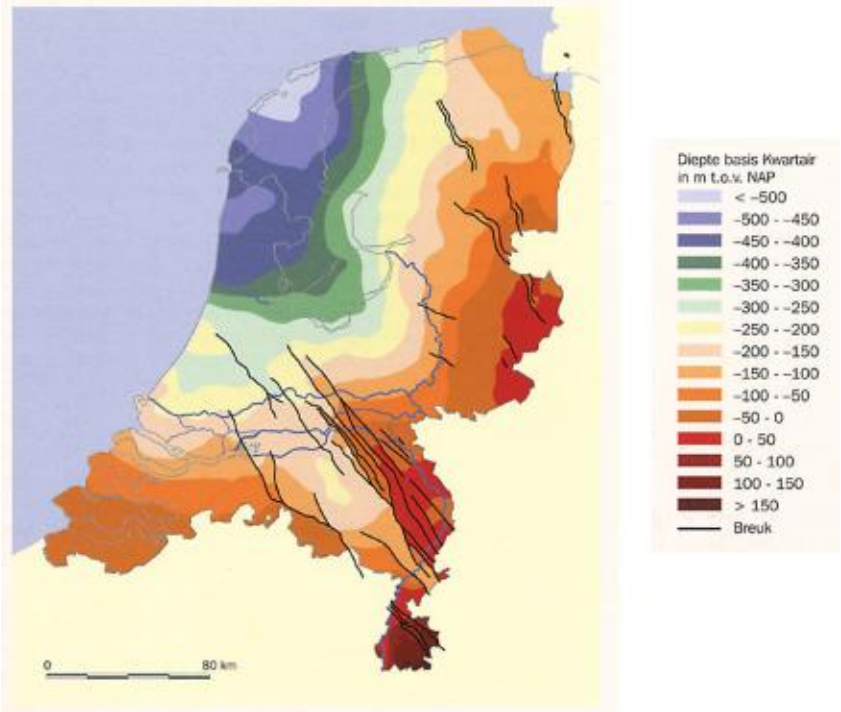

Figure 47 Spatial variability of the lower boundary of the Quaternary deposits (Source: Keijer, 2015)

7.9.1 Pleistocene Glaciation

The Pleistocene epoch is characterised by successive glacial periods, during which large ice caps formed in North-western Europe, particularly Scandinavia (Figure 48). During the cold periods, a significant amount of water was stored in the ice caps and glaciers, resulting in substantial lowering of the global sea level of up to 120 m lower than compared to today (Meijles, 2015). In the warmer interglacial periods between the ice ages, the glaciers melted, causing the sea level to rise again. Each glacial and interglacial period is characterised by their own distinct geological and geomorphological conditions, and therefore the nature of their sediment deposits.

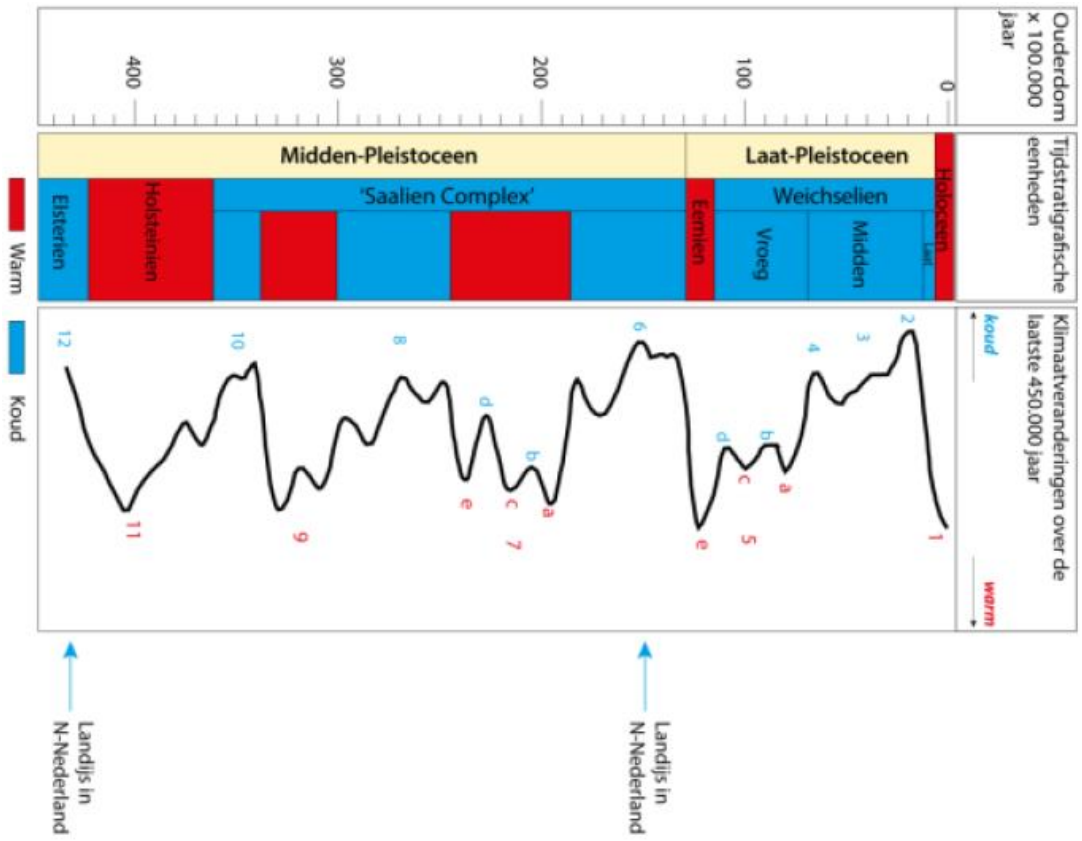

Figure 48 The global climate curve for the last 450.000 years along the Pleistocene and Holocene epochs subdivided in glacial and interglacial periods. Also, the periods of continental ice in the Northern Netherlands are indicated with blue arrows (Source: Meijles, 2015)

In Northern Netherlands three Pleistocene glacial periods are especially important: the Elsterian, the Saalian, and the Weichselian. Older glacial and interglacial periods have occurred, and it is possible that glaciers had reached the Northern Netherlands earlier, this however, remains unclear. Only during the Elsterian and Saalian periods the Northern Netherlands was covered by glaciers, as shown in Figure 48. During the Weichselian period, the land ice did not reach the Netherlands, but the region experienced colder temperatures.

Elsterian

During the Elsterian, the northern part of the Netherlands was covered with glacial ice. In this period, deep north-south-oriented trench systems known as tunnel valleys were formed, ranging from 20 to 100 kilometres in length, approximately 3 to 5 kilometres in width, and 100 to 300 meters in depth (Meijles, 2015). Glacial deposits from this period, classified as the Peelo Formation, consist of coarse sand with fine gravel, silt, and clay, varying in thickness from around 300 meters in the deepest tunnel valleys to 20 meters outside. Within these tunnel valleys, the settling of fine clay particles led to the formation of Pottery Clay, a dense clay layer that varies greatly in thickness from a few meters to several tens of meters and is classified as the Peelo Formatio''s Niewolda member. During the later Saalian glacial period, Pottery clay was compacted by glacial ice and served as a significant barrier to groundwater flow in the subsurface.

Figure 49. Maximum glaciation extent during the major glacial periods in from the mid-Pleistocene to present. In blue the Elsterien (ca. 465.000 – 418.000 BP), yellow: Saalien (ca. 238.000 – 128.000 BP) and red: Weichselien (ca. 116.000 – 11.500 BP) (Source: HvA, 2023)

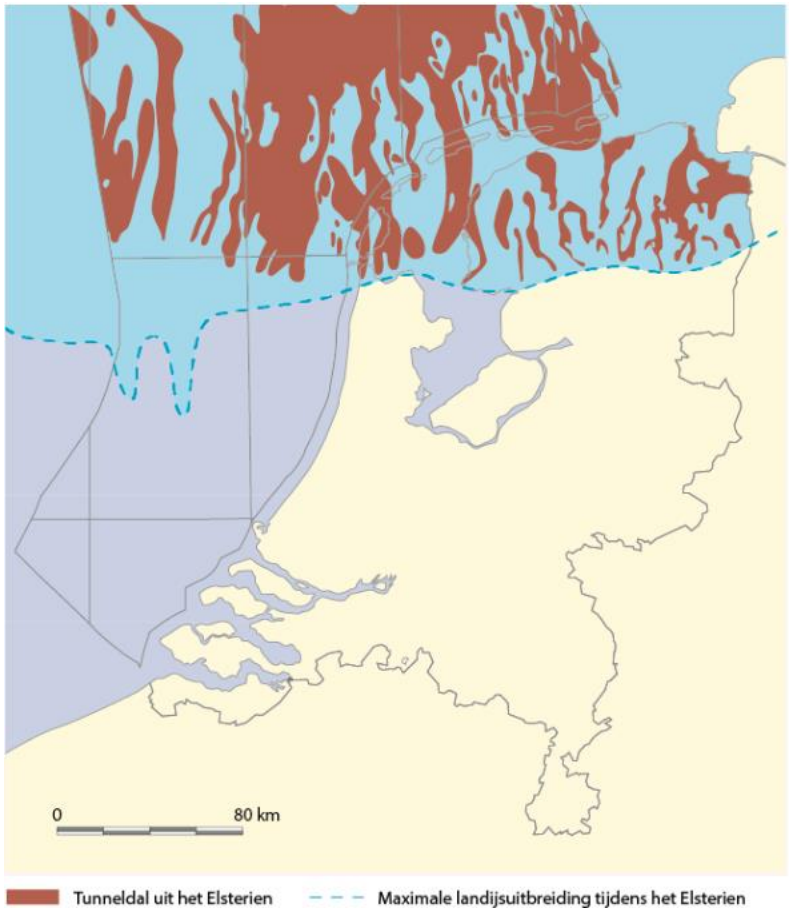

Figure 50. An overview of the tunnel valleys formed during the Elsterian period. The dotted line indicates the maximum extend of glacial ice (Source: Mulder et al., 2003).

Saalian

During the Saalian, glacial ice flowed from Scandinavia towards the southwest reaching approximately the Central Netherlands. The large hydraulic resistance of Elsterian Pottery clay and frozen sands underlying the glacial ice hindered meltwater to percolate into the subsurface, resulting in excess meltwater that acted as a lubricant beneath the glaciers, facilitating rapid glacial movement.

The glaciers pushed surface sediment ahead, forming push moraines (Figure 51). Also, glacial basins developed underneath the glacier where ground moraines were formed. These ground moraines consist of an unsorted mixture of clay, loam, sand, and larger stones referred to in Dutch as “Keileem”, which literally translates as boulder clay. These materials were carried into the lower layers of the glacier and are highly compacted by the glacial overburden, resulting in low hydraulic permeability. The glacial deposits from the Saalian are classified in the Drenthe Formation.

In the Groningen and Drenthe provinces, Saalian glacier movement has a significant impact on the landscape. A well-known example is the elongated Hondsrug system which is located between the cities of Groningen and Emmen. Within the project area, a ground moraine is found in the ridges (‘*gasten*’) of Noord- and Zuidhorn (Meijles, 2015). It has to be emphasized that these features are not pushed ground moraines as shown in Figure 51, but are considered ‘megaflutes’ (definition provided in chapter 10).

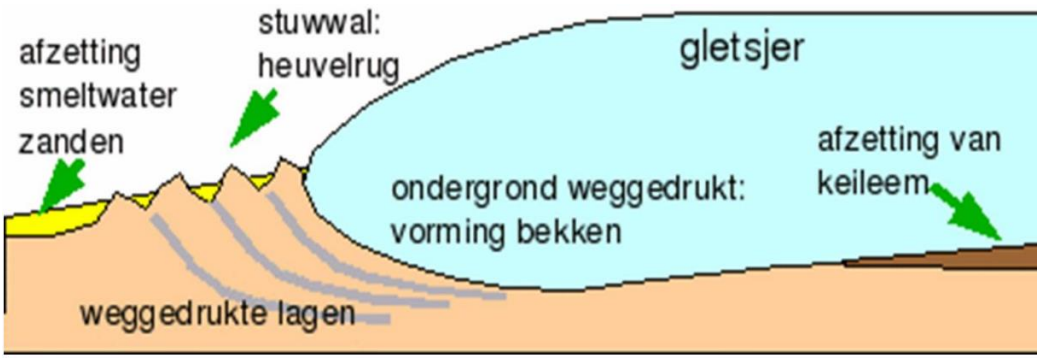

Figure 51. Illustration of glacial deposits during the Saalian. Glaciers push surface sediments forward forming push moraines like in the centre of the Netherlands (i.e. Utrechtse Heuvelrug and Hoge Veluwe). Also, ground moraines were formed beneath the glacial ice where Boulder Clay was deposited (source: Van Huissteden, 2024)

Eemian

During the Eemian interglacial, rising temperatures caused ice caps to melt, leading to significant meltwater release and a sea level rise of 4 to 6 meters above the current sea-level. The Netherlands was partly flooded, and clay was deposited in the glacial basins, known as Eem Clay. Coarse sands, grading upward into fine sands and clay, were deposited outside these basins. Today, these sediments are found at depths of 15 to 40 meters below the surface and belong to the Eem Formation, located at the north-eastern outskirts of the project area along the eastern Lauwersmeer-Groningen City line.

Weichselien

During the Weichselian period, the Netherlands were not covered by glacial ice, but it was intermittently a tundra and polar desert, following climate fluctuations. The land was sparsely vegetated, allowing wind and water to shape the landscape. The soil was deeply frozen in winter and thawing only happened at the soil surface during summer. This prevented melting water from infiltrating into the subsurface, leading to overland flow depositing sand and fine gravel in relatively broad streams in the lowest areas.

As a result of seasonal meltwater release, sand deposits are found, sometimes with thin layers of clay (meltwater deposits) in between. Also, because of sparse vegetation, fine aeolian sands were deposited as cover sand at a large scale over wide areas, known as the 'Wierden laagpakket'. The deposits formed during the Weichselian period belong to the Boxtel Formation and can be up to 15 meters thick.

7.9.2 Holocene

The current geological epoch, the Holocene, began approximately 11,700 BP. Compared to previous geological periods, the Holocene is relatively warm, causing glaciers and ice caps to melt, resulting in a significant sea-level rise. During the Holocene, the Dutch landscape and North Sea were formed, and is summarized in

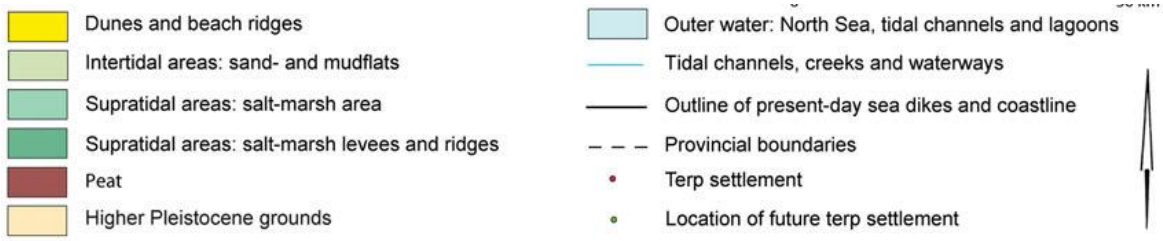

Figure 52.

Between 11,000 and 7,500 BP, rapid sea-level rise of 60 to 75 cm per century resulted in the gradual filling of the North Sea basin (Vermeersen et al., 2018). Around 7,500 BP, the sea had reached the location of what is now the current coastline of The Netherlands (Vos et al., 2021). Groundwater in the coastal areas followed the rising sea levels, transforming large parts of the low-lying coastal area into marshes where peat accumulated, forming the Basisveen (Nieuwkoop Formation). Under the influence of the ongoing sea level rise, coastal peatlands were pushed further inland, creating tidal areas along the coastline with tidal channels, mudflats, and salt marshes, like the current Wadden Sea and adjacent islands. Given the dynamics of these tidal environments, where tidal channels and mudflats are continuously on the move, significant variations in the Holocene lithostratigraphy can be found. In areas were water flows relatively quickly, such as tidal channels and regions under the influence of tidal currents or surface waves, sand is deposited in the form of sand banks and beaches. In calmer areas clay is allowed to settle, for example on mudflats and salt marshes.

Around 6000 BP, the rate of sea level rise decreased to approximately 30 to 40 cm per century. The upcoming centuries were characterised by the deposition of large amounts of marine sands and clay. The tidal areas of the Hunze and Fivel valleys gradually expanded, and the coastline remained open with Wadden Islands interrupted by large tidal inlets (Meijles, 2015).

Around 3500 BP, the rate of sea level rise decreased to approximately 15 to 25 cm per century. Despite being intersected by various channels and creeks, sedimentation in the tidal area was insufficient to keep up with the sea level rise. Also, expansion of peat areas along the Hunze and Fivel valleys occurred but was relatively limited compared to the Western Netherlands.

From around 500 BC (2500 BP), the sea level rise significantly decreased, resulting in less frequent flooding of the coastline. A large salty marshland emerged with sandy tidal salt marsh ridges along the coast, and riverbank ridges along tidal creeks. Small residential mounds, known as *wierden* in Groningen and eastern Fryslân, were built on these higher ridges (Meijles, 2015).

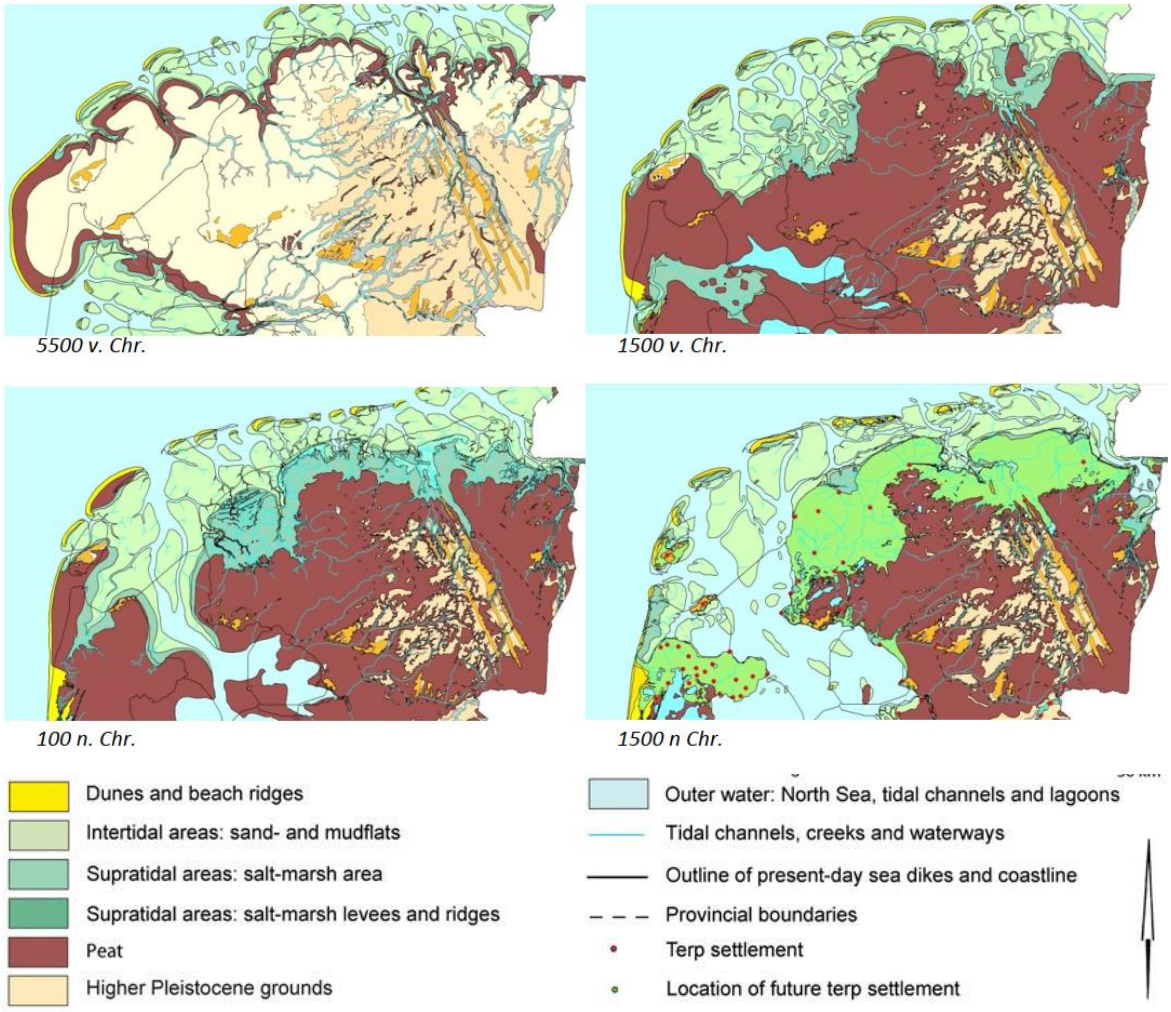

Figure 52. Landscape evolution during the Holocene for the northern Netherlands with the top left 7,500 BP, top right 3,500 BP, bottom left 1900 BP and bottom right 500 BP (Source: Vos and de Vries, 2013)

Around the beginning of the Common Era (2000 BP), the tidal areas of the Hunze and Fivel gradually silted up, leading to the expansion of salt marshes in the region. People began to make these areas suitable for habitation and started to exploit the peat along the edges, resulting in land subsidence. Consequently, large parts of the northern Netherlands were flooded by the sea (Meijles, 2015).

Around 800 AD (1200 BP), the tidal areas reached their maximum extent due to frequent sea flooding. As a result, peat became flooded, increasing water storage between low and high tide (tidal prism), tidal channels grew larger, and peat was eroded along the sea inlets (Vos et al., 2021). By this time a new tidal area was formed, named the Lauwerszee. Also, the course of the Hunze river shifted from the north towards the west, following the course of the Reitdiep.

Beginning in the 12th century (800 years ago), extensive peat cultivation occurred in the area, and dikes and dams were constructed along the rivers. Consequently, sedimentation could no longer occur inland. Former salt marshes were effectively drained through the construction of ditches and drainage systems, causing the land surface to gradually subside due to soil compaction and relative sea level rise (Vermeersen, 2018; Meijles et al., 2018). Meanwhile, farmers encouraged flooding of the salt marshes outside the dikes for the deposition of fertile sediments, leading to the formation of large contiguous areas with sandy clay soils. These accreted salt marshes could then be reclaimed, and because these polders were allowed to grow by natural sedimentation, they are located at higher grounds compared to the previous reclaimed lands. This process led to the formation of the Groninger Hoogeland. After the reclamation of especially the older clay areas, a varied landscape with numerous

winding ditches at the remnants of the former tidal creeks remained. In many areas, these ditches were filled up or were straightened for agricultural purposes over the past century. Around 1850 AD, the region acquired its current landscape shape.

7.10 Hydrogeology

The hydrogeological system is subdivided into three sections, namely the shallow, intermediate system, consisting of deposits from the Quaternary and late Neogene, and deep deposits from the Paleogene and older. It should be noted that the hydrogeological subdivision is made based on the available data and relevance on the hydrogeological system near the earth surface.

7.10.1 Shallow hydrogeology (0 – 20m)

In the Grijpskerk area, the shallow geology mainly consists of Holocene sediments, with a highly heterogeneous sequence of alternating clay and sand deposits overlying the Basisveen (Basal Peat). Below the Holocene, fine permeable sands belonging to the Quaternary Boxtel Formation are found. Near the sand dunes of Grootegast-Oldekerk and Noord-Zuidhorn, Boxtel coversand (NL: dekzand) can be found at the surface, covering the underlying Saalian Boulder Clay ridges from the Drente Formation.

The shallow hydrogeology refers to the position of the water table and its fluctuations. These fluctuations are affected by several factors including land use, the water management system, and climate conditions such as precipitation and evaporation.

The shallow hydrogeology is thus heavily influenced by:

- Weather conditions
- Polder water management, which is regulated by the location and position of weirs, pumping stations and waterways. Also, the maintenance of waterways, ditches and subsurface drainage systems on grasslands are important factors.
- Groundwater recharge by precipitation and evaporation
- Seepage fluxes between the shallow and intermediate hydrogeology

Due to its shallow depth, the groundwater levels are particularly sensitive to climate change events such as droughts, changes in the surface water management (Van den Eertwegh & Hiemstra, 2023). In summary, the characteristics of shallow geohydrology are thus influenced by a combination of local factors and broader climatic conditions. Due to the climate change we have already witnessed a number of extremely dry summers the past five years (Annex VIII).

7.10.2 Intermediate hydrogeology (20 – 500m)

The intermediate hydrogeological system mainly concerns groundwater flow in Quaternary sandy units and has been hydraulically parametrized by the REGIS ll model (TNO, 2019). At the bottom are the Oosterhout and Breda Formations, originating in the Neogene (Part of NU: Upper North Sea Group, see Annex VII). The Oosterhout Formation consists of an alternation of sandy and complex units, with the Breda Formation located beneath, which is a thick clay formation. Sandy units from the Peize, Waalre, and Appelscha Formations were deposited on top of the Oosterhout Formation during theIrnary.

As a result of the Pleistocene ice ages, the sand formations are deeply incised with deposits belonging to the Elsterian Peelo Formation, which is an alternation of thick clay and sandy layers. Subsequently, some remnants of Saalian Boulder Clay belonging to the Drente Formation can be found near

Grootegast and Zuidhoorn. A section of the REGIS II model shows that the subsurface along these depths is highly variable on a regional scale (see Figure 53).

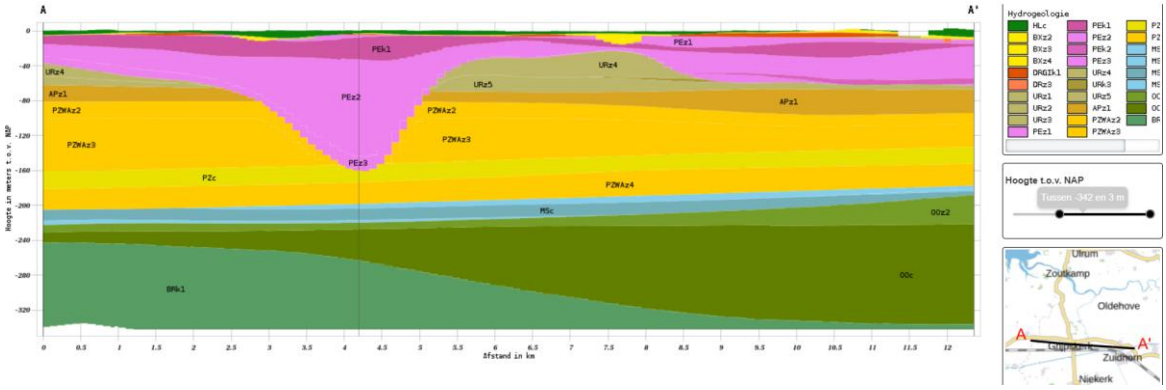

Figure 53 A cross section of the REGIS II model through the project area (Source: DINOloket).

Apart from the local geology, the hydraulic head at these depths is mainly determined by surface water levels (e.g. sea-level) and hydraulic heads in the hinterland (Germany to the east and Drenthe to the south. Locally, the hydraulic head may vary because of groundwater extractions for irrigation purposes or subsurface energy systems. In the marine clay areas this does not play a role since there is no possibility to extract fresh water. No large-scale drinking water extractions are undertaken within the project area (section 2.7.1).

7.10.3 Deep hydrogeology (500 – 1000m)

Below the Quaternary and Neogene, deep marine deposits from the Middle and Lower North Sea Group can be found. The groundwater at this depth is saline and/or hypersaline. The deep hydrogeology has limited influence on the intermediate and shallow geohydrology.

7.11 Surface characteristics

7.11.1 Geomorphology

An overview of the main geomorphological features is presented using the Geomorphological Map of the Netherlands (see Figure 95 in Annex V). In general, the geomorphology is tidal dominated with a few Pleistocene sand ridges in the south of glacial origin.

The central study area, roughly situated between Noordhoorn, Munnikezijl, Kollum, and Gerkesklooster, is primarily formed by tidal inlets intersected by tidal creek channels and levees, and is associated with thick clay deposits with local, loosely packed, sands representing former levees. South of Grijpskerk towards Lutjegast, and north of Munnikezijl, the landscape is dominated by former salt marsh flats and ridges, indicating thin interbedding of fine sands and clay.

Around Lutjegast and Grootegast, two parallel Pleistocene ground moraines or sand ridges with an east-west orientation are observed (megaflutes, see section 7.9.1), covered on both sides by aeolian sands. Between these ridges lie reclaimed peat valleys, filled with tidal sand and clay. Also, near the villages of Noordhorn and Zuidhorn, a clear Pleistocene ground moraine consisting of Boulder Clay covered with aeolian sand can be distinguished.

The area around Niehove and Ollehove is characterized by salt marsh deposits with a dense network of tidal creek channels. The expected stratigraphy is similar compared to the central study area. Further north around the Reitdiep the landscape is characterised by numerous tidal and river mouth channels, as well as residual channels. The subsurface is thus very variable and not mapped or documented at the scale to mtake these variations visible. These landscapes are associated with thick

clay deposits with local sand deposits in the former tidal channels. A similar landscape can be found in the western outskirts of the project area near Ingwierrum.

Throughout the entire area, dozens of dwelling mounds or 'wierden' have been counted, most of them are located on the east and north sides of the project area. Particularly, the surroundings of Niehove-Oldehove and Ulrum-Leens-Hoorn are marked by these dwelling mounds. The lithology of these dwelling mounds is highly variable, ranging from clastic sediments such as locally dug salt marsh sods sand towards manure rich layers (Meijles et al., 2016).

7.11.2 Hydrological setting

In the Grijpskerk area, water management is regulated by two water boards, namely: Wetterskip and Noorderzijlvest (Figure 97 in Annex V). These water boards address issues such as water nuisance, water scarcity, and water quality. The Dutch Environmental Planning Act (formerly Dutch Water Act) assigns responsibility to the water boards to maintain appropriate surface water levels within their area of jurisdiction, which are regulated using a complex system of watercourses, locks, weirs, and pumping stations.

A key factor in determining suitable surface water levels is the concept of freeboard, also known as "*drooglegging*" in Dutch. Freeboard refers to the area in the subsurface between ground level and the water levels in the surrounding watercourses (KEM-16, 2023). The groundwater levels within the freeboard are allowed to fluctuate under the influence of precipitation, evaporation, and seepage from and towards underlying confined aquifers. The susceptibility of the freeboard to fluctuate under these external fluxes is determined by the local geology, and distance to the nearest watercourse (Figure 10). The suitability of the freeboard is closely linked to land use practices, considering agriculture, nature conservation, urban development, water quality, cultural heritage, and archaeology. Around the Grijpskerk area where clayey soils are common, the use of watercourses alone is not sufficient to drain large areas of land. As a solution, many farmers installed subsoil drainage systems on their agricultural fields to reduce the drainage distance.

It is important to stress that freeboard is not the only factor in the decision-making process on regulating the surface water levels. Other factors such as watercourse depths, surface water discharge conditions, and space for navigation under bridges also play significant roles. To manage these varied needs effectively, the landscape is divided into numerous fixed drainage level areas, each maintaining specific surface water levels. The entire process of coordinating the different interests of stakeholders is complex and extensive. When the optimal surface level configuration is found, it is legally established in a water level adjustment decision, or "*peilbesluit*". It is important to point out that a peilbesluit is not an obligation of result, but rather an obligation of effort. Natural conditions may necessitate (temporary) deviations from the norm.

Monitoring of surface water levels, water level determining structures, and gauge scales typically happens every 5 years, followed by potential adjustments if necessary to comply with the peilbesluit. On average, a peilbesluit is updated approximately every 10 years. These are relatively long intervals in a dynamic system. In the meantime, the surface water level can be adjusted if necessary. Although a surface water level decision becomes effective 'virtually immediately, the actual implementation may lag for years, especially if new weirs and pumping stations need to be built. Considering the current standards for drainage and water table levels, the cumulative margin in surface water level management is on the order of decimetres. Natural variations in groundwater levels are a in the order of 1.5 to 2.0 meters.

7.11.3 Geotechnical characteristics

Buildings in the Netherlands either have pile or shallow foundations. With a shallow foundation, the load of the structure is directly transferred to the ground via load-bearing walls with an enlarged base. The shape of the enlarged base can be a strip or a pier, which can consist of brickwork (panel (A) in

Figure 54), rammed concrete (B), or a (reinforced) concrete slab (C). Nowadays, this method (C) is generally only applied if the ground is sufficiently load-bearing, such as sandy soils. In the presence of weak soil layers, such as clay and especially peat, soil improvement (D) will be necessary to transfer the force to the ground without experiencing significant compaction during or shortly after construction. Subsidence of the foundation element is highly dependent on the local stresses and compressibility of the soil within the area of influence under this element (typically a few meters in most cases). Hence the foundation element is sensitive to stress changes in this zone by e.g. a changing in groundwater level. If the weak soil underlying the foundation element is too thick, then pile foundations are used.

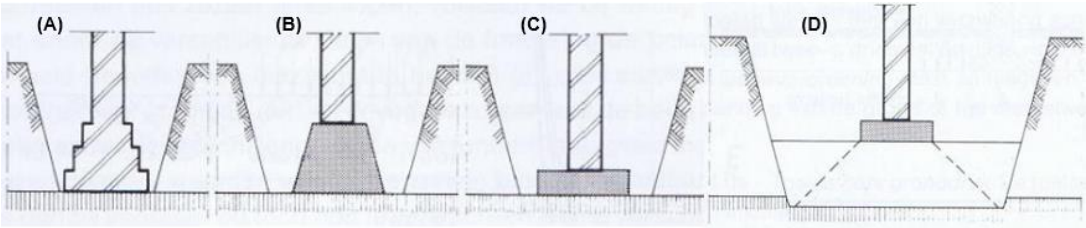

Figure 54 Overview of shallow foundations in the Netherlands (Source: Jellema, 1984)

Based on the soil structure, it is possible to roughly determine whether a building needs a shallow or pile foundation (Figure 55). It should be noted that the nature of the building (height, load, whether it has a basement, etc.) has not been considered. A comparison with the distribution of Holocene/Pleistocene soils at the surface shows that the foundation map was based on the thickness of the Holocene sediments, which is known for being rather heterogeneous including weak clay and peat layers (Figure 56). Considering that the project area, apart from the sand ridges of Grootegast and Zuidhorn, is entirely covered with Holocene deposits with several metres thickness, it can be concluded that the use of pile foundations is generally recommended.

Within the project area no direct information on the building foundations and structures is available. However, studies on foundations in neighbouring municipalities such as Zuidhorn and especially De Marne show that most buildings in the area have shallow foundations with only a few of them being piled (Borsje and de Richemont, 2011; Van Staalduinen et al., 2019). Shallow foundations have only been designed according to generally accepted guidelines since the introduction of the Guideline for Building Foundations (R.F.G.) in 1985. Many of the buildings examined within the studies date from before 1970 and therefore have a foundation that would have been chosen differently based on current knowledge and norms regarding the subsurface on which they are founded. In other words, instead of a shallow foundation, these buildings would likely have had pile foundations. After the 1970s pile foundations may be present in areas with shallow soft peat and clay soils.

In certain areas of Groningen, it is typical for buildings to have shallow foundations, either on dense clay soils such as Pottery clay (Peelo Formation) or Boulder Clay (Drente Formation), or in regions where the soil composition is highly heterogeneous, with different layers alternating over short distances horizontally (Kooi et al., 2021). Consequently, these foundations are more exposed to compaction compared to those on sandy soils. Additionally, it is a characteristic feature of Groningen and Fryslân that buildings with shallow foundations are constructed on elevated residential mounds known as *wierden* and *terpen*. This practice is similar to shallow foundation construction on clay dikes elsewhere in the Netherlands.

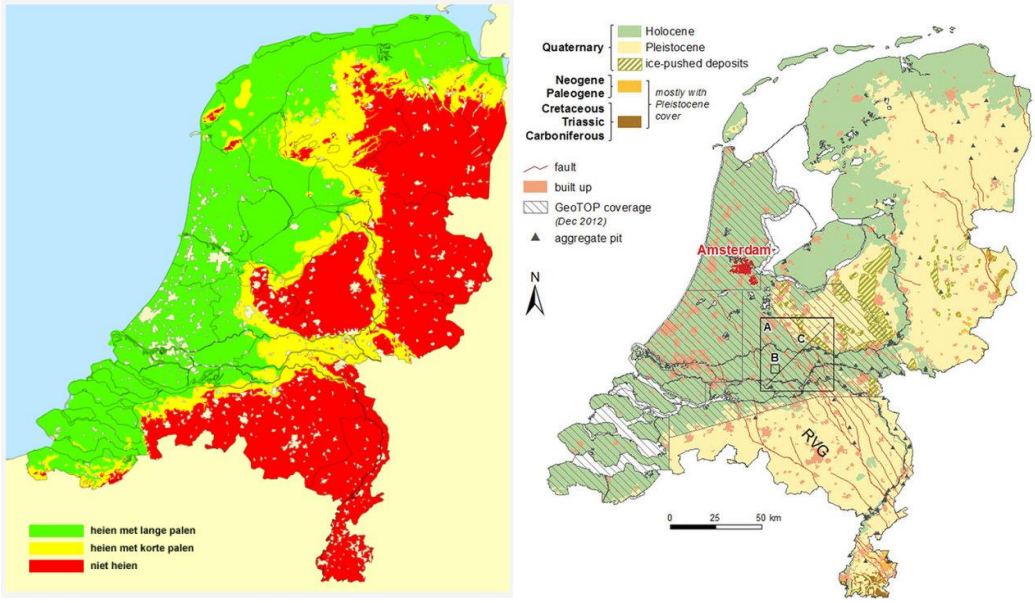

Figure 55 Left: global overview of recommended foundation type based on soil structure with green indicating long pile foundation, yellow indicating short pile foundation and red indicating shallow foundation (Source: IFCO). The map shows a clear correlation with the distribution of Holocene/Pleistocene sediments at the ground surface (Source: Maljers et al., 2015).

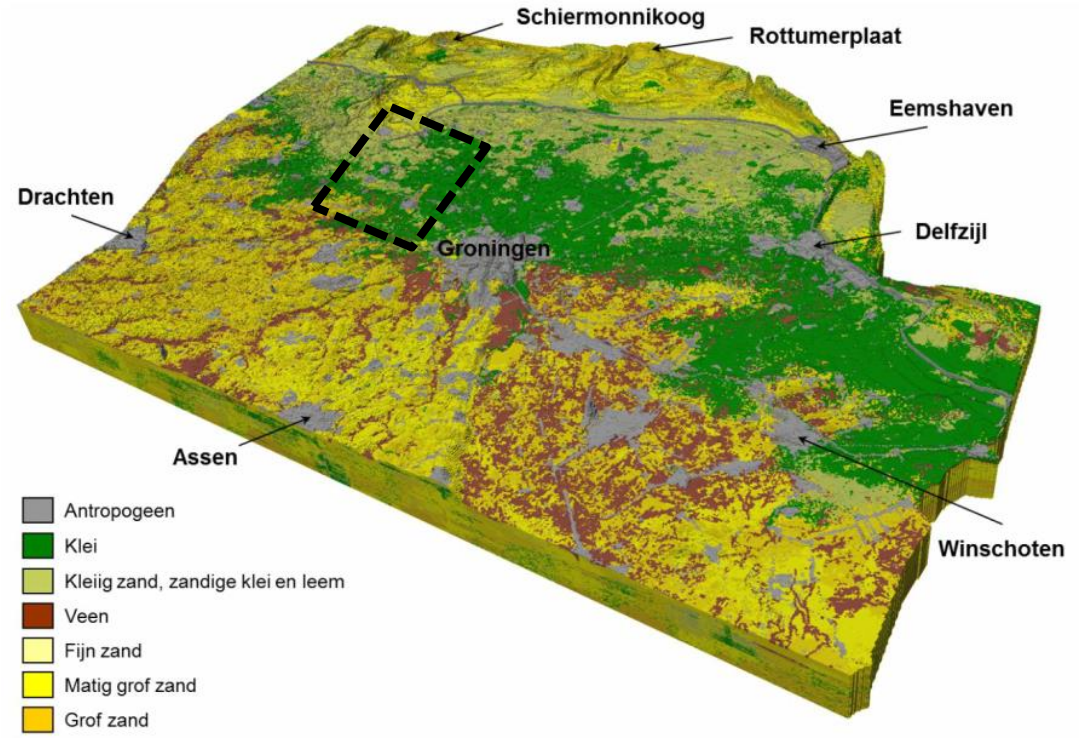

Figure 56. Based on Meijles, 2015: an overview of the most probable lithoclass at the ground surface based on the GeoTop model. The black dotted line delineates the project area.

8

FEASIBILITY STUDY MAIN APPROACH

8.1 Summary and conclusions

In this chapter we present a comprehensive feasibility study to assess the potential of advanced modelling techniques and innovative deformation analysis to understand the cumulative impacts and interactions of mining activities in the Lauwerszee Trough. For this purpose, the Annerveen gas field was selected as a showcase area, as the south side of this gas field was expected to be relatively isolated in terms of cumulative effects compared to other gas fields and has a long gas extraction history. The feasibility study is based on the foundation established by the KEM-19 study, which primarily addressed modelling of aquifer pressure dynamics. In this study we take the surface movements that are reported by citizens of the area as a starting point. Noting the large model uncertainty in the Lauwerszee Trough seen in KEM-19, the current study focusses on using reliable height observations to narrow down the parameter range of subsurface models as much as possible.

In this feasibility study we have used pressure measurements from production wells as provided by NLOG to understand reservoir pressure variations, revealing a predominant large gas compartment and two smaller ones. Utilizing the PySub library (TNO, 2023), we modelled subsidence. This modelling incorporates various parameters, including reservoir geometry and compaction models, followed by a sensitivity analysis on the implementation of these parameters.

A key part in the process is history matching of NAP levelling data before 1995, which achieved a good fit with a linear elastic compaction model, supported by an empirical relationship between porosity and compaction coefficient relevant to the Annerveen field. The residual subsidence signals post-1995 can be attributed to external factors such as salt production in the nearby Veendam area. Despite uncertainties in production volumes and the exact impact of external activities, the combined subsidence effects from Annerveen and Veendam have been estimated, providing a coherent explanation for observed subsidence patterns.

The advantage of NAP-data over InSAR or GNSS is that is provides a very long history of height data over a large area. The problem of NAP-data is that it was never intended to be used for this type of deformation analysis. Furthermore, while many NAP-points represent deep subsidence, this does not apply to all points in the dataset. In order to overcome this problem, we have elected to use the raw observation data for subsidence analysis. This means that all historically observed height differences are used for a large re-adjustment of the levelling network. This allows us to select a different height reference and to eliminate historical errors in the data, resulting in height data that is more precise and reliable. Also, the revision of heights of underground (or 1st order) NAP benchmarks have no longer effect on this re-adjusted data.

The modelled subsidence and raw NAP observations are combined in one large least squares adjustment of the observations. In such a geodetic adjustment the observations are related to the parameters to be estimated through a functional model and a probability model (Teunissen, 2003).

This allows for further error detection, in this case based on a functional model which integrates the geomechanical model of the deep subsidence. This approach, where we do not use the published NAP-heights but perform an adjustment of raw observations to obtain deformation parameters in combination with testing against the geomechanical model was newly developed for this KEM-48 study. This method will be referred to as the DELTA-method in this study. Application of the DELTA-method in the showcase area revealed points where the assumption that these points represent deep subsidence does not hold. These points can subsequently be removed as calibration points for the subsidence modelling.

In conclusion we observe that this new approach with the DELTA-method results in much better precision and accuracy. The combined adjustment with a geomechanical model allows for better selection of points that actually represent deep subsidence compared to other methods of point selection, such as assuming a linear subsidence. Thereby we are now able to model subsidence more reliably and link the results to real visible points on the surface. The technology has been tested and can be applied on larger scale in Phase II of this study.

8.2 Samenvatting en conclusies (NL)

In dit hoofdstuk presenteren we een uitgebreide haalbaarheidsstudie waarin we het potentieel van geavanceerde modelleringstechnieken en innovatieve deformatieanalyse beoordelen. Doelstelling hiervan is de cumulatieve effecten en interacties van mijnbouwactiviteiten in de Lauwerszeetrog te begrijpen. Voor dit doel is het Annerveen gasveld geselecteerd als showcase, omdat verwacht werd dat er aan de zuidzijde van dit gasveld relatief weinig cumulatieve effecten zouden optreden in vergelijking met andere velden. Ook heeft Annerveen een lange winningsgeschiedenis. De haalbaarheidsstudie is gebaseerd op de basis die is gelegd door de KEM-19-studie, waarin voornamelijk de modellering van de drukdynamiek in de watervoerende lagen aan de orde kwam. In deze studie nemen we de oppervlaktebewegingen die door bewoners uit het gebied worden gerapporteerd als uitgangspunt. Gezien de grote modelonzekerheid in de Lauwerszeetrog in KEM-19, richt de huidige studie zich op het gebruik van betrouwbare hoogtewaarnemingen om het parameterbereik van ondergrondmodellen zo veel mogelijk te beperken.

In deze haalbaarheidsstudie hebben we drukmetingen van productieputten gebruikt, zoals geleverd door NLOG, om inzicht te krijgen in reservoirdrukvariaties, waarbij een overheersend groot gascompartiment en twee kleinere gascompartimenten aan het licht kwamen. Met behulp van de PySub-library (TNO, 2023) werd een bodemdalingsmodellering uitgevoerd. Deze modellering omvat verschillende parameters, waaronder reservoirgeometrie en verdichtingsmodellen, gevolgd door een gevoeligheidsanalyse voor de implementatie van deze parameters.

Een belangrijk onderdeel van het proces is de historische matching van de NAP-peilgegevens van vóór 1995, die goed past bij een lineair elastisch verdichtingsmodel, ondersteund door een empirische relatie tussen porositeit en verdichtingscoëfficiënt die relevant is voor het Annerveen-veld. Het resterende bodemdalingssignaal na 1995 kan worden toegeschreven aan externe factoren zoals zoutwinning in het nabijgelegen Veendam. Ondanks onzekerheden in productievolumes en de exacte invloed van externe activiteiten, konden de gecombineerde bodemdalingseffecten van Annerveen en Veendam worden geschat. Deze resultaten kwamen dusdanig overeen dat ze een goede verklaring bieden voor waargenomen bodemdalingspatronen.

Het voordeel van NAP-gegevens ten opzichte van InSAR en GNSS is dat ze een zeer lange historie van hoogtegegevens over een groot gebied opleveren. Het probleem met NAP-gegevens is dat ze nooit bedoeld waren om te worden gebruikt voor dit type deformatieanalyse. Bovendien vertegenwoordigen veel NAP-punten diepe bodemdaling, maar dit geldt niet voor alle punten in de dataset. Om dit probleem te ondervangen, hebben we ervoor gekozen om de ruwe waarnemingsgegevens te gebruiken voor de analyse van de bodemdaling. Dit betekent dat alle historisch waargenomen hoogteverschillen worden gebruikt voor een grote aanpassing van het

waterpasnetwerk. Hierdoor kunnen we een andere hoogtereferentie kiezen en historische fouten in de gegevens elimineren, wat resulteert in hoogtegegevens die nauwkeuriger en betrouwbaarder zijn. Ook de herziening van de hoogtes van de ondergrondse (of 1e orde) NAP peilmerken heeft geen effect meer op deze aangepaste gegevens.

De gemodelleerde bodemdaling en de ruwe NAP-waarnemingen worden gecombineerd in één grote kleinste kwadratenvereffening van de waarnemingen. In een dergelijke geodetische vereffening worden de waarnemingen gerelateerd aan de te schatten onbekende parameters met behulp van een functiemodel en een kansmodel. Dit maakt verdere foutdetectie mogelijk op basis van het best mogelijke functiemodel van diepe bodemdaling dat beschikbaar is. Deze aanpak, waarbij we geen gebruik maken van de gepubliceerde NAP-hoogtes, maar een vereffening uitvoeren op de ruwe waarnemingen voor het schatten van deformatieparameters in combinatie met toetsing op basis van het geomechanische model is nieuw ontwikkeld voor KEM-48. Deze aanpak zal verder in de study aangeduid worden als de DELTA-methode. Door toepassing van de DELTA-methode in het showcase-gebied kwamen punten aan het licht waar de aanname dat ze diepe bodemdaling weergeven niet opgaat. Deze punten kunnen vervolgens worden verwijderd als kalibratiepunten voor de bodemdalingsmodellering.

Concluderend stellen we vast dat deze nieuwe benadering op basis van de DELTA-methode resulteert in een veel grotere precisie en nauwkeurigheid. De gecombineerde vereffening met een geomechanisch model maakt een betere selectie mogelijk van punten die daadwerkelijk diepe bodemdaling weergeven in vergelijking met een selectiemethodiek waarbij uit wordt gegaan van lineaire bodemdaling. Daardoor zijn we nu in staat om de bodemdaling betrouwbaarder te modelleren en de resultaten te koppelen aan echt zichtbare punten aan het oppervlak. De technologie is getest en kan op grotere schaal worden toegepast in fase II van dit onderzoek.

8.3 Introduction

The main research question to be addressed in the current study is on understanding cumulative effects on land subsidence, induced earthquakes, and interactions of the different mining activities around the Lauwerszee Trough. The same subject was addressed in the previous KEM-19 study, which focussed on a modelling approach of aquifer pressure. A main outcome of KEM-19 was that the evolution of the aquifer pressure in the southern Lauwerszee Trough is not well understood. A sensitivity analysis indicated a wide range of possible depletion scenarios.

At the same time, public concern has been expressed regarding observed surface movements in the area. To date, no model exists that (quantitatively) explains these movements and that could be used for making a prognosis of future deformations. This is the starting point for the current study. Noting the large model uncertainty in the Lauwerszee Trough seen in KEM-19, the current study focusses on using a new approach when using the NAP-data to narrow down the parameter range of subsurface models as much as possible.

Contrary to KEM-19 in this approach we use a new way to process the NAP-data as input for the geomechanical model. Where KEM-19 used the published NAP heights, which suffer from problems including a revision of the first order NAP-heights, we have opted to rely on the original observed height measurements and reprocess them with the goal to obtain deformations instead of heights. By doing so, we eliminate inaccuracies that stem from historic decisions in the NAP data processing. This new approach was developed for the KEM-48 study and will be referred to as the DELTA-method.

Crucially, the NAP dataset was never intended to be used for deformation analysis. As a result, the dataset is not a reliable source for deformation without proper testing of the validity of the observations (Fokker, 2018; Van der Weele, 1971). The following effects in particular make the NAP height data as-is unsuitable for deformation studies:

- Historic measurement errors are included in the historic NAP heights for a small set of selected points;
- Heights van be incorrect due to point misidentification errors.
- The NAP heights of first order benchmarks were revised in 2005. This causes a jump in the time series. This jump reflects a height change over more than 50 years but is similar (but arguably more complex) to a height change in 2nd order levelling over 5 or 10 years. (Brand, 2004)
- For smaller measurement campaigns there is no registration, how these were connected to the larger NAP measurement campaigns of NAP and whether points were assumed to be stable for this connection. SodM requires that networks are connected to a single point, which means that there is no testing to see if that point is stable. Connecting points may have subsided since their last measurement date.
- Points are measured in primary levelling campaigns, nationwide campaigns, and local campaigns. Each of these campaigns will have a different measurement frequency and have a different result on the variance-covariance matrix of these points.
- Spatial interpolation between neighbouring points is only allowed if the full variance-covariance matrix of the points is used (Technisch Platform Bodembeweging, 2014). Unfortunately, the variance-covariance matrix is not published as part of NAP.

As a result, the dataset is not a reliable source for the determination of deformations without proper testing of the validity of the observations (Fokker, 2018). For the primary purpose of NAP as a reference frame it is only important that the current height values of the benchmarks are reliable. There has never been the intention to obtain a reliable time series for the determination of deformations.

Consequently, it is better to use the original levelling observations instead of the published heights. In the context of KEM-48 we have therefore developed the DELTA-method. A new iterative approach for estimating deformation and handling measurement errors based on the DIA-concept (Detection, Identification, Adaptation) in combination with a geomechanical model. The method is based on the work by Velsink (2015) and the general principles of geodetical quality control (Teunissen, 2000). In order to test its effectiveness, the DELTA-method is applied to a test case, the Annerveen field, for demonstrating its performance. This test case was selected because this gas field was expected to be relatively isolated in terms of cumulative effects. Hence, the NAP levelling data to the South of the Annerveen field are expected to be impacted primarily by the Annerveen field. By performing the analysis on this test case, we can analyse if application of the DELTA-method will be feasible for performance in the second phase of this study. This chapter documents the feasibility of the DELTA-method. In section 8.4 we describe the way the geomechanical model is setup. In section 8.5 we describe the preparation of the height data using the levelling observations and in the integration of the data and the model.

8.4 Showcase Annerveen

8.4.1 Reservoir model

The platform NLOG.nl provides an extensive data collection for all gas fields in the Netherlands. These data include geological as well as operational data. For example, Figure 57 shows the outline of the Annerveen field including the location of the production wells.

In a first step, pressure measurements at each production well (Figure 58) are used to characterize the evolution of reservoir pressure at different reservoir locations (compartments). For the case of the Annerveen field, most production wells show a consistent pressure evolution, indicating that the reservoir is dominated by a single, large gas compartment (Figure 59). Two smaller compartments show a different pressure evolution. In the subsequent section, the Annerveen field is modelled as a system consisting of three independently compacting compartments.

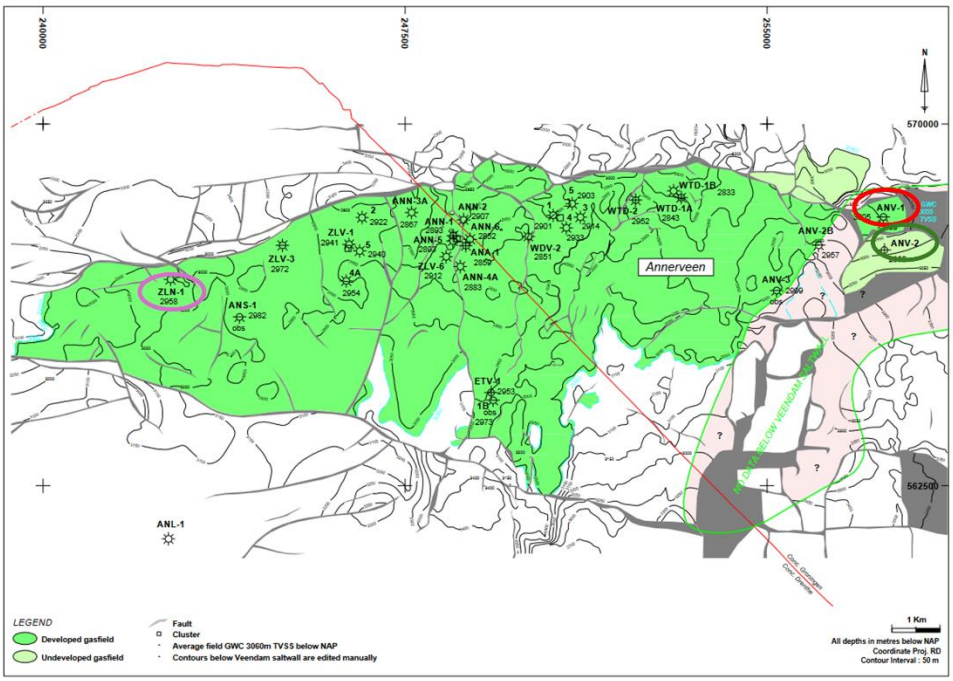

Figure 57. Map view of the Annerveen gas field, including wellbore locations. Source: NLOG.nl. Coloured ellipses indicate locations of wellbores ANV-1 (red), ANV-2 (green) and ZLN-1 (purple).

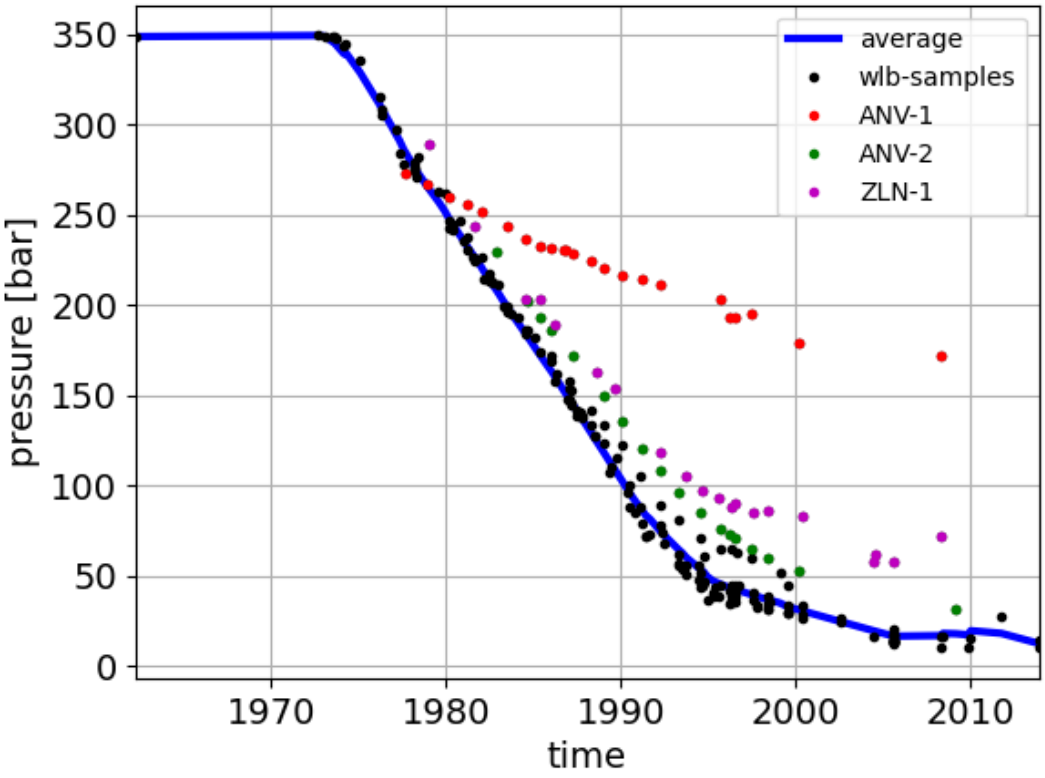

* Blue line indicates average pressure determined from measurements in various wells (black dots). Coloured dots indicate wellbores according to the legend, where measurements systematically deviate from the average pressure.

Figure 58. Pressure measured in Annerveen wells ANV-1, ANV-2 and ZLN-1 (compare previous figure) as a function of time. (Data source: NLOG.nl).

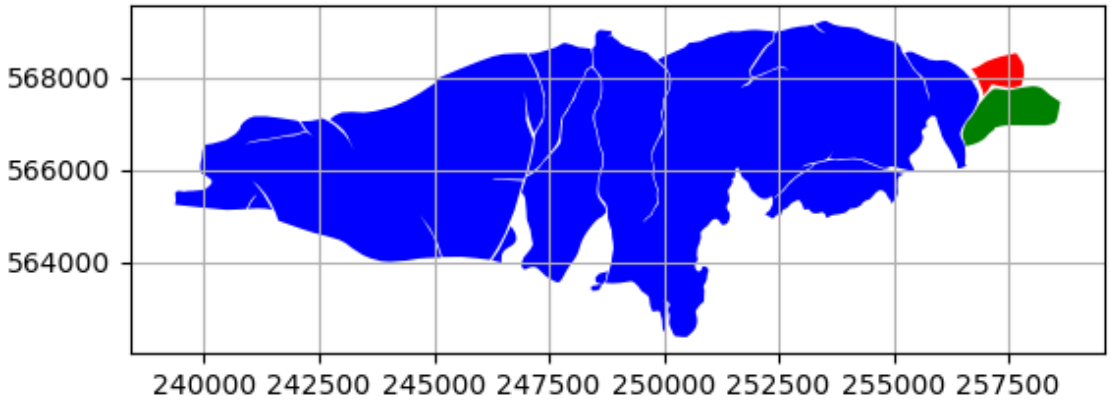

* The reservoir consists of a main compartment (blue) and two smaller compartments (red, green). In each compartment, spatially homogeneous pressure conditions are assumed with temporal depletion as indicated in Figure 58. Data from wellbore ZLN-1 (purple dots in Figure 58) indicates poor reservoir conditions at the Western rim. This data is ignored.

Figure 59. Simplified hydraulic reservoir model used for subsidence computation (Data source: NLOG.nl).

8.4.2 NAP levelling data

A total number of 176 NAP levelling points exist around the Annerveen gas field (Figure 60). An inversion scheme was set up to estimate relative height changes over time at each levelling point. The computation of the input for the NAP-modelling is described in more detail in section 8.5.

In principle, a compaction source, such as the Annerveen reservoir, can be “calibrated” using levelling data of a single benchmark. For the feasibility study, four benchmarks covering different areas around the Annerveen field were chosen. Data from these benchmarks is used for “calibrating” a subsidence model (section 8.4.3).

The choice of the four NAP benchmarks (Figure 61) is arbitrary and was based on visual inspection of height changes over time. The selection criterion for this showcase was a smooth subsidence signal with small scattering and a good coverage of the area. It should be noted that other benchmarks exhibit similar subsidence signals compared to the reference benchmarks. Once the full iterative procedure is completed, all benchmarks are equally relevant.

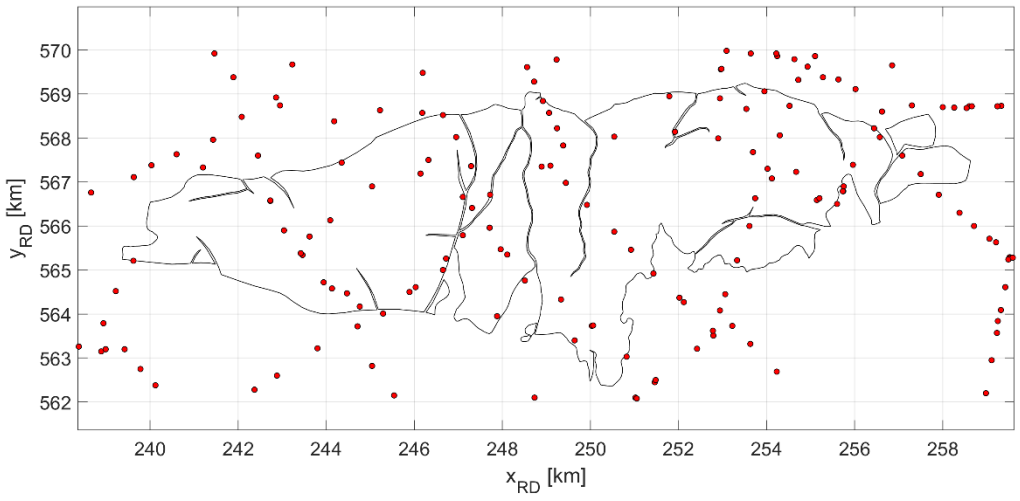

Figure 60: Locations of NAP benchmark points.

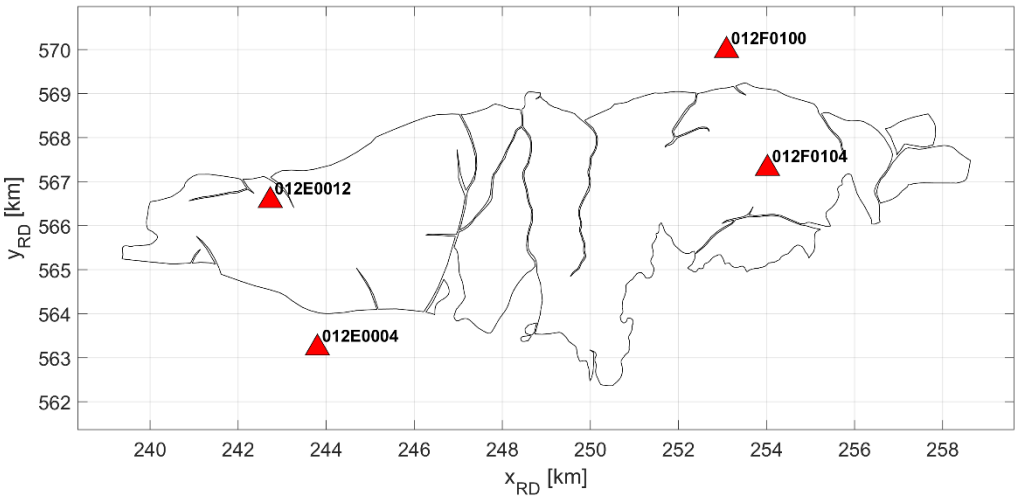

Figure 61: Location of 4 benchmarks selected for the feasibility test.

8.4.3 Subsidence modelling

Different approaches for modelling subsidence are presented in section 2.10.1. In the scientific literature, most subsidence computations are based on Geertsma's (1973) model, or similar analytic approaches. Following the same line, we use the Python library PySub developed in KEM16 (TNO, 2023) for modelling subsidence associated with natural gas and salt production. Subsidence calculations are based on the analytical half-space solution by Geertsma (1973), extended for Van Opstal's rigid basement implementation (see Tempone et al., 2010).

Input to the numerical model is the reservoir geometry (shape, thickness, depth), its depth to rigid basement, the compaction model (linear, rate-type, time decay), and the pressure history. Furthermore, Poisson ratio and several numerical parameters (e.g., resolution) need to be specified. Within a sensitivity analysis, however, it was found that choices of the latter parameters (Poisson ratio, numerical parameters) have a second order impact on the results.

For the feasibility study, we obtained improved deformation timeseries according to the method described in section 8.5. We performed the history matching with the reprocessed levelling data using linear, rate-type (RTiCM) and time decay compaction models, respectively. Initial comparisons between modelled and observed subsidence indicate several sources for deep subsidence. While the observed subsidence signal until 1995 can be well matched by gas production from Annerveen, strong deviations persist at later times, indicating interference from other geotechnical activities.

In a first step, we have calibrated the compaction process in the Annerveen field using the four NAP benchmarks defined in the previous section. For this, we restricted the history matching to times before 1995. Within a grid search we obtained the best fit using the linear elastic compaction model with a compaction coefficient of c_m = 6.98e-6 1/bar. This is illustrated in Figure 62 showing RMS-misfit between modelled and observed subsidence as a function of the compaction coefficient and the reference compaction coefficient in the rate-type compaction model. The best fit is obtained for c_m= c_{mref}, which is equivalent to the linear elastic compaction model. The best fit at c_m=6.97e-6 1/bar, however, shows little sensitivity to variations of c_{mref}, implying that a rate-dependent compaction model performs similar as the linear elastic compaction model. Time-dependent compaction models (not shown) do not provide a reasonable history match. A comparison of the best-fitting model and observed subsidence at the four reference benchmarks is shown in Figure 63.

We note that an empirical relationship between porosity and compaction coefficient for Groningen (TNO, 2013) yields the same compaction coefficient c_m=6.97e-6 1/bar for Φ=11.7%, which is the reservoir porosity for Annerveen (Fekkes, 2016).

For the time before 1995, the RMS difference between height changes resulting from the reprocessed NAP levelling data and the height changes resulting from subsidence modelling is approximately 4 mm. This RMS difference is consistent with the nominal data accuracy of the input levelling data.

Subsequently, we have analyzed the residual subsidence signal after 1995. Systematic deviations between modelled and observed subsidence after 1995 indicate a second (coherent) signal (Figure 63). The amplitude of this signal is largest at the benchmark located to the North of Annerveen, where salt is produced from a cavern field at Veendam (Figure 64). The first production at Veendam started in 1972 from a reservoir at 1300 - 1800 m depth. According to Leijen & Hanssen (2007), salt production started in May 1995, consistent with observations in Figure 63. Salt is produced from multiple wells with changing locations over time. Annual production data is publicly available only after the year 2001 and even the total production volume is subject to uncertainty (NLOG.nl states 5-10 Mio m^3). Given the lack of publicly available data and the level of uncertainty, we have not attempted to history match the Veendam subsidence signal. Instead, we have used simplified models to estimate the magnitude of the Veendam subsidence signal resulting from a specific salt production volume. Based on an estimate of the total salt production volume, we investigate if salt production at Veendam can in principle explain the amplitude of the residual subsidence signal after 1995.

We have made the following simplifying assumptions:

- 8 Mio m^3 total salt production since 1972.
- The cavern field is approximated by a single compaction source located in the center of the cavern field at 1300 m depth, with a height of 140 m.

After producing 10 Mio m^3 of salt, the modelled subsidence at the reference benchmark located to the North of Annerveen (index 115 in Figure 63) is approximately 255 mm. The combined compaction signals from Annerveen (50 mm in 2015) and Veendam (255 mm after producing 8 Mio m^3) approximately match the observed compaction of ~310 mm at the closest reference benchmark (index 115). We have not attempted to discriminate and isolate subsidence contributions from the Groningen gas field (compare Figure 64). This could be done following the same approach but is beyond the scope of the feasibility test.

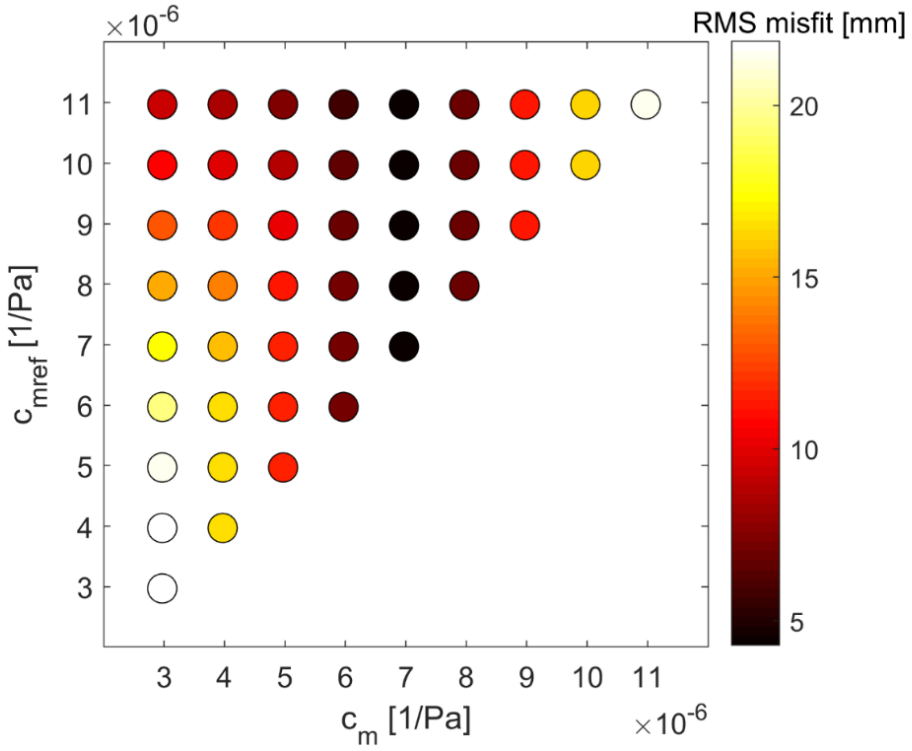

* Fixed parameters: ρ=2500 kg/m^3, $\dot{\sigma_{ref}}$= 1e-4 Pa/yr, b = 0.017, depth to rigid basement 5 km. The best fit is obtained for c_m= c_{mref}=6.97e-6 1/bar, which is equivalent to the linear elastic compaction model. The best fit at c_m=6.97e-6 1/bar, however, shows little sensitivity to variations of c_{mref} in the parameter range shown. Near the minimum, modelled subsidence is almost independent of the fixed parameters b and $\dot{\sigma_{ref}}$ Note that c_m cannot be larger than c_{mref}.

Figure 62: RMS misfit between modelled and observed subsidence (at 4 reference benchmarks) as a function of the two model parameters c_m and c_{mref} in the RTiCM compaction model.

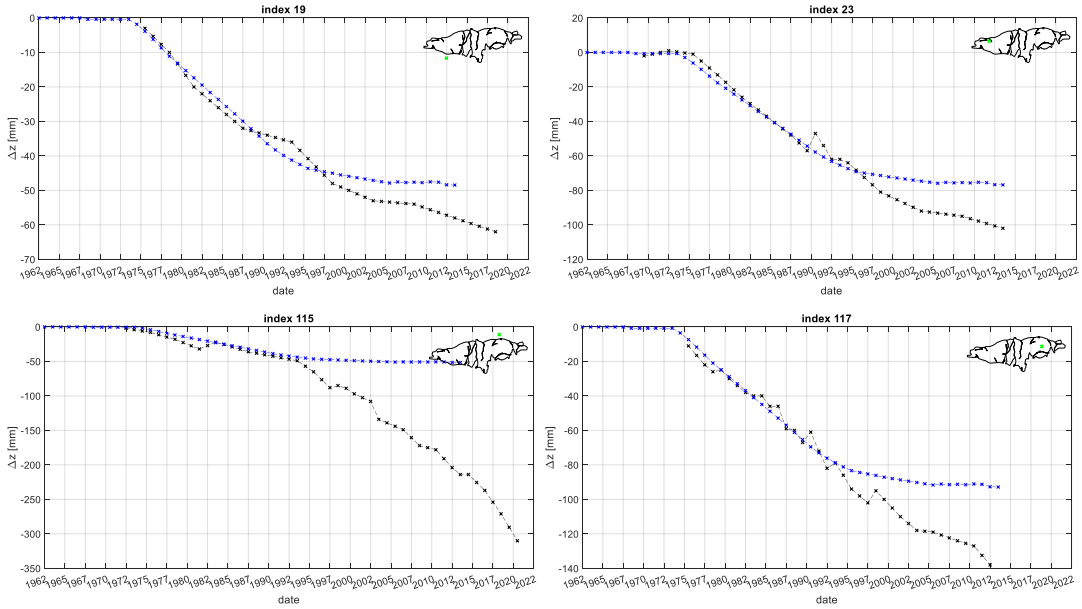

Figure 63: Best-fit modelled (blue) and observed (black) subsidence at the 4 benchmark locations as indicated in green on the inset-maps. Model fit restricted to times before 1995.

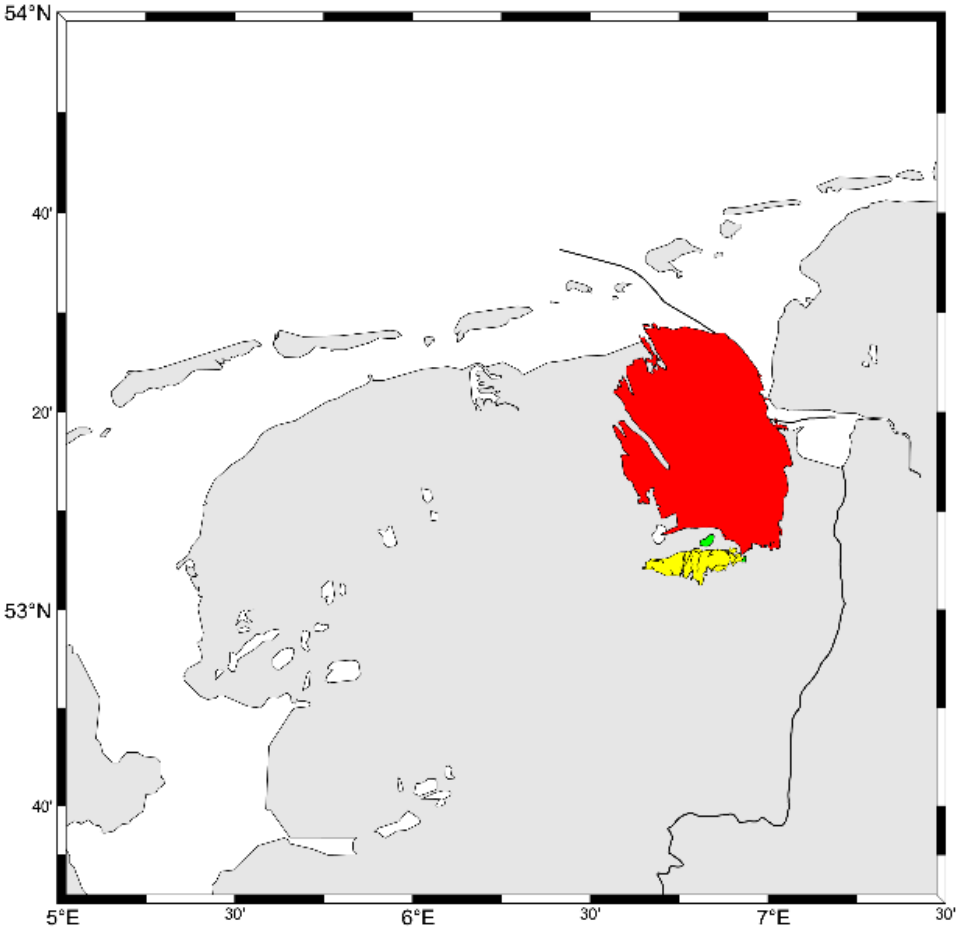

Figure 64: Map showing the location of the Groningen (red) and Annerveen (yellow) gas fields and salt production at Veendam (green).

8.5 Preparation of NAP-data for Annerveen area

8.5.1 NAP height data

The NAP, which is short for *Normaal Amsterdams Peil* (Amsterdam Ordnance Datum), is both the height reference system and the height reference frame of The Netherlands. As a height reference system, it defines a surface that is defined to be at height zero. This surface is approximately equal to the mean sea level at Amsterdam.

As a height reference frame, the NAP provides a realization of the system. This is achieved by placing benchmarks at locations throughout the country. These benchmarks can be bolts in buildings and civil engineering structures such as bridges, locks, etc. There are also underground benchmarks which are founded on a Pleistocene sand layer. The height of each benchmark, relative to NAP, is provided by Rijkswaterstaat. Surveyors use these bolts to obtain the NAP-height at their location. Further background to the history and properties of NAP, with an extensive list of references, can be found in section 2.11 as well as De Bruijne et al., 2005.

Many, but not all, NAP benchmarks are placed in buildings with foundations into the Pleistocene sand. Deformations that occur in the deep surface will therefore also result in a movement of the reference

benchmark bolt. By re-measuring the height of the bolt relative to NAP and computing the difference between multiple measurements, a magnitude for the deep surface deformation can be obtained.

However, the NAP was never intended to be used for deformation analysis, as described in section 8.3. In order to overcome the inherent limitations of NAP, we have proposed a novel approach to using the data from NAP. Rather than relying on the historically published values of NAP, we will recompute new reliable values within the context of KEM-48. To do so, we have obtained all original levelling observations from NAP since 1921. Using Geodelta's Least Squares Adjustment software Delfy, the goal of this work is to re-adjust all historical observations of the NAP to obtain reliable deformation time series.

8.5.2 Integrated deformation analysis based on a geomechanical model (DELTA-method)

Introduction

In total, we have received 505233 levelling observations from 1466 measurement campaigns, observed within the period from 1921 to 2021. The data covers 38311 benchmarks in the provinces of Friesland, Groningen, and Drenthe, as well as some benchmarks outside these provinces if they were part of a measurement campaign that crossed the border of a province. Figure 65 shows the location of the benchmarks, coloured by the first year of observation of the benchmark. In Figure 66 a cut-out is shown with the same data but zoomed in on Groningen.

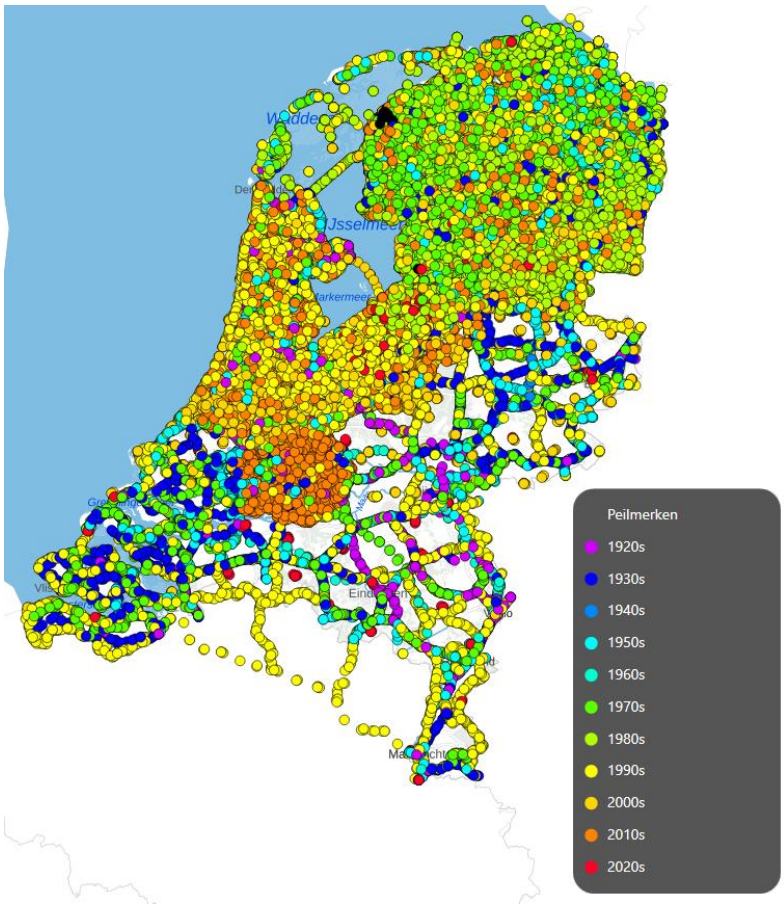

Figure 65. Map with the benchmarks used, coloured by first year of observation.

Figure 66. Map with the benchmarks, cut-out of the Groningen-area.

The data is organised in measurement campaigns or projects. Projects can be nationwide levelling campaigns, or very small local levelling campaigns. Also, levelling campaigns performed by mining concession holders as well as municipal levelling campaigns are included in the data. Some projects cover multiple years. In those cases, we have split the project into multiple sub-projects with a maximum time span of one year. Each project or sub-project is treated as an epoch in our analysis. In total this results in 1989 epochs. Figure 67 shows the epochs along a timeline for the Annerveen showcase region. The temporal accuracy of the epochs ranges from 1 day to 1 year, depending on the accuracy of date registration during the measurement campaign. For instance, in older primary levelling projects, all observations are registered at the first of January. In later projects, the actual date of observation is stored. In all cases, we select one date to serve as the epoch date.

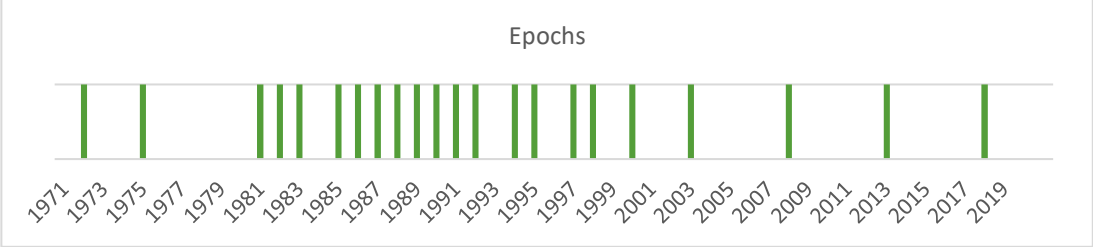

Figure 67. Plot with a timeline showing the epochs in the Annerveen region.

The DELTA-method is based on the work as published by Velsink (2018). In previous attempts to approximate the subsidence due to mining activities, several different mathematical functions have been used, without direct recourse to available geophysical models (Lorenz et al., 1991, De Heus et al., 1994, Kenselaar & Quadvlieg, 2001), or a simple geophysical model (Samiei-Esfahany & Bähr, 2015) was used. For the particular case of KEM-48, which deals with cumulative effects of mining, we preferred to compute the subsidence with as little as possible constraints on the actual measurements as possible. We refer to Annex II for further background on the challenges of correctly modelling subsidence. The DELTA-method furthermore uses the computation results to calibrate the

comprehensive geomechanical model of Q-con and, subsequently, to improve the computations in an iterative process of geodetic adjustment and geomechanical model inversion.

The DELTA-method relies on an iterative process. The first iteration is depicted in Figure 68. This iteration is slightly different from the subsequent iterations, because for the first iteration there is no geomechanical model data to serve as input.

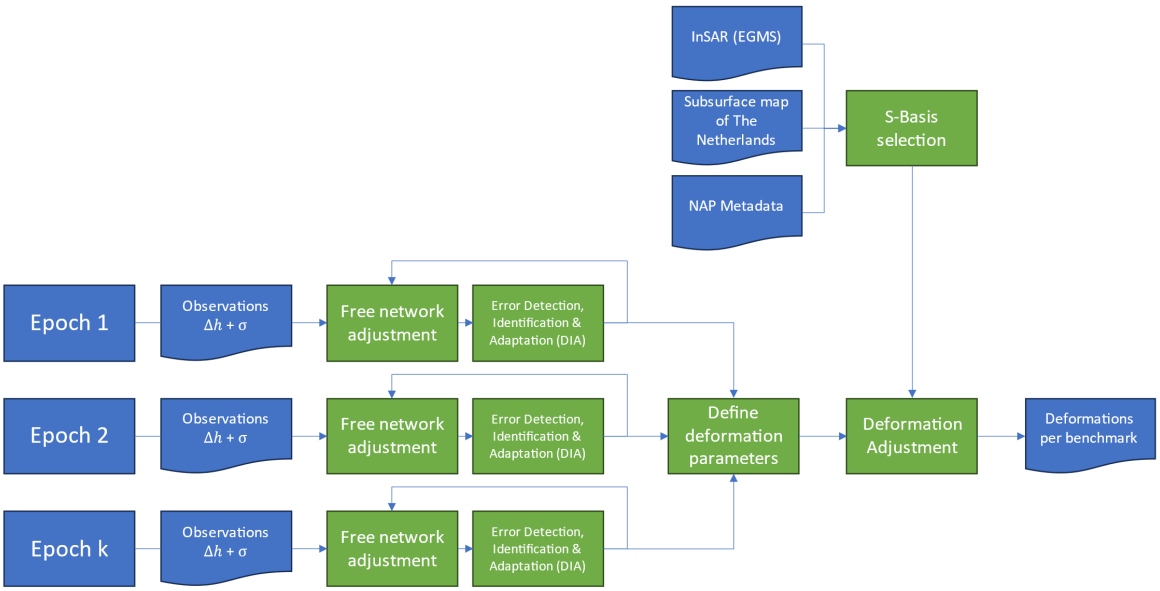

Figure 68. Workflow for the first iteration of the integrated deformation analysis

S-Basis selection

The step to go from observations to estimates of the unknown parameters is referred to as a geodetical least squares adjustment. In our work we follow the process for adjustment and testing as described among many others by Teunissen (2000, 2003) and Velsink (2015). In re-adjusting the NAP measurement data using the DELTA-method, we aim to obtain only deformation values. Contrary to traditional NAP-adjustments, no attempt is made to compute NAP heights. The computations are performed with the observation data of the NAP reference frame but are strictly not based on the NAP reference system. Therefore, even if a height is computed, this should not be confused with or compared to an NAP-height, only the height differences are a usable outcome of this computation.

Unfortunately, the problem of adjusting the observations to obtain deformations is ill-defined and some model parameters cannot be estimated from the measurements or cannot be estimated well enough. In particular, the height of one base point in just one epoch must be fixed, and for each interval between two consecutive epochs, the change of at least one height must be fixed. Therefore, it is necessary to constrain the adjustment problem. In Figure 69 this is visualized by showing a small levelling network at two epochs. The adjustment can only be solved for a single epoch if one height is fixed. For instance, the height of point A_1 can be fixed to 0 m. Additionally the change between epochs should be fixed for at least one point. For instance, the height difference between B_1 and B_2 can be fixed to 0 m if this point is assumed to be stable. In geodesy, the definition of these constraints is commonly referred to as the S-Basis (Baarda, 1973).

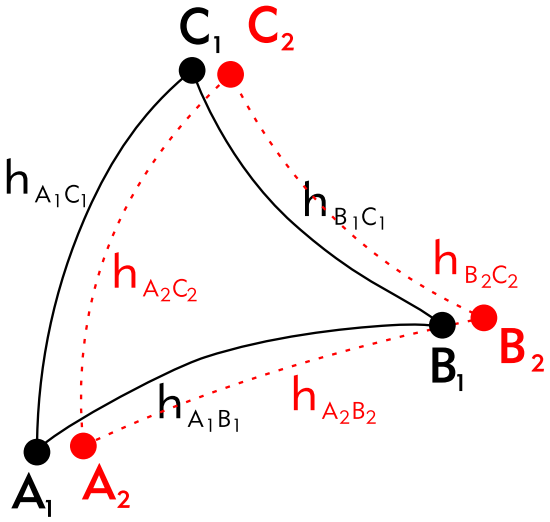

Figure 69. A levelling network with three points (A, B and C) measured in two epochs.

We have decided to select one point as S-Basis, and to fix the height of this point for all epochs. Technically, it does not matter which point is selected for this purpose. If we happen to select a point that subsides, the computation will still succeed. Fundamentally, it is impossible to select a truly stable point: the entire Netherlands is moving due to many different effects, including post-glacial rebound (see section 2.4.2). For this study we therefore prefer to select a point that is at least not influenced by mining activities.

For the selection of this point, we have reviewed all underground benchmarks which have a long history of observations. This means that these benchmarks are founded on a purpose-built pile in the deep Pleistocene sand layer. Furthermore, these benchmarks are unlikely to be disturbed by construction works, people, weather, etc. This subset of benchmarks is subsequently compared with the following data sources:

- Map with mining concessions;
- Map with soil types;
- InSAR data (Copernicus European Ground Motion Service, EGMS).

Only points that are well outside any mining concession, that are founded on Pleistocene sand and show no significant movement in the EGMS-data will be considered. It turns out that for the Annerveen showcase area no such point is available. For this reason, we decided to significantly extend the project area. We have now selected the benchmark 000A2080 at Gasselte as the fixed point for the computations. A picture of this point is shown in Figure 70.

It would be desirable, if more benchmarks, fulfilling the aforementioned conditions, and having no movement relative to benchmark 000A2080 at Gasselte, could be combined with that benchmark to form a reliable reference benchmark cluster, relative to which all subsidence in the North of the Netherlands can be computed. But such other benchmarks are not measured within the region of the showcase. For now, we rely on this one benchmark, which is really a trustworthy basis, especially for the Annerveen showcase, as our computations show. In the following this benchmark will be referred to as the S-basis.

Figure 70. The underground benchmark 000A2080 in Gasselte (source: Rijkswaterstaat).

Epochs and observations

As outlined above, we have defined epochs from the data based on the projects and measurement campaigns. In total there are 1989 epochs. However, not all epochs include the fixed point at Gasselte. In the first iteration, therefore, we include only the 22 epochs which contain an observation to Gasselte and cover the showcase area of Annerveen. These are identified as epochs 1 to *k* in Figure 68.

The observations constitute a list of observed height differences between benchmarks. Each height difference was observed using levelling. For each height difference an estimated standard deviation is provided. However, we have found that these values for the standard deviation are generally to pessimistic, especially for short distances. We have therefore decided to re-estimate the standard deviation for each observation. The standard deviation for levelling measurements is commonly expressed as a constant part and a part that is dependent on the square root of the distance between measurement points (Alberda, 2006). We have estimated new factors (constant part and range part) for computing the standard deviation by iteratively selecting two values such that the Overall Model Test, also known as, F-test (Baarda, 1968; Teunissen, 2000) is as close as possible to the critical value of the test. For the showcase the new standard deviation is now computed as $\sigma_{\Delta h} = 0.5mm + 0.25mm \cdot \sqrt{l}$ with l the distance of between measurement points in kilometres. The constant factor of 0.25 mm is already four times stricter than what is used by NAP. Further investigation revealed that a constant factor of 0.1 mm is also feasible. We have found that this stricter precision gives results for the Overall Model Test (F-test) of the free network adjustment per epoch between 0.3 and 0.9 with a critical value near 1.0, which indicates that it is a suitable value.

Per epoch, we have performed a free network adjustment. In a free network adjustment, the network is not constrained to more than one benchmark. This allows for testing of measurement errors in the data. In the DELTA-method we follow the B-method of testing (Baarda, 1968) using the DIA-procedure (Detection, Identification, Adaptation) which works as follows:

- Detection: discover if the epoch contains measurement errors or an incorrect stochastic model by performing the F-test (Overall Model Test).
- Identification: identify the most likely measurement error by performing the w-test on all observations (Teunissen and Salzmann 1988, 1989).
- Adaptation: resolve the error by adapting the observation data or by removing the measurement.

The DIA-procedure is performed iteratively, until no more gross errors are found in the data. Every time an error is resolved, the free network adjustment is restarted. The adaptation step in particular requires a specialist to analyse the measurement error and define the best way to resolve this error. As we are dealing with historical data, many of which was initially recorded in handwriting, small errors resulting from writing errors and digitisation errors are to be expected. Paragraph 8.5.3 documents two examples of errors that were corrected in this step. In total, 483 measurement errors were corrected for the Annerveen showcase.

If an epoch features insufficient redundancy, i.e. the measurements are too few to allow for the detection of errors, the entire epoch is disregarded and no longer used in the analysis. For the Annerveen region we have used a total of 22 epochs in the first iteration.

Creation of deformation parameters

Once all observations have been tested in a free network adjustment, we commence an integrated deformation adjustment. To this end, all observations from all epochs are added to a single least squares adjustment. In this step, we follow the approach as proposed by Velsink (2015, 2017). In this process, the deformation of a group of benchmarks is estimated as a parameter in the adjustment. This means that through our least squares estimation we estimate deformation parameters, without the need to estimate heights.

There are multiple ways to define deformation parameters in a one-dimensional levelling setup like the NAP-data. One method would be to estimate a linear deformation per benchmark. Alternatively, a deformation following a higher order polynomial, or two discontinuous deformations are possible (Lorenz et al., 1991, De Heus et al., 1994). Any choice made here is based on a deformation pattern hypothesis and should be made with great care. The interplay of various reservoirs may result in unexpected non-continuous deformation patterns. For that reason, it is better to start with unconstrained deformation parameters. This means that a deformation value is computed for every interval of two epochs for every benchmark.

Within the DELTA-method we use a least squares adjustment. Each height observation can mathematically be written as an observation equation:

$$\underline{dh_{ij} = H_j - H_i + e}$$

Here, dh_{ij} is the observed height difference and H_i and H_j are the heights of point i and j. The measurement noise is represented by $\underline{e}$. In this notation all stochastic variables are underlined. As we deal with many height difference observations, they can together be presented as a matrix equation as:

$$\underline{y} = Ax + \underline{e}$$

In this equation, $\underline{y}$ represents the observations, $\underline{e}$ are the stochastic errors in the observations and the matrix A relates the observations to the unknown parameters x.

When setting up the deformation equation, all height difference observations are added to the $\underline{y}$-vector. The heights are the unknowns in vector x. In addition, deformation equations are added to relate the observations from multiple epochs to deformations. This is achieved by adding the deformation model in the matrix D to the model matrix of the adjustment.

$$\begin{pmatrix} \underline{y}_{1,1} \\ \underline{y}_{1,2} \\ \vdots \\ \underline{y}_{1,n} \\ \underline{y}_{2,1} \\ \underline{y}_{2,2} \\ \vdots \\ \underline{y}_{2,n} \\ \vdots \\ \underline{y}_{k,1} \\ \underline{y}_{k,2} \\ \vdots \\ \underline{y}_{k,n} \\ 0 \\ \vdots \\ 0 \end{pmatrix} = \begin{pmatrix} A_1 & & & & \\ & A_2 & & & \\ & & \ddots & & \\ & & & A_k & \\ D_1 & D_2 & \dots & D_k & D_0 \end{pmatrix} x + \underline{e}$$

The submatrices D_i ensure that for each benchmark in each interval of two consecutive epochs a constraint is added to the model. It states that all deformations are in principle zero, which can be seen by the zeros in the lefthand side of the equation. A standard deviation of 0 mm was used for the constraints in the stochastic model. These constraints are relaxed by adding extra parameters in *x* and their coefficients in submatrix D_0, which enables the estimation of the deformation. In the first iteration adding this constraint results in an additional observation equation $0 = H_{1,1} - H_{1,2} + \Delta H_{1,1\to 2} + \underline{e}$. In this equation $H_{1,1}$ and $H_{1,2}$ represent the height of point 1 at epoch 1 and 2 respectively. $\Delta H_{1,1\to 2}$ is the height change of this point between two epochs. This parameter is only added for points that are not in the S-Basis.

Deformation adjustment

After the definition of the deformation parameters, the integrated least squares adjustment can be computed. We perform an adjustment using the prior selected S-Basis. All observations are weighted by the a priori standard deviation that was given to the observation using the equation given above. The adjustment problem is linear and can therefore be computed in a single iteration.

The result of the adjustment are the deformations per benchmark between epochs, as well as the a posteriori standard deviation per deformation as well as the Minimum Detectable Deformation. The Minimum Detectable Deformation is computed as the smallest deformation that can be detected with a certain probability using the w-test. In the current showcase a test power of 80% is applied ($\alpha_0 = 0.001$).

Model output integration

The results of the deformation adjustment are used to calibrate the model, as described in section 8.4.1. Once the geomechanical model is computed, the a posteriori deformation for each benchmark according to this model can be computed. These deformations act as input to the next iteration of the adjustment computations. The updated flowchart of the second iteration and onwards is shown in Figure 71.

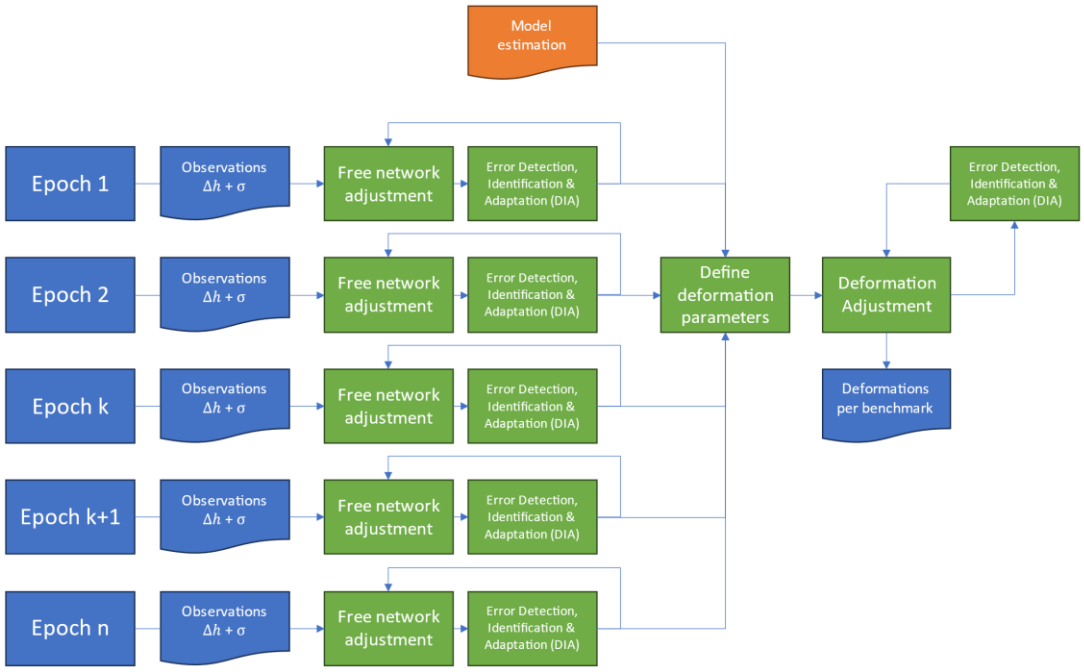

Figure 71. Flowchart for the second iteration onwards

Each geomechanically modeled deformation is added to the adjustment as an observation, like the height differences observed by surveyors using levelling. By combining both the geomechanical modeled deformations and the surveyed observations in one adjustment, both the adjustment model and the geomechanical model can be tested. This is an important step in further improving the quality of the estimated deformation within the DELTA-method. The testing is performed using w-tests, like the DIA-procedure that was applied to the original observations. A rejected w-test indicates that the observed deformation of the NAP-benchmark and the modeled deformation of the same benchmark are significantly different. There are several effects that could cause this situation:

– Problems with the geomechanical model

  - The model is not complete and is missing certain effects. For instance, the influence of reservoirs further away may have impact on the subsidence of benchmarks but may not be included in the model.
  - The model is not calibrated with the appropriate data. The selection of benchmarks to calibrate the model was not optimal, resulting in significant differences relative to the NAP-benchmark deformation at other locations.

– Problems with the NAP-data

  - Measurement errors. In the free network adjustment measurement errors were removed from the data as much as possible. However, there will always be a few errors that remain undetected. The very nature of the used B-method of testing means that there is a 20% chance that an observation is falsely accepted as being correct. By adding the data of the geomechanical model as observations, we increase the redundancy of the adjustment problem and thereby increase the detectability of measurement errors. Expert judgement is needed to decide if a rejection stems from the data or from the model.
  - Deep versus shallow subsidence. The working assumption during the first iteration of the adjustment has been that the NAP-benchmarks are placed on buildings with foundations into the Pleistocene sand and that any deep subsidence translates directly into a settlement of the benchmark. However, the foundation of NAP-benchmark locations has never been verified or enforced by Rijkswaterstaat. Rijkswaterstaat recommends placing new benchmarks in objects that are assumed to be stable, but foundations are not checked. Furthermore, founded objects

may not be available (as in rural areas often the case) or not publicly accessible. Consequently, many NAP-points have been placed into small bridges and electricity substations, buildings that often do not have a foundation. Furthermore, it is known that several houses in the region have been built without foundation. As a result, NAP-points may display a deformation that is a combination of both deep and shallow subsidence. These points will subside more than what is computed from the model and therefore can be detected now. These points should be removed as calibration points for the model.

Once all remaining measurement errors have been removed, and no outliers in the model data are detected, a new adjustment is performed. Now, the estimated deformations from this adjustment are the best estimates for the deformations of the benchmarks.

When adding the geomechanical model outcomes as observations, the new adjustment equation looks as follows:

$$\begin{pmatrix} \underline{y}_{1,1} \\ \underline{y}_{1,2} \\ \vdots \\ \underline{y}_{1,n} \\ \underline{y}_{2,1} \\ \underline{y}_{2,2} \\ \vdots \\ \underline{y}_{2,n} \\ \vdots \\ \underline{y}_{k,1} \\ \underline{y}_{k,2} \\ \vdots \\ \underline{y}_{k,n} \\ \underline{m}_1 \\ \vdots \\ \underline{m}_i \end{pmatrix} = \begin{pmatrix} A_1 & & & \\ & A_2 & & \\ & & \ddots & \\ & & & A_k \\ D_1 & D_2 & \dots & D_k \end{pmatrix} x + \underline{e}$$

Here, the zero values of the left side of the deformation equations are now replaced by the modeled deformations as stochastic variables m_1 to m_i for every benchmark with a small standard deviation. No extra parameters in x are needed anymore, so the submatrix D_0 has disappeared. The additional observation equations for modelling the deformation now look like $m_1 = H_{1,1} - H_{1,2} + \underline{e}$. Again, $H_{1,1}$ and $H_{1,2}$ represent the height of point 1 at epoch 1 and 2 respectively.

Inclusion of smaller epochs

So far only epochs with a measured connection to the S-Basis are used in the adjustment. The resolution of the data can be improved both spatially and temporally by including smaller epochs. These stem from measurement campaigns that only cover a small area, sometimes as little as only 3 benchmarks.

Because these epochs do not include the common point in Gasselte, the reference point that was selected in the S-Basis, adding such a network is not trivial. For the computation of the NAP these measurement campaigns are connected to other benchmarks in the NAP network. For campaigns that were also delivered to SodM and NLOG, the benchmark that was used for connecting the networks can be found in the available measurement reports of these campaigns as provided by NLOG. For most other measurement campaigns, the connecting benchmarks are not known.

In the computation of the NAP, it is generally assumed that the connecting benchmarks have remained stationary since the last publication of an NAP height. This is an unjustified assumption for the purpose of this project, as almost all points in the region are subject to subsidence. It is therefore better to include the estimated subsidence in the connection of the networks.

In our approach, for each unconnected epoch, this is an epoch without a measured connection to the S-basis (in the flowchart of Figure 71 these epochs are represented as the epochs k to n), another epoch is searched for, which has common points with the unconnected epoch. We also enforce that this other epoch was measured in approximately the same time frame.

The outcome of this densified network can now be used to recalibrate the model, which is the starting point of the next iteration which allows further improvement of the data.

8.5.3 Deformation results for Annerveen Showcase Region

This section describes the results from the showcase study that was conducted in the Annerveen region, using the DELTA-method as described in section 8.5.2.

Selected epochs

For the Annerveen showcase we have selected a subset of epochs:

Name	Interval	Total selected
NAP measurement campaign North Netherlands	5 years	7
Concession Slochteren	1 to 2 years	10
Concession Groningen	2 to 3 years	5

This amounts to a total of 22 epochs. These 22 epochs contain 93,759 observations, which is about 20% of the total number of observations for the North of the Netherlands.

Detection, Identification and Adaptation of measurement errors

For all epochs in the showcase project, we have performed the DIA-procedure. In total 483 errors have been corrected. For illustration purposes, we describe three situations of errors that were identified and corrected.

Epoch 347W12-NER

In the epoch 347W12-NER, the observations between 015E0086 and 015E0171 (forth and back) are rejected with a w-test of 722.270 (it should be below 3.29). The location of these two observations is shown with red arrows in Figure 72

Figure 72. Location of two rejected observations (red) between 015E0086 and 015E0171.

Inspection by a specialist shows that the rejection is due to a typographical error in the height difference. The two observations are:

- 015E0086 -> 015E0171: height difference is 0.8111 m (09/01/1993)
- 015E0171 -> 015E0086: height difference is 0.8100 m (09/01/1993)

One of these two observations should be negative. Based on analysis of the environment we have corrected the measurement from 015E0171 -> 015E0086 and changed it to -0.8100 m. After this adaptation, the observation is accepted by the w-test.

Epoch 199W64

In the project 199W64, there is a set of two observations between 012F0146 and 012E0040. This observation contains a typographical error because the map distance deviates from the written distance. The observation as registered by the surveyors is shown in Figure 73 as the long line across the map.

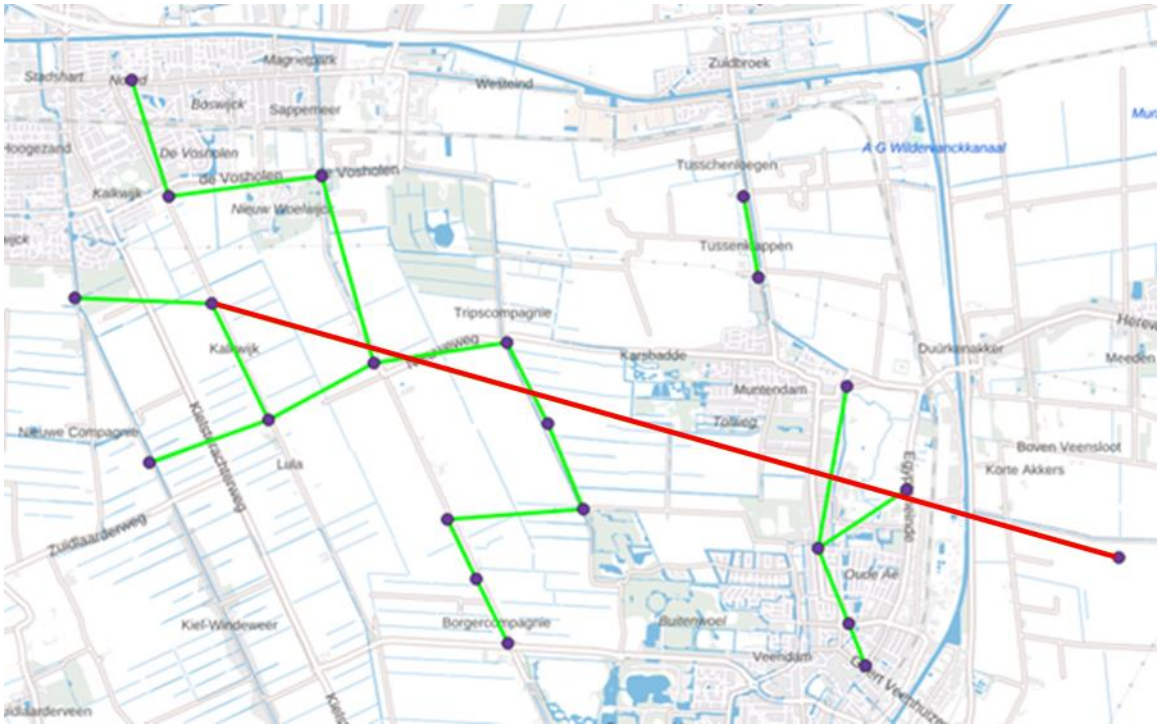

Figure 73. Map with observed height differences, one of them most likely connecting two wrong benchmarks (line in red).

The registered distance between the benchmarks was 1321 meters, while the distance on the map is 10115 meters. Through an examination of the benchmark locations, it was deduced that the E in 012E0040 is the typographical error. The correct benchmark name should have been 012F0040. After correction of the benchmark number, the distance on the map is like the distance registered by the surveyor.

Epoch 382=153

This epoch contains a set of four observations between the benchmarks 003D0143, 003C0141 and 003D0021. When plotting these observations on a map, as shown in Figure 74, they display an unlikely pattern. The survey starts from the right with small steps but then makes a large leap to a point on the left, only to return in the next step. It was not possible to discover a likely typographical error. Hence, the observation to benchmark 003C0141 was renamed, such that it connects to a temporary virtual benchmark. This allows for the completion of the calculations but renders this benchmark useless for the deformation analysis.

Figure 74. Observations in epoch 382=153 showing an unlikely path.

Deformation adjustment

The outcome of the deformation adjustment is a set of deformation values for every benchmark, including the estimated precision of the deformation. The result is a time series per benchmark. Figure 75 shows the estimated deformations of the benchmarks relative to the year 1972 for two different years: 1992 and 2012. Note that the area covered is much larger than Annerveen. As the entire Annerveen area is subsiding, we had to extend the network to outside the region. To successfully adjust the levelling networks, we have included all observations within the epoch. Consequently, the area outside Annerveen is also included, albeit with a lower temporal and spatial resolution.

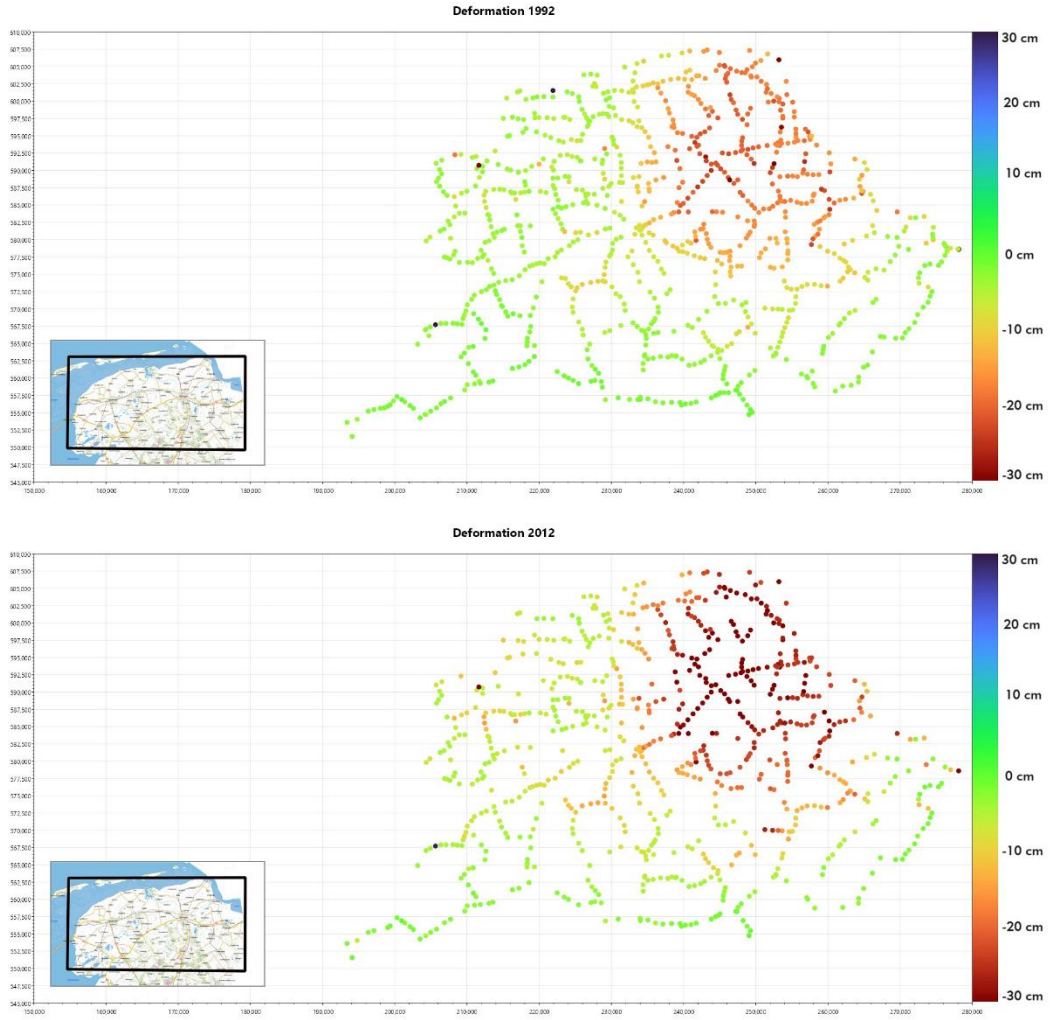

Figure 75. The estimated deformations relative to 1972 in 1992 and in 2021.

From Figure 75 it is visible that some points present a deformation of more than 10 centimeters while neighboring points do not show any deformation. **This shows that even after careful testing of the data for measurement errors, outliers may still be present in the outcomes.** This could be due to measurement errors and locally distorted benchmarks.

This is the reason why the testing against a geomechanical model, as performed in the DELTA-method, helps to further improve the result.

The precision of the estimated deformations is computed through error propagation of the a priori standard deviations. The precision is around 4 mm for most deformations, with spikes up to 8 mm. Figure 76 shows a histogram of the precision of all deformations.

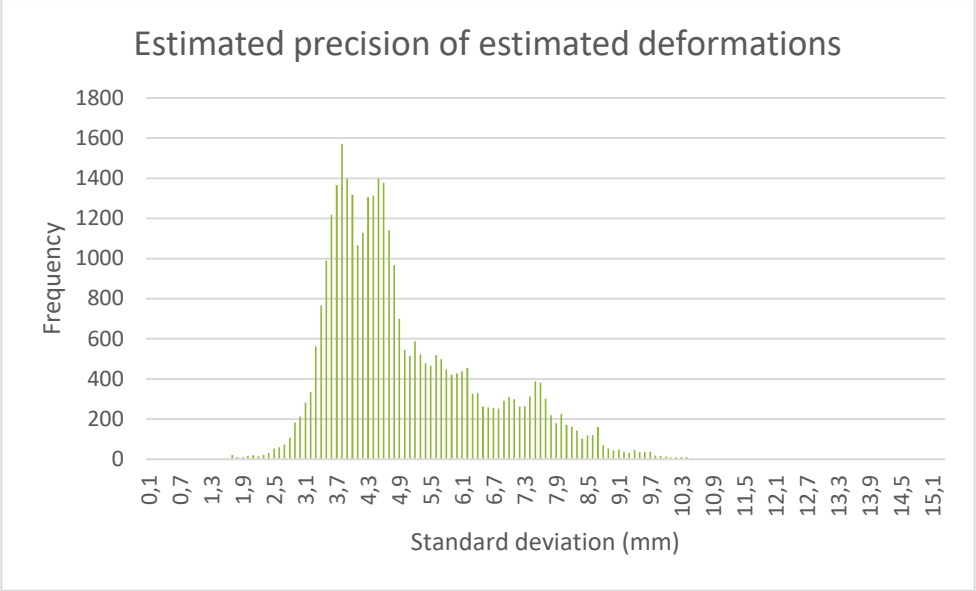

Figure 76. Histogram of deformation precisions

Model output integration

The output of the geomechanical model can be used to test the deformations that were estimated from the NAP-data. In most cases the data from the adjustment and the geomechanical model align very well, as can be seen in Figure 77 for benchmark 012E0002. The blue line shows the outcome of the deformation adjustment before inclusion of the geomechanical model in the adjustment. The sudden uplift in 1998 in the data is remarkable and leads to a rejection of the observation in the combined adjustment, reason for further analysis on what effects are at play in that year. It could be some residual measurement error or a wrongly recorded date. However, this movement can also stem from small effects that are not included in the model yet. Note that the model and the observations are no longer independent due to the integrated approach in the DELTA-method.

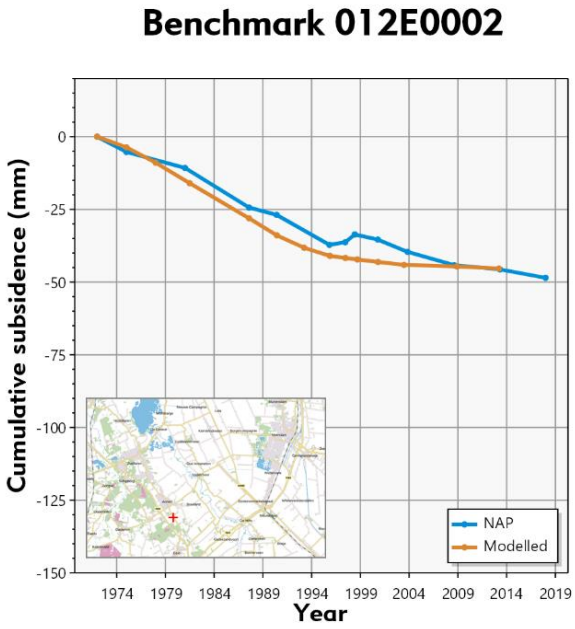

Figure 77. Deformation as estimated from the measurement data and as modelled.

As described in section 8.4.1 about the reservoir modelling, the effects of salt mining are not yet included in the model. Consequently, a further subsidence, probably due to salt extraction, since 1997

is visible in the observed data but not in the geomechanical model. This is for instance very clearly visible at benchmark 012E0012 as shown in Figure 78.

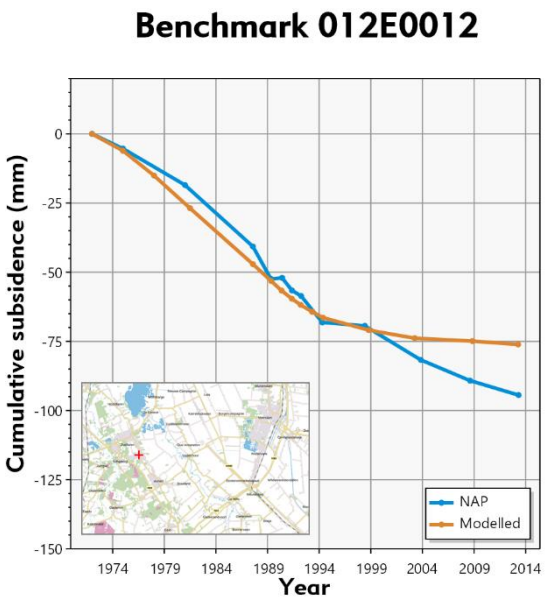

Figure 78. Deformations as estimated for 012E0012

The strongest rejection when testing the observations in combination with the geomechanical model occurs at benchmark 012E0124 with a w-test of 37 while the critical value is 3.29. Figure 79 shows the time series for this benchmark for both the NAP data and the geomechanical model. Further analysis of this benchmark reveals that this benchmark was placed on a culvert. This culvert was in an area with peat soil and therefore not founded on Pleistocene sands. The benchmark is therefore not representative of deep subsidence. Hence, this point should be discarded for analysis of deep subsidence.

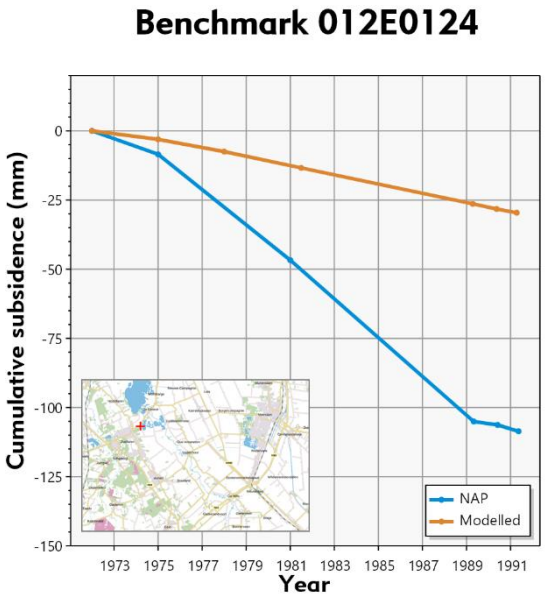

Figure 79. Deformations as estimated for 012E0124

Another strong rejection occurs at benchmark 012E0019, as shown in Figure 80. Here it is clearly visible that the NAP-data showcases a much stronger deformation than what is expected from the model. The hypothesis is that this represents a point where both shallow subsidence as well as deep subsidence play a role. To investigate the situation at this point, we have reviewed the images of this

point, of which Figure 81 is an example. Further analysis shows that the building has been demolished in 2009. The nearby point of 012E0160 does correctly follow the geomechanical model. This gives further reason to suspect that this building was not stable and therefore this benchmark was not a good representative for deep subsidence. Consequently, this benchmark should not be used for deformation analysis of deep subsidence and for the calibration of the geomechanical model.

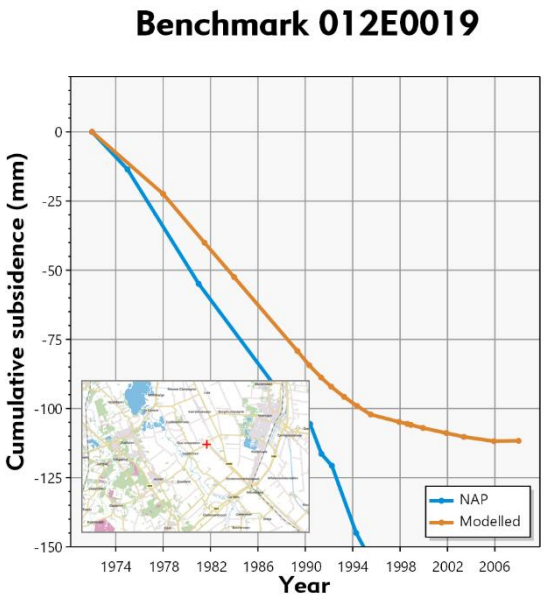

Figure 80. Deformations as estimated for 012E0019

Figure 81. Picture of point 012E0019 in 1958 (source: Rijkswaterstaat)

The current showcase has shown that it is possible to use NAP-data for large scale deformation analysis. The known problems with NAP, such as the revision in 2005 and the presence of measurement errors has been overcome by using only the original observation data. The uncertainty about deep and shallow subsidence has been addressed by comparing the NAP-data with the results from the geomechanical model.

The great benefit of using NAP-data is that it allows for historical analysis, all the way back to 1923. For the showcase we have used data starting from 1972. In the last two decades InSAR has become a viable option for subsidence analysis as well. In this showcase we did use InSAR data for selection of the S-Basis but did not include it in the deformation analysis. In Phase II a comparison will be made between the deformation adjustment and the InSAR data in the European Ground Monitoring Service

(EGMS). Additionally, the solution could benefit from the inclusion of permanent GNSS-observations. These were not included in the Annerveen showcase but could be included in the full computation. In this case it is important to note that InSAR and GNSS data use different reference systems that may affect estimated subsidence rates (Van der Marel, 2020).

.

9

RECOMMENDATIONS FOR FURTHER STUDY IN PHASE II

9.1 Introduction

This chapter gives an answer to the following research question as defined in section 1.4.1

4. What can be studied in more detail in Phase II for the Grijpskerk area?

This chapter describes the recommendations for further study in Phase II. In Phase I of this study, we have described the relevant processes leading to subsidence and seismicity. We have demonstrated feasibility for a new approach for calibrating multiple compaction sources based on differential height measurements. Applying this approach to the Grijpskerk area will be a main element of the phase II study (described in section 9.2 to 9.8). Additionally, topics identified during the literature study, the bicycle field tour (31-10-2023), the meetings with the guidance group and the HAZID-like session (on 22-01-2024) that could deserve (more) attention will be addressed in Phase II.

The literature review has indicated that the impact of anelastic reservoir compaction has not sufficiently been accounted for in previous geomechanical studies of seismicity induced by gas storage (section 3.7). This aspect will be addressed in Phase II.

Furthermore, consultation of inhabitants of the Grijpskerk area revealed several aspects that will be further investigated in Phase II. These include:

- Discrepancies in published data, i.e. between production data UGS Grijpskerk published on NLOG and European gas productions data. What is the impact of using different sources of information?
- Identified damage to buildings due to surface deformation.
- Felt vibrations which are not associated with earthquakes reported by the KNMI.
- Presence of a potentially leaking well (ID: GRK-43).

Additional aspects were identified in the HAZID-like session (Table 7, Table 8). In Phase II, these will be addressed in a qualitative manner. If knowledge gaps are identified, recommendations for further study will be made.

Table 7. Outcome of the HAZID-like session: an overview of the processes that have not been addressed in the Phase I literature study

Process	Concern	Addressed in phase II?
1. Swelling and shrinkage of deeper (over) consolidated clays such as Pot Clay	Widespread subsidence and heave patterns observed across the Netherlands are hypothesized to be linked to the shrinkage and swelling of deep consolidated clays.	Yes
2. Liquid loading	Concerns the accumulation of the liquid phase within gas wells and the nearby reservoir. The concern is that the accumulated liquids can result in dissolution of the Zechstein salts, reducing its sealing capacity.	Yes

Process	Concern	Addressed in phase II?
3. Salt creep in the Zechstein formation	Local thinning of the seal formation because of the creation of salt diapirs? Can the salt movement create/trigger movement in the faults above? (See also interaction item 3. Below.	Yes
4. Hydrogen storage	Status quo is that current reservoirs and wells are not useable for hydrogen storage because hydrogen gas corrodes certain steels, leading to well integrity failure. Hence new storage sites that are specifically designed for storing and transporting hydrogen gas need to be created, whereby salt deposits are deemed to be the ideal storage site, e.g. pilot at Zuidwending. It is also expected that in the future, if green hydrogen can be produced in large quantities, the Zechstein salts won't provide sufficient storage and traditional UGS might become relevant again.	No – beyond scope

Table 8. Outcome of the HAZID-like session: an overview of the interactions that have not been addressed in the Phase I literature study.

Interactions	Concern	Addressed in phase II?
1. Interaction between different subsidence/heave processes	When multiple subsidence/heave processes occur simultaneously within the subsurface, they could locally affect the subsidence curvatures near the ground surface. Think of the UGS and swelling/shrinking of both deeper consolidated clays and shallow clays.	Yes
2. Impact of gas storage/extraction on shallow fault movement	Faults have been identified and must be present above the Zechstein salt. It is not clear how far they extend. Can movement in the underlying reservoirs and UGS trigger movement in the shallower faults? And if so, what could be the impact at the surface? Can it create seismicity?	Yes
3. In what order of magnitude is deep subsidence irregular	These irregularities might affect the subsidence curvature near the surface. Effect of subsurface heterogeneity is investigated in the KEM-47 report.	No – beyond scope
4. Interference/amplification of different vibration sources within the subsurface	The concern is that vibrations of different sources can amplify each other by interference and reflection.	Yes
5. The extraction of cushion gas on subsidence/induced seismicity	Cushion gas is the gas that needs to be present within a reservoir to maintain adequate pressure that is needed for gas production. The fear is that the extraction of this gas before abandonment poses an augmented risk for subsidence and induced seismicity events.	Yes

9.2 Workflow geodetic and InSAR data

The novel approach of using the raw observations from the NAP dataset to construct changes in height differences (chapter 8) is a unique and a geodetically correct way to get high quality historical data. The vectors with height changes from NAP and the deformation trends from InSAR (EGMS) form the data to calibrate the model.

Importantly, the deeply founded benchmarks in the NAP data set are not subjected to shallow subsidence. Therefore, the NAP data set can be used for matching the cumulative effect of deep sources for subsidence.

However, as the historical data was never intended for this application, it requires specific processing as discussed in chapter 8. A process, like a forensic investigator-based statistics is needed. If all

observations but a few fit with the model, these observations should be reviewed and eventually rejected (compare chapter 8). But the fact that they are rejected is information in-itself. This information should be used to assess whether this is likely to be a measurement error, or whether this cluster hints at an unparametrized effect in the model. We intend to show which observations are used and which observations are rejected in our result. We are convinced that by demonstrating the way the model and the observations fit together, we can expect to increase the confidence in the computed results by all stakeholders. Ultimately, a sound analysis and interpretation of observations with the help of models helps to explain the deep subsidence since the start of natural gas extraction more than 60 years ago.

The feasibility analysis for employing geodetic and InSAR data in Phase II modelling hinges on several pivotal factors, all of which align favourably. Firstly, the availability of necessary data has been confirmed, ensuring a solid foundation for the project. Additionally, the presence of specialists within our network provides a substantial resource for technical expertise and guidance. The existence of previous reports on similar analyses offers a valuable reference point, enabling us to learn from past experiences and refine our approach. The crucial determinants of proceeding with the computations will be the efficiency and effectiveness of the process. These factors will be rigorously evaluated to ensure that the utilization of these data and tools aligns with the project's goals and resource constraints. This thorough preparation positions us well to leverage geodetic and InSAR data effectively in our modelling efforts.

As part of the feasibility study, we have also confirmed the availability of all relevant data, i.e.: NAP data, production, and reservoir data of geotechnical facilities in the wider vicinity of Grijpskerk.

9.3 Workflow seismicity observations

Subsurface activities can cause seismicity, and the occurrence of an earthquake is evidence for critical stress conditions at a particular location and time. Thus, induced earthquakes can provide constraints on geomechanical models, which need to reproduce earthquake failure conditions at the observed locations and times.

A clear association between an earthquake and a particular subsurface activity, however, may not always be possible due to earthquake location errors. In order to compare observed earthquakes and model predictions of this study, we will follow the approach of KEM-07 (Vörös & Baisch, 2018): we will update the classification scheme of KEM-07 (Figure 15), which accounts for the uncertainty in earthquake association. Subsequently we will investigate whether each observed earthquake in the Grijpskerk area (using the most recent catalogue of the KNMI) can be explained by stress changes caused by subsurface activities. For the latter step we will use the geomechanical models of KEM-07, which need to be extended for several gas fields that were previously excluded.

Following the consultation of inhabitants of the Grijpskerk area, we will also investigate reported cases of felt vibrations, which are not associated with earthquakes in the KNMI catalogue. Based on published estimates of the magnitude of completeness (Ruigrok et al., 2023) we will discuss the probability that a felt earthquake is not detected by the KNMI.

9.4 Workflow ultrasonic and low frequency noise vibrations

The literature review concluded that permanent changes in the soil structure due to vibrational-induced compaction is possible for well-known processes such as pile driving and vibratory sheet pile driving. Additionally, it was determined that compaction from traffic vibrations is only possible under extreme conditions, such as a bulldozer on very poor road surface. The area of influence remains limited to 10 meters.

Local stakeholders have urged the consortium to investigate the risk of vibration induced compaction stemming from the gas transport system, such as gas flow through pipelines and gas compressor

systems. While referencing a case in China where abnormal vibrations capable of inducing local compaction of loose sands were observed and modelled, it's important to note that these vibrations also pose a risk to the pipeline transport system and can be addressed through appropriate design and construction measures. Based on the assumption of proper usage of gas transport systems, we can reasonably conclude that gas infrastructure is unlikely to cause vibration-induced compaction. Low frequency noise could cause nuisance to people living in the vicinity of the gas infrastructure.

Given these conclusions and considering the scope of this study we believe that a further investigation in Phase 2 is unnecessary. The findings in the literature review will be considered when assessing the cumulative effects with vibrations caused by induced seismicity.

9.5 Workflow impact of salinization and future sea-level rise

Saltwater intrusion into freshwater systems occurs due to changes in the hydraulic gradient between the saltwater and freshwater systems. A prime example is the relative sea levels rise near coastal regions, which can be accelerated by subsidence events near coastal regions.

To assess the risks of mining-induced land subsidence on horizontal seawater intrusion, we examine the vertical extent of subsidence along the coastline and its implications for local changes in hydraulic head.

Regarding vertical seawater intrusion through seepage, we consider the position of the freshwater-saltwater interface in conjunction with the local geological composition and the impact of subsidence on this interface.

9.6 Workflow impact on water-holding capacity of water supply aquifers

The effect of subsidence and seismic events on the water holding capacity of water supply aquifers is supposed to be very small. The change in water holding capacity (expressed as $V_{\%}$) is the ratio between the compacted aquifer resulting from subsidence or seismic events, and the original aquifer depth ($D_{aquifer}$):

$$V_{\%} = 1 - \frac{(D_{aquifer} - Subsidence)}{D_{aquifer}}$$

Considering that water supply aquifers in the project area are located in deep Pleistocene sands that are already well compacted, their susceptibility to further compaction and vibration-induced cyclic loading is very low, typically in the millimetre to centimetre scale. Moreover, since the depth of the confining aquifers in the project area ranges in the order of meters, the resulting change in water storage capacity is limited to a few percent. Therefore, any impact on water storage capacity is expected to be negligible and unlikely to be noticeable in the field.

9.7 Workflow methane leakage

To assess methane leakage, borehole records within the project area are examined for potential indicators of suspicious conditions related to methane leaks. Indication of enhanced risks on methane leakage include age of gas wells, issues with installation or sealing (e.g., fugitive gas), and indications of an active water drive during production. The results will be summarized and reported in a table-like manner.

In case the workflow for modelling deep subsidence suggests the existence of depleting aquifers within the case study area, for example when deep subsidence is measured that cannot be explained by the gas field production. A conceptual model will be developed outlining key considerations regarding the expected aquifer pressure redistribution after abandonment of the gas fields around Grijpskerk in a schematic manner.

9.8 Modelling strategies

The study employs a systematic approach, starting with simple numerical models and increasing complexity as needed to match observations. Models focus on the Grijpskerk Underground Gas Storage, using a data-driven modelling strategy. The goal is to understand the impact of subsurface activities on deformation and seismicity. For shallow subsidence modelling, the impact of deep subsidence on the shallow hydrogeological system is examined by identifying the differential subsidence between water-level controlling objects such as weirs and pumping stations. The associated changes in the groundwater system are tested for different soil types to assess the risk of shallow subsidence on the environment.

9.8.1 Strategy for deep modelling

Our working method is to start with minimum complexity numerical models and attempt to match first order observations. Model complexity is introduced only if required by observation data. In the first step, we will simulate compaction induced strain as described in section 8.4.

A focus of this study is on the Grijpskerk UGS. As outlined in section 3.7, numerical models developed in previous KEM projects cannot explain observed earthquake occurrence at an early stage of storage operations. We speculate that non-elastic (irreversible) reservoir compaction might be a dominating process that needs to be accounted for simulating stresses during re-fill. If required by observation data (e.g., if observed subsidence and heave cannot be matched with a constant compaction coefficient), we will implement the Grijpskerk UGS as a 3D hydro-mechanical model utilizing the Comsol Multiphysics Finite-Element modelling suite. The focus will be on first-order effects using a geometrically simple model. Single-phase flow will be modelled, and the irreversible loss of pore space will be mimicked by reducing the effective reservoir height through a moving boundary condition.

We will follow a data-driven approach where the exact combination of modelling elements (modules and type of implementation) will be defined during the project. Although this is not very likely scenario, we will also consider the possibility (based on spatio-temporal correlation analysis) that observed earthquakes may result from local (space, time) stress perturbations such as hydraulic fracturing.

The superposition of strain and stress resulting from different modules will be compared to observation data (subsidence, earthquakes) for history matching. The matching procedure will be operated in a systematic way, starting when the first subsurface activity went online. The isolated signal of the first subsurface activity will be used for history matching the associated numerical module. In chronological order, subsequent modules will be history matched while accounting for the contribution of the previously “calibrated” modules. By this we attempt to determine the individual contributions of subsurface activities to the cumulative observation signal. We expect significant scattering of observational data due to near-surface processes that are not captured by our numerical models. This might require fitting trends of different length scale, informed by a modelled subsidence signature.

The main output will be a minimum complexity numerical model that best fits the observation data. The model will be used for making a prognosis of future deformation.

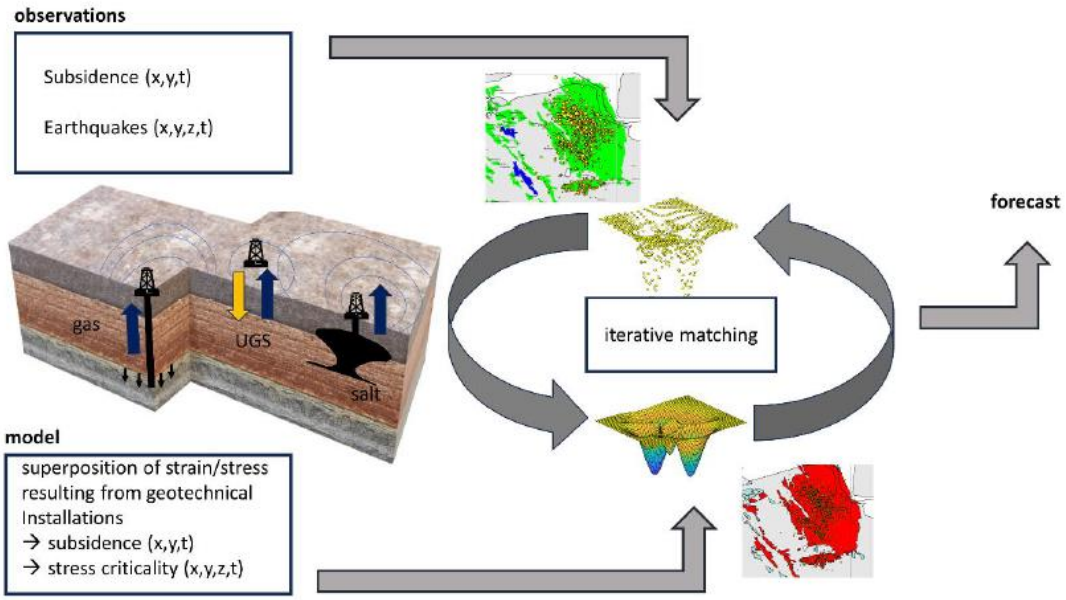

* The numerical model consists of several independent elements ("modules") representing different subsurface activities (gas fields, UGS, salt mines). The matching procedure will be operated in a forensic way, starting when the first subsurface activity went online. The isolated signal of the first subsurface activity will be used for history matching the associated numerical module. In chronological order, subsequent modules will be history matched while accounting for the contribution of the previously "calibrated" modules.

Figure 82. Sketch showing the workflow of the new approach.

9.8.2 Strategy for mining induced shallow modelling

To model mining induced shallow subsidence, we first model the effects of deep subsidence on the shallow hydrogeological system using a subsurface and groundwater model. The subsurface model is GeoTop (DINOloket, 2023), which is the best subsurface model publicly available in the region and is continuously improved. The GeoTop model has 100 equally probable realizations that can help to assess uncertainty around the spatial variability of soil types.

The groundwater model will be constructed based on the output of the deep subsidence model (section 8.4.1), providing us detailed subsidence contour levels that will be used to determine the differential subsidence between water-controlling objects such as weirs and pumping stations. The impact on the drainage depth in the surrounding watercourses is directly proportional to the differential subsidence between the concerning watercourse and the weir/pumping station downstream. Conservatively, the effect on the groundwater table between the watercourses will be linearly interpolated between the watercourses whereby the impact of local stratigraphy will be considered by means of impact factors provided by the KEM-16, (2023) study.

This workflow is highly sensitive to the spatial water management configuration. Given the absence of a comprehensive dataset on the spatial changes in water management since the start of the gas extraction, the most effective approach is to examine the current drainage configuration. Typically, land consolidation has resulted in larger parcels and fewer water-controlling objects, rendering the current situation most sensitive to the indirect effects of deep subsidence.

The resulting subsurface and groundwater models will provide a comprehensive overview of the expected lithology and groundwater lowering as a result of deep mining induced subsidence. Based on this data set, we assess the risk on environmental effects based on differential water levels and soil types.

9.9 Workflow effect of mining induced subsidence on local infrastructure

The effects of mining activities on both deep and shallow subsidence will be addressed on a regional scale. Given the large spatial discretization of the available shallow subsurface models (GeoTop, 100 x 100m), addressing individual damage cases will not be feasible as local variabilities in the soil stratigraphy are typically not captured by the model. When ignoring these small-scale influences, the risk of damage from shallow, mining induced subsidence may be underestimated. Furthermore, specific information regarding the condition of the local infrastructure and property-specific details such as foundation type and condition are not available.

Instead, our focus will be on identifying high-risk areas based on the absolute subsidence potential of different lithoclasses influenced by the modelled groundwater level changes (section 9.8.2). We will qualitatively consider the local subsurface variability using our knowledge of local geology, geomorphology, and land use.

Since local variations in the shallow subsurface do not impact the assessment of deep subsidence effects, we can evaluate the damage likelihood of deep subsidence by calculating the angular distortion and horizontal strain using the Limited Tensile Strain Method (LTSM). These results will then be incorporated into the analysis on the cumulative effects of deep and shallow subsidence.

Finally, the identified risks of mining induced damage will be placed in the context of non-mining-related processes occurring in the region. This will allow us to gain deeper understanding of the correlation and causality between observed damage and mining-related activities.

10

ABBREVATIONS AND TERMINOLOGY

10.1 Abbreviations

- CM: Commissie Mijnbouwschade (Committee Mining damage) This committee assesses damage due to gas extraction in The Netherlands outside Groningen field, UGS Norg and UGS Grijpskerk and damage due to salt mining in The Netherlands.
- Deep subsidence: surface movement due to oil- and gas extraction, gas storage and salt solution mining.
- GNSS: Global Navigation Satellite System. It is a generic term used to refer to a constellation of satellites that provide global positioning and navigation services.
- GPS: Global Positioning System. This is a specific type of GNSS developed and operated by the United States government.
- IMG: Institute Mijnbouwschade Groningen. Organisation that provides compensation and assessed damage due to gas extraction and storage from the Groningen field, UGS Norg and UGS Grijpskerk.
- InSAR: Interferometric Synthetic Aperture Radar. It is a remote sensing technique used to measure ground surface movements.
- NAP: Nieuw Amsterdams Peil: Netherlands national geodetic datum for elevation measurement. The NAP is considered the average sea level at low tide in the IJ near Amsterdam. It serves as a fixed elevation reference for geodetic measurements and mapping in the Netherlands.
- SodM: State Supervision of Mines/Staatstoezicht op de Mijnen
- Tcbb: Technische commissie bodembeweging
- UGS: Underground Gas Storage

10.2 Terminology

- Aquitard: An aquitard is a layer of rock or soil that restricts the flow of groundwater because it has low permeability. It acts as a barrier between aquifers or between aquifers and surface water bodies.
- *Borg*: historical, fortified dwelling or mansion in Groningen Province. Similar to the concept of a castle or manor house, a borg is a stately residence that often has defensive features and may be associated with the local nobility or affluent landowners.
- Confined aquifer: A confined aquifer is a groundwater system where water is trapped between impermeable layers, creating pressure. Wells drilled into these aquifers can cause water to rise above the ground level due to this pressure.
- Freeboard (NL: *Drooglegging*): A key factor in determining suitable surface water levels is the concept of freeboard: it refers to the area in the subsurface between ground level and the water levels in the surrounding watercourses.
- *Gast*: a natural sand ridge or elevation in the landscape formed during the last glacial period.

- *Heemschar*: areas of common land that were traditionally used for communal grazing of livestock or other shared purposes.
- Hemrik: see Heemschar.
- Induced seismicity: earthquakes caused by movement along faults in reservoir rock due to gas extraction, water injection or other changes in the geomechanical stress regime.
- *Keileem*: till or boulder clay. *Keileem* is a type of glacial till, a sedimentary material that is deposited directly by a glacier. It is characterized by a mixture of clay, silt, sand, and a significant number of unsorted rocks and boulders, which are often embedded in the fine-grained loamy matrix.
- Knikklei or Knipklei: clay soil that exhibits a tendency to crack or split upon drying, typical for salt marsh soils.
- Megaflute: A 'flute' is a narrow ridge formed by the movement of a glacier, composed of sand, till, and debris. Resembling flutes when viewed from above, they align parallel to the glacier's flow direction. Multiple flutes can form in parallel, with larger ones spanning several kilometers, called megaflutes, ranging from centimeters to tens of meters in height. The Hondsrug feature is well-known example of a megaflute.
- Old marine clay polders (NL: *Oude zeekleipolders*): formed by diking inhabited salt marsh areas.
- *Peilbesluit*: water level adjustment decision, i.e. an optimal surface level configuration, which is legally validated. Important to point out is that a *peilbesluit* is not an obligation of result, but rather an obligation of effort. Natural conditions may necessitate (temporary) deviations from the norm.
- Phreatic aquifer: A phreatic aquifer, also known as an unconfined aquifer, lacks confining layers. Water in this type of aquifer moves freely and is not under pressure. The water table, the upper surface of the saturated zone, fluctuates depending on factors like precipitation and groundwater extraction.
- *Polder*: An area protected by a water barrier from external water, allowing for controlled water levels within. (Definition from the water boards)
- *Ruilverkaveling*: land consolidation or land reallotment: a process where land holdings are rearranged and reorganised to obtain larger parcels that are more efficient to manage primarily from an agricultural perspective, but also from a water management point of view.
- Salt marsh (NL: *Kwelder*): Inhabitable vegetated outer dike area (land) that remains above water during average high tides.
- Salt marsh ridges (NL: *Kwelderwallen*): elevated sections of the salt marsh where coarser materials are deposited during floods. Many village belts are built on salt marsh ridges, often used for agriculture due to the easier soil cultivation compared to more clayey areas.
- Shallow subsidence: surface movement due to consolidation of shallow soil layers, peat oxidation and swelling and shrinking of clay. Shallow subsidence is mostly driven by changes in the shallow groundwater regime.
- Small gas fields: these are gas reservoirs that are not part of the large Groningen field. The term small is not good denominator but needs to be viewed in comparison to the size of the Groningen gas field.
- *State*: historical, fortified dwelling or mansion in Fryslân Province. Similar to the concept of a castle or manor house, a borg is a stately residence that often has defensive features and may be associated with the local nobility or affluent landowners.
- *Stinsen/stinswieren*: A medieval fortified house or defensive tower built to protect residents from hostile invasions. *Stinswier* is the artificial dwelling mound on which the structure is built.
- *Terp*: Frisian term for an artificial (dwelling) mound used as a refuge for residents during spring tides or floods.
- Tidal flat (NL: *wadden/wadplaten*): Uninhabitable intertidal area (sea), without vegetation, consisting of sandy areas interchanged with soft clay deposits.
- Unconventional reservoir: Unconventional reservoirs are characterized by low permeability and often require special extraction techniques like fracking to recover hydrocarbons effectively. Shale gas reservoir are typical unconventional reservoirs.

- *Wierde*: Groningen term for an artificial (dwelling) mound used as a refuge for residents during spring tides or floods.
- Young marine clay polders (NL: Jonge zeekleipolders): formed by embanking sea incursions and new land reclamation.

11

REFERENCES

11.1 Literature references

A'Campo, Y. W. L., Baisch, S., Buter, E., Slob, S., Laenen, B., Besseling, F., & Boter, E. L. (2020). *Risk assessment for UDG and EGS and an inventory of preventive and mitigating measures* (Final report project KEM-06 No. 105911/20–005.135) (p. 142). Witteveen+Bos. Retrieved from https://kemprogramma.nl/file/download/57979640/kem-06-report-on-risk-assessment-udg-and-egs-rewrite-1-0.PDF

ACSG, (2019). Het invloedsgebied van grondwateronttrekkingen voor droogteschade.

Aki, K., & Richards, P. (2002). Quantitative Seismology, 2nd Ed.

Alberda, J.E., Ebbinge, J.B., 2006, Inleiding landmeetkunde, VSSD, Delft.

Allan, R. P., & Soden, B. J. (2008). Atmospheric warming and the amplification of precipitation extremes. Science, 321(5895), 1481-1484.

Allison, M., Yuill, B., Törnqvist, T., Amelung, F., Dixon, T. H., Erkens, G., et al. (2016). Global risks and research priorities for coastal subsidence. Eos, 97, 22–27. https://doi.org/10.1029/2016EO055013

Ambraseys, N.N. (1988). Engineering seismology, Earthquake Engineering & Structural Dynamics 17, 1-105.

Asselen, S. van, H. Kooi, J.J.H. van den Akker (2020), *STOWA Deltafact Bodemdaling*, versie 3.1

Athanasopoulos, G. A., & Pelekis, P. C. (2000). Ground vibrations from sheetpile driving in urban environment: measurements, analysis and effects on buildings and occupants. Soil dynamics and earthquake engineering, 19(5), 371-387.

Auersch, L. (2005). The excitation of ground vibration by rail traffic: theory of vehicle–track–soil interaction and measurements on high-speed lines. Journal of Sound and Vibration, 284(1-2), 103-132.

Aveco de Bondt. (2023) Aanvullend onderzoek drinkwaterwinning Hammerflier e.o. Referentie: 223320_AdB_RAP_0001_AVG.

Baarda, W. 1973. S-transformations and Criterion Matrices. Publications on Geodesy New Series, vol. 5, no 1. Netherlands Geodetic Commission.

Babaryka, A., & Benndorf, J. (2023). Ground Subsidence above Salt Caverns for Energy Storage: A Comparison of Prediction Methods with Emphasis on Convergence and Asymmetry. Mining, 3(2), 334–346. https://doi.org/10.3390/mining3020020

Baisch, S., Carbon, D., Dannwolf, U., Delacou, B., Devaux, M., Dunand, F., et al. (2009). Deep Heat Mining Basel - Seismic Risk Analysis (p. 553). SERIANEX study prepared for the Departement für Wirtschaft, Soziales und Umwelt des Kantons Basel-Stadt, Amt für Umwelt und Energie. Retrieved from http://www.wsu.bs.ch/geothermie

Baisch, S., Rothert, E., Stang, H., Vörös, R., Koch, C., & McMahon, A. (2015). Continued Geothermal Reservoir Stimulation Experiments in the Cooper Basin (Australia). Bulletin of the Seismological Society of America, 105(1), 198–209. https://doi.org/10.1785/0120140208

Baisch, S., Seidemann, M., Vörös, R., & Bartels, T. (2023). Numerical Simulation of Seismicity Induced by Gas Production - Implications for the Seismic Hazard Assessment. Journal of Geophysical Research: Solid Earth, 128(9), 16. https://doi.org/10.1029/2023JB027025

Baisch, S., Vörös, R., Carstens, P., Koch, C., Stang, H., & Rothert, E. (2021). *Induzierte Seismizität bei der Gewinnung von Kohlenwasserstoffen aus unkonventionellen Lagerstätten* (p. 204). Berlin: Report for the Expert Commission on Fracking (German Federal Ministry of Education and Research). Retrieved from https://expkom-fracking-whg.de/lw_resource/datapool/systemfiles/elements/files/BF72FB64A7EC14E8E0537E695E862A2F/live/document/2021_Studie_induzierteSeismizitaet.pdf

Baisch, S., Weidler, R., Vörös, R., Wyborn, D., & de Graaf, L. (2006). Induced Seismicity during the Stimulation of a Geothermal HFR Reservoir in the Cooper Basin, Australia. Bulletin of the Seismological Society of America, 96(6), 2242–2256. https://doi.org/10.1785/0120050255

Baisch, Seidemann, Vörös, Bartels: Numerical simulation of seismicity induced by gas production – implications for the seismic hazard assessment. Submitted to Jour. Geophys. Res.

Bakker, J.W. van den Akker, J J.H., Cornelissen, P., Boels, D. (1995). Oorzaak en preventie van schade aan wegen door vochtonttrekking door bomen, DLO Staring Centrum, rapport 318, ISSN 0927-4499.

Barciela Rial, M. (2019). Consolidation and drying of slurries: A building with nature study for the Marker Wadden (Doctoral dissertation). TU Delft. https://doi.org/10.4233/uuid:ae11c3e7-86f2-4c6a-8d53-ee8781d56a72

Barends, S. (2010). Het Nederlandse landschap: een historisch-geografische benadering. Utrecht. Matrijs.

Barkan, D. (1962). Dynamics of bases and foundations. New York: McGraw-Hill Book Cy Inc. (original publication in Russian 1948)

Barlet-Gouedard, V., Rimmele, G., Goffe, B., & Porcherie, O. (2006). Mitigation strategies for the risk of CO2 migration through wellbores. In IADC/SPE drilling conference. OnePetro.

Bartholomeus, R. P., van der Wiel, K., van Loon, A. F., van Huijgevoort, M. H., van Vliet, M. T., Mens, M., .& Pot, W. (2023). Managing water across the flood–drought spectrum: Experiences from and challenges for the Netherlands. Cambridge Prisms: Water, 1, e2.

Bear, J. (2012). Hydraulics of groundwater. Courier Corporation.

Bear, J., & Corapcioglu, M. Y. (1981). Mathematical model for regional land subsidence due to pumping: 2. Integrated aquifer subsidence equations for vertical and horizontal displacements. Water Resources Research, 17(4), 947-958.

Békési, E., Fokker, P. A., Martins, J. E., Limberger, J., Bonté, D., & Van Wees, J. D. (2019). Production-induced subsidence at the Los Humeros geothermal field inferred from PS-InSAR. Geofluids, 2019.

Benson, C. H., & Trast, J. M. (1995). Hydraulic conductivity of thirteen compacted clays. Clays and clay minerals, 43, 669-681.

Bhunia, G. S., Chatterjee, U., & Shit, P. K. (2021). Emergence and challenges of land reclamation: Issues and prospect. Modern Cartography Series, 10, 1-15.

Birkholzer, J. T., Zhou, Q., & Tsang, C. F. (2009). Large-scale impact of CO2 storage in deep saline aquifers: A sensitivity study on pressure response in stratified systems. international journal of greenhouse gas control, 3(2), 181-194.

Bishop, A. W. (1969). Creep characteristics of two undisturbed clays. Proc. 7th ICSMFE, Mexico City, 1969, 1, 29-37.

Bjerrum, L. (1967). Engineering geology of Norwegian normally-consolidated marine clays as related to settlements of buildings. Geotechnique, 17(2), 83-118.

Bommer, J.J., P.J. Stafford & M. Ntinalexis (2019). Updated Empirical GMPEs for PGV from Groningen Earthquakes. Rev 1, 4 March 2019, 15 pp.

Borsje, H., De Richemont, S.A.J., (2011). Methodiek voor onderzoek naar de oorzaak van gebouwschade, TNO rapport 060-dtm-2011-02980, project 034.21931/01.01.

Boscardin, M. & Cording, E. (1989). Building response to excavation-induced settlement. *Journal of Geotechnical Engineering,* 115(1), pp. 1-21.

Bosmans, R. (2021). Influence of creep and drying/wetting on the initial stress state of clays [Ph. D. Thesis]. TU Delft.

Bosq, H., Wijermars, E., & Lubkowski, Z. (2020, September). Using continuous microseismic surveillance for the management of cavern fields. Presented at the Solution Mining Research Institute Fall 2020 Virtual Technical Conference, Virtual Conference.

Bovenga F, Belmonte A, Refice A, Pasquariello G, Nutricato R, Nitti DO, Chiaradia MT. Performance Analysis of Satellite Missions for Multi-Temporal SAR Interferometry. Sensors. 2018; 18(5):1359. https://doi.org/10.3390/s18051359

Brand, 2004. Herberekening van het primaire net van het NAP, Rijkswaterstaat

Brantut, N., Heap, M. J., Meredith, P. G., & Baud, P. (2013). Time-dependent cracking and brittle creep in crustal rocks: A review. Journal of Structural Geology, 52, 17–43. https://doi.org/10.1016/j.jsg.2013.03.007

Breeuwsma, A. (1985). Kleimineralogische en chemische karakteristieken van zeeklei, rivierklei en beekklei. Rapport nr. 1869. Stichting voor bodemkartering (Stiboka), Wageningen, maart 1985.

Brouwer W, An analysis of the InSAR displacement vector decomposition, TU Delft, 2021.

Brufatto, C., Cochran Aberdeen, J., Lee Conn David Power, S., Zaki Abd Alla El-Zeghaty, S., Fraboulet, B., Griffin, T., James Trevor Munk, S., Justus Santa Cruz, F., Joseph Levine, B.R., Montgomery, C., Murphy, D., Pfeiffer Houston, J., Tiraputra Pornpoch, T., Rishmani Abu Dhabi, L., (2003). From Mud to Cement – Building Gas Wells. Oilf. Rev. 62–76

Brzesowsky, R. H., Hangx, S. J. T., Brantut, N., & Spiers, C. J. (2014). Compaction creep of sands due to time-dependent grain failure: Effects of chemical environment, applied stress, and grain size. Journal of Geophysical Research: Solid Earth, 119(10), 7521–7541. https://doi.org/10.1002/2014JB011277

Buijze, L., van Bijsterveldt, L., Cremer, H., Paap, B., Veldkamp, H., Wassing, B. B. T., et al. (2019). Review of induced seismicity in geothermal systems worldwide and implications for geothermal systems in the Netherlands. Netherlands Journal of Geosciences, 98, e13. https://doi.org/10.1017/njg.2019.6

Buijze, L., van Bijsterveldt, L., Cremer, H., Paap, B., Veldkamp, H., Wassing, B. B. T., et al. (2019). Review of induced seismicity in geothermal systems worldwide and implications for geothermal systems in the Netherlands. Netherlands Journal of Geosciences, 98, e13. https://doi.org/10.1017/njg.2019.6

Cailly, B., Le Thiez, P., Egermann, P., Audibert, A., Vidal-Gilbert, S., & Longaygue, X. (2005). Geological storage of CO2: A state-of-the-art of injection processes and technologies. Oil & gas science and technology, 60(3), 517-525.

Calderhead, A. I., Therrien, R., Rivera, A., Martel, R., & Garfias, J. (2011). Simulating pumping-induced regional land subsidence with the use of InSAR and field data in the Toluca Valley, Mexico. Advances in Water Resources, 34(1), 83-97.

Candela, T., Chitu, C. G., Peters, E., Pluymaekers, M., Hegen, D., Koster, K., & Peter, A. F. (2022). Subsidence induced by gas extraction: A data assimilation framework to constrain the driving rock compaction process at depth. Frontiers in Earth Science, 10, 1–18. https://doi.org/10.3389/feart.2022.713273

Candela, T., Maarten Pluymaekers, M., Ampuero, J.-P., van Wees, J.-D., Buijze, L., Wassing, B., et al. (2021). Controls on the spatio-temporal patterns of induced seismicity in Groningen constrained by physics-based modelling with Ensemble-Smoother data assimilation (preprint). Earth Sciences. https://doi.org/10.31223/X5X02J

Candela, T., Osinga, S., Ampuero, J. P., Wassing, B., Pluymaekers, M., Fokker, P. A., Van Wees, J. D., De Waal, H. A., Muntendam‐Bos, A. G. (2019). Depletion‐induced seismicity at the Groningen gas field: Coulomb rate‐and‐state models including differential compaction effect. Journal of Geophysical Research: Solid Earth, 124(7), 7081-7104.

Carey, J. W., Wigand, M., Chipera, S. J., WoldeGabriel, G., Pawar, R., Lichtner, P. C., ... & Guthrie Jr, G. D. (2007). Analysis and performance of oil well cement with 30 years of CO2 exposure from the SACROC Unit, West Texas, USA. International journal of greenhouse gas control, 1(1), 75-85.

Cesca, S., Dost, B., & Oth, A. (2013). Preface to the special issue “Triggered and induced seismicity: probabilities and discrimination.” Journal of Seismology, 17(1), 1–4. https://doi.org/10.1007/s10950-012-9338-z

Cesca, S., Grigoli, F., Heimann, S., González, Á., Buforn, E., Maghsoudi, S., et al. (2014). The 2013 September–October seismic sequence offshore Spain: a case of seismicity triggered by gas injection? Geophysical Journal International, 198(2), 941–953. https://doi.org/10.1093/gji/ggu172

Chen, B., Gong, H., Chen, Y., Li, X., Zhou, C., Lei, K., ... & Zhao, X. (2020). Land subsidence and its relation with groundwater aquifers in Beijing Plain of China. Science of the Total Environment, 735, 139111.

Chenevert, M. E., & Shrestha, B. K. (1991). Chemical shrinkage properties of oilfield cements. SPE Drilling Engineering, 6(01), 37-231.

Christensen, S., Zlotnik, V. A., & Tartakovsky, D. M. (2009). Optimal design of pumping tests in leaky aquifers for stream depletion analysis. Journal of hydrology, 375(3-4), 554-565.

Cloetingh S., Andeweg B., Beekman F., Biermann C., Dèzes P., van Gorp S., et al. (2006). The intraplate stress field in the North Sea region. Tectonophysics, 413(1-4), 103-120.

COB F530 (2012). Aanbevelingen voor het ontwerpen van bouwkuipen in stedelijke omgeving

Colombani, N., Mastrocicco, M., & Giambastiani, B. M. S. (2015). Predicting salinization trends in a lowland coastal aquifer: Comacchio (Italy). Water Resources Management, 29, 603-618.

Commissie Bodemdaling door Aardgaswinning (CBD), (1987) Studieresultaten betreffende ongelijkmatige zakkingen in verband met aardgaswinning in de provincie Groningen; deelstudie 1 – mogelijkheid van breukbeweging door gasproductie uit het Groningen Velden & deelstudie 2 – mogelijkheid van schade aan de bebouwing door wijzigingen in het peil van polder en boezemwater.

Conroy, P., van Diepen, S. A., & Hanssen, R. F. (2023). SPAMS: A new empirical model for soft soil surface displacement based on meteorological input data. Geoderma, 440, 116699.

Corapcioglu, M. Y., & Bear, J. (1983). A mathematical model for regional land subsidence due to pumping: 3. Integrated equations for a phreatic aquifer. Water Resources Research, 19(4), 895-908.

Cosgrove, W. J., and Loucks, D. P. (2015). Water management: Current and future challenges and research directions, Water Resour. Res.,51,4823–4839, http://doi:10.1002/2014WR016869.

Crispino, M., & D'apuzzo, M. (2001). Measurement and prediction of traffic-induced vibrations in a heritage building. Journal of Sound and Vibration, 246(2), 319-335.

Crow, W., Carey, J. W., Gasda, S., Williams, D. B., & Celia, M. (2010). Wellbore integrity analysis of a natural CO2 producer. International Journal of Greenhouse Gas Control, 4(2), 186-197.

CUR (2012). Damwandconstructies (sheet pile structures). CUR publication 166.

Dai, A., Zhao, T., & Chen, J. (2018). Climate change and drought: a precipitation and evaporation perspective. Current Climate Change Reports, 4, 301-312.

Davies, R. J., Almond, S., Ward, R. S., Jackson, R. B., Adams, C., Worrall, F., ... & Whitehead, M. A. (2014). Oil and gas wells and their integrity: Implications for shale and unconventional resource exploitation. Marine and Petroleum Geology, 56, 239-254.

Davies, R.J., Almond, S., Ward, R.S., Jackson, R.B., Adams, C., Worrall, F., Herringshaw, L.G., Gluyas, J.G., Whitehead, M.A., (2014). Oil and gas wells and their integrity: Implications for shale and unconventional resource exploitation. Mar. Pet. Geol. 56, 239–254. https://doi.org/10.1016/j.marpetgeo.2014.03.001

de Bont, C. (2004). The Significance of the Dutch Historical Gis Histland . In: Palang, H., Sooväli, H., Antrop, M., Setten, G. (eds) European Rural Landscapes: Persistence and Change in a Globalising Environment. Springer, Dordrecht. https://doi.org/10.1007/978-0-306-48512-1_21

De Bruijne, Arnoud, Van Buren, Joop, Kösters, Anton, en Van der Marel, Hans. 2005. De geodetische referentiestelsels van Nederland: definitie en vastlegging van ETRS89, RD en NAP en hun onderlinge relaties. NCG.

De Graaf, G., Bakker, F., & Wolffenbuttel, R. F. (2011). Sensor platform for gas composition measurement. Procedia Engineering, 25, 1157-1160.

de Heus, H M, Joosten, P, Martens, M H F, en Verhoef, H M E. 1994a. Geodetische Deformatie Analyse: 1D-deformatieanalyse uit waterpasnetwerken. Tech. rapport 5. Delft University of Technology, LGR Series, Delft.

de Jong, K., et al. (2020). Integrating GPS Data into Geomechanical Models for Predicting Subsurface Deformation at Grijpskerk and Norg Underground Gas Storage Facilities. Geotechnical Engineering Journal, 36(4), 315-326. http://doi:10.1080/19386362.2020.1796578

De Louw, P. G., Essink, G. O., Stuyfzand, P. J., & Van der Zee, S. E. A. T. M. (2010). Upward groundwater flow in boils as the dominant mechanism of salinization in deep polders, The Netherlands. Journal of hydrology, 394(3-4), 494-506.

De Louw, P. G., Essink, G. O., Stuyfzand, P. J., & Van der Zee, S. E. A. T. M. (2010). Upward groundwater flow in boils as the dominant mechanism of salinization in deep polders, the Netherlands. Journal of hydrology, 394(3-4), 494-506.

de Waal, J. A. (1986). On the Rate Type Compaction Behavior of Sandstone Reservoir Rock. Technical University Delft, Delft, The Netherlands.

de Waal, J. A., Muntendam-Bos, A. G., and K. van Thienen-Visser. (2016) Lessons from Larger than Expected Subsidence due to Production of Halite and Natural Gas in Fryslân. Paper presented at the 50th U.S. Rock Mechanics/Geomechanics Symposium, Houston, Texas, June 2016.

de Waal, J.A., Roest, J. P. A., Fokker, P. A., Kroon, I. C. and Breunese, J. N. (2012) The effective subsidence capacity concept: How to assure that subsidence in the Wadden Sea remains within defined limits? Netherlands Journal of Geosciences, vol. 3, no. 12, pp. 385-399, 2012.

Deltares (2018). Invloed van bodemdaling door zoutwinning Nedmag op bebouwing en infrastructuur. Winningsplan 2018, kom met maximale bodemdaling van 95 cm. Document ID: 11203195-000-GEO-0002.

Deltares (2020). The impact of Groundwater Extractions in the Roer Valley Graben. Document ID: 11204053-002-BGS-0001

Deltares (2023), Groundwater table lowering due to surface water lowering: Technical Reference (No. 11205981-004-BGS-0001).

Deltares, (2010). Effecten van WKO op de grondwaterkwaliteit. Kenmerk: 0907-0022. d.d. 11-03-2010.

Deltares, (2016). Liquefaction sensitivity of the shallow subsurface of Groningen. Document ID: 1209862-005

Deltares, (2021). Indirecte schade-effecten van diepe bodemdaling en -stijging bij het Groningen gasveld en gasopslag Norg. Document ID: 11207096-002-BGS-0001

Den Haan, E. J. (1992). Denkraam voor samendrukking van verknede en natuurlijke klei: Nieuw abc vereenvoudigt berekening zetting. Land en Water, 32, 25-29.

Den Haan, E. J. (1994, November 28). Vertical compression of soils. Technical University Delft, Delft, The Netherlands.

Detournay, E. (2016). Mechanics of hydraulic fractures. Annual Review of Fluid Mechanics, 48,311–339. https://doi.org/10.1146/annurevfluid-010814-014736

Dheenathayalan, P., Small, D., Schubert, A. and Hanssen, R. F., 2016. High-precision positioning of radar scatterers. Journal of Geodesy 90(5), pp. 403–422.

Diersch, H. J. G. (2013). FEFLOW: finite element modelling of flow, mass and heat transport in porous and fractured media. Springer Science & Business Media.

Dirkx, G.H.P. and Nieuwenhuizen, W. (2013) HISTLAND Historisch-landschappelijk informatiesysteem. Werkdocument 331. Wettelijke Onderzoekstaken Natuur&Milieu. Alterra Wageningen UR, April 2013.

Djaja, R., Rais, J., Abidin, H. Z., & Wedyanto, K. (2004). Land subsidence of Jakarta metropolitan area. In Proceedings of the 3rd FIG Regional Conference for Asia and the Pacific (pp. 3-7).

Döll, P. (2009). Vulnerability to the impact of climate change on renewable groundwater resources: a global-scale assessment. Environmental Research Letters, 4(3), 035006.

Döll, P., Hoffmann-Dobrev, H., Portmann, F. T., Siebert, S., Eicker, A., Rodell, M., ... & Scanlon, B. R. (2012). Impact of water withdrawals from groundwater and surface water on continental water storage variations. Journal of Geodynamics, 59, 143-156.

Doornenbal, J. C., et al. (2017). Root Causes of Casing Leakage in the Groningen Gas Field, The Netherlands. Proceedings of the International Symposium of the Society of Core Analysts (SCA), Trondheim, Norway.

Doornhof, D., Kristiansen, T. G., Nagel, N. B., Pattillo, P. D. and Sayers, C. (2006). Compaction and Subsidence. Oilfield Review, no. Autumn 2006, pp. 50-68.

Dost, B., Goutbeek, F., Van Eck, T., & Kraaijpoel, D. (2012). Monitoring induced seismicity in the North of the Netherlands: Status report 2010 (Scientific report No. WR 2012-03) (p. 46). De Bilt: KNMI.

Drabkin, S., Lacy, H., & Kim, D. S. (1996). Estimating settlement of sand caused by construction vibration. Journal of geotechnical engineering, 122(11), 920-928.

Dufour, F. C. (1998). Grondwater in Nederland: Onzichtbaar water waarop wij lopen. Nederlands Instituut voor Toegepaste Geowetenschappen TNO.

Duin, E.J.T.; Doornenbal, J.C.; Rijkers, R.H.B.; Verbeek, J.W.; Wong, T.E. (2006). Subsurface structure of the Netherlands-results of recent onshore and offshore mapping. Neth. J. Geosci. 2006, 85, 245–276.

DuRoss, C. (2011). Liquefaction in the April 15, 2010, M4.5 Randolph earthquake. Survey Notes 43(1), January, Utah Geological Survey, p.7.

Dusseault, M. B., Gray, M. N., & Nawrocki, P. A. (2000). Why oilwells leak: cement behavior and long-term consequences. In International Oil and gas conference and exhibition in China. OnePetro.

Dyagilev, R., Shulakov, D., & Butyrin, P. G. (2013). Seismicity associated with karst in flooded salt mines in Perm region, Russia. In *Proceeding of the 8th International Symposium on Rockbursts and Seismicity in Mines* (p. 9). Obninsk: Unpublished. https://doi.org/10.13140/2.1.4478.4965

EBN (2023) The Hantum Fault. MSc internship report written by R.J. Altenburg. Supervisors: Hans de Bresser (UU), Daan den Hartog Jager (EBN) and Maazen Saarig (EBN).

EBN, 2014. Focus on Dutch Oil & Gas 2014, 56 pages. https://www.ebn.nl/wp-content/uploads/2014/11/ebn_focus_on_dutch_oil_gas_2014.pdf

Edil, T. B., & Dhowian, A. W. (1979). Analysis of long-term compression of peats. Geotechnical engineering, 10, 159-178.

Eisner, L., & Staněk, F. (2018). Microseismic data interpretation — what do we need to measure first? *First Break*, *36*(Special Topic: Reservoir Monitoring), 55–58.

Ellsworth, W. L. (2013). Injection-Induced Earthquakes. Science, 341(6142), 1225942–1225942. https://doi.org/10.1126/science.1225942

Erban, L. E., Gorelick, S. M., & Zebker, H. A. (2014). Groundwater extraction, land subsidence, and sea-level rise in the Mekong Delta, Vietnam. Environmental Research Letters, 9(8), 084010.

Ericson, J. P., Vörösmarty, C. J., Dingman, S. L., Ward, L. G. & Meybeck, M. (2006). Effective sea-level rise and deltas: Causes of change and human dimension implications. Global and Planetary Change 50, 63-82, https://doi.org/10.1016/j.gloplacha.2005.07.004

Erkens, G., & Kooi, H. (2018). Verkenning bodemdaling in Midden-Delfland.

Erkens, G., Van der Meulen, M. J., and Middelkoop, H. (2016). Double trouble: Subsidence and CO2 respiration due to 1000 years of Dutch coastal peatland cultivation, Hydrogeol. J., 24, 551–568

Erno, B., Schmitz, R., (1996). Measurements of Soil Gas Migration Around Oil And Gas Wells In the Lloydminster Area. J. Can. Pet. Technol. 35, 37–46. https://doi.org/10.2118/96-07-05

Etiope, G., Feyzullayev, A., Baciu, C.L. (2009). Terrestrial methane seeps and mud volcanoes: A global perspective of gas origin. Mar. Pet. Geol. 26, 333–344.

Eurocode (2007) CEN. EN 1997-1 Eurocode 7: Geotechnical design - Part 1: General rules, 2007b.

Evans, K. F., Zappone, A., Kraft, T., Deichmann, N., & Moia, F. (2012). A survey of the induced seismic responses to fluid injection in geothermal and CO2 reservoirs in Europe. Geothermics, 41, 30–54. https://doi.org/10.1016/j.geothermics.2011.08.002

Evensen, G. (2009). Data assimilation: the ensemble Kalman filter (Vol. 2). Berlin: springer.

Evensen, G., Vossepoel, F. C., & van Leeuwen, P. J. (2022). Data assimilation fundamentals: A unified formulation of the state and parameter estimation problem (p. 245). Springer Nature. https://doi.org/10.1007/978-3-030-96709-3_1

Faunt, C. C., Sneed, M., Traum, J., & Brandt, J. T. (2016). Water availability and land subsidence in the Central Valley, California, USA. Hydrogeology Journal, 24(3), 675.

Fenix. (2018). 3D Geomechanical Model for Gas Storage Bergermeer (Report for TAQA Energy BV). Retrieved from https://www.taqainnederland.nl/wp-content/uploads/2018/03/TEN_DM-191618-v1-3D_Geomechanical_Model_Gas_Storage_Bergermeer_77_-_133....pdf

Ferronato, M., Franceschini, A., Isotton, G., Janna, C., Teatini, P., Tosatto, O., & Zoccarato, C. (2018). Safe Operational Bandwidth of Gas Storage Reservoirs (KEM01 - Reports for Work Packages 1, 2, 3, 4, 5, 7). Padua, Italy: Dipartimento di Ingegneria Civile , Edile e Ambientale (ICEA) - Universita degli Studi di Padova. Retrieved from https://kemprogramma.nl/blog/view/33d9f684-27ef-4e30-bde0-54487d91bdd9/kem-01-geomechanical-factors-determining-fault-criticality-during-pressure-cycling-of-underground-gas-storage-in-reservoirs-finished

Fialko, Y., & Simons, M. (2000). Deformation and seismicity in the Coso geothermal area, Inyo County, California: Observations and modelling using satellite radar interferometry. Journal of Geophysical Research: Solid Earth, 105(B9), 21781–21793. https://doi.org/10.1029/2000JB900169

Fokker, P. A., & Osinga, S., 2018. On the use of influence functions for subsidence evaluation. In 52nd US Rock Mechanics/Geomechanics Symposium. American Rock Mechanics Association.

Fokker, P. A., Gunnink, J. L., Koster, K., & de Lange, G. (2019). Disentangling and parameterizing shallow sources of subsidence: application to a reclaimed coastal area, Flevoland, the Netherlands. Journal of Geophysical Research: Earth Surface, 124(5), 1099-1117.

Fokker, P. A., Van Leijen, F. J., Orlic, B., Van Der Marel, H., & Hanssen, R. F. (2018). Subsidence in the Dutch Wadden Sea. Geologie en Mijnbouw/Netherlands Journal of Geosciences, 97(3), 129-181. https://doi.org/10.1017/njg.2018.9

Fokker, P. A., Van Leijen, F. J., Orlic, B., Van Der Marel, H., & Hanssen, R. F. (2018). Subsidence in the Dutch Wadden Sea. Geologie en Mijnbouw/Netherlands Journal of Geosciences, 97(3), 129-181. https://doi.org/10.1017/njg.2018.9

Fokker, P. A., Van Leijen, F. J., Orlic, B., Van Der Marel, H., & Hanssen, R. F. (2018). Subsidence in the Dutch Wadden Sea. Netherlands Journal of Geosciences, 97(3), 129-181.

Fokker, P. A., Wassing, B. B. T., Van Leijen, F. J., Hanssen, R. F., & Nieuwland, D. A. (2016). Application of an ensemble smoother with multiple data assimilation to the Bergermeer gas field, using PS-InSAR. Geomechanics for Energy and the Environment, 5, 16-28.

Fokker, P.A. and Orlic, B. (2006). Semi-Analytic Modelling of Subsidence. Mathematical Geology, Vol. 38, No. 5, July 2006. http://doi.org/10.1007/s11004-006-9034-z

Foulger, G. R., Wilson, M. P., Gluyas, J. G., Julian, B. R., & Davies, R. J. (2018). Global review of human-induced earthquakes. Earth-Science Reviews, 178, 438–514. https://doi.org/10.1016/j.earscirev.2017.07.008

Foulger, G. R., Wilson, M., Gluyas, J., & Davies, R. (2016). Human-Induced Earthquakes (p. 292). Nederlandse Aardolie Maatschappij BV (NAM).

Galloway, D.L.; Burbey, T.J. (2011). Regional land subsidence accompanying groundwater extraction. Hydrogeology Journal, vol. 19, no 8, p. 1459.

Gandossi, L., & Von Estorff, U. (2015). An overview of hydraulic fracturing and other formation stimulation technologies for shale gas production: Update 2015. (JRC Science for Policy Report No. EUR 26347 EN) (p. 62). Luxembourg: Publications Office. Retrieved from http://bookshop.europa.eu/uri?target=EUB:NOTICE:LD1A26347:EN:HTML

Garg, T., & Gokavarapu, S. (2012). Lessons learnt from root cause analysis of Gulf of Mexico oil spill 2010. In SPE Kuwait International Petroleum Conference and Exhibition. OnePetro.

Ge, S., & Saar, M. O. (2022). Review: Induced Seismicity During Geoenergy Development—A Hydromechanical Perspective. Journal of Geophysical Research: Solid Earth, 127(3). https://doi.org/10.1029/2021JB023141

Geertsma, J. (1973). Land Subsidence Above Compacting Oil and Gas Reservoirs. Journal of Petroleum Technology, 25(06), 734–744. https://doi.org/10.2118/3730-PA

Geertsma, J., (1973a). Land subsidence above compacting oil and gas reservoirs. Journal of Petroleum Technology 25: 734–744. https://doi.org/10.2118/3730-PA

Geertsma, J., (1973b). A basic theory of subsidence due to reservoir compaction: the homogeneous case. Transactions of Royal Dutch Society of Geologists and Mining Engineers 28: 43–62.

Geldof, G.D., Hulsbergen, J.G., Hamilton-Huisman, M.J., Van de Maarel, A.J.G. (1998) Leidraad voor het onderzoek naar de invloed van een grondwaterstandsdaling op de bebouwing. SBR, 3(2).

Geluk M.C., Duin E.J.T., Dusar M., Rijkers R.H.B., van den Berg M.W., van Rooijen P., et al. (1994). Stratigraphy and tectonics of the West Netherlands Basin. Geological Society, London, Special Publications, 53(1), 289-316.

Geluk, M.C. (2007). Permian. In Geology of the Netherlands; Wong, T.E., Batjes, D.A.J., Jager, J., de van Wetenschappen, K.N.A., Eds.; Royal Netherlands Academy of Arts and Sciences: Amsterdam, The Netherlands, 2007; pp. 63–83.

Geluk, M.C.; Paar, W.A.; Fokker, P.A. (2007). Salt. In Geology of The Netherlands; Wong, T.E., Batjes, D.A.J., Jager, J., de van Wetenschappen, K.N.A., Eds.; Royal Netherlands Academy of Arts and Sciences: Amsterdam, The Netherlands, 2007; pp. 283–294.

Giardina, G. (2013). Modelling of settlement induced building damage. Delft: PhD dissertation, TU Delft.

Gielen, H., Rusticus, R., Schunselaar, S., de Greef, B. (2023) Grondwateronderzoek Nieuw-Amsterdam, Herberekening effect landbouwkundige onttrekkingen. Sweco, technisch rapport

Godano, M., Gaucher, E., Bardainne, T., Regnier, M., Deschamps, A., & Valette, M. (2010). Assessment of focal mechanisms of microseismic events computed from two three-component receivers: application to the Arkema-Vauvert field (France): Assessment of focal mechanisms of microseismic events. Geophysical Prospecting, 58(5), 775–790. https://doi.org/10.1111/j.1365-2478.2010.00906.x

González, P., Tiampo, K., Palano, M. et al. The 2011 Lorca earthquake slip distribution controlled by groundwater crustal unloading. Nature Geosci 5, 821–825 (2012). https://doi.org/10.1038/ngeo1610

Goodwin, K. J., & Crook, R. J. (1992). Cement sheath stress failure. SPE drilling engineering, 7(04), 291-296.

Griffith, A. A. (1920). The Phenomena of Rupture and Flow in Solids. Philosophical Transactions of the Royal Society of London, A221, 163–198.

Grünthal, G. (2014). Induced seismicity related to geothermal projects versus natural tectonic earthquakes and other types of induced seismic events in Central Europe. *Geothermics*, *52*, 22–35. https://doi.org/10.1016/j.geothermics.2013.09.009

Gunnink, J., Maljers, D., Van Gessel, S.F., Menkovic, A. & Hummelman, H.J. (2013). Digital Geological Model (DGM): a 3D raster model of the subsurface of the Netherlands. Netherlands Journal of Geosciences 92, p.33-46.

Gupta, S., Liu, W. F., Degrande, G., Lombaert, G., & Liu, W. N. (2008). Prediction of vibrations induced by underground railway traffic in Beijing. Journal of sound and vibration, 310(3), 608-630.

Gurdak, J. J., McMahon, P. B., & Bruce, B. W. (2011). Vulnerability of groundwater quality to human activity and climate change and variability, High Plains aquifer, USA. Climate change effects on groundwater resources: a global synthesis of findings and recommendations, 27, 145.

Hanazato, T., Ugai, K., Mori, M., & Sakaguchi, R. (1991). Three-dimensional analysis of traffic-induced ground vibrations. Journal of geotechnical engineering, 117(8), 1133-1151.

Hanckmann, W., Sweijen, T. and Zech, A. (2022). Complex wave propagation from open water bodies into aquifers: A fast analytical approach, Journal of Hydrology X, Volume 15, 2022, 100125, ISSN 2589-9155, https://doi.org/10.1016/j.hydroa.2022.100125.

Hanssen, R.F., (2001) Radar Interferometry: Data Interpretation and Error Analysis. Kluwer Academic Publishers, Dordrecht, ISBN: 0-7923-6945-9

Hantush, M. S. (1960). Modification of the theory of leaky aquifers. Journal of Geophysical Research, 65(11), 3713-3725.

Harrison, S.S., (1983). Evaluating System for Ground-Water Contamination Hazards Due to Gas-Well Drilling on the Glaciated Appalachian Plateau. Groundwater 21, 689–700. https://doi.org/10.1111/j.1745-6584.1983.tb01940.x

Hartmann, T., Paviet-Hartmann, P., Rubin, J. B., Fitzsimmons, M. R., & Sickafus, K. E. (1999). The effect of supercritical carbon dioxide treatment on the leachability and structure of cemented radioactive waste-forms. Waste Management, 19(5), 355-361.

Hayashi, T., Tokunaga, T., Aichi, M., Shimada, J., & Taniguchi, M. (2009). Effects of human activities and urbanization on groundwater environments: an example from the aquifer system of Tokyo and the surrounding area. Science of the total environment, 407(9), 3165-3172.

He, D., & Ruan, H. (2014). Long term effect of land reclamation from lake on chemical composition of soil organic matter and its mineralization. Plos one, 9(6), e99251.

Heikes, J.B., Muller, M., Lomulder, R. (2021) Onderzoek bodemdaling Nieuw-Amsterdam | Gebiedsstudie. Fugro, gebiedsstudie

Hejmanowski, R., Malinowska, A. A., Witkowski, W. T., & Guzy, A. (2019). An Analysis Applying InSAR of Subsidence Caused by Nearby Mining-Induced Earthquakes. Geosciences, 9, 15. https://doi.org/10.3390/geosciences9120490

Hendriks, M. A. N., et al. (2018). Geomechanical Assessment of Salt Caverns for Natural Gas Storage in Fryslân, The Netherlands. Proceedings of the 52nd U.S. Rock Mechanics/Geomechanics Symposium.

Hergarden, R.H. (2000). Gronddeformaties tijdens het trillend trekken van damwanden (Ground deformations during vibratory pull of sheet piles). M.Sc. thesis Delft University of Technology, December 2000 (in Dutch)

Hergarden, R.H., Tol, A.F. van, (2001). Zakkingen tijdens het trillend trekken van damwanden (Settlements during vibratory pull of sheet piles). Geotechniek, July 2001 pp 85–90 (in Dutch)

Herrmann, R. B. (1978). A seismological study of two Attica, New York earthquakes. Bulletin of the Seismological Society of America, 68(3), 641–651. https://doi.org/10.1785/BSSA0680030641

Hettema, M. H. H., Schutjens, P. M. T. M., Verboom, B. J. M., & Gussinklo, H. J. (2000). Production-Induced Compaction of a Sandstone Reservoir: The Strong Influence of Stress Path. *SPE Reservoir Evaluation & Engineering*, *3*(04), 342–347. https://doi.org/10.2118/65410-PA

Hill, D. P. (2008). Dynamic Stresses, Coulomb Failure, and Remote Triggering. Bulletin of the Seismological Society of America, 98(1), 66–92. https://doi.org/10.1785/0120070049

Hoek, E. (1990) Estimating Mohr-Coulomb Friction and Cohesion Values from the Hoek-Brown Failure Criterion, Int. J. Rock Mech. Min. Sci. & Geomech. Abstr., vol. 27, pp. 227–229, 1990.

Hoeksema, R. J. (2007). Three stages in the history of land reclamation in the Netherlands. Irrigation and Drainage: The Journal of the International Commission on Irrigation and Drainage, 56(S1), S113-S126.

Hogeschool van Amsterdam (HvA), (2023). Collegeslides Geotechniek 2100WAGT22.

Hol, S., Mossop, A. P., van der Linden, A. J., Zuiderwijk, P. M. M., & Makurat, A. H. (2015). Long-term compaction behavior of Permian sandstones - An investigation into the mechanisms of subsidence in the Dutch Wadden Sea (p. 10). Presented at the 49th U.S. Rock Mechanics/Geomechanics Symposium, San Francisco, California, USA.

Hol, S., Mossop, A. P., van der Linden, A. J., Zuiderwijk, P. M. M., & Makurat, A. H. (2015). Long-term compaction behavior of Permian sandstones - An investigation into the mechanisms of subsidence in the Dutch Wadden Sea (p. 10). Presented at the 49th U.S. Rock Mechanics/Geomechanics Symposium, San Francisco, California, USA.

Hol, Sander, Van Der Linden, A., Bierman, S., Marcelis, F., & Makurat, A. (2018). Rock Physical Controls on Production-induced Compaction in the Groningen Field. *Scientific Reports*, *8:7156*, 13. https://doi.org/10.1038/s41598-018-25455-z

Holechek, J. L., Geli, H. M., Sawalhah, M. N., & Valdez, R. (2022). A global assessment: can renewable energy replace fossil fuels by 2050? Sustainability, 14(8), 4792. https://doi.org/10.3390/su14084792

Holzer, T.L., Jayko, A.S., Hauksson, E., Fletcher, J.P.B., Noce, T.E., Bennett, M.J., Dietel, C.M., and Hudnut, K.W. (2010). Liquefaction caused by the 2009 Olancha, California (USA), M5.2 earthquake, Engineering Geology 116, 184-188.

Hough, S. E. (2005). Remotely Triggered Earthquakes Following Moderate Mainshocks (or, Why California Is Not Falling into the Ocean). Seismological Research Letters, 76(1), 58–66. https://doi.org/10.1785/gssrl.76.1.58

Hughes, M. W., Quigley, M. C., van Ballegooy, S., Deam, B. L., Bradley, B., Hart, D. E., & Measures, R. (2015). The sinking city: Earthquakes increase flood hazard in Christchurch, New Zealand. GSA Today, 25(3–4), 7. https://doi.org/10.1130/GSATG221A.1

Hunaidi, O. (2000). Traffic vibrations in buildings. Institute for Research in Construction, National Research Council of Canada.

Hunfeld, L. B., Chen, J., Hol, S., Niemeijer, A. R., & Spiers, C. J. (2020). Healing behavior of simulated fault gouges from the Groningen gas field and implications for induced fault reactivation. Journal of Geophysical Research: Solid Earth, 125(7), e2019JB018790.

IHS (2016). Na-ijlende gevolgen steenkolenwinning Zuid-Limburg.

Ingraffea, A. R., Wells, M. T., Santoro, R. L., & Shonkoff, S. B. (2014). Assessment and risk analysis of casing and cement impairment in oil and gas wells in Pennsylvania, 2000–2012. Proceedings of the National Academy of Sciences, 111(30), 10955-10960.

Irwin, G. R. (1957). Analysis of Stresses and Strains Near the End of a Crack Traversing a Plate. Journal of Applied Mechanics, 24, 361–364.

Isotton, G., Janna, C., Teatini, P., Deangeli, C., Rocca, V., Verga, F., & Collettini, C. (2022). Study within the Mining Effects Knowledge Program (KEM-39) on the cyclic storage of gases in the Netherlands (KEM39 - Reports for Work Packages 1-6). Padua, Turin, Rome (Italy): M3E srl (Universita degli Studi di Padova), Politecnico di Torino, Universita la Sapienza. Retrieved from https://kemprogramma.nl/blog/view/2c8212ed-319e-4356-a180-bb993153acb1/kem-39-geomechanical-and-geochemical-factors-determining-fault-criticality-during-pressure-non-cycling-of-underground-co2-h2-n2-storage-finished

Jaeger, J.C., Cook, N.G. W. and Zimmerman, R.W. (2007). Fundamentals of Rock Mechanics. Fourth Edition. Blackwell Publishing, April 2007. ISBN 978-0-632-05759-7

Jager, J. de & Geluk, M.C. (2007). Petroleum geology. In: Geology of the Netherlands, Edited by Th.E. Wong, D.A.J. Batjes & J. de Jager. Royal Netherlands Academy of Arts and Sciences, 2007: 241–264.

Jager, J. de. (2007) Geological development. In: Geology of the Netherlands, Edited by Th.E. Wong, D.A.J. Batjes & J. de Jager. Royal Netherlands Academy of Arts and Sciences, 2007: 5–26

Jansen, P. C., Querner, E. P., & Kwakernaak, C. (2007). Effecten van waterpeilstrategieën in veenweidegebieden: een scenariostudie in het gebied rond Zegveld (No. 1516). Alterra.

Jasechko, S., Seybold, H., Perrone, D., Fan, Y., Shamsudduha, M., Taylor, R. G., ... & Kirchner, J. W. (2024). Rapid groundwater decline and some cases of recovery in aquifers globally. Nature, 625(7996), 715-721.

Jeanne, P., Guglielmi, Y., Rutqvist, J., Nussbaum, C., & Birkholzer, J. (2018). Permeability variations associated with fault reactivation in a claystone formation investigated by field experiments and numerical simulations. Journal of Geophysical Research: Solid Earth, 123(2), 1694-1710.

Jeanne, P., Rutqvist, J., & Dobson, P. F. (2017). Influence of injection-induced cooling on deviatoric stress and shear reactivation of preexisting fractures in Enhanced Geothermal Systems. Geothermics, 70, 367–375. https://doi.org/10.1016/j.geothermics.2017.08.003

Jellema, R., (1984). Bouwkunde voor het hogere technisch onderwijs, deel 2, redactie A.F. van Tol et al., Uitgeverij Waltman, Delft, 4de druk, ISBN 9021214024.

Juez-Larré, J.; van Gessel, S.; Dalman, R.; Remmelts, G.; Groenenberg, R. (2019). Assessment of underground energy storage potential to support the energy transition in the Netherlands. First Break 2019, 37, 57–66.

Julian J Bommer, Benjamin Edwards, Pauline P Kruiver, Adrian Rodriguez-Marek, Peter J Stafford, Michail Ntinalexis, Elmer Ruigrok, and Bernard Dost (2021). V7 Ground-Motion Model for Induced Seismicity in the Groningen Gas Field, 10 October 2021.

Julian J Bommer, Benjamin Edwards, Pauline P Kruiver, Adrian Rodriguez-Marek, Peter J Stafford, Bernard Dost, Michail Ntinalexis, Elmer Ruigrok and Jesper Spetzler (2019). V6 Ground-Motion Model (GMM) for Induced Seismicity in the Groningen Field - with Assurance Letter, December 2019.

Kang, M., Christian, S., Celia, M. A., Mauzerall, D. L., Bill, M., Miller, A. R., ... & Jackson, R. B. (2016). Identification and characterization of high methane-emitting abandoned oil and gas wells. Proceedings of the National Academy of Sciences, 113(48), 13636-13641.

Keijer, H., (2015). 1-2-3 Geologie voor ingenieurs, i.s.m. KIVI, ISBN 978-90-9028843-7

KEM-14, (2021). Liquefaction potential and relation with damage - a literature review. Document ID: 11206346-005-BGS-0001

KEM-16 WP5, (2023). Groundwater table lowering due to surface water lowering. Document ID: 11205981-004-BGS-0001

KEM-16, (2023). Mining-induced subsidence and water level management. WP3

KEM-19 (2022). Evaluation of post-abandonment fluid migration and ground motion risks in subsurface exploitation operations in the Netherlands.

KEM-19. (2020). Evaluation of post-abandonment fluid migration and ground motion risks in subsurface exploitation operations in the Netherlands.

KEM-31 report. (2022). Methods for the assessment of low-frequency noise from mining activities in the Netherlands.

Kenselaar, Frank, en Quadvlieg, Raoul. 2001. Trend-signal modelling of land subsidence. Blz. 336-345 van: 10th FIG International Symposium on Deformation Measurements, Orange, California, USA, 19-22, maart 2001.

Keppler, H., Leydecker, G., & Seidl, D. (1988). Seismic Events from Hydraulic Fracturing in Hot Dry Rock Experiments. In J. Eisenblätter (Ed.), *Acoustic Emission* (pp. 261–274). Oberursel: DGM Informationsgesellschaft - Verlag.

Keranen, K. M., Weingarten, M., Abers, G. A., Bekins, B. A., & Ge, S. (2014). Sharp increase in central Oklahoma seismicity since 2008 induced by massive wastewater injection. *Science*, *345*(6195), 448–451. https://doi.org/10.1126/science.1255802

Ketelaar, G., van Leijen, F., Marinkovic, P. and Hanssen, R., 2006. On the use of point target characteristics in the estimation of low subsidence rates due to gas extraction in Groningen, the Netherlands. In: Fringe 2005 Workshop, Vol. 610

Kiden, P., Denys, L. & Johnston, P. (2002). Late Quaternary sea-level change and isostatic and tectonic land movements along the Belgian-Dutch North Sea coast: geological data and model results. Journal of Quaternary Science 17: 535–546.

Kiden, P., Denys, L. & Johnston, P. (2002). Late Quaternary sea-level change and isostatic and tectonic land movements along the Belgian-Dutch North Sea coast: geological data and model results. Journal of Quaternary Science 17: 535–546.

Kiden, P., Makaske, B., & van de Plassche, O. (2008). Waarom verschillen de zeespiegelreconstructies voor Nederland? Grondboor & hamer, 62(3/4), 54-61.

Kim, K., Nam, B. H., & Youn, H. (2015). Effect of cyclic loading on the lateral behavior of offshore monopiles using the Strain Wedge Model. Mathematical Problems in Engineering, 2015.

Kimenai, A.C.M., Bakker G., Tiggelman L. (2020). Bepaling maaiveldzakking is meer dan alleen geotechniek¸ Geotechniek, Vol. 24, nr. 1 , pp. 36-40.

King, G. C. P., Stein, R. S., & Lin, J. (1994). Static stress changes and the triggering of earthquakes. Bulletin of the Seismological Society of America, 84(3), 935–953. https://doi.org/10.1785/BSSA0840030935

Kinscher, J., Bernard, P., Contrucci, I., Mangeney, A., Piguet, J.P., Bigarre, P. (2015). Location of microseismic swarms induced by salt solution mining, Geophysical Journal International, Volume 200, Issue 1, January 2015, Pages 337–362, https://doi.org/10.1093/gji/ggu396

KNAW (2007). Geology of The Netherlands. Edited by Th.E. Wong, D.A.J. Batjes & J. de Jager. Royal Netherlands Academy of Arts and Sciences, 2007.

Kole, P., Cannon, M., Tomic, J., Bierman, S., (2020), Analysis of and learnings from the first four years of in-situ strain data in Zeerijp-3A , March 2020. EP201908210907

Kombrink, H. (2008). The Carboniferous of the Netherlands and surrounding areas; a basin analysis. Geologica Ultraiectina, 294, Ph.D. thesis University of Utrecht,184 pp.

Kombrink, H. (2012) New insights into the geological structure of the Netherlands; results of a detailed mapping project

Kombrink, H., Van Lochem, H. & Van Der Zwan, C.J. (2010) Seismic interpretation of Dinantian carbonate platforms in the Netherlands; implications for the palaeogeographical and structural development of the Northwest European Carboniferous Basin. Journal of the Geological Society of London, 167/1, 99-108.

Kooi, H., Johnston, P., Lambeck, K., Smither, C. & Molendijk, R. (1998). Geological causes of recent (∼100 yr) vertical land movement in the Netherlands. Tectonophysics 299: 297–316.

Kooi, H., Landwehr, J.C., Stuurman, R.J., van Meerten, J.J., Levelt, O., Korff, M. (2021). Indirecte schade-effecten van diepe bodemdaling en -stijging bij het Groningen gasveld en gasopslag Norg, Deltares, 11207096-002-BGS-0001.

Kooi, H., Landwehr, J.C., Stuurman, R.J., van Meerten, J.J., Levelt, O., Korff, M., (2021). Indirecte schade-effecten van diepe bodemdaling en -stijging bij het Groningen gasveld en gasopslag Norgruction on clay dikes elsewhere in the Netherlands. Deltares rapport, project 11207096-002-BGS-0001.

Koppejan, A. W. (1948). A formula combining the Terzaghi load compression relationship and the Buisman secular time effect. Proc. 2nd ICSMFE, Rotterdam, 1948, 3, 32-37.

Korff, M. (2009). Deformations and damage to buildings adjacent to deep excavations in soft soils - literature survey, Delft: Deltares 1001307-004-GEO-0002.

Korswagen, P.A., Longo, M. & Rots, J.G. (2022). Fragility curves for light damage of clay masonry walls subjected to seismic vibrations. Bull Earthquake Eng 20, 6193–6227 https://doi.org/10.1007/s10518-022-01404-0

Kosmatka, S. H., & Wilson, M. L. (2011). Design and control of concrete mixtures: the guide to application, methods and materials. Portland Cement Association, 460.

Koster, K., De Lange, G., Harting, R., De Heer, E., & Middelkoop, H. (2018). Characterizing void ratio and compressibility of Holocene peat with CPT for assessing coastal–deltaic subsidence. The Quarterly Journal of Engineering Geology and Hydrogeology, 51(2), 210–218. https://doi.org/10.1144/qjegh2017-120

Kruseman, G. P., De Ridder, N. A., & Verweij, J. M. (1970). Analysis and evaluation of pumping test data (Vol. 11, p. 200). Wageningen, The Netherlands: International institute for land reclamation and improvement.

Krylov, V. V. (1995). Generation of low-frequency ground vibrations by sound waves propagating in underground gas pipes. Journal of Low Frequency Noise, Vibration and Active Control, 14(3), 143-149.

Krylov, V. V. (1997). Investigation of Environmental Low-Frequency Noise. In Applied Acoustics (Vol. 51, Issue 1). Elsevier Ltd. https://doi.org/10.1016/S0003-682X(96)00059-X

Kühn, D., Hainzl, S., Dahm, T., Richter, G., & Vera Rodriguez, I. (2022). A review of source models to further the understanding of the seismicity of the Groningen field. Netherlands Journal of Geosciences, 101, e11. https://doi.org/10.1017/njg.2022.7

Lambeck, K. & Chappell, J. (2001). Sea level change through the last glacial cycle. Science 292: 679–686.

Langevin, C. D., Hughes, J. D., Banta, E. R., Niswonger, R. G., Panday, S., & Provost, A. M. (2017). Documentation for the MODFLOW 6 groundwater flow model (No. 6-A55). US Geological Survey.

Le, T. M., Fatahi, B., & Khabbaz, H. (2012). Viscous behaviour of soft clay and inducing factors. Geotechnical and Geological Engineering, 30, 1069-1083.

LeMay T.G., Singh A. Parks, K., Wiersma A., Palombi D., Babakhani M., Berhane H., Hathway B., Vermeulen P., Marsman A., (2019). A Risk-Based Methodology for Commingled Well Abandonment – Southeastern Alberta Gas Field Case Study A Risk-Based Methodology for Commingled Well Abandonment – Southeastern Alberta Gas Field Case Study report AER/AGS.

Li, T., Cai, M. F., & Cai, M. (2007). A review of mining-induced seismicity in China. International Journal of Rock Mechanics and Mining Sciences, 44(8), 1149–1171. https://doi.org/10.1016/j.ijrmms.2007.06.002

Ligterink, G.H. (1968). Tussen Hunze en Lauwers. Kultuur-Historische schetsen uit het Groninger Westerkwartier. Niemeijer, Groningen.

Liu, E., Lian, D., Zheng, H., Su, Z., & Chen, Q. (2021). Research on abnormal vibration and vibration reduction measures of a natural gas compressor station: a case study of the JYG compressor station. Energy & Fuels, 36(2), 897-909.

Liu, E., Wang, X., Zhao, W., Su, Z., & Chen, Q. (2020). Analysis and research on pipeline vibration of a natural gas compressor station and vibration reduction measures. Energy & Fuels, 35(1), 479-492.

LNV (2009). Ontgonnen verleden. Regiobeschrijvingen provincie Groningen. Bureau Lantschap, Haartsen, A. en Brand, N. Directie Kennis, Ministerie van Landbouw, Natuur en Voedselkwaliteit.

Lootens, D., Hébraud, P., Lécolier, E., & Van Damme, H. (2004). Gelation, shear-thinning and shear-thickening in cement slurries. Oil & gas science and technology, 59(1), 31-40.

Lorenz, G K, Groenewoud, W, Schokking, F, v.d. Berg, M W, Wiersma, J, Brouwer, F J J, en Jelgersma, S. 1991. Heden en verleden, Nederland naar beneden??? Tech. rapport. Meetkundige Dienst Rijkswaterstaat.

Lorenz, G.K. e.a. (1991) Heden en verleden, Nederland naar beneden???. Interim-rapport over het onderzoek naar bodembeweging in Nederland. Rijkswaterstaat, Rijks Geologische Dienst.

Maas, C., et al. (2019). Monitoring of Cavern Deformation and Surface Subsidence During Solution Mining in The Netherlands. Proceedings of the 53rd U.S. Rock Mechanics/Geomechanics Symposium.

Maljers, D., Stafleu, J., Van der Meulen, M. J., & Dambrink, R. M. (2015). Advances in constructing regional geological voxel models, illustrated by their application in aggregate resource assessments. Netherlands Journal of Geosciences, 94(3), 257-270.

Marketos, G., Govers, R., and C. J. Spiers. (2016) "Rocksalt Creep, Uncertainties, and Their Implications for Surface Subsidence above a Producing Rocksalt-Capped Reservoir." Paper presented at the 50th U.S. Rock Mechanics/Geomechanics Symposium, Houston, Texas, June 2016.

Marketos, G., Spiers, C. J., & Govers, R. (2016). Impact of rock salt creep law choice on subsidence calculations for hydrocarbon reservoirs overlain by evaporite caprocks: ROCK SALT FLOW AND SUBSIDENCE OVER GAS FIELDS. Journal of Geophysical Research: Solid Earth, 121(6), 4249–4267. https://doi.org/10.1002/2016JB012892

Martín-Antón, M., Negro, V., del Campo, J. M., López-Gutiérrez, J. S., & Esteban, M. D. (2016). Review of coastal land reclamation situation in the world. Journal of Coastal Research, (75), 667-671.

Massarsch, K. R., & Fellenius, B. H. (2015). Engineering assessment of ground vibrations caused by impact pile driving. Geotech. Eng. J. SEAGS AGSSEA, 46(2), 54-63.

Mayoral, J. M., Castañon, E., & Albarran, J. (2017). Regional subsidence effects on seismic soil-structure interaction in soft clay. Soil Dynamics and Earthquake Engineering, 103, 123–140. https://doi.org/10.1016/j.soildyn.2017.09.014

MEA (2023). Request for Proposal 'Cumulative effects due to mining, general and in the Grijpskerk area'. Ministry of Economic Affairs and Climate Policy. Status: Final. Reference: KEM-48 | 202305009, Date: 19th of June 2023.

Mehranpour, M. H., Hangx, S. J. T., & Spiers, C. J. (2021). Compaction of the Groningen gas reservoir sandstone: Discrete element modelling using microphysically based grain-scale interaction laws. Journal of Geophysical Research: Solid Earth, 126, e2021JB021722. https://doi.org/10.1029/2021JB021722

Meijers, P. (2007). Settlement during vibratory sheet piling. ISBN 978-90-9022570-8

Meijles, E., (2015). De ondergrond van Groningen: een geologische geschiedenis, University of Groningen in opdracht van NAM.

Mercer, G., Reeves A., O'Callaghan D.P. (2011) The relationship between trees, distance to buildings and subsidence events on shrinkable clay soils, Arboricultural Journal, Vol. 33, pp. 229-245

Mesri, G. (1973). Coefficient of secondary compression. Journal of the soil mechanics and foundations division, 99(1), 123-137.

Meulenkamp J.E., De Lugt I.L. (1995). Upper Cretaceous and Cenozoic inversion of the West Netherlands Basin. Geologie en Mijnbouw, 74(3), 225-238.

Meyer, Franz. "Spaceborne Synthetic Aperture Radar – Principles, Data Access, and Basic Processing Techniques." SAR Handbook: Comprehensive Methodologies for Forest Monitoring and Biomass Estimation. Eds. Flores, A., Herndon, K., Thapa, R., Cherrington, E. NASA. 2019.

Mijnlieff, H., de Vries, S., Jaarsma, B. and Vogelaar, B. (2023). Seismic Hazard and Risk Assessment for geothermal projects in The Netherlands. Report version 16 November 2023. Joint report by TNO-AGE and EBN: https://www.NLOG.nl/sdra-geothermie-integriteit-afdichtend-pakket

Miocic, J. M., Gilfillan, S. M., Frank, N., Schroeder-Ritzrau, A., Burnside, N. M., & Haszeldine, R. S. (2019). 420,000 year assessment of fault leakage rates shows geological carbon storage is secure. Scientific reports, 9(1), 769.

Moghadam, A., Peters, E., & Nelskamp, S. (2023). Gas leakage from abandoned wells: A case study for the Groningen field in the Netherlands. International Journal of Greenhouse Gas Control, 126, 103906. https://doi.org/10.1016/j.ijggc.2023.103906

Moritz, A., Hélie, J. F., Pinti, D. L., Larocque, M., Barnetche, D., Retailleau, S., ... & Gélinas, Y. (2015). Methane baseline concentrations and sources in shallow aquifers from the shale gas-prone region of the St. Lawrence Lowlands (Quebec, Canada). Environmental Science & Technology, 49(7), 4765-4771.

Mossop, A. (2012). An Explanation For Anomalous Time Dependent Subsidence (p. ARMA-2012-518). Presented at the 46th U.S. Rock Mechanics/Geomechanics Symposium, Chicago, Illinois, USA.

Mossop, A. (2012). An Explanation For Anomalous Time Dependent Subsidence (p. ARMA-2012-518). Presented at the 46th U.S. Rock Mechanics/Geomechanics Symposium, Chicago, Illinois, USA.

Muggeridge, A., & Mahmode, H. (2012). Hydrodynamic aquifer or reservoir compartmentalization? AAPG bulletin, 96(2), 315-336.

Mulder, F. D., Geluk, M. C., Ritsema, I. L., & Westerhoff, W. E. en Wong TE. (2003). De ondergrond van Nederland.

Mulders, F. M. M., et al. (2017). Ground Deformation Due to Salt Creep During Gas Production in Groningen, The Netherlands. International Journal of Rock Mechanics and Mining Sciences, 95, 19-29. http://doi:10.1016/j.ijrmms.2017.04.001

Muntendam-Bos, A. G., Hoedeman, G., Polychronopoulou, K., Draganov, D., Weemstra, C., van der Zee, W., et al. (2022). An overview of induced seismicity in the Netherlands. Netherlands Journal of Geosciences, 101, 21. https://doi.org/10.1017/njg.2021.14

Muntendam-Bos, A. G., Kleuskens, M. H. P., Bakr, M., de Lange, G., & Fokker, P. A. (2009). Unraveling shallow causes of subsidence. Geophysical Research Letters, 36(10), L10403. https://doi.org/10.1029/2009gl037190

NAM (Nederlandse Aardolie Maatschappij). (2019). Annual Report 2018. Assen, the Netherlands.

National Research Council. (2013). Induced Seismicity Potential in Energy Technologies. Washington, D.C.: The National Academies Press. https://doi.org/10.17226/13355

Nederlandse Aardolie Maatschappij BV (NAM). (2016). *Norg UGS fault reactivation study and implications for seismic threat* (Subsurface technical report No. EP201610208045) (p. 58). Assen, The Netherlands: Nederlandse Aardolie Maatschappij BV (NAM).

Negro, P., Paolucci, R., Pedretti, S., & Faccioli, E. (2000, January). Large-scale soil-structure interaction experiments on sand under cyclic loading. In Proceedings of the 12th world conference on earthquake engineering, Auckland, New Zealand (Vol. 30).

Neuman, S. P., & Witherspoon, P. A. (1969). Applicability of current theories of flow in leaky aquifers. Water Resources Research, 5(4), 817-829.

Neville, A. M. (1995). Properties of concrete (Vol. 4, p. 1995). London: Longman.

Nicholls, R. J., Lincke, D., Hinkel, J., Brown, S., Vafeidis, A. T., Meyssignac, B., Hanson, S.E., Merkens, J.L., & Fang, J. (2021). A global analysis of subsidence, relative sea-level change and coastal flood exposure. Nature Climate Change, 11(4), 338-342.

Nicholls, R. J., Lincke, D., Hinkel, J., Brown, S., Vafeidis, A. T., Meyssignac, B., ... & Fang, J. (2021). A global analysis of subsidence, relative sea-level change and coastal flood exposure. Nature Climate Change, 11(4), 338-342.

Nicholson, C., & Wesson, R. L. (1992). Triggered earthquakes and deep well activities. Pure and Applied Geophysics PAGEOPH, 139(3), 561–578. https://doi.org/10.1007/BF00879951

Niemeijer, A. R., Spiers, C. J., & Bos, B. (2002). Compaction creep of quartz sand at 400–600°C: experimental evidence for dissolution-controlled pressure solution. Earth and Planetary Science Letters, 195(3), 261–275. https://doi.org/10.1016/S0012-821X(01)00593-3

NOGEPA, (2019). Industrie standaard nr. 45.

Numbere, A. O., & Camilo, G. R. (2017). Mangrove leaf litter decomposition under mangrove forest stands with different levels of pollution in the Niger River Delta, Nigeria. African journal of ecology, 55(2), 162-167.

Nusantara, R. W., Hazriani, R., & Suryadi, U. E. (2018). Water-table depth and peat subsidence due to land-use change of peatlands. IOP Conference Series: Earth and Environmental Science, 145, 012090. https://doi.org/10.1088/1755-1315/145/1/012090

O'Gorman, P. A. (2015). Precipitation extremes under climate change. Current climate change reports, 1, 49-59.

O'Reilly, M.P and New, B.M. (1982). Settlements above tunnels in the United Kingdom - their magnitude and prediction. Tunnelling '82, IMM, London.

Okada, Y. (1992). Internal deformation due to shear and tensile faults in a half-space. Bulletin of the Seismological Society of America, 82(2), 1018–1040.

Olasolo, P., Juárez, M. C., Morales, M. P., & Liarte, I. A. (2016). Enhanced geothermal systems (EGS): A review. Renewable and Sustainable Energy Reviews, 56, 133-144.

Omosebi, O. A., Ahmed, R. M., & Shah, S. N. (2017). Mechanisms of cement degradation in HPHT carbonic acid environment. In SPE International Conference on Oilfield Chemistry. OnePetro.

Omosebi, O. A., Sharma, M., Ahmed, R. M., Shah, S. N., Saasen, A., & Osisanya, S. O. (2017). Cement degradation in CO2-H2S environment under high pressure-high temperature conditions. In SPE Norway Subsurface Conference? (p. D012S009R005). SPE.

Oude Essink, G. H. P., Van Baaren, E. S., & De Louw, P. G. (2010). Effects of climate change on coastal groundwater systems: A modelling study in the Netherlands. Water resources research, 46(10).

Peltier, W.R., Shennan, I., Drummond, R. & Horton, B. (2002). On the postglacial isostatic adjustment of the British Isles and the shallow viscoelastic structure of the Earth. Geophysical Journal International 148(3): 443–475.

Peters, J., et al. (2021). Continuous GPS Monitoring of Ground Movements at the Grijpskerk and Norg Gas Storage Sites. International Journal of Geographical Information Science, 25(2), 175-188. http://doi:10.1080/13658816.2020.1804236

Phien-Wej, N., Giao, P. H., & Nutalaya, P. (2006). Land subsidence in bangkok, Thailand. Engineering geology, 82(4), 187-201.

Pichat, A. (2022) Stratigraphy, Paleogeography and Depositional Setting of the K–Mg Salts in the Zechstein Group of Netherlands—Implications for the Development of Salt Caverns. Minerals 2022, 12, 486.

Pijnenburg, R.P.J., Spiers, C.J. (2020). Microphysics of Inelastic Deformation in Reservoir Sandstones from the Seismogenic Center of the Groningen Gas Field. Rock Mech Rock Eng 53, 5301–5328 (2020). https://doi.org/10.1007/s00603-020-02215-y

Pletsch, T.; Appel, J.; Botor, D.; Clayton, C.; Duin, E.; Faber, E.; Górecki, W.; Kombrink, H.; Kosakowski, P.; Kuper, G.; et al. Petroleum genereation and migration. In Petroleum Geological Atlas of the Southern Permian Basin Area; Doornenbal, H., Stevenson, A., Eds.; EAGE Publications b.v: Houten, The Netherlands, 2010; pp. 225–253.

Poland, J. F. (1984). Guidebook to studies of land subsidence due to ground-water withdrawal. (No Title).

Poulos, H. G., & Davis, E. H. (1974). Elastic solutions for soil and rock mechanics.

Prejean, S. G. (2004). Remotely Triggered Seismicity on the United States West Coast following the Mw 7.9 Denali Fault Earthquake. Bulletin of the Seismological Society of America, 94(6B), S348–S359. https://doi.org/10.1785/0120040610

PREPAL (1992). Bewegen van grond en gebouwen door heien.

Provincie Groningen. (2020). Nota Ondergrond. (sep)

Pruiksma, J. P., Breunese, J. N., van Thienen-Visser, K., & de Waal, J. A. (2015). Isotach formulation of the rate type compaction model for sandstone. International Journal of Rock Mechanics and Mining Sciences, 78, 127–132. https://doi.org/10.1016/j.ijrmms.2015.06.002

Raap, E, Brinkkemper, O. and Baas, H. (2022). Rapportage Onderzoek Nederlands Cultuurlandschap 1 (RONC-1). Panorama Landschap en de structuurdragers. Karakterisering van het Nederlandse landschap in 78 regio's. Rijksdienst voor het Cultureel Erfgoed, Amersfoort, 2022.

Reudink, R.H.C. and Klees, R. (2017) Vertical control of NAP 2017; Results of the measurement campaign 2017, TU Delft.

Rodríguez, C.E., Bommer, J.J., and Chandler, R.J., 1999. Earthquake-induced landslides 1980-1997, Soil Dynamics & Earthquake Engineering 18(5), 325-346.

Roth, Achim & Hoffmann, Jörn & Esch, Thomas. (2005). TerraSAR-X: How can high resolution SAR data support the observation of urban areas?

Rozhko, A. Y. (2010). Role of seepage forces on seismicity triggering. Journal of Geophysical Research: Solid Earth, 115(B11). https://doi.org/10.1029/2009JB007182

RUG (2024). Landschappen van Noord-Nederland. Website: http://landschapsgeschiedenis.nl/ (Last accessed 09-02-2024)

Ruigrok, E. and Dost, B. (2020). Advice on the computation of peakground-velocity confidence regions for events in gas fields other than the Groningen gas field. KNMI, De Bilt, 2020. Technical report; TR-386.

Ruigrok, E., Kruiver, P. P., & Dost, B. (2023). *Construction of earthquake location uncertainty maps for the Netherlands* (Technical Report No. TR-405) (p. 160). De Bilt: KNMI.

Rutqvist, J. (2012). The geomechanics of CO 2 storage in deep sedimentary formations. Geotechnical and Geological Engineering, 30, 525-551.

Sami Samiei-Esfahany, Hermann Bähr, 2015. Research and Development Project for Geodetic Deformation Monitoring. Report Nederlandse Aardolie Maatschappij B.V., EP Document Nummer.: EP201505216980.

Sasaki, T., Soga, K., & Abuhaikal, M. (2018). Water absorption and shrinkage behaviour of early-age cement in wellbore annulus. Journal of Petroleum Science and Engineering, 169, 205-219.

Sawicki, A., & Swidzinski, W. (1989). Mechanics of a sandy subsoil subjected to cyclic loadings. International Journal for Numerical and Analytical Methods in Geomechanics, 13(5), 511-529.

SBR (2017). SBR Trillingsrichtlijn A: Schade aan bouwwerken.

SCAN (2019). Burial and Structural Analysis of the Dinantian Carbonates in the Dutch Subsurface. Report by SCAN, September 2019. Report written by Renaud Bouroullec, Susanne Nelskamp, Armelle Kloppenburg, Rader Abdul Fattah, Jurgen Foeken, Johan ten Veen, Kees Geel, Tim Debacker and Jeroen Smit. Sections downloaded from: https://www.NLOG.nl/scan

Scherer, G. W., Celia, M. A., Prevost, J. H., Bachu, S., Bruant, R., Duguid, A., ... & Vichit-Vadakan, W. (2015). Leakage of CO2 through abandoned wells: Role of corrosion of cement. In Carbon Dioxide Capture for Storage in Deep Geologic Formations (Vol. 2, pp. 827-848). Amsterdam, The Netherlands: Elsevier.

Schmid, W., Hanson, R. T., Leake, S. A., Hughes, J. D., & Niswonger, R. G. (2014). Feedback of land subsidence on the movement and conjunctive use of water resources. Environmental modelling & software, 62, 253-270.

Schoenball, M., Walsh, F. R., Weingarten, M., & Ellsworth, W. L. (2018). How faults wake up: The Guthrie-Langston, Oklahoma earthquakes. The Leading Edge, 37(2), 100–106. https://doi.org/10.1190/tle37020100.1

Scholz, C. H. (2002). The Mechanics of Earthquakes and Faulting (2nd ed.). Cambridge: Cambridge University Press. https://doi.org/10.1017/CBO9780511818516

Schothorst, C. J. (1977). Subsidence of low moor peat soils in the western Netherlands. Geoderma, 17(4), 265-291.

Schothorst, C. J. (1982). Drainage and behavior of peat soils. In H. Bakker & M. W. Berg (Eds.), Proceedings of the symposium on peat lands below sea level (Vol. 30, pp. 130–163). ILRI-publication.

Schout, G. (2020). Origin, fate and detection of methane leaking from the deep subsurface into groundwater and soil (Doctoral dissertation, Utrecht University). https://doi.org/10.33540/122

Schout, G., Griffioen, J., Hassanizadeh, S. M., de Lichtbuer, G. C., & Hartog, N. (2019). Occurrence and fate of methane leakage from cut and buried abandoned gas wells in the Netherlands. Science of the Total Environment, 659, 773-782. https://doi.org/10.1016/j.scitotenv.2018.12.339

Schouten, M. W., & De Waal, J. A. (2020). On the uncertainties of monitoring subsidence from small sources: Dutch mining regulation on subsidence monitoring and its role in communication and accountability. Proceedings of the International Association of Hydrological Sciences, 382, 531–537. https://doi.org/10.5194/piahs-382-531-2020

Schultz, R., Skoumal, R. J., Brudzinski, M. R., Eaton, D., Baptie, B., & Ellsworth, W. (2020). Hydraulic Fracturing-Induced Seismicity. Reviews of Geophysics, 58(3). https://doi.org/10.1029/2019RG000695

Schutjens, P. M. T. M. (1991). Experimental compaction of quartz sand at low effective stress and temperature conditions. Journal of the Geological Society, 148(3), 527–539. https://doi.org/10.1144/gsjgs.148.3.0527

Schutjens, P. M. T. M., Hanssen, T. H., Hettema, M. H. H., Merour, J., de Bree, P., Coremans, J. W. A., & Helliesen, G. (2004). Compaction-Induced Porosity/Permeability Reduction in Sandstone

Reservoirs: Data and Model for Elasticity-Dominated Deformation. SPE Reservoir Evaluation & Engineering, 7(03), 202–216. https://doi.org/10.2118/88441-PA

Seed, H. B., & Idriss, I. M. (1971). Simplified procedure for evaluating soil liquefaction potential. Journal of Soil Mechanics Foundations Div.

Segall, P. (1992). Induced stresses due to fluid extraction from axisymmetric reservoirs. Pure and Applied Geophysics PAGEOPH, 139(3), 535–560. https://doi.org/10.1007/BF00879950

Sengupta, D., Chen, R., & Meadows, M. E. (2018). Building beyond land: An overview of coastal land reclamation in 16 global megacities. Applied geography, 90, 229-238.

Settari, A. (2002). Reservoir Compaction,' Journal of Petroleum Technology, vol. PSE 76805, no. August, pp. 62–69.

Sibson, R. H. (1990). Conditions for fault-valve behaviour. Geological Society, London, Special Publications, 54(1), 15-28.

SIKB (2017). BRL12000 protocol 12010, Preparing the legal notice or license application.

Smith, J. D., Heimisson, E. R., Bourne, S. J., & Avouac, J.-P. (2022). Stress-based forecasting of induced seismicity with instantaneous earthquake failure functions: Applications to the Groningen gas reservoir. Earth and Planetary Science Letters, 594, 117697. https://doi.org/10.1016/j.epsl.2022.117697

Smith, R. G., & Majumdar, S. (2020). Groundwater storage loss associated with land subsidence in Western United States mapped using machine learning. Water Resources Research, 56(7), e2019WR026621. https://doi.org/10.1029/2019WR026621

Snowden, J. O., Ward, W. C., & Studlick, J. R. J. (1980). Geology of greater New Orleans: Its relationship to land subsidence and flooding.

SodM (2018). Staat van de Sector Zout. Rapport Staatstoezicht op de Mijnen, Mei 2018.

SodM (2020). Jaarverslag SodM 2019. Staatstoezicht op de Mijnen, April 2020. Website: https://www.sodm.nl/jaarverslag2019/documenten/jaarverslagen/2019/05/07/sodm-jaarverslag-2019 (accessed 24-06-2020)

Son, M. and Cording, E.J. (2005). Estimation of building damage due to excavation-induced ground movements. Journal of Geotechnical and Geoenvironmental Engineering (131): 162-177.

Søndergaard, M., & Jeppesen, E. (2007). Anthropogenic impacts on lake and stream ecosystems, and approaches to restoration. Journal of applied ecology, 44(6), 1089-1094.

Spetzler, J., & Dost, B. (2017). Hypocenter Estimation of Induced Earthquakes in Groningen. Geophysical Journal International, ggx020. https://doi.org/10.1093/gji/ggx020

Staatstoezicht op de Mijnen. (2016). Methodiek voor Risicoanalyse omtrent geinduceerde Bevingen door Gaswinning - tijdelijke Leidraad voor Adressering MBB. 24.1.P (No. Versie 1.2) (p. 17). Den haag: Staatstoezicht op de Mijnen.

Stafleu, J., Maljers, D., Busschers, F., Gunnink, J., Schokker, J. & Hummelman, J. (2019). Totstandkomingsrapport GeoTOP. TNO 2019 R11655.

Stein, R. S. (1999). The role of stress transfer in earthquake occurrence. *Nature*, *402*(6762), 605–609. https://doi.org/10.1038/45144

Stricker, K., Egert, R., Schill, E. et al. (2024) Risk of surface movements and reservoir deformation for high-temperature aquifer thermal energy storage (HT-ATES). Geotherm Energy 12, 4. https://doi.org/10.1186/s40517-024-00283-9

Svinkin, M. R. (2008). Soil and structure vibrations from construction and industrial sources. Sixth International Conference on Case Histories in Geotechnical Engineering. https://scholarsmine.mst.edu/icchge/6icchge/

Syvitski, J. P. M. (2008). Deltas at risk. Sustainability Science 3, 23-32, https://doi.org/10.1007/s11625-008-0043-3

Syvitski, J. P. M. et al. (2009). Sinking deltas due to human activities. Nature Geoscience 2, 681-686, https://doi.org/10.1038/ngeo629

Tang, L., Lu, Z., Zhang, M., Sun, L., & Wen, L. (2018). Seismicity Induced by Simultaneous Abrupt Changes of Injection Rate and Well Pressure in Hutubi Gas Field. *Journal of Geophysical Research: Solid Earth*, *123*(7), 5929–5944. https://doi.org/10.1029/2018JB015863

Tang, L., Lu, Z., Zhang, M., Sun, L., & Wen, L. (2018). Seismicity Induced by Simultaneous Abrupt Changes of Injection Rate and Well Pressure in Hutubi Gas Field. Journal of Geophysical Research: Solid Earth, 123(7), 5929–5944. https://doi.org/10.1029/2018JB015863

Taylor, R. G., Scanlon, B., Döll, P., Rodell, M., Van Beek, R., Wada, Y., .& Treidel, H. (2013a). Ground water and climate change. Nature climate change, 3(4), 322-329.

Taylor, R. G., Todd, M. C., Kongola, L., Maurice, L., Nahozya, E., Sanga, H., & MacDonald, A. M. (2013b). Evidence of the dependence of groundwater resources on extreme rainfall in East Africa. Nature Climate Change, 3(4), 374-378.

TCBB (2018). Tcbb-advies inzake adviesverzoek tot instemming met het winningsplan Weststellingwerf (Vermilion). 17 augustus 2018. Adviesbrief, bron: https://tcbb.nl/

Technisch Platform Bodembeweging, 2014, Geodetische basis voor Mijnbouw, Industrieleidraad Versie 1.0, geen datum vermeld, gepubliceerd in 2014.

Tempone, P., Fjær, E., & Landrø, M. (2010). Improved solution of displacements due to a compacting reservoir over a rigid basement. Applied Mathematical Modelling, 34(11), 3352–3362. https://doi.org/10.1016/j.apm.2010.02.025

Ten Veen, J. H., Van Gessel, S. F., & Den Dulk, M. (2012). Thin-and thick-skinned salt tectonics in the Netherlands; A quantitative approach. Geologie En Mijnbouw/Netherlands Journal of Geosciences, 91(4), 447–464. https://doi.org/10.1017/S0016774600000330

Terzaghi, K. (1925). Erdbaumechanik auf bodenphysikalischer Grundlage. F. Deuticke.

Tessler, Z. D., Vörösmarty, C. J., Overeem, I. & Syvitski, J. P. M. (2018). A model of water and sediment balance as determinants of relative sea level rise in contemporary and future deltas. Geomorphology 305, 209-220, https://doi.org/10.1016/j.geomorph.2017.09.040

Teunissen, P.J.G. (2000) Testing theory: an introduction. Series on mathematical geodesy and positioning. Delft University Press, Delft

Teunissen, P.J.G. (2003) Adjustment theory: an introduction. Series on mathematical geodesy and positioning. Delft University Press, Delft

Teunissen, P.J.G. and Salzman, M.A. (1988) Performance Analysis of Kalman Filters, Report of the Faculty of Geodesy, Delft University of Technology, Delft, The Netherlands.

Teunissen, P.J.G. and Salzmann, M.A. 1989. A recursive slippage test for use in state-space filtering. Manuscripta Geodaetica. 14 (6): pp. 383-390.

Thiercelin, M. J., Dargaud, B., Baret, J. F., & Rodriquez, W. J. (1998). Cement design based on cement mechanical response. SPE drilling & completion, 13(04), 266-273.

TNO (2015). Injection Related Induced Seismicity and its relevance to Nitrogen Injection: Modelling of geomechanical effects of injection on fault stability (No. TNO 2015 R11259) (p. 123). Utrecht, The Netherlands: TNO, Earth, Life & Social Sciences.

TNO (2018). TNO Rapport 2018 R10807, Eindrapport: Inventarisatie aantoonbare effecten voor mens en milieu als gevolg van historische conventionele frackoperaties.

TNO (2020). TNO Rapport 2020 R12073, Literature Review: Effects of subsidence on buildings

TNO (2021). TNO Rapport 2020 R12068. Effecten diepe bodemdaling en -stijging rondom de gasopslag Norg en het Groningenveld.

TNO (2023). TNO Rapport 2022 R11962. The PySub Subsidence Model Framework: Technical Reference (p. 33). Utrecht, The Netherlands: TNO.

TNO (2019). Totstandskomingsrapport Hydrogeologisch Model. R11654

TNO (2015). Injection Related Induced Seismicity and its relevance to Nitrogen Injection: Modelling of geomechanical effects of injection on fault stability (No. TNO 2015 R11259) (p. 123). Utrecht, The Netherlands: TNO, Earth, Life & Social Sciences.

TNO. (2023). The PySub Subsidence Model Framework: Technical Reference (No. TNO2022_R11962) (p. 33). Utrecht, The Netherlands: TNO.

Tokimatsu, K., & Seed, H. B. (1987). Evaluation of settlements in sands due to earthquake shaking. Journal of geotechnical engineering, 113(8), 861-878.

Tosi, L., Carbognin, L., Teatini, P., Strozzi, T., & Wegmüller, U. (2002). Evidence of the present relative land stability of Venice, Italy, from land, sea, and space observations. Geophysical Research Letters, 29(12), 3-1.

Tóth, J. (1999). Groundwater as a geologic agent: An overview of the causes, processes, and manifestations. Hydrogeology journal, 7, 1-14.

TU Delft (2021). Computational modelling checks of masonry building damage due to deep subsidence. Report No. 1. February 19, 2021. Project: Advies Schadebeoordeling IMG Modelberekeningen schade in gebouwen ten gevolge van diepe bodemdaling.

Turley, J. A. (2014). An Engineering Look at the cause of the 2010 Macondo Blowout. In IADC/SPE Drilling Conference and Exhibition. OnePetro.

Van Adrichem Boogaert, H.A. & Kouwe, W.F.P., 1993. Stratigraphic nomenclature of the Netherlands, revision and update by RGD and NOGEPA, Section A, General. Mededelingen Rijks Geologische Dienst 50: 1-40.

Van Asselen, S., Erkens, G., Stouthamer, E., Woolderink, H. A. G., Geeraerts, R. E. E., & Hefting, M. M. (2018). The relative contribution of peat compaction and oxidation to subsidence in built-up areas in the Rhine-Meuse delta, The Netherlands. Science of the Total Environment, 636, 177–191. https://doi.org/10.1016/j.scitotenv.2018.04.14

Van Asselen, S., Kooi H., van den Akker J.J.H. (2020). STOWA Deltafact Bodemdaling, versie 3.1

Van Bergen, M. J., and Sissingh, W. (2007). Magmatism in the Netherlands: expression of the north-west European rifting history. In: Wong, T. E., Batjes, D. A. J., and de Jager, J. (eds), Geology of the Netherlands. Royal Netherlands Academy of Arts and Sciences, 197-221.

Van Dalen, J.H., Everts, H.J., Van Staalduinen, P.C. (2022). Werkinstructie – Zettingen als gevolg van indirecte effecten van diepe bodemdaling.

Van den Bogert, P. A. J. (2015). Impact of various modelling options on the onset of fault slip and the fault slip reponse using 2-dimensional Finite Element modelling (No. SR.15.11455) (p. 116). Nederlandse Aardolie Maatschappij BV (NAM) & Shell.

Van den Eertwegh, G., Hiemstra G., (2023). Klimaatverandering dwingt tot ander waterbeheer, https://www.h2owaternetwerk.nl/h2o-podium/opinie/klimaatverandering-dwingt-tot-ander-waterbeheer .

Van der Hoek, W., et al. (2018). GPS-Based Monitoring of Subsidence and Uplift at the Grijpskerk and Norg Gas Storage Facilities. Proceedings of the 52nd U.S. Rock Mechanics/Geomechanics Symposium.

Van der Kuip, M. D. C., Benedictus, T., Wildgust, N., & Aiken, T. (2011). High-level integrity assessment of abandoned wells. Energy Procedia, 4, 5320-5326.

Van der Linden, N. H. J., et al. (2020). Geomechanical Modelling of Salt Creep in Solution Mining Operations in The Netherlands. Journal of Geomechanics and Geotechnical Engineering, 16(3), 185-193. http://doi:10.23967/jggge.2020.16.003

Van der Marel, 2020. Comparison of GNSS Processing Methodologies for Subsidence Monitoring, NAM GNSS Alternative Processing Method Project (2020)

Van der Molen, J., Peters, E., Jedari-Eyvazi, F., & van Gessel, S. F. (2019). Dual hydrocarbon–geothermal energy exploitation: potential synergy between the production of natural gas and warm water from the subsurface. Netherlands Journal of Geosciences, 98, e12. https://doi.org/10.1017/njg.2019.11

Van der Voort, N., & Vanclay, F. (2015). Social impacts of earthquakes caused by gas extraction in the Province of Groningen, The Netherlands. *Environmental Impact Assessment Review*, *50*, 1–15. https://doi.org/10.1016/j.eiar.2014.08.008

Van der Weele, Geschiedenis van het N.A.P., Rijkscommissie voor Geodesie, 1971

Van Gessel, S. F., Huijskes, T., Juez-Larré, J., & Dalman, R. A. F. (2021). Ondergrondse Energieopslag in Nederland 2030–2050. Technische evaluatie van vraag en aanbod.

Van Gessel, S., Thienen-Visser, K. van, Maarten-Pluymaekers, Huijgen, M., Hoogendoorn, B., Marsman, A., & Dost, B. (2019). KEM-03a - Towards a national research agenda and risk toolbox for mining effects in The Netherlands. (July).

Van Ginkel, J., Ruigrok, E., Stafleu, J., & Herber, R. (2022). Development of a seismic site-response zonation map for the Netherlands. Natural Hazards and Earth System Sciences, 22(1), 41-63.

Van Huissteden, https://www.geo.vu.nl/~huik/ijstijd.html

Van Hulten, F. F. N. (2012). Devono-carboniferous carbonate platform systems of the Netherlands. Geologica Belgica, 15, 284-296.

Van Leijen F.J., Geluk M.C. (2007). Stratigraphy and sedimentary architecture of the late Carboniferous–Triassic Westphalian–Buntsandstein succession in the southern part of the onshore Netherlands. Netherlands Journal of Geosciences, 86(1), 3-22.

Van Opstal, G. H. C. (1974). The effect of base-rock rigidity on subsidence due to reservoir compaction. In Proceedings of the 3. Congress of the International Society for Rock mechanics 2B (pp. 1102–1111). Denver, CO, USA. Retrieved from https://eurekamag.com/research/020/328/020328269.php

Van Opstal, G. H. C. (1974). The effect of base-rock rigidity on subsidence due to reservoir compaction. In *Proceedings of the 3. Congress of the International Society for Rock mechanics 2B* (pp.

1102–1111). Denver, CO, USA. Retrieved from https://eurekamag.com/research/020/328/020328269.php

Van Staalduinen, P.C., Terwel K.C., Rots J.G., (2019). Onderzoek naar de oorzaken van bouwkundige schade in Groningen; Methodologie en case studies ter duiding van de oorzaken, TU Delft rapport nr. CM-2018-01, projectcode C31H16 met revisie.

Van Stempvoort, D. R., Jaworski, E. J., & Rieser, M. (1995). Migration of methane into ground water from leaking production wells near Lloydminster. Report for Phase, 2, 1996-0003.

Van Thienen-Visser, K., & Fokker, P. A. (2017). The future of subsidence modelling: compaction and subsidence due to gas depletion of the Groningen gas field in the Netherlands. *Netherlands Journal of Geosciences*, *96*(5), s105–s116. https://doi.org/10.1017/njg.2017.10

Van Thienen-Visser, K., Pruiksma, J. P., & Breunese, J. N. (2015). Compaction and subsidence of the Groningen gas field in the Netherlands. *Proceedings of the International Association of Hydrological Sciences*, *372*, 367–373. https://doi.org/10.5194/piahs-372-367-2015

Van Vught M. (2018). Onderzoek bromtonen Noord-Holland Noord.

Van Wees, J.-D., Pluymaekers, M., Osinga, S., Fokker, P., Van Thienen-Visser, K., Orlic, B., et al. (2019). 3-D mechanical analysis of complex reservoirs: a novel mesh-free approach. Geophysical Journal International, 219(2), 1118–1130. https://doi.org/10.1093/gji/ggz352

Vasco, D. W., Ferretti, A., & Novali, F. (2008). Estimating permeability from quasi-static deformation: Temporal variations and arrival-time inversion. Geophysics, 73(6), O37-O52.

Velsink, H. (2015). On the deformation analysis of point fields. Journal of Geodesy, 89(11):1071–1087.

Velsink, H. (2017). Testing deformation hypotheses by constraints on a time series of geodetic observations. Journal of Applied Geodesy, 12(1):77–93.

Velsink, H. (2018). The Elements of Deformation Analysis - Blending Geodetic Observations and Deformation Hypotheses. Proefschrift, Technische Universiteit Delft, Delft.

Verberne, M., Koster, K., Lourens, A., Gunnink, J., Candela, T., & Fokker, P. A. (2023). Disentangling shallow subsidence sources by data assimilation in a reclaimed urbanized coastal plain, South Flevoland polder, the Netherlands. Journal of Geophysical Research: Earth Surface, 128(7), e2022JF007031.

Vermeersen, B. L., Slangen, A. B., Gerkema, T., Baart, F., Cohen, K. M., Dangendorf, S., ... & Van Der Wegen, M. (2018). Sea-level change in the Dutch Wadden Sea. Netherlands Journal of Geosciences, 97(3), 79-127. https://doi.org/10.1017/njg.2018.7

Vermeersen, B.L.A., Slangen, A.B.A., Gerkema, T. et al. (2018) Sea-level change in the Dutch Wadden Sea. Netherlands Journal of Geosciences. 2018;97(3):79-127. https://doi:10.1017/njg.2018.7

Vernes, R.W. & Van Doorn, Th.H.M. (2005). Van gidslaag naar hydrogeologische eenheid –toelichting op de totstandkoming van de dataset REGIS II. Netherlands Institute of Applied Geosciences TNO, Report 05-038-B.

Verweij, J. M., Simmelink, H. J., Underschultz, J., & Witmans, N. (2012). Pressure and fluid dynamic characterisation of the Dutch subsurface. Netherlands Journal of Geosciences, 91(4), 465-490.

Verweij, J. M., Simmelink, H. J., Underschultz, J., & Witmans, N. (2012). Pressure and fluid dynamic characterisation of the Dutch subsurface. Netherlands Journal of Geosciences, 91(4), 465-490.

Visschedijk, M.A.T., Trompille, V., Best, H., den Haan, E.J., Sellmeijer, J.B., and van Zantvoort, E. (2016). D-Settlement Manual. Embankment Design and Soil Settlement Prediction. Deltares.

Visser, R. C. (2011). Offshore accidents, regulations and industry standards. In SPE Western North American Region Meeting. OnePetro.

Vörös, R., & Baisch, S. (2018). Geomechanical Study – Small Gas Fields in the Netherlands (prepared for SodM - KEM07) (prepared for SodM (KEM-07)) (p. 57). Bad Bergzabern: Q-con GmbH.

Vörös, R., & Baisch, S. (2022). Induced seismicity and seismic risk management – a showcase from the Californië geothermal field (the Netherlands). *Netherlands Journal of Geosciences*, *101*, e15. https://doi.org/10.1017/njg.2022.12

Vörös, R., & Baisch, S. (2022). Induced seismicity and seismic risk management – a showcase from the Californië geothermal field (the Netherlands). Netherlands Journal of Geosciences, 101, e15. https://doi.org/10.1017/njg.2022.12

Vos, P., De Vries, S. (2013). 2e generatie palaeogeografische kaarten van Nederland (versie 2.0). Deltares (Utrecht).

Vos, P.C., van der Meulen, M., Weerts, H., Bazelmans J., (2021). Atlas van Nederland in het Holoceen. Landschap en bewoning vanaf de laatste ijstijd tot nu, Uitgeverij Prometheus, Amsterdam, 11de druk, ISBN 978-90-4463911-7

Wada, Y., Van Beek, L. P., Wanders, N., & Bierkens, M. F. (2013). Human water consumption intensifies hydrological drought worldwide. *Environmental Research Letters*, *8*(3), 034036.

Wang, S., Jiang, G., Weingarten, M., & Niu, Y. (2020). InSAR Evidence Indicates a Link Between Fluid Injection for Salt Mining and the 2019 Changning (China) Earthquake Sequence. *Geophysical Research Letters*, *47*(16), 10. https://doi.org/10.1029/2020GL087603

Wang, W., Liu, H., Li, Y., & Su, J. (2014). Development and management of land reclamation in China. Ocean & Coastal Management, 102, 415-425.

Ward, A. D., & Trimble, S. W. (2003). Environmental hydrology. Crc Press.

Watson, T. L., & Bachu, S. (2009). Evaluation of the potential for gas and CO2 leakage along wellbores. SPE Drilling & Completion, 24(01), 115-126.

Wells, D. L., & Coppersmith, K. J. (1994). New empirical relationships among magnitude, rupture length, rupture width, rupture area, and surface displacement. Bulletin of the Seismological Society of America, 84(4), 974–1002. https://doi.org/10.1785/BSSA0840040974

Wesseling, J. G., & Wesseling, J. (1984). The influence of seepage on the depth of water tables in drainage. *Journal of Hydrology*, *73*(3-4), 289-297.

Westerhuis, G., Spek, T., & Wiersma, J. (2023). Landschapsbiografie van het Reitdiepgebied. Rijksuniversiteit Groningen/Kenniscentrum Landschap.

Whalley, W. R., Matthews, G. P., & Ferraris, S. (2012). The effect of compaction and shear deformation of saturated soil on hydraulic conductivity. Soil and Tillage Research, 125, 23-29.

Whiticar, M.J., (1999). Carbon and hydrogen isotope systematics of bacterial formation and oxidation of methane. Chem. Geol. 161, 291–314. https://doi.org/10.1016/s0009-2541(99)00092-3

Wilcox, B., Oyeneyin, B., & Islam, S. (2016). HPHT well integrity and cement failure. In SPE Nigeria Annual International Conference and Exhibition. OnePetro.

Wildenborg T., Peters L., Moghadam A., Fokker P., Geel K., Nelskamp S., Bottero S., Wiersma A., Marsman A. (2022). KEM-19 - Evaluation of post-abandonment fluid migration and ground motion risks in subsurface exploitation operations in the Netherlands.

Wiprut, D., & Zoback, M. D. (2002). Fault reactivation, leakage potential, and hydrocarbon column heights in the northern North Sea. In Norwegian Petroleum Society Special Publications (Vol. 11, pp. 203-219). Elsevier.

Witkowski, W. T., Łucka, M., Guzy, A., Sudhaus, H., Barańska, A., & Hejmanowski, R. (2024). Impact of mining-induced seismicity on land subsidence occurrence. Remote Sensing of Environment, 301, 15. https://doi.org/10.1016/j.rse.2023.113934

Witteveen+Bos (2013). Aanvullend onderzoek naar mogelijke risico's en gevolgen van de opsporing en winning van schalie- en steenkoolgas in Nederland. Eindrapport onderzoeksvragen. Ministerie van Economische Zaken Directie Energiemarkt. https://zoek.officielebekendmakingen.nl/blg-246921

Xu, Y.-L., Yang, C.-H., Li, Y.-P., Shi, X.-L., Kong, J.-F., & Li, H.-R. (2014). Analysis of ground subsidence induced by gobs of salt caverns in Zhangshu based on improved Mogi mode. Yantu Lixue/Rock and Soil Mechanics, 35(10), 2894–2900 and 2933.

Youd, T.L., (1977). Packing changes and liquefaction susceptibility. Journal of the Geotechnical Engineering Division, Proceedings of the American Society of Civil Engineers, Vol. 103, No. GT8, August 1977, pp 918-922

Yousuf, N., Olayiwola, O., Guo, B., & Liu, N. (2021). A comprehensive review on the loss of wellbore integrity due to cement failure and available remedial methods. Journal of Petroleum Science and Engineering, 207, 109123.

Zang, A., Oye, V., Jousset, P., Deichmann, N., Gritto, R., McGarr, A., et al. (2014). Analysis of induced seismicity in geothermal reservoirs – An overview. Geothermics, 52, 6–21. https://doi.org/10.1016/j.geothermics.2014.06.005

Zimmermann, G., Blöcher, G., Reinicke, A., & Brandt, W. (2011). Rock specific hydraulic fracturing and matrix acidizing to enhance a geothermal system—concepts and field results. Tectonophysics, 503(1-2), 146-154.

Zoback, M. D., & Gorelick, S. M. (2012). Earthquake triggering and large-scale geologic storage of carbon dioxide. Proceedings of the National Academy of Sciences, 109(26), 10164-10168.

Zoccarato, C., Bau, D., Ferronato, M., Gambolati, G., Alzraiee, A., & Teatini, P. (2016). Data assimilation of surface displacements to improve geomechanical parameters of gas storage reservoirs. Journal of Geophysical Research: Solid Earth, 121(3), 1441-1461.

Zomer, J. (2016). Middeleeuwse veenontginningen in het getijdenbekken van de Hunze: Een interdisciplinair landschapshistorisch onderzoek naar de paleogeografie, ontginning en waterhuishouding (ca 800-ca 1500). [, Rijksuniversiteit Groningen]. Rijksuniversiteit Groningen.

11.2 Websites

Centraal Bureau voor de Statistiek (CBS). (2021). Hernieuwbare energie in Nederland. Website: https://longreads.cbs.nl/hernieuwbare-energie-in-nederland-2021/ (Last accessed 22/11/2023)

Corre Energy (2023). Hydrogen Based Energy Storage. Website: https://correenergystorage.nl/caes/ (Last accessed 16/11/2023)

DINOloket (2024). Stratigraphic Nomenclature. Website: https://www.DINOloket.nl/en/stratigraphic-nomenclature (Last accessed: 01/02/2024)

Hystock (2024). HyStock is working on the first large-scale underground storage of hydrogen in the Netherlands. Website: https://www.hystock.nl/en (Last accessed: 08/03/2024)

ICS (2024). International Commission on Stratigraphy. Website: https://stratigraphy.org/chart (Last accessed: 01/02/2024)

IFCO (2024) https://www.ifco.nl/funderingsadvies (Last accessed: 01/02/2024)

IMG (2023). Instituut Mijnbouwschade Groningen. Website: https://www.schadedoormijnbouw.nl/ (Last accessed 30/11/2023)

KEM (2020). Knowledge Programme on Effects of Mining. Website: https://www.kemprogramma.nl (Last accessed 13/07/2023)

KNMI (2024). Magnitude of Completeness Maps for the Netherlands. KNMI data platform. Website: https://dataplatform.knmi.nl/dataset/access/netherlands-earthquake-magnitude-completeness-1-0 (Last accessed 10/05/2024)

LFG (2024). Stichting Laagfrequent Geluid. Website: https://laagfrequentgeluid.nl/ (Last accessed 09/05/2024)

Nedmag (2023). Bodemdaling door zoutwinning. Website: https://www.nedmag.nl/ (Last accessed 15/11/2023).

NPLW (2024) Warmteopslag, Website: https://www.nplw.nl/technieken/warmtebronnen/warmteopslag (Last accessed 15/03/2024)

WKOtool (2023) Ontdek de mogelijkheden van bodemenergie. Ministerie van Economische Zaken/RVO. Website: https://wkotool.nl/ (Last accessed 30/11/2023)

RCE (2024a). PanoramaLandschap Website/GIS viewer : https://rce.webgispublisher.nl/Viewer.aspx?map=PanoramaLandschap# (last accessed 14/02/2024)

RCE (2024b). HISTLAND Website/GIS viewer: https://rce.webgispublisher.nl/Viewer.aspx?map=HISTLAND# (last accessed 14/02/2024)

RCE (2024c). Erfgoedthesaurus. Website: https://thesaurus.cultureelerfgoed.nl/ (last accessed 14/02/2024)

RUG (2024). Landschappen van Noord-Nederland. Website: http://landschapsgeschiedenis.nl/ (last accessed 14/02/2024)

Solution Mining Research Institute (2023). Homepage. Website: https://www.solutionmining.org/ Last accessed 15/11/2023

Wageningen University & Research. (2023). Parameters grondwaterdynamiek. Website: https://www.wur.nl/nl/onderzoek-resultaten/onderzoeksinstituten/environmental-research/faciliteiten-tools/software-en-modellen/grondwaterdynamiek/parameters.htm (Last accessed 15/11/2023)

WKOTool (2024). WKO-bodemenergietool. Ontdek de mogelijkheden van bodemenergie. Website: https://www.wkotool.nl/ (Last accessed 08/03/2024)

11.3 Data sources

- AHN: https://www.ahn.nl/
- Bodemdalingskaart: https://bodemdalingskaart.nl/nl/
- BRO: https://basisregistratieondergrond.nl/
- DINOloket: https://www.DINOloket.nl/
- EGMS: https://egms.land.copernicus.eu/
- KNMI: https://www.knmi.nl/nederland-nu/seismologie/aardbevingen
- NAPinfo: https://maps.rijkswaterstaat.nl/geoweb55/

- NLOG: https://www.NLOG.nl/
- Stabialert: https://www.stabialert.nl/nl/

ANNEXES

ANNEX I. GEODETIC MEASURING TECHNIQUES

Geodetic Measurements for Ground Movement

Levelling and NAP

Technology

Levelling is the oldest and, to this day, a frequently applied method for measuring height differences. The concept is extremely simple. An instrument is placed level, perpendicular to the vector indicating the direction of gravity. Then the height difference between two beacons can be established (Figure 83. Levelling for establishing the NAP).

Figure 83. Levelling for establishing the NAP

By performing height differences in a continuous levelling operation, the height difference relative to a reference point can be established. In this way, a height network can be created. This method was applied in the Netherlands for the Normal Amsterdam Level (NAP). Starting from a reference point, originally located on the dam in Amsterdam, benchmarks were placed throughout the country and the height difference of this benchmark relative to the reference point was calculated. This height difference is the NAP height.

The first levellings for the NAP were carried out at the request of the Prussian government from 1875 (Weele, 1971). These measurements of the first precision levelling are now considered unreliable. The first reliable measurements in the Netherlands date from the second precision levelling of 1935. This makes the NAP a dataset with the longest history regarding height information in the Netherlands.

The NAP was never intended to establish ground movement and without additional processing layers, the NAP is also not suitable for this. Measurement errors, registration errors, and a lack of a probability model contribute to this. In the north of the Netherlands, additional levellings have been carried out for monitoring by the State Supervision of Mines, which are explicitly intended for monitoring ground movement. These measurements are often also included in the NAP calculations. To use the NAP for analyzing ground movement, outliers must be removed through statistical testing. It is much better to use the raw measurement data to determine ground movement, as described in section 5.3.3.

Properties

Time Span	From 1935
Covered Area	All of the Netherlands
Temporal Resolution	5 years (2)
Density	500 m
Geometric Quality of Subsidence	5 mm standard deviation (3)
Geometric Quality of Ground Stretch	n/a (4)

Time Span

The oldest available measurements come from the first precision levelling carried out between 1875 and 1885. These measurements are now considered unreliable. The second precision levelling began in 1926. The measurements in the Fryslân, Groningen, and Drenthe region were carried out between 1933 and 1935 (Waalewijn, 1979). These are therefore the oldest measurements that can be relied upon.

Temporal Resolution

For the NAP, the renewal frequency is ten years. However, a frequency of five years is maintained in the north of the country due to mining activities. Locally, the frequency is higher because additional measurements are or were carried out by the concession holders. These measurements are also included in the NAP.

Density

The median distance between the NAP benchmarks is 500 m, but there is a large variance in the distance between them. Most benchmarks are located along main roads. The distance along the road may be 500 m, but the distance perpendicular to the road can be up to 5 kilometres.

Geometric Quality of Subsidence

The standard deviation of the absolute heights in the NAP is about 5 mm. Better quality can be achieved by looking at the height differences between two benchmarks. A levelled height difference between two points 1 km apart is 0.5 mm. To ensure that the deformation analysis is carried out at the highest possible quality, it is best to use the raw measurement data for the deformation calculations. Section 5.3.3 revisits methods for using raw measurement data in deformation analysis.

Geometric Quality of Ground Stretch

The benchmark data is only available in height. Any horizontal stretch can only be derived from the data model-wise.

GPS/GNSS

For seasonal deformation changes, GNSS measurements are used in Norg and Grijpskerk. These are the most reliable data available to monitor the deformations at these locations. The GNSS receivers are mounted on deeply founded structures. They provide continuous height measurements which are available through NLOG.

A comprehensive study by van der Hoek et al. (2018) demonstrated the accuracy and effectiveness of GPS measurements in detecting surface subsidence and uplift, providing real-time data for subsurface deformation analysis. The research revealed that the GPS-based monitoring approach offered valuable insights into the geomechanical behaviour of the salt caverns and their surrounding rock mass during gas injection and withdrawal operations.

Additionally, a study by Peters et al. (2021) highlighted the use of continuous GPS measurements in detecting temporal variations in ground movements at the Grijpskerk and Norg storage sites. The researchers demonstrated that the GPS monitoring system allowed for early detection of potential anomalies, enabling operators to take timely actions to prevent subsidence-related risks and ensure the safety of the storage facilities.

Furthermore, GPS data has been integrated into advanced geomechanical models to predict the long-term behaviour of the storage reservoirs. Research by de Jong et al. (2020) showed that the combination of GPS measurements with geomechanical simulations improved the understanding of subsurface stress distribution and deformation mechanisms, aiding in the optimization of gas injection and withdrawal strategies.

Due to the continuous nature of the measurements, seasonal changes at Norg and Grijpskerk can be monitored. In this work, we will attempt to correlate the measurement data from these GNSS receivers with both NAP levelling data as well as the InSAR data (see following section), that latter which also have a sufficiently high temporal frequency to detect seasonal changes.

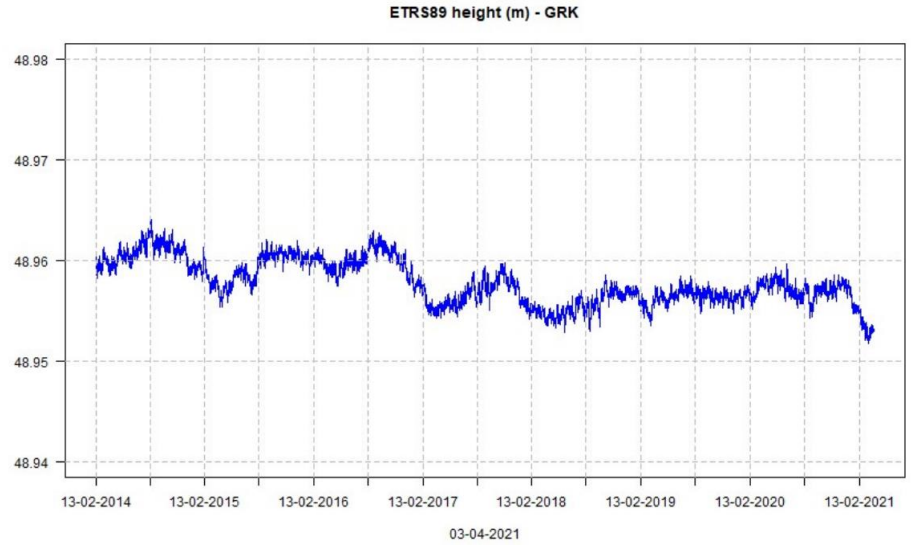

Figure 29. Continuous GPS measurements at the location Grijpskerk [Source: NLOG]

Radar Interferometry

Technology

Radar interferometry from satellites, known as Interferometric Synthetic Aperture Radar (InSAR), is a revolutionary technique that has become essential in monitoring and measuring ground movement. InSAR uses the principle of radar interferometry, which is based on comparing phase information from radar images of the same area obtained at different times. This comparison makes it possible to obtain very accurate measurements of surface deformation, on the order of millimetres to centimetres.

The operating principle of InSAR is that radar beams are transmitted from a satellite to the earth's surface. These beams are reflected and received by the satellite, where the phase information is stored. By comparing the phase information from two or more images, the relative change in position of the surface can be derived (Hanssen, 2001).

An important concept within InSAR is Persistent Scatterers (PS) interferometry. Persistent Scatterers refers to points within a radar image that exhibit high reflectivity and stable phase properties over time. This means they give a stable radar response in multiple radar images, making them very suitable for detecting small changes in surface height. PS interferometry allows for reconstructing a time series of surface deformations. Even though the PS-InSAR points are represented as individual points, the source of the deformation signal is, in general, less accurately known. Geolocation estimates of PS-InSAR are known with metres precision at best, depending on the sensor (Dheenathayalan et al., 2016), but generally allow for analysis up to street level (Ketelaar et al., 2006).

There is currently a large constellation of radar satellites for performing interferometry (Figure 84). The oldest data dates to 1992, but for reliable analyses, it is best to fall back on data from Radarsat-2, TerraSAR-X, and Sentinel. The Sentinel data is freely available and makes historical analyses possible from around 2016 (Bovenga, 2018).

SAR wavelengths, commonly known as bands, are identified by letters like X, C, and L. The choice of wavelength is crucial in SAR applications because it influences the interaction of the radar signal with the surface and its penetration depth into various materials. For instance, X-band radar, with a wavelength around 3 cm, has limited ability to penetrate dense foliage, primarily interacting with the uppermost leaves of the tree canopy, but allows for a high resolution due to its smaller wavelength. Conversely, an L-band radar, with its longer wavelength of about 23 cm, can penetrate deeper into forests, enabling more substantial interactions with thicker branches and tree trunks, but will result in low resolution modelling. The Sentinal data is observed in the C-band, which provides a middle ground for a range of InSAR applications. The TerraSAR-X data is observed in the X-band and therefore allows for more detailed calculations. This is particularly useful in urban environments, where the more precise geolocation and high resolution allow for better analysis of the deformation of urban structures (Roth, 2005). A comparison of radar bands is presented in Table 9.

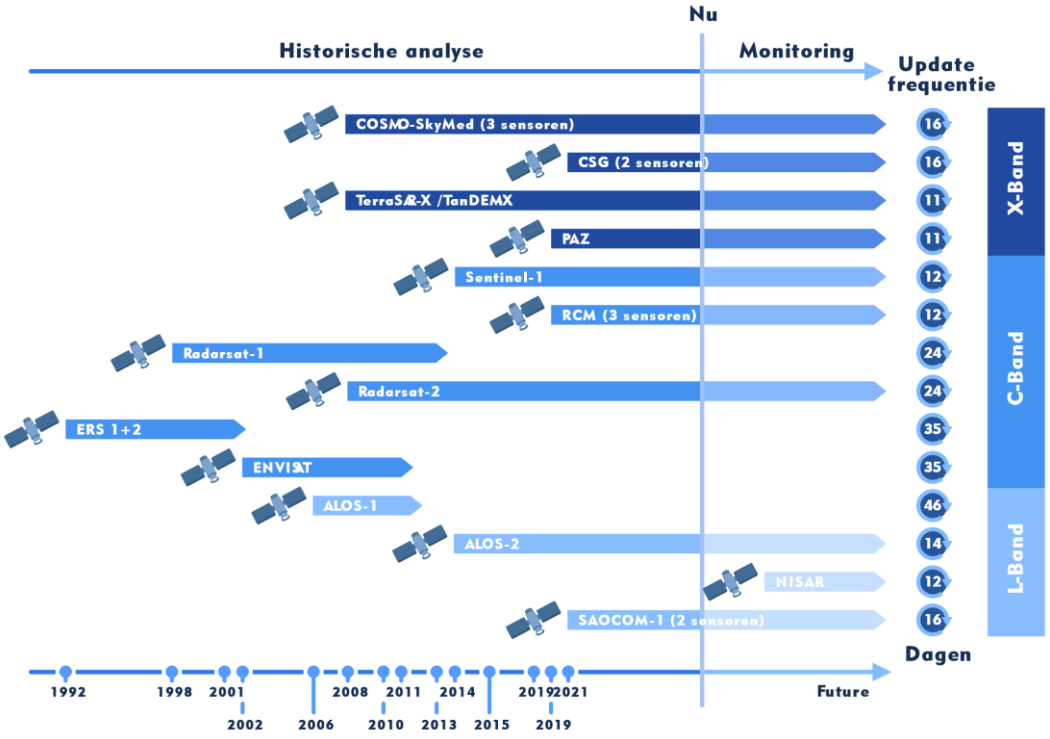

Figure 84. Radar satellites in the past, now, and in the future.

Table 9. Comparison of radar bands for InSAR processing (after Meyer, 2019)

Band	Frequency	Wavelength	Applications
X	8–12 GHz	3.8–2.4 cm	Detailed SAR Imaging, ideal for urban monitoring and tracking ice and snow.
C	4–8 GHz	7.5–3.8 cm	SAR Workhorse, used for global mapping and change detection.
S	2–4 GHz	15–7.5 cm	Little but increasing use for SAR-based Earth observation; agriculture monitoring (NISAR will carry an S-band channel; expends C-band applications to higher vegetation density).
L	1–2 GHz	30–15 cm	Medium resolution SAR, useful for geophysical monitoring, biomass and vegetation mapping)

The radar signal is transmitted at an angle. Depending on the satellite and the location on earth, this angle is between 20 and 30 degrees relative to the vertical. The line that runs under this angle from the satellite to the point on the earth is the Line-Of-Sight (LOS). The deformation established from multiple measurements relates to the movement in this direction (Figure 4). This is therefore not a vertical ground movement.

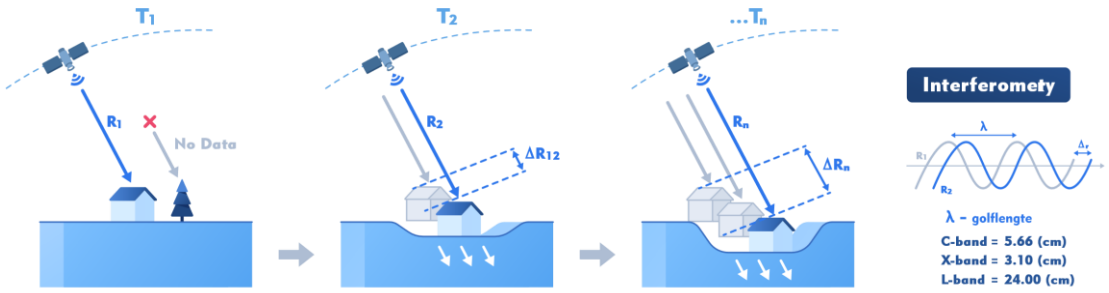

Figure 85. Establishing ground movement in the Line-Of-Sight (LOS)

There are techniques for deriving vertical ground movement from this diagonal movement. One method is to assume that there is no horizontal movement. By tilting the point accordingly, the vertical component can be calculated.

Another approach is to combine InSAR data from two different directions. If it can be established for a point that it has been observed from two directions, both a horizontal component and a vertical component can be determined (Brouwer, 2021). In practice, this means reporting an east-west movement and a vertical movement. A possible north-south movement is difficult to determine due to the dominant north-south direction of the satellite orbit. Figure 86 shows a section of north of the Netherlands with the east-west movements according to EGMS.

Based on the Sentinel data, a ground movement map is available for all of Europe. This map can be found at https://egms.land.copernicus.eu/. Both the vertical and east-west components can be requested via this service. Note that for distinguishing these two components, model assumptions have been made that are not necessarily the best for the Netherlands. For example, EGMS uses a grid of 100m x 100m and all points therein are averaged (Ferretti, Passera, & Capes, 2023) and combined into one point. This causes a lot of detail at the building level to be lost. Furthermore, it is important that the movements are displayed relative to a GNSS network that has the best fit for all of Europe. Since the Netherlands is tilting (post-glacial uplift), this is not the best fitting reference for the Netherlands. Further, there is a risk of errors in the determination of phase ambiguity. This can particularly be the case with very large horizontal shifts. Therefore, an unusual value in the EGMS cannot be concluded to indicate a problem without prior research.

On the other hand, the EGMS is very easily available and offers a wealth of insight. This makes the EGMS highly suitable for an initial inventory, after which detailed studies can be carried out at locations noticed in the EGMS. For these detailed studies, for example, a detailed study with TerraSAR-X can be carried out. A combination with NAP data based on an analysis of the raw height measurements is recommended in this, but this still requires some research.

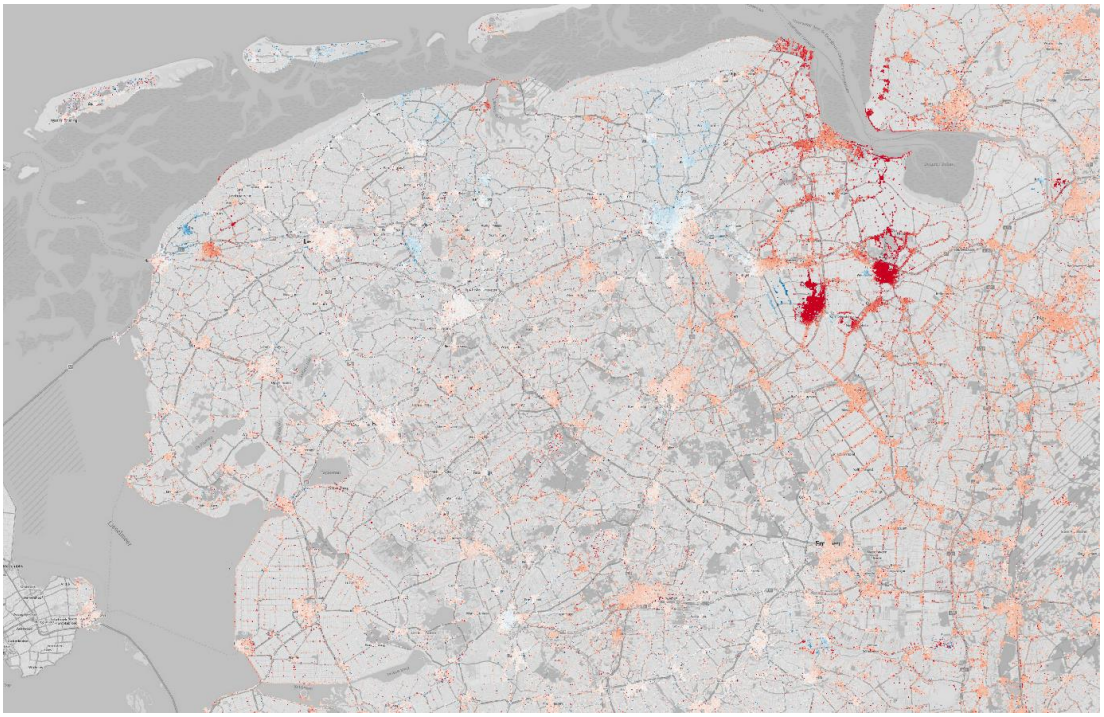

Figure 86. Horizontal ground movement according to the EGMS.

Properties

Time Span	From 2010 (TerraSAR-X) or 2016 (EGMS via Sentinel)
Covered Area	Entire world
Temporal Resolution	Two days
Density	Varies. In EGMS 100m x 100m
Geometric Quality of Subsidence	Precision of the trend: 1mm/year (EGMS)
Geometric Quality of Ground Stretch	Precision of the trend: 1mm/year (EGMS)

Time Span

The timespan is the period over which this data is available. See Figure 84 for the time span of different satellites.

Temporal Resolution

The temporal resolution depends on the satellite and the location on earth. The temporal resolution can be higher than the revisit time of the satellite. With each overflight, the Radarsat-2 satellite scans a 250-km wide strip of the Earth's surface. Towards the poles, these overflight paths overlap. This means that data are acquired more often. Consequently, in the Netherlands, a temporal resolution of 2 to 3 days is achievable.

Density

In urban areas, the persistent scatterers, the stable points on which a deformation analysis can be carried out, can have a density between 5 and 10 meters. This density is entirely dependent on the presence of sufficient stable reflective points. In rural areas, the density is much lower with virtually no points in pastures and in arable farming. For area-covering analyses, it is common to combine multiple points into a grid. The EGMS, the European Ground Monitoring Service, uses a grid of 100 meters for this purpose.

Geometric Quality of Subsidence

The EGMS reports a precision of 1mm/year. Note that there may be systematic errors as described in the introduction (Kotzerke, 2022).

Geometric Quality of Soil Strain

The EGMS reports a precision of 1mm/year. Note that systematic errors may be present as described in the introduction (Kotzerke, 2022; Brouwer, 2021).

Laser Scanning (AHN)

Technology

Airborne Laser Scanning (ALS), also known as Light Detection and Ranging (LiDAR), is a technology used to create detailed and accurate 3D models of the earth's surface. The technology is based on the emission and reception of laser pulses from a sensor typically mounted on an aircraft or drone.

The operating principle of ALS is relatively simple. A laser beam is emitted from the airborne sensor and reflected off objects on the ground. The reflected laser beam is then detected by the sensor. The distance between the sensor and the object is calculated based on the time it takes for the laser beam to return to the sensor (time of flight) and the speed of light. By combining these distance measurements with the exact position and orientation of the aircraft at the time of each pulse (usually obtained using GPS and an Inertial Measurement Unit), a very precise 3D point of the surface can be calculated (Figure 87).

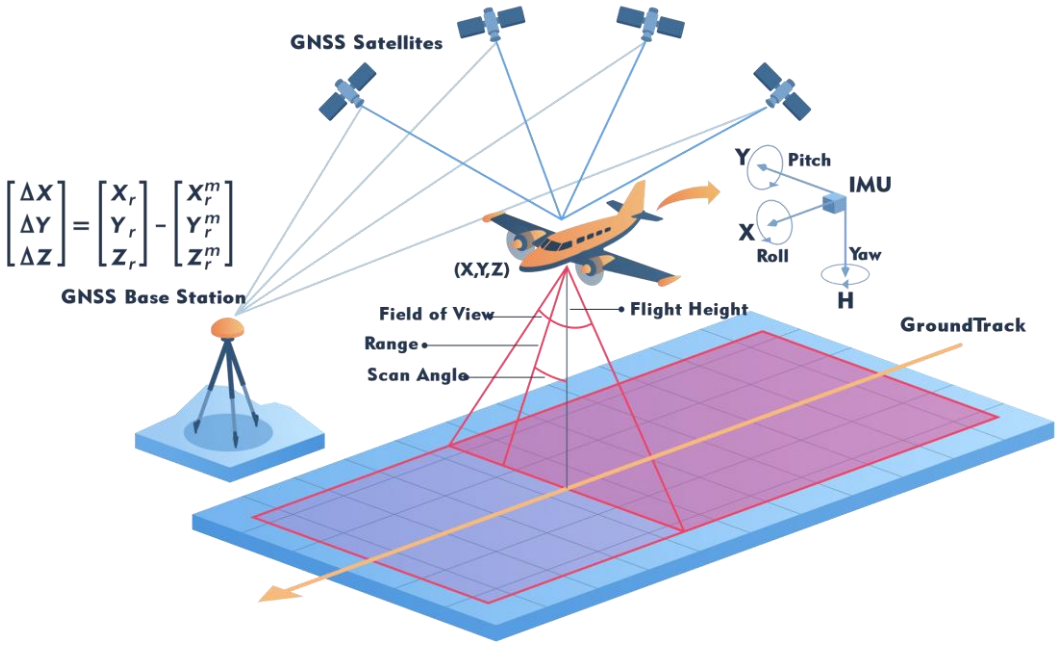

Figure 87. Operating Principle of Airborne Laser Scanning

Since 1997, Airborne Laser Scanning has been used to create a national elevation database called the Actueel Hoogtebestand Nederland (AHN). A 3D visualization of the AHN is shown in Figure 88. The AHN is inherently unsuitable for determining soil movements smaller than 16 centimetres. Geodelta, in collaboration with Het Waterschapshuis, has developed a new calculation methodology that allows soil movement from the AHN to be calculated with centimetre-level precision. However, this soil movement refers only to shallow subsidence.

Figure 88. The AHN4 Visualized in the City of Groningen

Properties

Time Span	From 2019 (1)
Covered Area	All of the Netherlands
Temporal Resolution	3 years
Density	6 to 14 points per m^2
Geometric Quality of Subsidence	5 cm stochastic and 5 cm systematic
Geometric Quality of Soil Strain	Maximum error of 80 mm

Time Span, Temporal Resolution, and Density

The following table shows the recording times for the AHN in the Groningen region.

Edition	Acquisition Period Groningen	Density
AHN1	1997-1999	1 point/16 m^2
AHN2	2009	6 to 10 points/m^2
AHN3	2019	6 to 10 point/m^2
AHN4	2022	10 to 14 points/m^2
AHN5	2025	10 to 14 point/m^2

Geometric Quality of Subsidence

From AHN2 onwards, the specifications require that the height component must have a quality of 5 cm stochastic and 5 cm systematic. This means that points in the AHN may have a systematic shift of up to 5 centimetres. Additionally, there may be a noise band of 5 cm. Due to unfavourable wording in the specifications, there can be a systematic shift of up to about 8 centimetres in practice.

This means that when comparing two datasets, the error in height can be up to 16 centimetres.

Geodelta has developed a new methodology to perform a better height comparison. This work is done for analysis in peat meadow areas, where there is typically little reflection present from InSAR data. This methodology is deployed with the AHN3 as a reference point. The data from the AHN2 is unsuitable for this purpose. With this methodology, a precision of soil subsidence can be achieved at the centimetre level. However, it explicitly concerns shallow subsidence. This means that the AHN is unsuitable for determining

deep subsidence. Yet, this information could be useful for GEMMA, for example, for determining the consequences of changes in groundwater levels. An integration with both NAP data and InSAR data would be very interesting from an academic perspective.

Geometric Quality of Soil Strain

The requirements set in the AHN for horizontal positioning are very broad. An error of up to 80 centimetres is allowed. It is technically feasible to use the AHN to determine relative displacements between buildings over a distance of up to 100 meters at the centimetre level. However, this is custom work.

Photogrammetry

Photogrammetry is a technique that derives geometry from photos. The principle involves measuring points on the terrain from multiple photos, allowing a 3D coordinate to be calculated from the intersection of multiple photos (Figure 89).

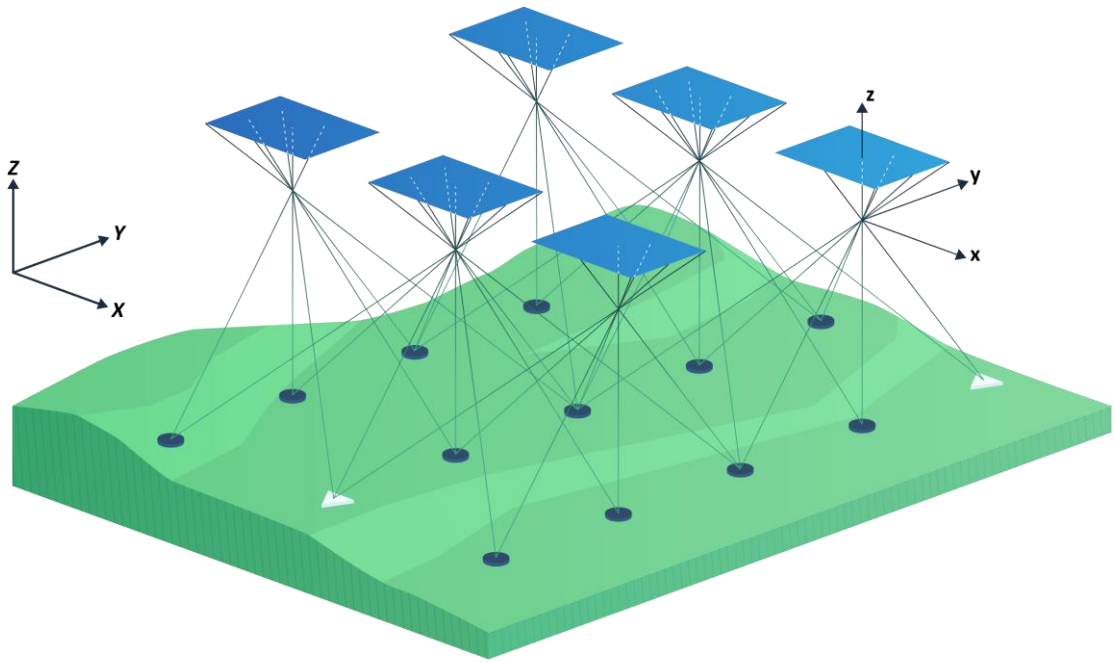

Figure 89. Operating Principle of Photogrammetry

The beauty of photogrammetry is that this technique is scale independent. This means that photogrammetry can be used at short distances and over very long distances. The achievable quality is directly dependent on the distance between the photo and the object. Geodelta has developed software to determine deformations in quay walls photogrammetrically with a precision of 2.5 mm. If the same technique were deployed from aerial photos, a precision in the order of centimetres would follow.

We mention the technology here because there is a long history of aerial photos in the Netherlands. The archives with photogrammetric recordings go back to the middle of the last century. Determining vertical and horizontal soil movement from these photos is, however, very labour-intensive and would provide insufficient precision for the application of the IMG.

Drones also commonly use photogrammetry. At a sufficiently low flying height, it is possible to achieve centimetre-level precision with drones. However, there is currently no history of drone images that can be used to look back in time.

Gravimetry

The gravitational field generated by the earth due to its mass, known as gravitational force, affects all objects. In addition, rotating objects on Earth experience a centrifugal force. The combined action of these forces results in what we call gravity. Interestingly, when the earth moves vertically - such as during processes of deep subsidence, the gravity on a co-moving object increases. Tracking these gravity fluctuations can therefore help identify vertical soil movements.

Advanced gravimeters, developed to follow this phenomenon, are capable of detecting gravity changes significantly smaller than the general gravity. The use of these instruments offers a unique advantage over other measurement techniques described earlier in this report, namely that they can measure absolute soil movements. However, it is important to recognize that to obtain an accurate measurement of absolute soil movement, long-term observations are necessary at specifically selected locations.

In the Netherlands, we have been actively monitoring gravity at various locations since the 1990s. TU Delft has been conducting these observations annually since 2005, resulting in a network of six stations (Kootwijk, Westerbork, Epen, Zundert, Oudemirdum, and Texel). Westerbork and Epen have the most extensive and accurate time series, while the Oudemirdum and Texel stations are relatively new and still in the early stages of data collection.

The importance of these gravity measurements lies in evaluating the stability of the NAP zero level. This level is established by stable-assumed underground marks on the Veluwe and the Utrechtse Heuvelrug. The assumption is that the height of these points does not change over time. It is questionable whether this assumption is correct. Gravity measurements can measure this.

The importance for determining deep subsidence lies in the fact that a possible tilting of the NAP zero level is not visible in the analysis as described in the previous section Radar Interferometry. For the analysis of subsidence at the building level, however, this effect is considered negligible, so we do not elaborate further.

ANNEX II. GEOMETRY MODELS FOR DEFORMATION ANALYSIS

Everyone involved in subsidence in Northern Netherlands seems to know that measuring subsidence amounts to measuring the heights of points at two or more points in time and subtracting these heights. However, this is just a very simple geometric model. We will hereafter call this simple model the basic geometric model. This model does not suffice in many cases. There are various reasons for this, which are related to:

- the definition of the concept of height;
- the measurement noise, measurement errors, temporal noise, and the uncertainty of measurement, geometry, and geomechanical models;
- the scaling in space and time.

These will be discussed in more detail in the following sections.

Definition of the concept of height

Subtracting two measured heights of the same point to determine a deformation is different from subtracting, for example, two measured lengths of a rod, first measured at 0°C and then at 20°C. With the rod, the starting point and endpoint are clear. This is not the case with a height measurement. Should we go to the zero point in Amsterdam for a height measured relative to NAP? We will go into this in more detail later. It will become clear that the measured height difference of one point has no value. This undermines an important premise of the basic geometric model.

Noise, measurement errors, and uncertainty of models

A difference in height measured at two different times is not only the result of, for example, ground movement, but there are also other causes.

- The measurement noise of the levelling instrument causes small differences in the observations. This is unavoidable. The possible size of the differences is described by the standard deviation.
- Errors were made in conducting the measurements, which were not noticed, despite the control measurements.
- The measurement model is incorrect. For example, the measurement model assumes that the light beam went in a straight line from staff to levelling instrument, but variations in temperature caused by hot asphalt have made the light beam wobble.
- The geometry model or the geomechanical model is incorrect, or both are incorrect, or they are only roughly correct, which means they are an oversimplification or only valid under certain conditions.

To get a good estimate of ground movement, it is necessary to know how large the mentioned noise, errors, and uncertainties are. The basic geometric model cannot make any statements about this and therefore does not suffice. To be able to make a statement about it, the observations must be tested against the models to separate noise and model from each other. This is sometimes called separating signal and noise, where the model is equal to the signal. Sometimes the term signal is reserved for deviations and details of the model, which are part of the model, but in the calculations are treated as noise, i.e., as a stochastic phenomenon.

Separation of noise and model by adjustment

In geodesy, it is good practice to ensure that there are always control measurements. Because each observation is checked in some way, all observations can be adjusted. This means that they are adjusted so that they collectively meet the model.

What “the model” is can be illustrated with an example. Suppose there are five levelling bolts, named A, B, C, D, and E. The bolts are placed in buildings, and the shortest distance between two bolts is 500 m, and the largest distance is 3 km. With a levelling instrument, height differences between benchmarks are measured, with the distance between two benchmarks being approximately 60 m. Starting with a benchmark at bolt A, levelling is done in 60 m strokes to point B, then to C, to D, and finally to E. Then the “levelling circle” is closed by levelling directly from E back to A. The resulting height of A must correspond to the starting height of A. In other words: all height differences measured in the circle must add up to zero. This is the first “condition”. Then direct levelling is done from A to C and finally from C to E. This provides two additional conditions and there are various ways to form circles, of which the measured height differences should add up to zero. We choose the circles: ABCA, ACEA, CDEC. Through an adjustment using the method of least squares, the measured height differences are adjusted so that the observations meet the three circle conditions (the sum of the height differences in the circle is zero).

The three circles form the model, and we say that the adjusted observations meet the model. This not only tracks errors in the observations, but the adjusted observations (the adjusted observations) also have better precision (smaller standard deviation) than the unadjusted observations.

For determining subsidence, a second model is then used, the deformation model. To set up the deformation model, we assume that later, for example, a year later, the height differences between the five levelling bolts A, B, C, D, and E are measured again. We carry out an adjustment again and note that the adjusted height differences strongly resemble the height differences measured a year earlier but are slightly different. There are various causes for the changed height differences, such as measurement noise, temporal noise, and of course deformations, such as subsidence.

The deformation model states that either the height differences between the five points at the first and second points in time are the same or have undergone a change. The change is caused, for example, by the subsidence of two points, C and D. There are three possible ways to determine the extent of the subsidence of both points.

Basic Geometric Model

The most common is the basic geometric model. From the adjusted height differences, the heights of the five points are first calculated for each of the two measurement times. The heights are entered into a spreadsheet, and the differences between the first and second measurement moments are calculated. These differences are considered as subsidence. The problem that now arises is that all points will show differences between the two times. Therefore, a threshold value is chosen, below which a difference is not considered as subsidence or deformation. Choosing a threshold value is difficult to substantiate statistically. Usually, an experiential value is chosen without proper justification.

If height differences are not measured, but measurements are made from which two- or three-dimensional coordinates (2D or 3D) are calculated, a similar approach is used. The x and y coordinates (2D) or x, y, and z coordinates (3D) are entered into a spreadsheet and the differences are calculated for each type of coordinate (x, y, z). Again, a threshold value is needed.

The choice of the threshold value is not the only problem. Directly comparing coordinates from two different times means that the reference systems at both times must have been the same. It involves operationally defined reference systems, which depend on the choice of the base. These concepts are explained further on. Here, it is only noted that the operational definition causes inaccuracy. As a result, this inaccuracy directly affects the calculated differences. This can be prevented by transforming the coordinates of the second time. This involves a similarity transformation or a congruence transformation. In the first case, a rotation, translation, and scaling are applied; in the second case, only a rotation and translation. For height measurements, only a translation is performed. Often the transformation parameters are calculated by making the coordinates of one, two, or three points, respectively in 1D, 2D, and 3D, equal at both times. We call this point, or these points the base, calculation base, or scaling base. The problem is that the coordinate differences calculated afterward depend on the scaling base: a different base choice gives different coordinate differences. It is possible to choose the base as a kind of average of all points, which makes the effect slightly less, but it

would be better to estimate deformations in a way that is independent of the base. And that is possible but is rarely done in practice.

We note that in the basic geometric model:

- coordinates are calculated per point in an operationally defined reference system.
- a similarity transformation or a congruence transformation of all coordinates of the second time to the reference system of the first time is needed.
- coordinate differences dependent on the base are calculated per point between two times.
- the coordinate differences are compared with a threshold value that is not statistically substantiated.

In the basic geometric model, the calculated coordinate differences are compared with the threshold value to test which differences represent a deformation. The coordinate differences are also the estimate of the size of the deformation. Unfortunately, the coordinate differences are not optimally suited for testing and are not the optimal estimates of the deformations. A different approach must be chosen for statistically justified testing. The testing must be done by calculating the ratio between a function of the coordinate differences and the precision with which those differences have been determined. This allows for the testing to be performed. The estimate of the size of the deformation can then be calculated in such a way that the estimate does not change if a different scaling base is used. Before we describe how this works, we first describe how an adjustment can make a better estimate of the deformations.

Adjustment per Point

It is possible - we return to the example just given of the five levelling bolts A, B, C, D, and E - to make an assumption about the subsidence, for example, that it is proportional to time (a point sinks the same distance each month). Then we can carry out an adjustment of the subsidence, giving us an estimate in millimetres. It is customary to perform the adjustment for a single point for all times of measurement. This is also referred to as filtering or regression. If the formulas of the regression are linear (this is not explained here), it is a case of linear regression.

By adjustment, the noise is separated from the model. From the previous sections, it has become clear that both the noise and the model consist of different parts, namely different types of noise and different sub-models. The types of noise and their behaviour are described in the probability model. The different sub-models are in the function model. Formulating the probability model and the function model correctly is crucial for drawing the right conclusions. It is often difficult to obtain good numerical values (usually standard deviations and correlation coefficients) for all types of noise and good (mathematical) descriptions for all sub-models. It is important always to make at least an estimate of the order of magnitude of the neglects, if simple assumptions for standard deviations, correlations, and sub-models are taken.

The adjustment provides a better estimate of the movement a point has undergone than directly taking the coordinate difference at a certain time. But if the coordinate differences are base dependent, the adjusted values are also base dependent. This can be done better, and that is described in the following third method of determining the deformations.

Integral Adjustment of the Point Field

The third way to determine the deformations is the integral adjustment of the point field, which has been measured at two or more times (Velsink, The Elements of Deformation Analysis - Blending Geodetic Observations and Deformation Hypotheses, 2018).

When using the basic geometric model - the first way to determine deformations - the differences are calculated between two times. When adjusting each point separately - the second way to determine deformations - measurements from more than two times are used. We have seen that there are two problems

for both methods: 1.) the choice of the scaling base and its influence on the calculated coordinate differences, and 2.) the lack of statistical substantiation for the threshold value. The integral adjustment of the point field overcomes these two problems. A brief description follows. The adjustment is described in more detail in (Velsink, Statistical Testing of Deformations, 2020).

The adjustment starts with the observation that if no point of the point field has moved relative to any other point of the point field, the calculated coordinates of all points at the first, second, and each subsequent time should be the same.

In this case, it is assumed that the various sub-models accurately describe reality. If there are differences, they must be explainable as measurement noise or temporal noise, or possibly as a residual signal. The adjustment ensures that the coordinates of each point for all two or more times get equal values. For this, all coordinates need corrections. These corrections are the basis for testing, but more is needed. In the least squares adjustment, the standard deviations of these corrections are also calculated. Now, dimensionless functions of the corrections and their standard deviations and correlations can be calculated, which are independent of the base and can be statistically tested for significant deformations. They are the test variables. The threshold value is now called the critical value and is statistically substantiated.

If test variables are rejected, the question arises as to which points have moved due to deformation. To this end, one or more points are 'released' in the adjustment. This means that it is not required for that point or those points that the coordinates are the same for all times. The differences after adjustment are thus the least squares estimates of the deformations.

It is important that the test variables are independent of the base. This is achieved by transforming the coordinates of each time to a reference time, for example, the time of the zero measurement. This must be a similarity transformation or a congruence transformation because we are interested in deformations, that is, changes in shape or size (Latin: forma = shape; deformation = shape change). A similarity transformation leaves the shape of the point field unchanged; a congruence transformation leaves the shape and size unchanged. After the transformation, the remaining differences can only be explained by a change in shape or size, or by a deformation.

By the similarity transformation or the congruence transformation, two sets of coordinates of the same point field are brought to the same scaling base. Not only the coordinates must be transformed but also the standard deviations and correlations. These are combined for an entire point field in the so-called covariance matrix. Therefore, we say that the covariance matrix must be scaled to the base of the reference time. For height measurements, the transformation is usually one-dimensional and involves only a shift (= translation) and possibly a scale change (the latter is generally not necessary because the scales of measuring instruments and the NAP differ very little from each other). It may be that the heights do not change through the transformation, but the covariance matrix does.

Section 3.5 addresses the concept of scaling. For this, it is necessary to understand how the national reference systems are defined in the Netherlands. Therefore, this will be discussed first.

Dutch National Reference Systems

The concept of scaling is used in geodesy to indicate that for practical applications, coordinates and heights are calculated in an operationally defined reference system. There are various types of coordinates, such as Cartesian or rectilinear coordinates, spherical coordinates, ellipsoidal coordinates, cylindrical coordinates, barycentric coordinates, and so forth. Here we limit ourselves to rectilinear coordinates, although for geodesy other types of coordinates are also important. For this discussion, it is sufficient to consider only rectilinear coordinates. Heights are regarded here as coordinates in a one-dimensional reference system.

Two national geodetic reference systems are important for monitoring subsidence in the Netherlands: The Rijksdriehoeksmeting system (RD system) and the Normaal Amsterdams Peil (NAP system).

The RD system allows points in European Netherlands to be fixed with an x and a y coordinate on a flat plane. This plane intersects the globe with a circle, which has the Onze Lieve Vrouwetoren in Amersfoort as its center and a radius of about 122 km. The globe is assumed to be an ellipsoid according to the parameters established by Bessel. The position of the ellipsoid relative to the Earth was determined in the early twentieth century by first conducting directional measurements in a triangulation network with sides of about 30 km. Then, the entire network was positioned relative to the Netherlands through astronomical measurements at several observatories. From this, the RD coordinates of the national triangulation network were derived. These RD points form the operational definition of the RD system. In 2000, the definition of the RD system was changed so that its basis is now formed by nineteen points spread across the Netherlands, which are continuously fixed in position using GPS and other positioning systems. These are the points of the Active GNSS Reference System. The RD system is managed by the Kadaster.

Heights of points in European Netherlands can be recorded relative to the NAP system. The zero point of this one-dimensional system is in Amsterdam, but this point is not stable. Like the RD system, the NAP system is operationally defined by many points spread across the Netherlands. These points together form a network. The network is regularly measured with precision levelling. The fifth national precision levelling in 2004 led to adjustments in the heights of all NAP points. The stable basis of the NAP system is formed by several points on the Veluwe and the Utrechtse Heuvelrug. The NAP system is managed by Rijkswaterstaat. Rijkswaterstaat and the Kadaster work together to use RD and NAP as a joint three-dimensional network.

To determine the position of points, GPS is almost always used directly or indirectly (and more broadly, Global Navigation Satellite Systems (GNSS), which includes the American GPS, the European Galileo, the Russian Glonass, the Chinese Beidou, and other satellite positioning systems). A GNSS receiver provides the coordinates of the center of the antenna in the World Geodetic System 1984 (WGS84). This reference system uses an ellipsoid that has different parameters and is positioned differently relative to the Earth than the ellipsoids of the RD and NAP systems. Therefore, a transformation is needed, which causes additional inaccuracy, especially for height. The height is less accurately determined because only satellites well above the horizon can be used and because a model of the Earth's gravitational field (the geoid) is needed for the transformation.

It should be noted that GNSS can be used directly for positioning, but is also used for positioning drones, airplanes, and satellites, which are employed for other positioning techniques (photogrammetry, remote sensing, InSAR).

Precision of a Point Field

Usually, when discussing the required precision of a point, what is meant is the possible deviation that the coordinates of the point can or may have (hereafter, the term 'coordinates' also refers to heights). It's about deviations from the actual position. As a measure of these deviations, the standard deviation is commonly used in Europe. Although this interpretation of a point's precision is common, it is problematic. Four reasons can be mentioned for this:

1. The precision of a point only has meaning in relation to a point field of at least three (1D and 2D) or four points (3D).
5. Defining what the term 'true value' means is not simple.
6. The statistical correlation between coordinates is, alongside the standard deviation, an important part of the precision of a point field.
7. The standard deviation is different from the maximum spread.

This will be elaborated in the following four subsections.

Precision of a Point is Relative

From the previous section, it has become clear that it is not possible to measure the coordinates of a point directly in the RD and NAP systems, i.e., to directly measure the position and orientation relative to the coordinate axes. This also applies to measuring coordinates in a local system. One must determine the position

of a point in a geodetic network relative to points whose coordinates are already known, the base points. If one uses a local reference system for their network (which could range in size from a hundred by a hundred meters to an entire province), one must first create a base. Even when using GNSS, a ground network is used, usually a network that is commercially offered or managed by the government, so one does not have to set it up themselves.

The consequence is that it is pointless to talk about the precision of a single point. One must always mention (which unfortunately rarely happens) in relation to which base the precision is defined. An example of where this went wrong is the height of the first platform of Den Haag Centraal station. This height was set during construction relative to a different base bolt than the heights of the other platforms. The height difference is clearly visible. Note that NAP heights were used. Due to the operational definitions of the RD and NAP systems, there is not one RD system and one NAP system, but each time a new operational definition is realized through the choice of base points.

In deformation measurements, it is about changes in the shape and size of objects on, under, or above the earth's surface, of that surface itself, or of the earth. In the flat plane, you can talk about the shape of a triangle, not the shape of a straight line. Therefore, three points are needed to discuss shape. They together form a point field, and three points are the smallest possible point field. In three-dimensional space, the smallest possible point field consists of four points, which together form a tetrahedron.

Suppose we want to establish the precision of three points in the flat plane with standard deviations. The three points form a triangle, and we want to know the precision of the shape and size of the triangle to say something about the precision of a deformation of the triangle. We have determined the coordinates of the three points from measurements and want to do so again later for deformation analysis. We are not interested in the position of the triangle relative to the RD or NAP system. Those systems might assist in deformation analysis, but if it can be done without them, that is also fine. To determine the precision of the triangle, we first need to choose a scaling basis. This means that we select arbitrary values for three coordinates of the triangle, for example, one of the points gets the coordinates (0,0) and another point the coordinates (100 m, y), with y being an unspecified value. Now the standard deviations of the remaining three coordinates can be calculated from the measurements (and their standard deviations), which are used to calculate the coordinates. We see that for this field of three points the standard deviations are related to a scaling basis (also known as a calculation basis or S-basis) of three coordinates. Each standard deviation of an x or y coordinate in the flat plane is relative to a scaling basis of three coordinates. A scaling basis can also consist of more points, but the calculation technique required for this is not discussed here.

A point field whose x, y, and z coordinates in three-dimensional space are known requires a scaling basis of six coordinates from at least three points. In one-dimensional space (heights determined from height difference measurements), the concept of shape is not immediately obvious, but can be defined by the ratio of two height differences. From this, it follows that a scaling basis of three points is needed.

The conclusion is that standard deviations of coordinates in a point field are always relative to a scaling basis. Naming a standard deviation without specifying this relation can lead to errors.

True Value

A standard deviation is described above as the deviation from the true value. But how is the true value defined? This is a philosophical question and touches on whether and how we can know the world. We will not go into it extensively here. We limit ourselves to the observation that our measurements provide an estimate of something that we think might be the true value. The precision of that estimate is thus also difficult to define. We use different measures, such as standard deviation, to describe precision and base their definitions on statistics, which means repeating measurements, making histograms, calculating numbers for those histograms, and so forth. We hope to make a good statement about the precision of the measurement results with this.

Correlation of Coordinates

The standard deviation is a measure of the precision of a coordinate. For an accurate description of precision, it is important to also have information about the statistical correlation between coordinates, both between the two or three coordinates of the same point and between coordinates of different points. Nowadays, we are accustomed to receiving measurements in large quantities. Without further discussion, it is usually assumed that all these measurements are independent of each other, meaning that each measurement is a new piece of information that says something about reality. However, this is often not the case. The measurements are often heavily correlated. This means that, for example, out of a million measurements, perhaps only a hundred are independent of each other, and the rest contain no additional information. Let's illustrate this with a very simple example.

Let's measure a distance of 100 meters between points A and B twice. We do this with a laser distance meter, which we know (from calibration) has a standard deviation of 2 mm. We average the two distances and wonder what the standard deviation of that average is. A standard statistics book tells us that the standard deviation is √n times smaller than the standard deviation of a single measurement. In this case, it's $2 / \sqrt{2} \times 2$ mm ≈ 1.4 mm. The precision thus improves, as the standard deviation of 2 mm decreases to 1.4 mm. Measuring twice makes sense.

Now let's assume that the two measured distances are correlated. A common measure for correlation is the correlation coefficient, a number between -1 and +1, where 0 indicates no correlation, +1 indicates full positive correlation (if one variable increases, the other also increases) and -1 indicates full negative correlation (if one variable increases, the other decreases). Let's take the correlation coefficient as 0, 0.5, and 0.9999, respectively. We calculate the standard deviation of the average by applying the method of least squares. We get the following table with the standard deviation of the average (s.d. avg.) for four values of the correlation coefficient (c.c.):

c.c.	s.a. avg.
0	1,41 mm
0,5	1,73 mm
0,9	1,95 mm
0,999	1,99 mm

With a correlation coefficient of 0.9999, the second measurement hardly adds anything extra. The observation could just as well have been omitted.

For a point field measured with laser scanning or with InSAR, this means that much less valuable information may have been collected than it appears at first glance.

Measures of Spread

The standard deviation is a commonly used measure to describe precision. If it concerns a single variable that follows a normal distribution (Laplace-Gauss distribution), we can draw a diagram indicating the standard deviation. This has been done on the internet. It shows that only 68% of the measurements stay within the standard deviation. This is because the standard deviation is a kind of "average deviation", and it is very possible that measurements have a value that, loosely speaking, falls outside it. Therefore, often not the standard deviation, but twice the standard deviation is taken as a measure. The value "two" is then the rounding off the number 1.96. This number is the value within which, loosely speaking, 95% of the observations remain, for a single variable. If there are more variables involved (as with two- or three-dimensional coordinates), other values apply.

This means that no value of the standard deviation says anything with 100% certainty about the maximum spread a measurement can have. Values can be calculated for 95%, 99%, or 99.9%, but these are not standard deviations. Often in such cases, we talk about confidence intervals.

Scaling in Space and Time

In the previous sections, various reasons have been mentioned why the basic geometric model does not suffice for good deformation analysis. In this section, we specifically focus on the reason that an analysis with the basic geometric model is dependent on scaling in space and time. We have seen in section 3.3.1 what a scaling basis is. It concerned a scaling basis in space. In section 3.3.3, we saw how a testing of deformations can occur that is independent of the spatial scaling basis. Scaling in time is also necessary. A deformation is measured from a certain moment in time. That zero time is the scaling basis in time. Choosing the zero time is challenging. Points disappear and new ones are created. There are few points where the height position has been recorded throughout the entire period for which information is desired. Moreover, the geographic distribution of the points is usually not regular. An additional problem is that different measuring techniques use different points.

Through functional models and covariance functions (Kriging, collocation, Kalman filter, etc.), everything can be calculated in relation to each other (Kenselaar & Quadvlieg, 2001), both in the three spatial dimensions (x, y, z), and in time. In doing so, it is important to keep a close eye on where the scaling bases are located and how the similarity transformations or congruence transformations should be performed.

ANNEX III. GEODETIC DEFORMATION ANALYSIS IN THE NETHERLANDS

We have seen that for geodetic deformation analysis, geodetic models (consisting of measurement models and geometry models) and geomechanical models are needed. The geometry models have been examined in more detail to show how estimates of deformations should be determined and how their precision should be described. In this chapter, we look at the way geodetic deformation analysis is performed in the Netherlands. There are seven sectors in the Netherlands for which geodetic deformation analysis is essential:

1. Residential and utility construction. In the construction and maintenance of structures, geodetic deformation analysis is mainly used to monitor desired and undesired movements of the work itself and the environment. The private sector and the government are active here: project developers, construction companies, national services, provinces, and municipalities. An important role is played by the Association of Insurers, where construction companies insure themselves against damage caused by themselves. For these so-called CAR insurances, the insurance companies set requirements, including that adequate monitoring takes place.
2. Hydraulic engineering and water infrastructure. In the construction and maintenance of waterways, ports, and other surface water, and in the construction and maintenance of the water supply, geodetic deformation analysis ensures the monitoring of movements caused by human actions and natural causes. Especially the government is active here: Rijkswaterstaat, the water boards, the provinces, and the municipalities.
3. Road infrastructure. Monitoring the roads for movements is crucial for the safety of transport and the environment in the construction and maintenance of roads. Especially the government is active here: Rijkswaterstaat, the provinces, and the municipalities.
4. Rail infrastructure. The construction and maintenance of railways and tramlines require a lot of monitoring. The positioning of the rails must be good to the millimetre level and remain so, the ground should not move, and the environment should not suffer any damage. ProRail is an important player here, as well as the municipalities that operate tramlines.
5. Mining. The extraction of minerals (coal, gas, oil, salt, etc.) requires a lot of geodetic deformation analysis.
6. Industrial installations. Oil refineries, water purification plants, large industrial complexes, etc., cause movements of their own installations and structures, of the ground, and possibly of the environment. Monitoring of this is needed.
7. Long-term movements of the earth's surface (continental drift, earthquakes, movements due to climate change, etc.). Research into the long-term movements of the earth's surface is mainly carried out at academic universities.

Within these seven sectors, three major clients operate, whose influence on geodetic deformation analysis extends further than just their own task setting. Their influence is great because they continuously outsource work concerning geodetic deformation analysis on a considerable scale, for which they publish guidelines that are detailed and thereby help determine what is seen as good and bad geodetic deformation analysis. These are Rijkswaterstaat, the NAM (with the State Supervision of Mines (SodM) as the regulating government agency), and ProRail. The guidelines of these organizations are briefly mentioned here.

1. Rijkswaterstaat publishes a product specification for performing deformation measurements of structures (Rijkswaterstaat, 2020). This protocol is also used in the tendering of work by many other clients (municipalities, water boards, contractors, etc.).
2. State Supervision of Mines (SodM) took the initiative in the last century to develop a guideline for the execution of deformation measurements (Tcbb, 2014). The guideline was developed in consultation with the mining companies, including NAM as the largest. The guideline is managed by the Technical Committee on Soil Movement: https://tcbb.nl.
3. ProRail has guidelines for measuring a geometric basis and for absolute track geometry.

The following paragraphs discuss which of the geometry models, discussed in paragraphs 3.3.1 to 3.3.3, are used by whom.

Rijkswaterstaat: basic geometry model

In the product specification for deformation measurements on structures of Rijkswaterstaat (Rijkswaterstaat, 2020), the basic geometry model discussed in paragraph 3.3.1 is used. Therefore, the previously described disadvantages of this model also apply to this product specification. These can be mentioned:

- Being able to compare only two points in time with each other.
- The heavy weight of the results of the initial measurement compared to the other measurements.
- Not using available precision information in the deformation analysis.
- Drawing conclusions based on coordinate differences and not on statistical tests.
- The point-wise approach (not as a point field).
- The dependence of the conclusions on the choice of the adjustment base.

TU Delft: modelling per point

On December 14, 1990, a cooperation agreement was signed for the research project 'Geodetic Deformation Analysis' between the Nederlandse Aardolie Maatschappij B.V. (NAM), the Surveying Service of Rijkswaterstaat (MD), and the Laboratory for Geodetic Computing Techniques (LGR) of the Faculty of Geodesy of the Delft University of Technology. This resulted in a final report (De Heus, Joosten, Martens, & Verhoef, 1994) and a software package, SCAN-1DEFO. The method developed in the research is based on levelling measurements and consists of two phases. In the first phase, the geodetic network of levelling measurements is adjusted according to the least squares method and tested for stability. In the second phase, a polynomial is estimated per point, using the adjusted heights of all points in time at which measurements were taken. This is the method described in paragraph 3.3.2. The method is characterized by the disadvantages mentioned there.

TU Delft/NAM Integral adjustment of point field

The article by (Kenselaar & Quadvlieg, 2001) describes a method that corresponds to what is described in paragraph 3.3.3: an integral adjustment of the point field. About the method described in the previous paragraph 4.2, the following is stated in the introduction of the article:

Although this procedure worked quite well, certain drawbacks were experienced. Absolute deformation analysis, by connection of the levelling networks to stable benchmarks, was complicated by the expanding subsidence area and the suspicion of unstable reference points. Stability analysis, in order to identify stable reference points, turned out to be the most difficult part of the data processing. Moreover, the benchmark-oriented analysis was frustrated because many benchmarks disappeared during the years, and new benchmarks in larger levelling networks had to be established to cover the growing subsidence area. Finally, the smooth spatial and temporal character of the subsidence bowl was not fully exploited in the analysis. Although it was possible to estimate spatial-temporal polynomials to model the behaviour of local groups of benchmarks, their interpretation was rather indiscriminate.

Ir. F. Kenselaar (TU Delft) and Ir. R.C.H. Quadvlieg (NAM) proposed an alternative, which in the author's opinion of this note is the best proposal for carrying out subsidence analyses. What this method adds to the method of the previous paragraph 4.2 is that covariance functions are used to combine measurements without common points. The technique used for this is known under many names and has many variants: Kriging, collocation, Kalman filter, Wiener-Kolmogorov filtering, smoothing, etc.

TU Delft/NAM: integrated geodetic processing.

In addition to levelling, GNSS and InSAR have become important new techniques for subsidence measurements in this century. (Van Leijen, Van der Marel, & Hanssen, 2021) describe the way, according to the current insights of Delft University of Technology, these different techniques can be used together to arrive at the best possible estimate of subsidence. Specific software has been developed for this purpose (called Integrated Geodetic Processing [IGP]), which can process massive amounts of measurement data using transformations and specialized data storage.

Soil movement and NAP points

The soil movement caused by mining must be monitored according to the mining law. The State Supervision of Mines (SodM) supervises this on behalf of the government. On behalf of the SodM, the mining sector has drawn up a guideline for monitoring (Tcbb, 2014).

The idea of using the NAP heights of thousands of bolts published by Rijkswaterstaat to analyze what movements these bolts have undergone is not new. In a conversation with Bas Alberts, an employee of Rijkswaterstaat, he said that he had already performed such calculations before, but he did not publish the results because he finds them too unreliable: there is too little known about the earlier calculations of the heights and there is too little known about the location and subsoil of the bolts.

According to the aforementioned guideline of SodM:

- Benchmark movements are not necessarily representative of soil movement due to mining activities. Autonomous movements and identification errors cannot be detected in a 'per epoch' analysis.
- Only time series with the same reference point and the same starting epoch can be directly compared with each other.
- The result of the above two points is that interpolation of the subsidence signal is not representative. The results can only be viewed at benchmark level.
- The guideline also contains much information about the correct handling of benchmarks and the interpretation of their heights and height differences.

Geodetic deformation analysis method of Velsink

In the dissertation by Velsink (Velsink, The Elements of Deformation Analysis - Blending Geodetic Observations and Deformation Hypotheses, 2018), it is described how an integral adjustment and validation of a point field for geodetic deformation analysis, as described in section 5.3.3, can be carried out. For the dissertation, software was developed to perform the described methods. The software includes the packages CoDefAn and MeDefAn. This software is more specifically designed for geodetic deformation analysis than the software package that is the de facto standard in the Dutch geodetic market, MOVE3. The following points are mentioned as advantages of the method:

1. Advanced methods have been implemented to search for the best deformation hypothesis.
2. The unchanged status of points in a time interval can be strictly tested ("hard" restrictions are tested), and their threshold values (at what value does a deformation exceed a specified chance of detection?) can be calculated.
3. Unlike traditionally used methods, the method does not require stable points to perform the deformation analysis. The deformations that are detected are movements of parts of the point field relative to other parts of the point field. The point field is chosen as large as necessary to detect those movements that pose risks or that are relevant for any application.
4. Unlike many traditionally used methods, more than two points in time of measurement are analyzed simultaneously, so that trends can be estimated through least squares adjustment.
5. In two government-subsidized research projects (DefoGuide and ValidDefo), the methods were validated in collaboration with a broad representation of the professional field of geodetic deformation analysis. The

reports describe, among other things, how the methods can be used for standardization of geodetic deformation analysis (Velsink, Final report of the DefoGuide project, 2016).

Meanwhile, the method is being applied in practice, for example for deformation monitoring with photogrammetry, see Geodelta (Geodelta, 2023), for which the geodetic technique was used (Kodde & Velsink, 2020).

ANNEX IV. SALT SOLUTION MINING CONFIGURATIONS

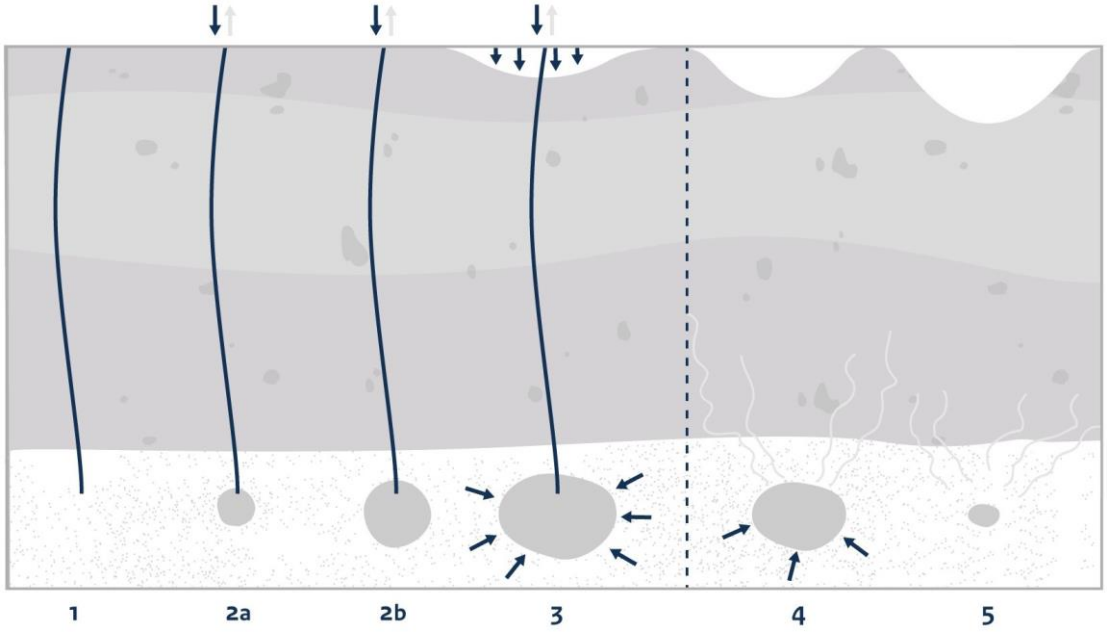

Figure 90. Schematic of the different phases in the salt solution mining process. From: SodM (2018)

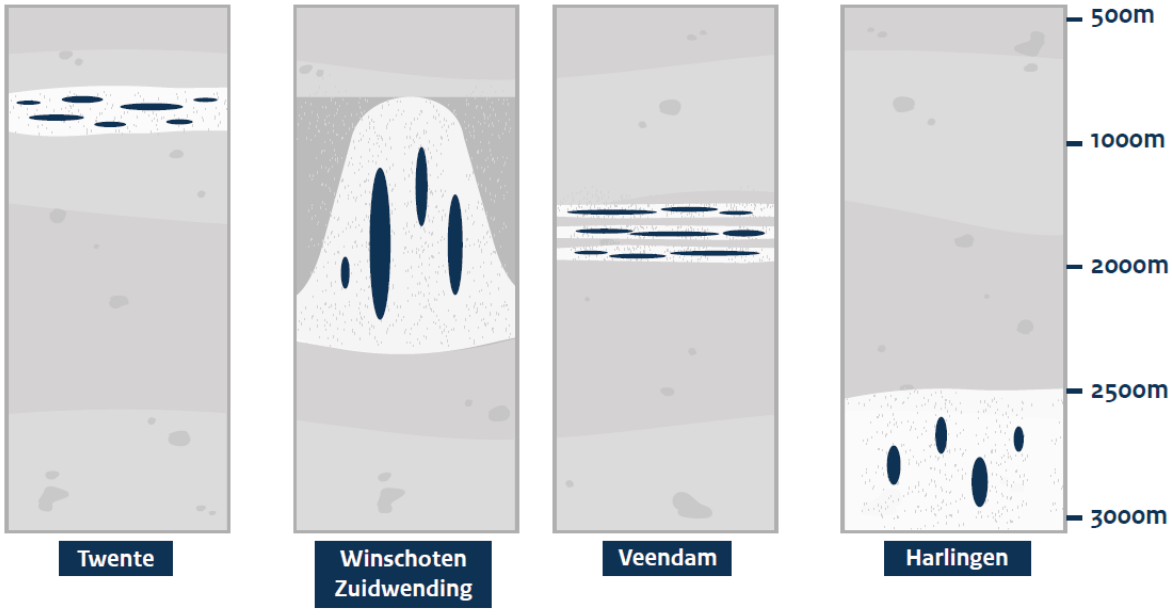

Figure 91. Schematic representation of the shape and depth of the various forms of salt extraction occurring in the Netherlands, in relation to the salt layer from which the extraction takes place. From: SodM (2018).

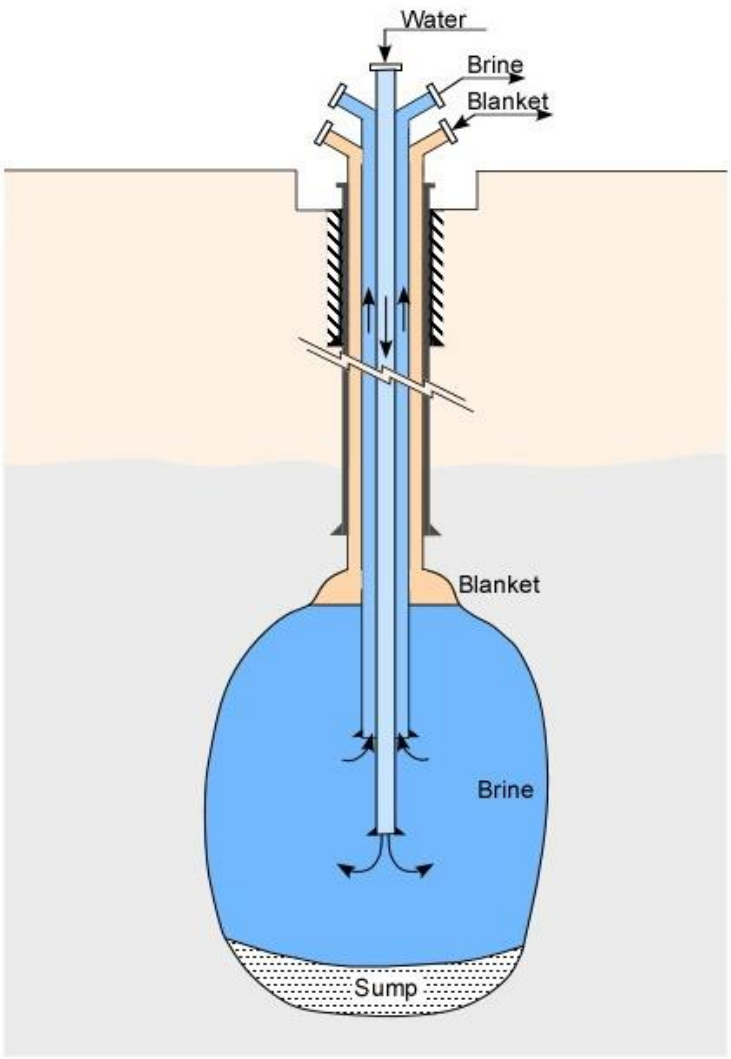

Figure 92. Illustrations of salt solution mining created cavern. From: Solution Mining Research Institute (2023)

ANNEX V. MAPS STUDY AREA

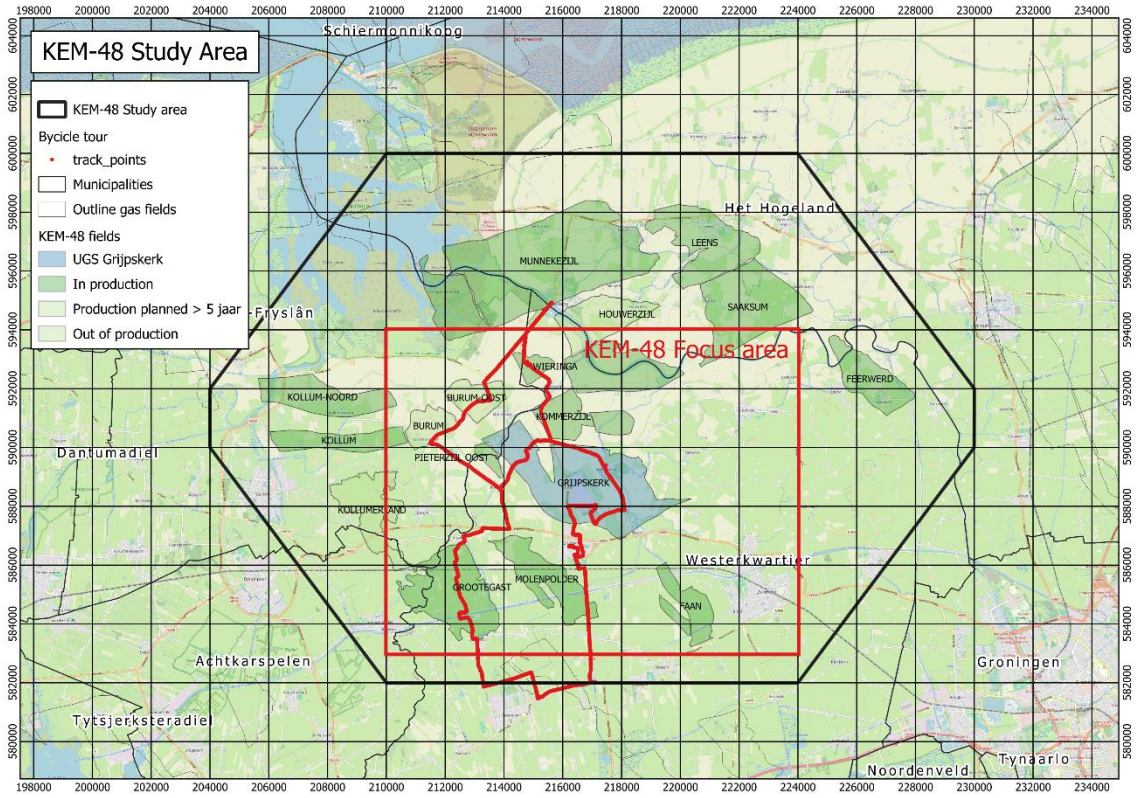

Figure 93. Case study area outline, with focus area in red. In red dots the route of the field visit.

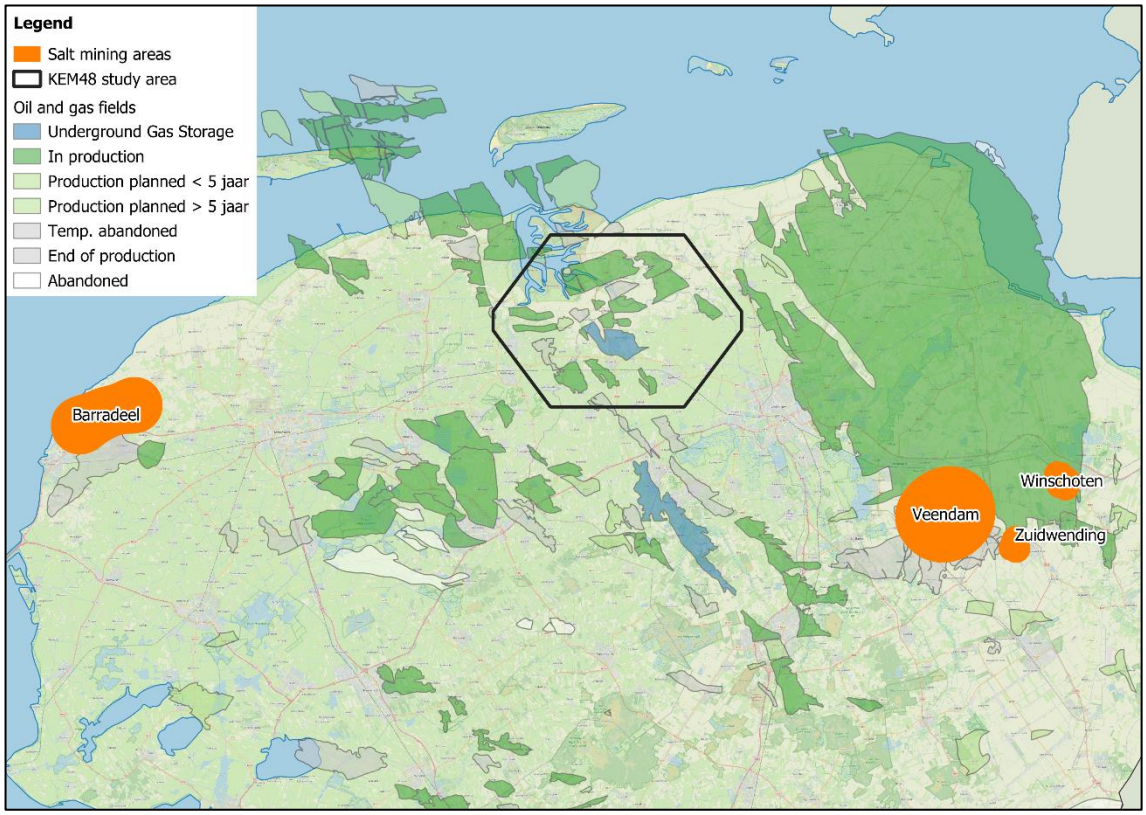

Figure 94. Location of the four salt mining areas in the northern part of the Netherlands. Currently, the Barradeel operations is abandoned and shifted offshore outside Harlingen.

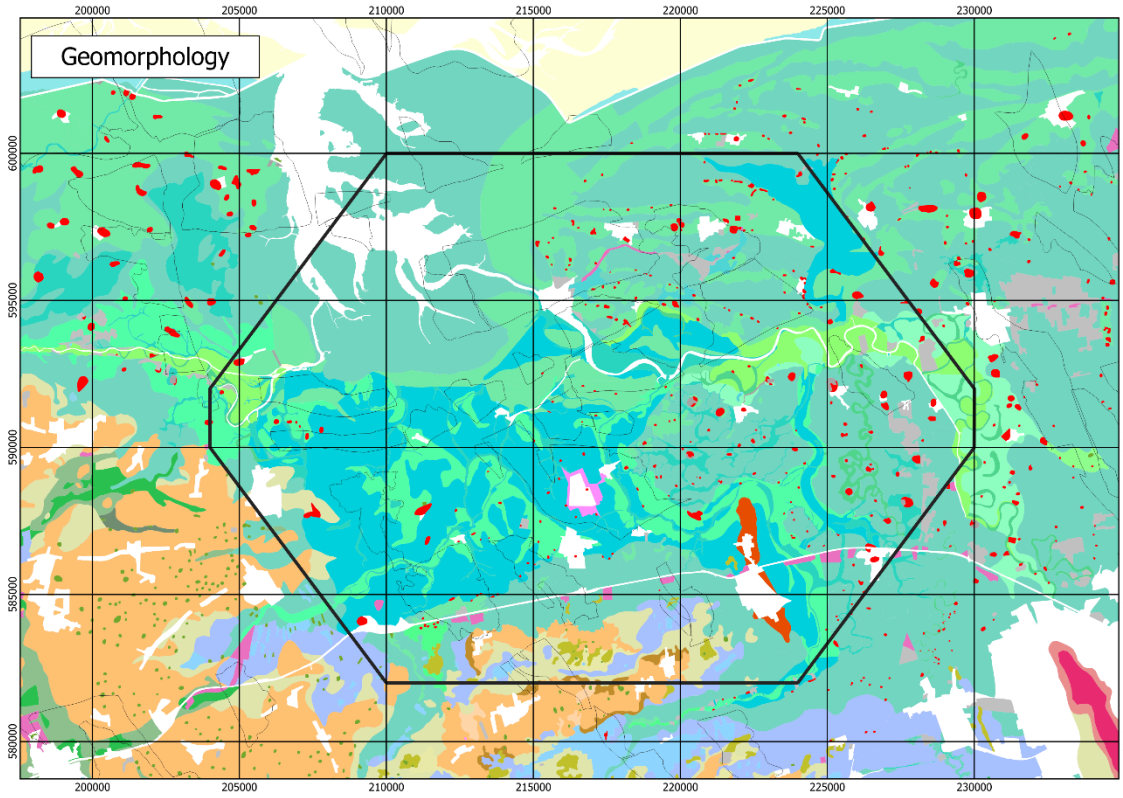

Geomorphology legend

KEM48_studyarea
Gasfields outline
BRO-GMM-DownloadGeomorfologischekaart_V2023-01_1
geomorphological_area
Grondmorenerug
IJsstroomheuvelrug, 'megaflute'
Dekzandkopje
Getij-inversierug
Getij-oeverwal
Getij-riviermondrug
Kwelderwal
Terp (wierd) of hoogwatervluchtplaats
Plateau-achtige storthoop, opgehoogd of opgespoten terrein, of kunstmatig eiland
Grondmorenegloolling of smeltwatergloolling met resten van grondmorene
Gloolling van hellingafspoelingen
Grondmorenewelvingen
Dekzandwelvingen
Storthopen met grind-, zand-, kleigaten of ijzerkuilen
Vlakte van grondmorene
Rivierkom- en oeverwalachtige vlakte
Dekzandvlakte
Vlakte van ten dele verspoelde dekzanden of löss
Vlakte van getij-afzettingen
Vlakte van getij-riviermondafzettingen
Zeeboezemvlakte
Strandvlakte, zandplaat of slik
Aanwasvlakte
Ontgonnen veenvlakte
Ontgonnen veenvlakte met petgaten
Boezemland, vlietland, moerassige vlakte
Vlakte ontstaan door afgraving en/of egalisatie
Rivier-erosielaagte, kolk/wiel
Uitblazingskom
Zee-erosielaagte
Laagte ontstaan door afgraving
Droogdal
Dalvormige laagte
Beekdalbodem
Restgeul
Getij-kreekbedding, zee-erosiegeul

Figure 95. Geomorphological map (Source: BRO/DINOloket)

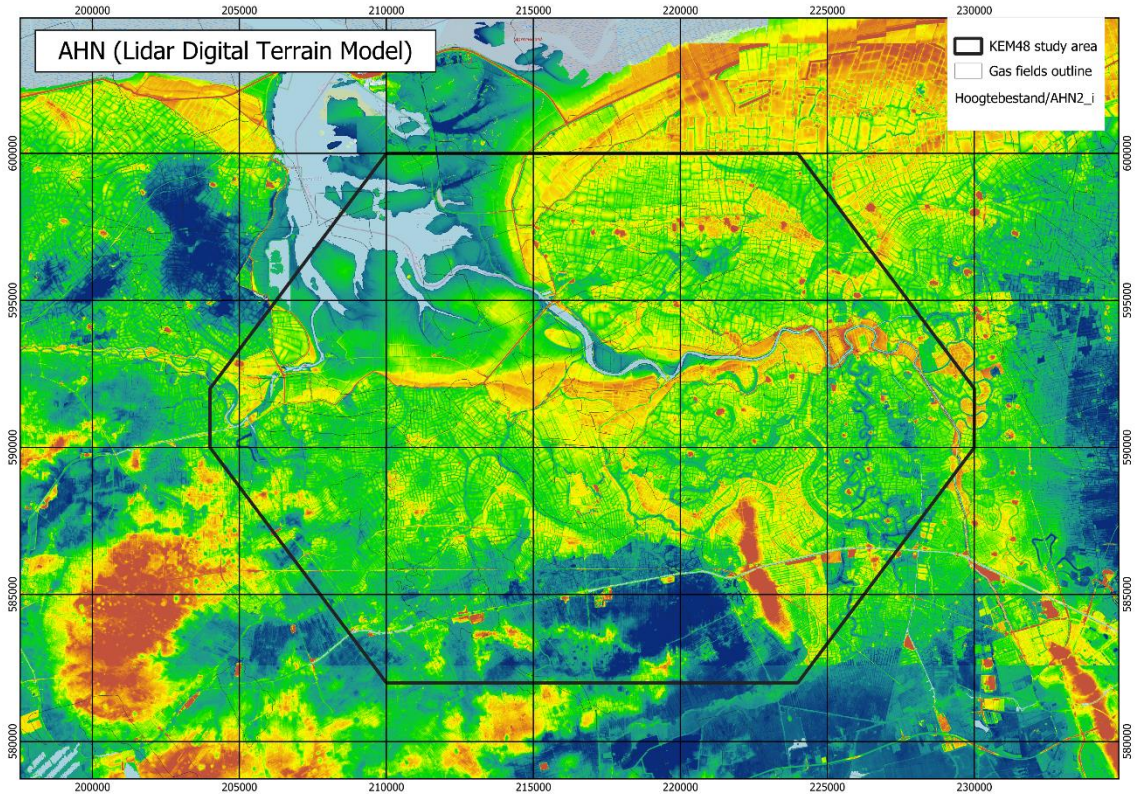

Figure 96. Map of the case study area with AHN (lidar) digital terrain model.

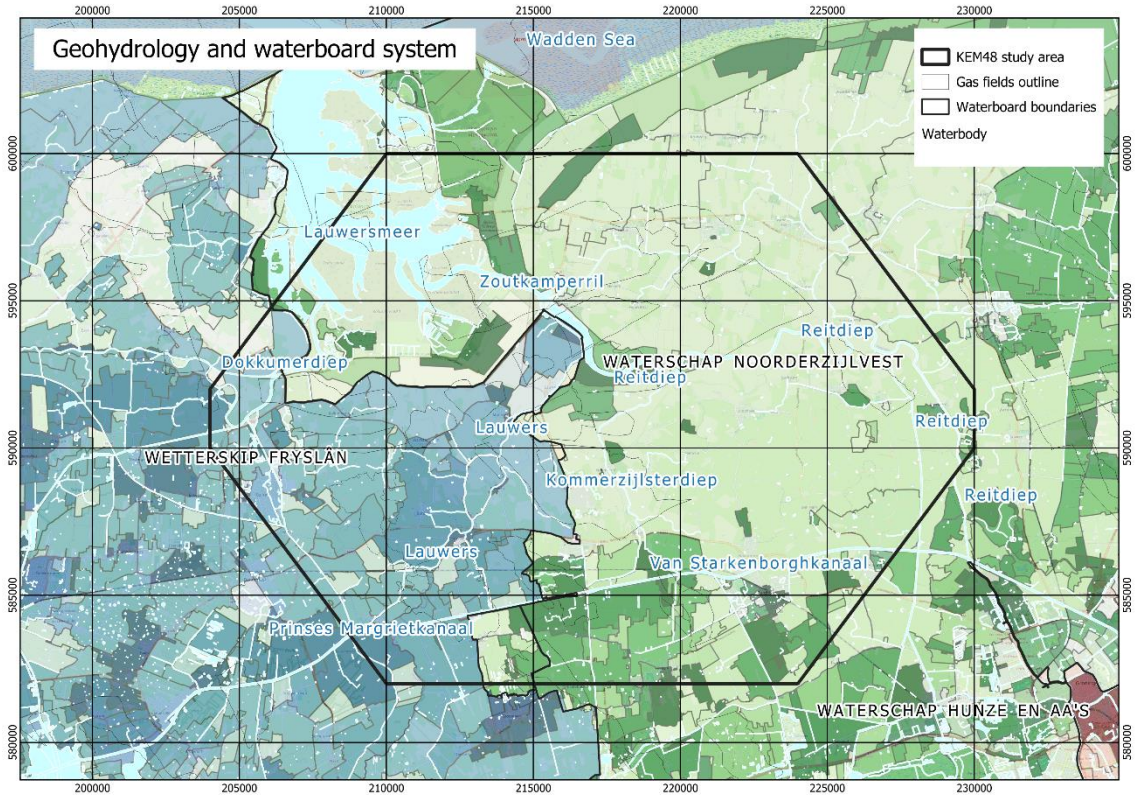

Figure 97. Geohydrology and waterboard system.

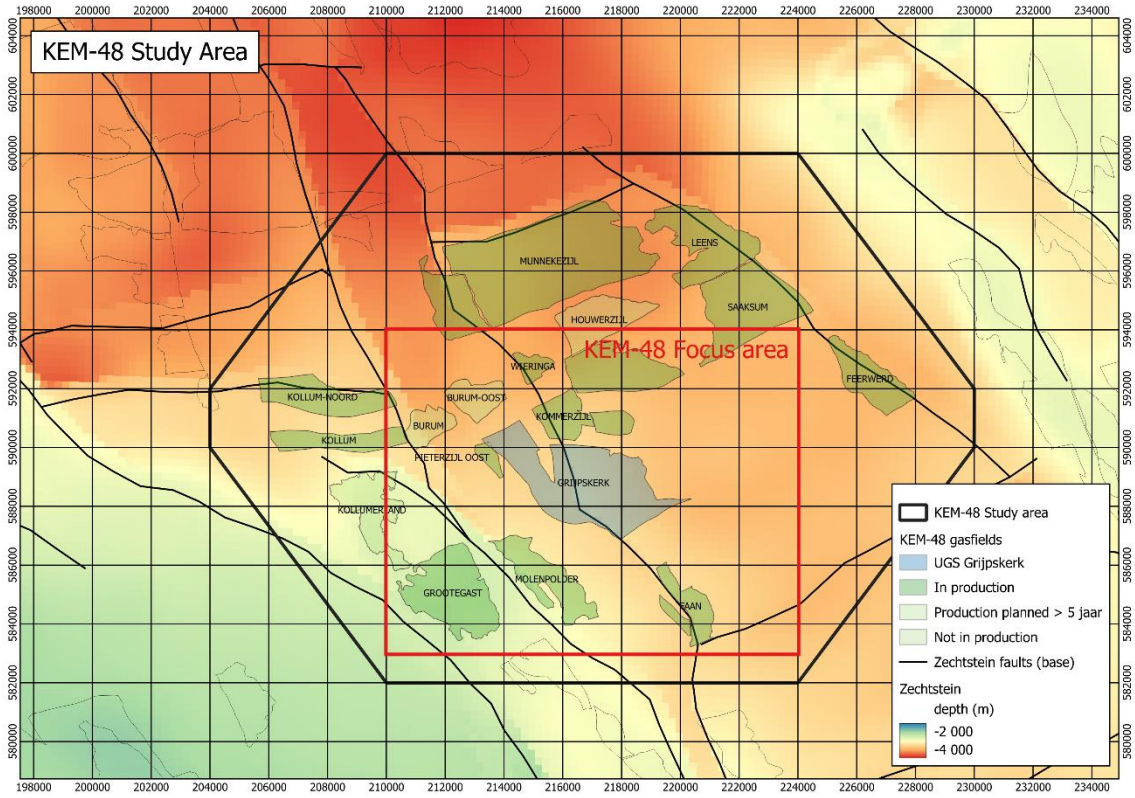

Figure 98. The depth of the base of the Zechstein salt layers (top of Rotliegend reservoir sandstone) with the outline of the gasfields (GWC) in the case study area. The structure of the Lauwerszee Trough is clearly visible also in this map. Compare also with the thickness map of the Zechstein (see Figure 46).

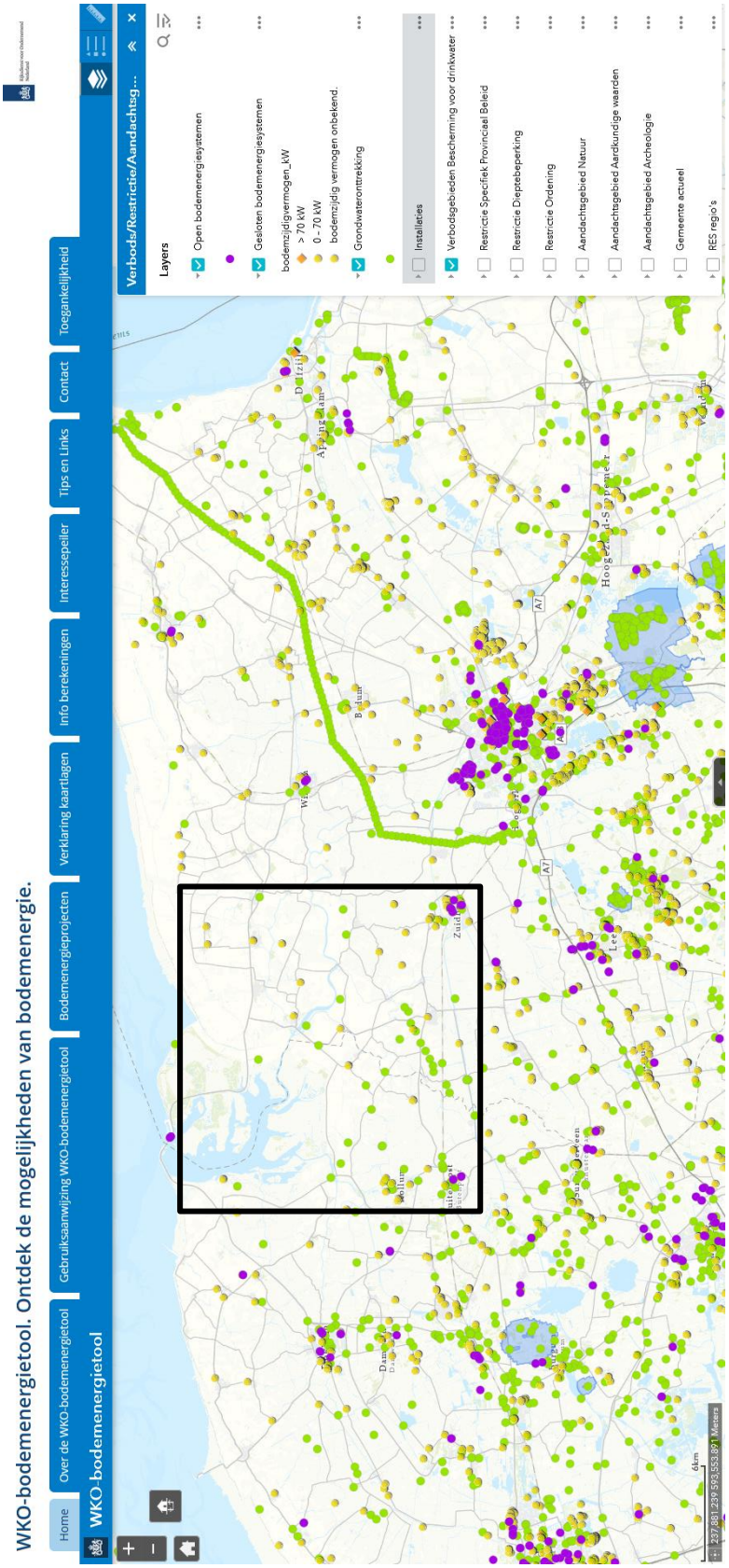

Figure 99. Map of the northern part of the Netherlands with open (purple) en closed (yellow/orange) ATES systems and the permitted and registered groundwater extraction locations (green). There are no drinking water extraction locations in the project area (outlined by the black box). The nearest drinking water area are between Leek and Roden, near Burgum and in Glimmen (SE of Groningen City). Source: WKOTool (2024).

ANNEX VI. PHOTO'S BICYCLE TOUR CASE STUDY AREA

Figure 100. NAM UGS complex Grijpskerk

Figure 101. Geodetic marker on house (right) north of Niezijl

Figure 102. Old sluice in Kommerzijlsterriet river at Kommerzijl

Figure 103. Remnant of dike structure (Ooster-Waarddijk)

Figure 104. Sluice complex near Zoutkamp (Friesche sluis) where the Lauwers rivers empties into the Lauwersmeer

Figure 105. NAM locatie Kommerzijl

Figure 106. Remnant of dike structure (Ooster-Waarddijk) in the distance

Figure 107. Discussion during the lunchbreak.

Figure 108. Near Eibersburen view on old Farmhouse with clear visible damage which has a geodetic marker

Figure 109. NAM location Grootegast-100 (Grootegast gas field)

Figure 110. Around Lutjegast en Grootegast change to a different landscape and landuse, clear relation with the shallow subsurface.

Figure 111. Around Lutjegast en Grootegast change to a different landscape (sandridge or ‘Gast’) and landuse, clear relation with the subsurface.

ANNEX VII. STRATIGRAPHIC UNITS

In this Annex we describe all the major soil and rock units in the Grijpskerk area that we encounter when we would drill a borehole from the surface to 10 km depth. In geological terms it is common to refer to 'stratigraphic units'. A stratigraphic unit is a distinct layer or combination of layers of rock or soil that differentiate it from adjacent layers. The units are usually differentiated and described based on age, lithology, and genesis. Here the typical depths and thickness of the various units, specifically for the Grijpskerk area are also provided. Genesis explains the origin and method of formation of the unit. The units are described below from young to old, in a normal stratigraphic sequence. The depths are indicative, based on a typical profile from the centre of the Grijpskerk area, based on the DGMdiep V5.0 model. References used here are the publication by Kombrink (2014), the book Geology of The Netherlands (KNAW, 2007) and the Stratigraphic Nomenclature database that can be found online (DINOloket, 2024). The Dutch Stratigraphic Nomenclature is after Van Adrichem Boogaert and Kouwe (1993) and is also used in the naming used below, which corresponds to the geological section provided in Figure 15. The ages and colours used in mapping should adhere to international standards set by the International Commission on Stratigraphy, and a Dutch version of the International Stratigraphic Chart (ICS, 2024) is provided in Figure 113.

NU (Upper North Sea Group) Depth: 0-500 m.

Age: Miocene - Holocene (23 – 0 Ma) (Neocene and Quaternary)

Lithology: Clay and fine-grained to coarse sand, locally gravel or peat and brown-coal seams. In The Netherlands there is a general trend from coarse- to fine-grained sediments towards the north and west.

Depositional setting: Shallow marine, river deposits and glacial deposits in the upper part.

Remark: The upper part of the NU Group consists of Pleistocene and Holocene deposits, which are further differentiated in Section 8.5. The Pleistocene and Holocene stratigraphic subunits (series or epochs) are classified under the Quaternary Period. The Pleistocene stage was one with alternating glaciations. The most recent glaciation occurred approximately 20,000 years ago and ended about 12,000 years ago, which marked the end of the Pleistocene. The lower part of the NU Group consists of Miocene and Pliocene deposits, grouped together under the Neogene Period. The Paleogene and Neogene periods were before grouped together as 'Tertiairy', but this name is no longer in official use.

NML (Middle and Lower North Sea Group) Depth: 500-1100 m.

Age: Middle Paleocene - Oligocene (60 - 23 Ma) (Paleogene)

Lithology: Middle North Sea group: Sands, silt, and clay, primarily of marine origin. The sands are mainly found along the southern edge of the North Sea Basin. Lower North Sea Group: A group of formations consisting of alternating grey sands, sandstones, and clays. They are the result of several small- and large-scale clastic sedimentation cycles in a marine environment at the edges of the North Sea Basin.

Depositional setting: Mainly marine deposits.

CK (Chalk Group) Depth: 1100-2000

Age: Upper Cretaceous (100-66 Ma)

Lithology: Mainly composed of carbonate rocks, the majority consists of white, buff, cream, and light-grey, hard, fine-grained, bioclastic limestones and marly limestones. Initially possessing a more chalky nature, these limestones underwent substantial compaction and densification due to deep burial. In some areas, marls, calcareous claystones, and glauconitic sands can be found. Chert (flint) concretions, either isolated or in layers parallel to the bedding, are common.

Depositional setting: The chalks are characterised by stable marine deposition over an extended period. Sediment features suggest varying water depths. Generally agreed upon is a depositional depth of 50-300 meters. Hardgrounds throughout may result from sea-level fluctuations or tectonic uplift.

KN (Rijnland Group) Depth: 2000-2100 m.

Age: Lower Cretaceous (145-100 Ma)

Lithology: A set of clay-rich and occasionally marly formations that may include sandstone layers at the bottom and, in some instances, comparable coarse clastic intercalations at upper levels adjacent to the basin margin.

Depositional setting: Characterized by coastal, shallow to deep, open-marine conditions (ranging from littoral to outer-neritic). Fines and carbonates settled from suspension, while sands were transported by waves, storms, tidal, and longshore currents. The concentration of sands occurred through sorting into coastal-barrier bars and offshore shoals.

GT (German Triassic Group) Depth: 2100-2800 m.

Age: Triassic (252-201 Ma)

Lithology: Usually, a distinction is made between the Lower and Upper Germanic Triassic Groups. The Lower Group consist red-bed-type sandstones, siltstones and claystones, often referred to as Buntsandstein. The Upper Group consist of varicoloured, silty claystones, evaporites, carbonates and sandstones. The Muschelkalk (carbonates) and Keuper (anhydrites and claystones) are distinct formations in here. The name 'Trias' (trisection) is derived from the recognisable distinction between the three Buntsandstein, Musschelkalk and Keuper formations.

Depositional setting: The sediments are deposited in the German basin. The Upper group is deposited in a marine setting, specifically in an alternating shallow, restricted-marine, inland-playa lake, and floodplain settings. The Lower group is deposited in more continental setting: lacustrine and fluvial with local aeolian influences.

ZE (Zechstein Group) Depth: 2800-3500 m.

Age: Late Permian: Lopingian (260-252 Ma)

Lithology: The sequence consists of evaporites and carbonates with occasional thin layers of claystone. Evaporites include anhydrite, rock salt, and small quantities of bitter salts, often influenced by halokinetic movements in certain areas, i.e. the development of salt diapirs and salt walls.

Depositional setting: Deposition of the Zechstein Group took place in a peri-marine to marine setting in the extensive Permian basin under warm and arid climatic conditions. During deposition of the Zechstein Group the basin became increasingly shallow. By the end of this deposition, continental and more humid conditions had returned. The Zechstein Group comprises five evaporite cycles (Z1 to Z5). In terms of thickness the Z1 and Z2 cycles are the most prominent. Minor extensional fault movements occurred during lower (Z1) and upper Zechstein (Geluk, 1999; 2005; Geluk et al., 1997).

Remark: The thick Zechstein salt deposit form the most important trap for the hydrocarbons in the Rotliegend reservoir rock. Rock salt (Halite) and Magnesium salts are mined with salt solution mining and using the squeeze method in various parts of The Netherlands (see Section 2.8.2)

RO (Upper Rotliegend Group) Depth: 3500-3800 m.

Age: Late Permian: Capitanian/Wuchiapingian (264-260 Ma)

Lithology: Group of formations, comprising conglomerates, claystones, sandstones predominantly of red-bed type and evaporites. The group consists of two separate formations, from young to old: Silverpit Formation and Slochteren Formation. The Silverpit formation consist of a sequence of red-brown, silty, often anhydritic claystones with some sand- or siltstone stringers and thin beds, and with rock-salt intercalations in the centre

of the basin. The Ten Boer Member form the top of the Silverpit formation and due the presence of clay forms the first seal for the trapped gas in the underlying Slochteren Formation. The Slochteren Formation consists of predominantly red to pale red-brown, occasionally yellow or grey, sandstones and conglomerates with lesser amounts of intercalated dark red, red-brown, or green-grey silty claystones. The sandstones exhibit diverse grain sizes, textures, and sedimentary structures. Due to the porosity and permeability, it forms a good reservoir rock for possible trapped hydrocarbons. The gas fields in the Grijpskerk area are all located within the Slochteren Formation.

Depositional setting: Deposited in the Southern Permian Basin, this formation originated in a large inland saline lake at the basin centre, characterized by clay with minor evaporite sediments (halite). Moving towards the basin fringe, the clay domain transitions to sand and finally conglomeratic domains. These depositional zones include playa lake/salt pan, mudflats, sandflats, 'aeolian' sand seas, and fluvial/alluvial fans with wadi systems. The widespread presence of aeolian and evaporitic sediments suggests a desert/playa-lake complex formation. The Slochteren Formation consist of aeolian features including dunes and sand flats (dry, damp, and wet). Water-laid features consist of fluvial channel fills (low- and high-sinuous, highly ephemeral to perennial) and sheet floods. Fine-grained deposits are associated with lakes, interdune ponds, and sabkha mudflats.

DC (Limburg Group) Depth: 3800-8000 m. (lower boundary highly uncertain)

Age: Late Carboniferous: Serpukhovian – Moscovian (331-307 Ma) (Old names: Silesian: Namurian – Westphalian)

Lithology: This formation consists of thick, predominantly grey to black, fine-grained siliciclastic sediments with intermittent coal seams in the middle and upper sections. Older segments include fossil-rich marine beds, becoming scarce in the middle and absent in the youngest interval. Light-coloured sandstones, primary red-bed intervals without coal seams, and sporadic volcanic beds are also present. The basal interval contains black, bituminous shale and intrusive rocks.

Depositional setting: The sediments from the Limburg Group formed in a foredeep basin due to the collision of drifting Gondwana and Laurussia continents. The Variscan mountain belt, the collision centre, served as the sediment source for the southern basin, while sediments in the north came from the Caledonian Mountains. Lithology varies from claystone to conglomerate. Initially deposited in a lacustrine/marine basin, it transitioned to deltaic, alluvial, and finally fluvial, red-bed environments.

Remarks: The peat layer turned into coal, which was mined in Limburg in the southern Netherlands until 1974. The maturation of the peat into coal also resulted in the creation of the hydrocarbons (methane and oil) that migrated and became trapped in the overlying Rotliegend (Slochteren) sandstone layers. The age of the Limburg Group has in NW Europe been referred to as ‘Silesian’ with the stages Namurian and Westphalian. While no longer employed in official international terminology, this name is still widely used.

CL (Carboniferous Limestone Group) Depth: 8000 – 8100 m (depths highly uncertain)

Age: Early Carboniferous (also: Dinantian or Zeeland Formation): Tournaisian-Visean (359-331 Ma)

Lithology: Group of mainly light-grey, brown, and black carbonates. Variable number of claystones can be intercalated. In places bedded cherts occur. Within the research area the top part of the Dinantian probably consists of black limestones and shales, due to the presence of the early deeper Lauwerszee basin. On the adjacent Fryslân platform and Groningen High limestone reefs can be present.

Depositional setting: An important element is a series of carbonate platforms and intervening shale-dominated troughs. Three platforms have been interpreted, with the largest platforms (>20 km in length) occurring on the Fryslân Platform and the Groningen High. The Lauwerszee Trough, situated between these platforms, likely represents a Dinantian basin (Kombrink, 2008).

Remark: the MSc study by Hoornveld (2013) investigated the possibility of the Dinantian carbonates to host a petroleum system. Several prospective areas were identified, with key risks including high temperatures, gas

quality issues, and potential faults affecting the seal. If not gas-bearing, Enhanced or Ultra-deep Geothermal Systems (EGS/UDG) for electricity generation could be a viable option for these ultra-deep leads.

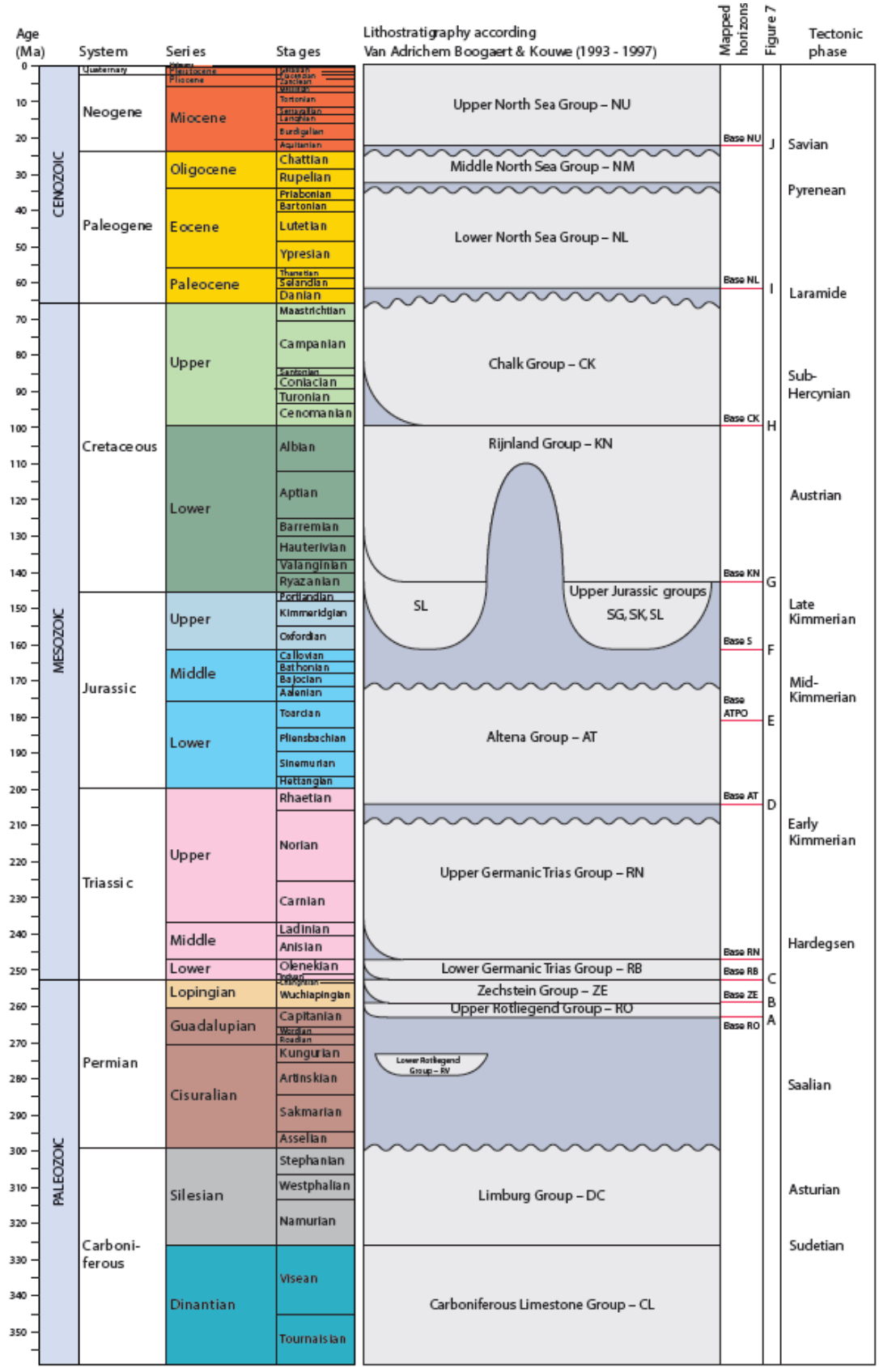

Figure 112. Simplified stratigraphic diagram of the Netherlands (Kombrink, 2012)

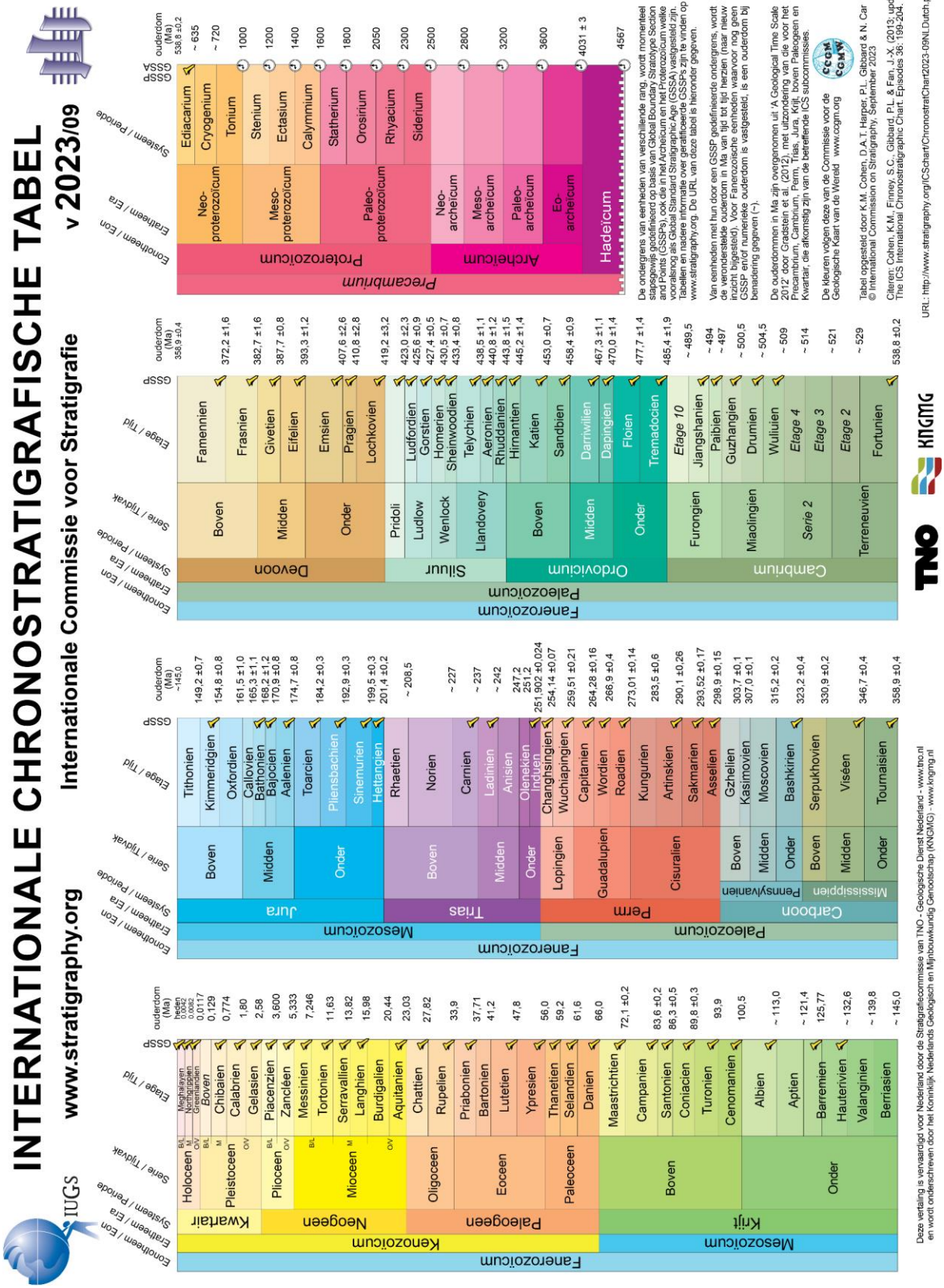

Figure 113. Dutch translation of the IUGS international stratigraphic table (IUGS, 2024)

ANNEX VIII. KNMI ANNUAL DROUGHT DATA

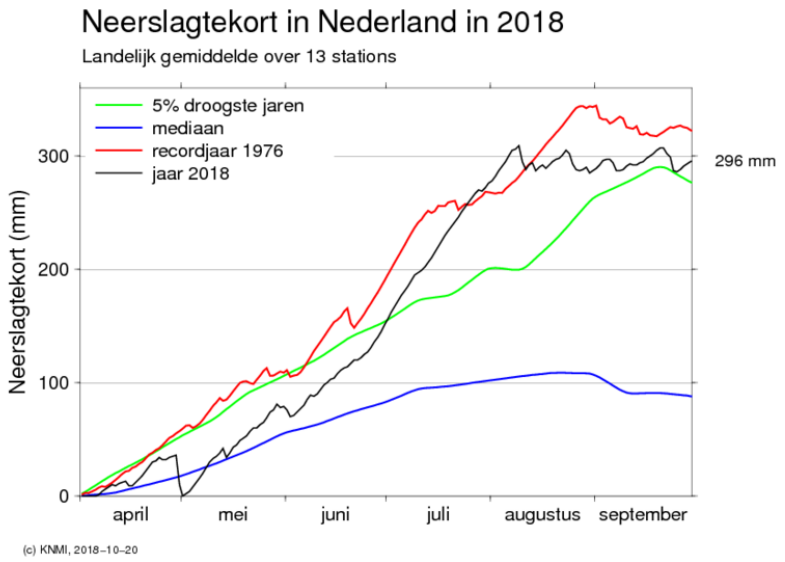

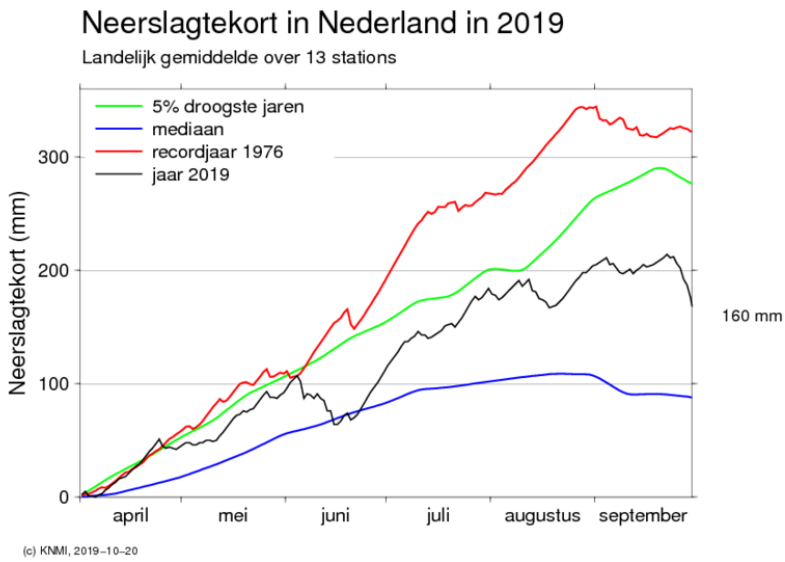

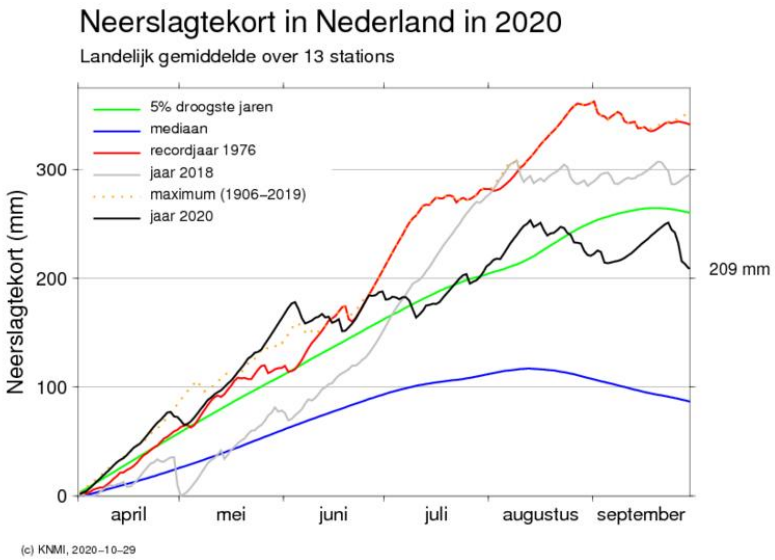
Neerslagtekort in Nederland in 2020
Landelijk gemiddelde over 13 stations
5% droogste jaren
mediaan
recordjaar 1976
jaar 2018
maximum (1906–2019)
jaar 2020
Neerslagtekort (mm)
300
200
100
0
april
mei
juni
juli
augustus
september
209 mm
(c) KNMI, 2020-10-29

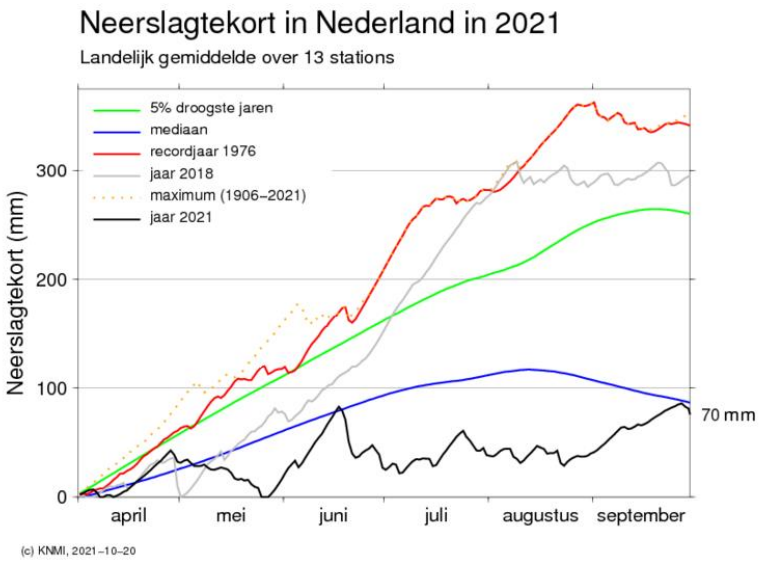
Neerslagtekort in Nederland in 2021
Landelijk gemiddelde over 13 stations
5% droogste jaren
mediaan
recordjaar 1976
jaar 2018
maximum (1906–2021)
jaar 2021
Neerslagtekort (mm)
300
200
100
0
april
mei
juni
juli
augustus
september
70 mm
(c) KNMI, 2021-10-20

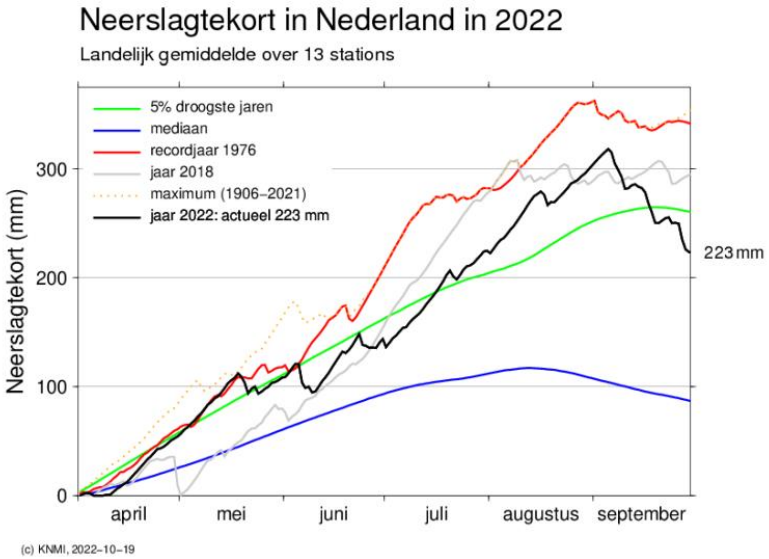
Neerslagtekort in Nederland in 2022
Landelijk gemiddelde over 13 stations
5% droogste jaren
mediaan
recordjaar 1976
jaar 2018
maximum (1906–2021)
jaar 2022: actueel 223 mm
Neerslagtekort (mm)
300
200
100
0
april
mei
juni
juli
augustus
september
223 mm
(c) KNMI, 2022-10-19